SCHOLARLY PUBLICATIONS

A CURRENT AWARENESS BULLETIN
OF RESEARCH OUTPUT

@DTU

(14th Edition)

FEBRUARY 2014

BY: CENTRAL LIBRARY

DELHI TECHNOLOGICAL UNIVERSITY
(FORMERLY *DELHI COLLEGE OF ENGINEERING)*
GOVT. OF N.C.T. OF DELHI
SHAHBAD DAULATPUR, MAIN BAWANA ROAD
DELHI 110042

PREFACE

This is the Twelfth Issue of Current Awareness Bulletin started by Delhi Technological University, Central Library. The aim of the bulletin is to compile, preserve and disseminate information published by the faculty, students and alumni for mutual benefits. The bulletin also aims to propagate the intellectual contribution of Delhi Technological University (DTU) as a whole to the academia.

The bulletin contains information resources available in the internet in the form of articles, reports, presentations published in international journals, websites, etc. by the faculty and students of DTU. The publications of faculty and student which are not covered in this bulletin may be because of the reason that the full text either was not accessible or could not be searched by the search engine used by the library for this purpose.

The learned faculty and students are requested to provide their uncovered publications to the library either through email or in CD, etc to make the bulletin more comprehensive.

This issue contains the information published during February 2014. The arrangement of the contents is alphabetical. The full text of the article which is either subscribed by the university or available in the web is provided in this bulletin.

Central Library

CONTENTS

10. Fuzzy-Genetic Algorithm For Patient Data Processing In Telemedicine, ***Richa Gupta***, Department of Information Technology and ***Dr. Parmod Kumar*** Department of Electrical Engg.

11. Graft-Interpenetrating Polymer Networks of Epoxy with Polyurethanes Derived from Poly(ethyleneterephthalate) Waste, ***Saurabh Chaudhary***, Surekha Parthasarathy, ***Devendra Kumar***, Department of Applied Chemistry and Polymer Technology Chitra Rajagopal and Prasun Kumar Roy

12. GUAR GUM AND THEIR DERIVATIVES: A RESEARCH PROFILE, ***Anek Pal Gupta*** and ***Devendra Kumar Verma,*** Department of Applied Chemistry and Polymer Technology

13. Magnetized Viscous Fluid Anisotropic Models in String Cosmology ***C.P.Singh*** Applied Mathematics and A. Beesham

14. Molecular Interaction Studies of Shrimp Antiviral Protein, PmAV with WSSV RING Finger Domain in silico, MNV Prasad Gajula, ***Garima Soni***, Babu G, Rai A and ***Bharadvaja N,*** Department of Biotechnology

15. NFC Based Secure Mobile Healthcare System, ***Divyashikha Sethia, *Daya Gupta, *Tanuj Mittal, *Ujjwal Arora,*** Department of Computer Engineering and Huzur Saran

16. Novel single input five output voltage mode universal filter based on DDCCTA, ***Neeta Pandey***, ***Rajeshwari Pandey***, Department of Electronics and Communication Engineering and Sajal K. Paul

17. Reaffirmation of Measurement Uncertainty in Pressure Sensitivity Determination of Ls2p Microphones by Reciprocity Method, ***N. Garg***, Anil Kumar, Arif Sanjid M, K.P. Chaudhary, ***S. Maji***, Deptt of Mechanical, Production & Industrial Engg.

18. Real Time Object Tracking Using Different Mean Shift Techniques–a Review, ***Snekha, Chetna Sachdeva*** and ***Rajesh Birok***, Electronics and Communication Department

19. Role of technological advancements in enhancing sustainable development, ***£Ujjwal Raheja*** and Abhinav Malik

20. Sensing Performance Evaluation over Multihop System with Composite Fading Channel, Deepti Kakkar1, Arun Khosla and ***~Moin Uddin***

21. Spectrophotometric Determination of Complexation of Ruthenium (IV) with 2-[(5-Bromo-2-Pyridylazo)]-5-Diethylaminophenol and N-Hydroxy-N, N'-Diphenylbenzamidine, Pushpa Ratre and Devendra Kumar, Department of Applied Chemistry and Polymer Technology

22. UNFAIR ADVERTISING AND SALES PROMOTION: CONSUMERS' PERCEPTION, Dr. P.V. Khatri* and ***#Ms. Rashmi***,

23. Vehicular traffic noise modeling using artificial neural network approach, Paras Kumar, ***S.P. Nigam*** and ***Narotam Kumar***, Mechanical Engineering Department,

International Journal of Application or Innovation in Engineering & Management (IJAIEM)
Web Site: www.ijaiem.org Email: editor@ijaiem.org, editorijaiem@gmail.com
Volume 2, Issue 6, June 2013 ISSN 2319 - 4847

A Novel Approach of Calculating Affective Cost in Cost Cognizant Regression Testing

Harsh Bhasin[1], Satpal[2] and Deepkiran Munjal[3]

[1]Delhi Technological University, Delhi
[2]BSAITM, Faridabad
[3]BSAITM, Faridabad

ABSTRACT

The present methods of cost cognizant regression testing are based on the execution time of a test case. However, it has been observed that in the testing of a professional enterprise resource planning system, a test case may take different time to run in different testing cycles. This may be because of different number of concurrent processes running on the system or because of the updates. The work proposes a method for the calculation of effective cost of a test suite in such situation. This would facilitate the application of 'cost cognizant regression testing'. Owing to the huge number of possible test cases, Genetic Algorithms has been applied in order to achieve optimization.

Keywords: Regression testing, Cost Cognizant, APFD, Coefficient of Variation

1. INTRODUCTION

It is a known fact that software undergoes many changes in its life cycle. After every change the older test cases must be re-executed to analyze the effect of changes on components developed in the older version. This exercise is referred as regression testing and may consume a huge amount of time and resources. It is, therefore, desirable to minimize the test suite or to order it in such a way that the important test cases are executed first. This mythology is referred to as minimization. Minimization is one of the three techniques of regression testing. The other two being selection and prioritization. Many techniques have been proposed in order to accomplish the above task. Cost Cognizant is one of them. It takes into account the cost of each test case in order to determine the final ordering. However, the existing techniques fail to handle the situation wherein many test cycle have been executed and a particular test case is taking different time to execute in different cycles. This may happen due to different background processes running at that time or the updates. The execution of the process and the amount of the RAM used also affect the running time of the test case. This work presents a solution to handle such problems. The Novel and path-breaking technique will change the way the cost factor is perceived as of now.

The work is a part of our endeavor to study various testing techniques [1-5] and test data generation techniques [6-9].The work is a continuation of earlier attempt in which time aware and cost cognizant regression testing techniques were presented [11, 12]. The rest of the paper has been divided as follows: Section 2 of the paper examines genetic algorithms. Section 3 throws light on applicability of genetic algorithms. Section 4 presents proposed work and section 5 presents results and conclusion.

2. GENETIC ALGORITHMS

Genetic algorithms are heuristic search processes which are based on the theory of natural selection. They are generally applied when the population can be arranged on the basis of some value referred to as fitness value. It may be noted that genetic algorithms are applied only when the search space is large. The steps of Simple Genetic Algorithm are as follows.

Population Generation: A population of chromosomes is generated. A chromosome contains cells. The cells can be binary or numeric. It may be noted that each cell represents some attribute.

Crossover: The crossover mingle the features of two chromosomes. There are many types of crossovers like one point cross over, multi point cross over etc.

Mutation: The mutation operator breaks the local minima/maxima and helps to achieve optimization.

Selection: Selection is selecting the chromosome from amongst the population. This can be done by one of the many techniques like roulette wheel selection.

It may be stated that in many experiments were carried out to find the crossover rate and the mutation rate at which maximum optimization can be achieved [10, 13-19]. It was found the crossover rate of 2% and the mutation rate of 0.5% provides best results. However, it may also be stated that these rates just give an idea and not the exact value of the rates. In the present work the effect of factors on the optimization was also analyzed.

3. PROPOSED WORK

Since the cost of a particular test case is different in different cycles of testing, the affective cost of a test case needs to be evaluated. In order to accomplish the task, the following steps must be carried out.

Step 1. Gather the cost of a test case in different cycles. The cost of the test cases can be gathered by the previous test cycles carried out.

Step 2. Find the mean cost of each test case. The mean cost of text cases is given by Formula 1.

$$\overleftrightarrow{x} = \frac{\sum_{i=1}^{n} x_i}{n} \quad (1)$$

Step 3. Find the standard deviation of each test case. The formula of standard deviation is as follows.

$$\sigma = \sqrt{\frac{(\sum_{i=1}^{n} x_i - \overleftrightarrow{x})^2}{n}} \quad (2)$$

Step 4. Divide the mean and the standard deviation to evaluate the coefficient of variation of each test case. The coefficient of variation(CV) is given by the following formula.

$$CV = \frac{\sigma}{\overleftrightarrow{x}} \quad (3)$$

Step 5. Evaluate the fitness function of a test suite. The fitness function of a test suite is the sum of finesses of each test case.

Step 6. Arrange the test suites in order of their fitness function. The test suites can be created by using Genetic Algorithms initial population.

Step 7. The new order of the test suite is the result, as per the technique.

The technique has been depicted in Figure 1.

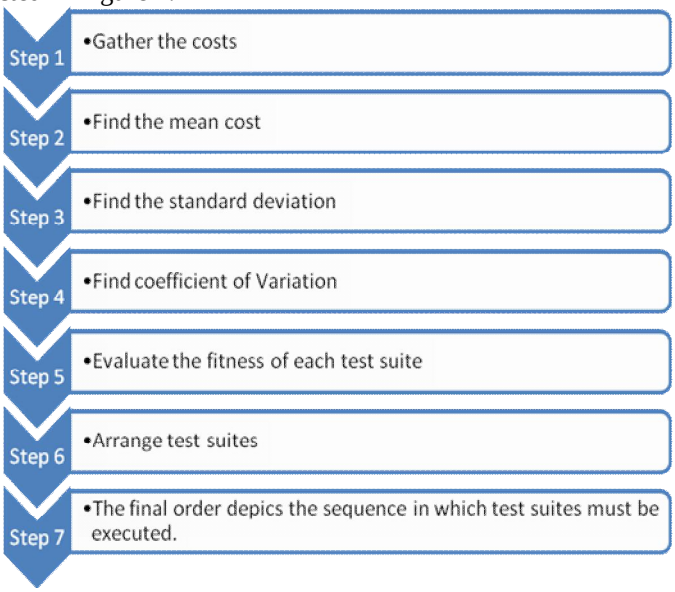

Figure 1: Effective Cost Calculation

4. VERIFICATION

In order to verify the above technique, a Software develop by Sahib Soft has been taken. The Software is of around 3K lines of code. The four cycles of Software testing have already been carried out. The following test suites are to be prioritized using the proposed technique. Here, Ti represents i^{th} test suite and TCj represents j^{th} test case. The following steps depict the implementation of the proposed technique.

First of all, an initial population is generated using the Genetic Tool. The number of test cases is 10.Therefore the no. of cell in each chromosome of the genetic population should be 10.Table 1 depicts the initial Population generated by the tool. Each Chromosome is then mapped against requisite test cases for example 1101000000 depicts test suite {T1, T2, T3, T4}. Table 2 represents the running time of each test case in millisecond. On the basis of Step no. 3 effective cost of each test case is calculated. It may be noted that at this point the cost is remains same in different cycles. Then those values should be taken the final values. Otherwise the mean error and standard deviation should be calculated and the statistically analysis should give the effective cost that can be used to calculate the fitness of each test case. On the basis of data of the above step values of fitness of test suite are evaluated .These values are shown in Table 3. Then,

Crossover is applied on the initial Population and new Population is generated. One point Crossover has been applied with a crossover rate of 2.0. The new chromosome generated is then mapped with test cases and their fitness is again calculated. This is followed by the application of mutation operator. The mutated population is shown in Table 3. The coefficient of variation is then calculated for each test case. Table 4 shows the requisite data. The APFD of the final test suite is coming out to be 0.94, which is much better then the random ordering.

Table1 Initial Population

0	0	1	0	0	1	0	1	0	1
1	1	0	1	0	1	1	0	0	0
1	0	1	0	0	1	0	1	0	0
0	0	0	1	1	0	0	1	1	0
0	1	1	0	0	1	0	0	0	0
1	1	0	0	1	1	0	1	0	0
1	1	0	1	1	1	0	1	0	0
0	1	0	0	0	0	1	0	1	0
1	1	0	0	0	0	1	0	1	1
0	1	0	0	1	1	0	0	0	0
1	1	0	0	0	1	0	1	1	0
1	0	1	0	0	0	0	0	1	0
0	0	1	1	0	0	0	1	1	1
1	0	0	1	0	0	0	1	0	1
0	0	1	1	0	0	1	0	1	0
0	0	1	1	0	1	0	0	1	0
1	1	0	1	0	1	0	1	0	0
0	0	0	0	1	1	0	1	0	1
1	1	1	0	0	1	1	1	0	0
0	0	0	1	1	0	0	0	1	0
0	0	0	1	0	0	1	1	1	0

Table 2: Running time in previous cycles.

67	451	129	343
196	348	496	7
413	76	415	134
141	336	320	86
324	305	25	432
348	14	130	168
301	76	253	144
277	208	400	364
167	87	306	356
307	223	173	454

Table 3: Mutation

	TC1	TC2	TC3	TC4	TC5	TC6	TC7	TC8	TC9	TC10
T1	1	0	0	1	0	0	0	1	1	1
T2	1	0	1	1	0	0	0	1	0	1
T3	1	1	1	1	0	1	1	1	1	0
T4	1	0	0	1	1	1	0	1	1	0
T5	1	1	1	1	1	0	1	1	0	0

T6	0	1	0	1	1	1	1	1	1	0
T7	0	1	0	0	0	1	1	0	1	1
T8	0	1	1	0	1	1	0	0	1	0
T9	1	0	1	0	0	1	0	1	0	1
T10	0	1	1	0	0	1	0	0	1	0
T11	0	1	1	0	1	1	0	1	1	1
T12	0	0	0	1	1	1	1	1	0	1
T13	0	0	1	0	1	1	1	0	1	1
T14	0	1	1	1	0	1	0	0	0	1
T15	1	0	1	1	0	0	0	1	1	0
T16	0	1	1	1	1	1	1	1	1	1
T17	1	0	1	0	0	1	1	1	0	0
T18	0	1	1	0	1	0	1	0	0	0
T19	1	1	1	1	0	1	0	1	0	1
T20	1	1	1	1	1	1	0	1	1	0
T21	1	0	1	0	0	0	0	1	1	1
T22	0	1	0	0	1	0	1	1	1	1
T23	1	0	1	0	0	1	0	1	1	1
T24	1	0	1	0	0	1	1	1	1	0

Table 4: CV of each Test Case

TC1	SD	155.8453
	CV	0.629678
TC2	SD	181.3345
	CV	0.692777
TC3	SD	155.8533
	CV	0.600591
TC4	SD	109.1407
	CV	0.494409
TC5	SD	150.3305
	CV	0.553703
TC6	SD	119.9166
	CV	0.726768
TC7	SD	88.52824
	CV	0.45751
TC8	SD	74.97458
	CV	0.240111
TC9	SD	107.3103
	CV	0.468604
TC10	SD	106.4856
	CV	0.368144

5. CONCLUSION

The cost of a test case can be perceived as the time it takes to execute the test case. The cost cognizant technique relies on the cost of a test case. However, there is no definite procedure of calculating the effective cost when the value of cost caries in different cycles of testing. The above work proposes a technique that evaluates the effective cost of testing. The proposed technique is applied on professional software developed in C#, .NET framework. The results obtained are encouraging and thus instills confidence in the technique. However, it is intended to amalgamate the concept of cost and time in order to develop a technique which is more effective. The concept is being developed and being applied to a professional Enterprise Resource Planning System.

References

[1.] Harsh Bhasin et. al., "Regression testing using Fuzzy Logic", International journal of Computer Science and Information Technology, Vol. 4, No. 2, 2013.

[2.] Harsh Bhasin et. al., "Implementation of Regression testing Using Fuzzy Logic", International Journal of Application or Innovation in Engineering and Management, Vol. 2, No. 4, 2013.

[3.] Harsh Bhasin et. al., "Orthogonal Testing Using genetic Algorithms", International Journal of Computer Science and Information Technology, Vol. 4, No. 2, 2013.

[4.] Harsh Bhasin et. al., "Software Architecture Based Regression Testing", IJCSE, Vol. 5, No. 04, 2013.

[5.] Harsh Bhasin et. al., "Software Architecture Based Regression Testing Implementation", International Journal of Computer Science and Engineering (IJCSE), Vol. 2, No. 3, 1-4, July 2013.

[6.] Harsh Bhasin et. al., "Test Data Generation using Artificial Life", International Journal of Computer Applications, Vol. 67, No. 12, 2013.

[7.] Harsh Bhasin et. al., "On The Application Of Artificial Life Based Test Data Generation", International Journal of Computer Science and Engineering, Vol. 5, 2013.

[8.] Harsh Bhasin, Neha Singla, "Test Data Generation Using Cellular Automata", ACM Sigsoft Software Engineering Notes, to be published in July 2013.

[9.] Harsh Bhasin, Neha Singla, "Cellular Genetic Test data Generation", Communicated in ACM sigsoft Software Engineering notes.

[10.] Harsh Bhasin, Surbhi Bhatia, "Use of Genetic Algorithms for Finding Roots of Algebraic Equations", IJCSIT, Volume 2, No. 4, Pages 1693-1696, 2011.

[11.] Harsh Bhasin et. al., **"**Novel Time Aware Regression Testing Technique", International Journal on Computer Science and Engineering (IJCSE), Vol. 5 No. 05, 2013.

[12.] Harsh Bhasin et al., "A Novel Approach to Cost Cognizant Regression Testing", International Journal of Computer Science and Management Research, Vol. 2, No. 5, 2013.

[13.] Harsh Bhasin, Neha Singla, "Genetic based Algorithm for N – Puzzle Problem", International Journal of Computer Applications, Vol. 51, No.22, 2012.

[14.] Harsh Bhasin, Rohan Mahajan, "Genetic Algorithms Based Solution To Maximum Clique Problem", International Journal on Computer Science and Engineering (IJCSE), Vol. 4, No. 08, 2012.

[15.] Harsh Bhasin and Neha Singla, "Harnessing Cellular Automata and Genetic Algorithms To Solve Travelling Salesman Problem", International Conference on Information, Computing and Telecommunications, (ICICT - 2012), pp. 72 – 77, 2012.

[16.] Harsh Bhasin, Neha Singla, "Modified Genetic Algorithms Based Solution to Subset Sum Problem", (IJARAI), International Journal of Advanced Research in Artificial Intelligence, Vol. 1, No. 1, 2012.

[17.] Harsh Bhasin, Nishant Gupta, "Randomized algorithm approach for solving PCP", International Journal on Computer Science and Engineering (IJCSE), Vol. 4, No. 01, 2012.

[18.] Harsh Bhasin et. al., "Hybrid Genetic Algorithm for Maximum Clique Problem", International Journal of Application or Innovation in Engineering & Management, Volume 2, No. 4, April 2013

[19.] Harsh Bhasin, Gitanjali Ahuja, "Harnessing Genetic Algorithm for Vertex Cover Problem", International Journal of Computer Science and Engineering, Vol. 4, No. 2, 2012.

ISSN: 2319-8753

International Journal of Innovative Research in Science, Engineering and Technology

(An ISO 3297: 2007 Certified Organization)

Vol. 3, Issue 2, February 2014

A Sustainable Approach towards the Construction and Demolition Waste

Shishir Bansal[1], S K Singh[2]

Research Scholar, Department of Environmental Engineering,Delhi Technological University, Delhi, India[1]

Head, Department of Environmental Engineering,Delhi Technological University, Delhi, India[2]

Abstract:With the growth of society on all the fronts, lot of construction activities are seen everywhere. Mega construction activities are increasing exponentially. Also, the demolition of existing structures, which have outlived its service life, is going on simultaneously. It is not essential that the structures need to be demolished only after their service life span is over, but also due to ongoing trend of reconstruction of even healthy structures just for creating more space in order to meet the present requirement. All such activities are generating huge amount of waste, called the Construction and Demolition (C&D) waste. Disposal of such debris in a sustainable manner is a big challenge for the builders, developers and owners.

While the disposal of debris is a challenge, on the other hand there is an acute shortage of naturally available aggregates for construction of buildings. Reduction of this demand in a small way is possible with the reusing or recycling of construction and demolition waste generated from the construction activities. Hence, the construction sector must accept the use of C& D waste wherever feasible.

Keywords:Construction & Demolition, Recycling, Sustainability, Waste management.

I. INTRODUCTION

The concept of C& D waste management is new and it is essentially required to spread the education and information in order to gain the public support. The present mindset of public and their attitude towards the waste generated from construction and demolition sites is required to be changed which is possible only with the education in this field. It is required to sensitise not only the Engineers, but all stakeholders including regulatory authorities in construction industry. One must understand the reuse potential of C& D waste and existing practices in implementation and enforcement for achieving the aim with an ultimate motive of Environmental sustainability.

Recycling cost is influenced by transportation distance and amount of waste concrete to be recycled. CO_2 emission is influenced by transportation distance. It is important to minimize C&D waste generation and maximize reuse/recycling as the construction industry is consumer of tremendous amount of natural resources and energy as well as emitter of GHGs. Establishment of effective strategies and enactment of laws and regulations is essential to achieve this. In addition, provision for some incentives to users of the recycled products deems to be necessary to promote the use. It is essential to assess the life-cycle as it provides quantitative tool to assess environmental impact of C&D waste reuse/recycling.

The work in this paper is divided mainly in three stages. Section II explains the reuse and recycling potential of different C&D waste products. Simple guidelines to be followed in recycling the wastes are covered in section III. C&D waste recycling facilities in Delhi are furnished in Section IV, while the waste recycling in global forum is covered under Section V with specific examples of Korea and Japan. Finally, Section VI presents conclusion.

II. REUSING AND RECYCLING POTENTIAL OF DIFFERENT C&D WASTE

Reusing of construction and Demolition waste is different from Recycling. Reusing does not require any further processing to convert into a useful product. The items which are usable directly are screened out from the debris and

ISSN: 2319-8753

International Journal of Innovative Research in Science, Engineering and Technology

(An ISO 3297: 2007 Certified Organization)

Vol. 3, Issue 2, February 2014

put into the intended use without further processing or further energy input for conversion into the useful product. For example, full bricks can be screened out of the demolition debris and used as it is for building a partition walls. Otherwise for recycling, it would have been converted into smaller pieces for using it as an aggregate or brick bats for plinth protection etc. Since the reusing of C&D waste is always more advantageous, it is essential that to identify and segregate more and more reusable materials in debris. This is possible, if sufficient precautions are taken while a building is demolished. There should be an effective deconstruction plan instead of just converting the standing structure into debris within minutes. Useful products like doors and windows, bricks, reinforcement, from RCC components, structural steel can be taken out with little extra efforts and put into reuse without much processing. Once the reusable items are taken out, the leftover waste is now available for recycling. Recycling of this waste into useful products to extend the service to environment is a challenge. Worldwide in Japan, Korea, Norway, Singapore etc., recycling of such wastes is taking place and we must understand the potential of different waste products for their effective and useful recycling.

Different waste products covered under this section are Concrete, Bricks, tiles, Metals and Plastics.

2.1 Concrete

Concrete is primarily a composition of cement, coarse aggregates, fine aggregates and water, further processed by addition of industrial products/ by products for enhancing the properties. Engineers are mainly dependent on nature for obtaining the Coarse and Fine aggregates as well as water for the chemical reaction with cement. Scarcity is there for all these naturally occurring materials and need is there to explore alternative sources. Even for the water with required properties, shift is towards the use of waste water after due treatment. One of the alternative sources of coarse aggregates is recycled concrete aggregates (RCA) which are obtained from the processed Construction and Demolition (C&D) waste. During and after the demolition of any concrete structure, the demolished concrete waste is taken to a recycling plant and there crushed into the required sizes which is called the Recycled concrete aggregate (RCA).

Sometimes, good sized precast element are also obtained during the demolition, which have a potential of being reused or otherwise, these are also crushed and converted into the recycled aggregates. Thus, use of recycled aggregates can be there with different quantum of their share by suitable replacing the component of naturally occurring aggregates. It will help out not only in meeting the situation where there is acute shortage of natural resources, but also a step towards the sustainability.

2.2 Brick

Bricks are important building material in the construction of residential as well as non –residential buildings in every country. It is also a significant component of the total C&D waste on new residential construction sites. Its demand figures are next to concrete as a building material. Bricks are largely treated as waste when broken or damaged from the brick production line or from construction site due to poor internal handling and excessive cutting. Brick is a maintenance-free component of the structure which is durable during the complete service life of the building. The high durability property of the brick makes it environmental friendly in the sense that after the demolition of the structure, it can be reused repeatedly and the left over volume which is non-reusable can be recycled for other beneficial purposes. Generally, a building is not required to be demolished due to deterioration in the Engineering properties of the bricks. It is for different reason or different needs other reasons that the building has outlived its useful/economical service life and required to be replaced with new structure. During the demolition process itself, bricks obtained are stacked for next use in its original form after the removal of mortar which is chiseled out and make the brick ready for reuse or recycling, if not reusable.

Bricks, after the removal of the stuck up mortar remain reusable for restoration or for new homes and projects. Recovered bricks can be used like a fresh lot of bricks without any further processing. These can also be laid on as brick pavers or for landscaping or any other artistic creations. Brick paved streets are aesthetically pleasing and rain water also percolates through the pavement. Also, a brick surface is cooler in hot months. These street advantages make bricks a good choice in driveways. Bricks on edge are also sometimes used as economical pavement solutions in smaller compounds.

Bricks which cannot be reused directly can be disintegrated into smaller sized aggregates or brick chips to be used as construction materials. These recycled bricks products are strong and durable enough in comparison to the original

ISSN: 2319-8753

International Journal of Innovative Research in Science, Engineering and Technology

(An ISO 3297: 2007 Certified Organization)

Vol. 3, Issue 2, February 2014

brick. Bricks from demolition sites can be recycled as Road base and construction fill and also as light weight concrete. Construction debris consisting of bricks can be recycled into brick aggregate through screening, crushing, re-screening and blending, which can then be used as pavement base material by proper mix proportions with cement and fly ash. Brick waste which are not suitable for recycling into the pavement base materials can be used in construction/land fill. Concrete prepared from crushed brick aggregate has good engineering and also better thermal properties but has greater shrinkage than ordinary concrete. Sometimes, during the manufacturing of bricks, due inadequate burning, or sometimes due to over burning, whole lot is turned into the production waste. Though this waste is different from construction and demolition waste, but it can also be recycled like C& D waste and can be suitable used for production of precast elements like paver blocks, kerb stones, interlocking tiles by mixing with cement and using as a concrete mix.

2.3 Tiles

Generally, it is difficult to extract tiles from the walls in proper shape and size in order to find them suitable for reuse. It also depends upon the type of the tiles, their life span and the existing conditions. Still tiles extracted from walls, even if these are broken pieces, provide an excellent opportunity to the artists /designers for making murals or other decorative master pieces. Broken tiles can also be used aggregate after crushing. If the tiles can be extracted or removed from the wall in good shape and size, these are reused for the same purpose after the removal stuck up mortar and then glued with suitable adhesives available in market today. Creative items like artifacts, table tops, special effects in drive ways, pedestrian subways etc. can be smartly created by reusing for a wide variety of projects. Nek Chand's Rock Garden in Chandigarh, which is internationally renowned, is a perfect example of such reuses.The broken tiles can be further crushed into smaller sizes and can be a partial replacement of gravel and crushed stone in making concrete.

2.4 Timber

The waste timber is not only produced from the demolition of the building, but also from construction of wooden building wherein lot of timber waste is generated. Each source has its own system of recycling and reuse of recovered timber from the demolition of a building or the construction of a building. Whenever a building is decided to be dismantled, timber products like doors and windows are the items which are removed as first step and that too in original form. Timber products have a quality of a long service life which is much longer than the life of the building itself. Hence, in general such products unless eaten by the termites or damaged due to fire do not lose the Engineering properties for a long time and can be used multiple times and thus an environmentally friendly product.

The waste timber which does not been recovered in its original form or non-usable in same shape and size, can be recycled into new particleboard, medium density fibre boards, animal bedding or used to make renewable energy. Timber used for recycling has to be free from any other demolition products like concrete, mortar, aggregates, sand, bricks, plastic, metals, tiles etc. Wood chips are produced from good quality wooden waste such as large size lumbers. Some of the particleboard producing companies and the pulp and paper producing companies are still using the recycled chip for their products. Chipped or shredded wood is also used as a sewage sludge bulking medium and other products lime pallets.

2.5 Metals

Amongst the metals, steel and Aluminium are the two major products obtained as waste during the construction as well during the demolition of a building. Structural steel obtained during the demolition of a steel structure or left over steel during the construction can be reused directly without much processing. The members can be resized as op the requirement and can be reused directly. Aluminium scrap can be put into reuse by the solid bonding process. If a care is taken in initial stages i.e. during designing with a valid deconstruction plan, then the reusable scrape can be increased to a much greater extent like house hold appliances, without taking the routing the scrap through a foundry. Reusing a steel beam its existing form is better than re-melting it and rolling a new steel beam, i.e. the energy used to re-melt the beam is saved.

Steel waste occurs during the construction and refurbishment of buildings and when they are ultimately demolished and the material becomes available for recycling. Waste from the manufacture of steel construction products can be easily collected and segregated for recycling. Steel generates almost nil wastage on the construction site. Waste steel

ISSN: 2319-8753

International Journal of Innovative Research in Science, Engineering and Technology

(An ISO 3297: 2007 Certified Organization)

Vol. 3, Issue 2, February 2014

which is reusable is equally good in durability criteria and the quality is also well maintained while making products like fire hydrants, steel furniture and also ecologically sustainable.
As far as Aluminium is concerned, it is recyclable multiple times and is always on demand with the need to preserve the environment. Our raw materials vary considerably based on whether we are using primary or recycled aluminum. We must take into account the different sustainability impacts of sourcing primary aluminum from the mined substance bauxite, or recycled aluminum from either pre- or post-consumer sources. Recycling scrap aluminium requires very less energy in comparison to the energy requirement of new aluminium. Because aluminum is infinitely recyclable, it can be reused in applications vastly different from its previous purpose, and it can also be recast into its original form. These properties make aluminum an ideal material for use in premium applications, even after being recycled many times.

2.6 Plastic

Scrap or waste plastic recovered from demolition or construction site is reprocessed and transformed into the entirely different useful products. Typically a plastic is not recycled into the same type of plastic, and products made from recycled plastics are often not recyclable. When compared to other materials like glass and metals, plastic polymers require greater processing to be recycled. The most-often recycled plastic HDPE (high-density polyethylene) is reduced to plastic lumber, tables, roadside curbs, benches, truck cargo liners, stationery (e.g. rulers) and other durable plastic products and is usually in demand. Other application of recycled plastic is in the preparation of a road surface that includes recycled plastic: aggregate, bitumen (asphalt) with plastic that has been shredded and melted at a temperature below 220° C (428 °F) to avoid pollution. Such road surfaces are very durable and monsoon rain resistant.

III. SIMPLE GUIDELINES TO BE FOLLOWED IN RECYCLING OF DEMOLITION WASTE

The agencies responsible for generation of wastes should separate the generated wastes having potential for reuse/recycling. The Engineer-in-charge will select structure's type and materials that are suitable for reuse/recycling, use recycled aggregates, and ensure proper treatment of wastes generated from such development. The waste generation from construction should not only be minimised, but should also minimise the hazardous effect from the generated wastes.

3.1 Agencies (or sub-contractors)

Various agencies or sub-contractors to be involved are to be linked up with the steps in this process of C& D waste reuse and recycling. Some of such steps can be listed as waste collection and transportation, intermediate waste treatment i.e. receiving the waste, its segregation and further suitable comprehensive treatment before putting into the use. The cost for C&D waste separation, storage, treatment, reuse/recycling should be included in the Estimated Cost by the Engineer-in-charge while according Technical sanction and preparing tender documents.
There are important duties to be either assigned or as a dutiful contractor, he may be establishing himself like, he should establish step-by-step demolition plan. Contractor may establish treatment facility at site only. He should report expected amount of wastes by type and treatment plan at the beginning of construction. There should be effective utilization of recycled aggregates and Safe treatment of hazardous waste like asbestos.
Contractor may be asked to submit Environmental Management Plan during Construction.

3.2 C&D waste information on web

All C&D waste information by contractor and by those involved in its treatment waste treatment companies are to be put on public domain in order to improve the rate of use of demolished concrete for e.g. application of recycled aggregates. Further to have a stronger data base of C&D waste, users reusing the C&D waste or recycled waste after treatment and processing can contribute a lot. This will help in substantial reduction on the amount of wastes and promotion of recycling or reusing the C&D waste.

3.3 Demolition Plan

It is required to adopt a systematic approach while demolishing a building in order to minimise the waste and its best use. A recommended approach can be to follow a sequence of segregation of household waste as first step followed

ISSN: 2319-8753

International Journal of Innovative Research in Science, Engineering and Technology

(An ISO 3297: 2007 Certified Organization)

Vol. 3, Issue 2, February 2014

by mechanical and electrical equipment, exterior and interior finishing materials, roof finishing and water-proofing materials, then structure as a last resort. Demolished C&D wastes need to be brought out of field immediately or temporarily stored in a designated area for the C&D wastes.

IV. C&D WASTE RECYCLING FACILITY IN NEW DELHI

At present, in India, the recycling of Construction and Demolition waste has started now only and we have to go a long way in this direction. In New Delhi, 1st pilot plant is functioning at Burari in North Delhi, but it requires many such plants to fulfil the needs in Delhi looking at the recycling potential of waste generated daily in New Delhi. About 5000 MT of recyclable waste is believed to be generated daily in New Delhi. Fig. 1 shows the one pilot plant set up IL&FS Environmental Infrastructure and Facilities Ltd. for North Delhi Municipal Corporation is functioning at Burari, Delhi.

Fig 1 C&D Waste Management Plant setup by IL&FS at Burari, Delhi

After the collection of Construction and Demolition waste, the material is routed through the Weighbridge to the processing site, wherein silt and loose soil is separated and used for land filling. Processed C&D waste is used for sub base of roads and for making bricks, paver blocks & kerb stones. The capacity of the plant is 500 T per day.

Fig 2 Containers and skips

Fig 3 Mobile crusher

ISSN: 2319-8753

International Journal of Innovative Research in Science, Engineering and Technology

(An ISO 3297: 2007 Certified Organization)

Vol. 3, Issue 2, February 2014

There are designated collection points where containers and skips (Fig. 2) are placed as a first storage point of C&D waste where the waste is brought in by private persons. As an additional measure, sufficient vehicles are also in operation to collect the waste from various locations of the city as per the services required from pick up points.
In 2012, 153000 T of C&D waste has been processed for making useful products. Out of this 11700 T of aggregates, 5632 T of Granular sub-base and 4289 T of sand has been produced. Further, 2000 cum of cast products and 6000 Cum of Ready Mix Concrete has been produced in this plant in 2012. Fig. 4 shows the Pavement Blocks and Kerb stones being produced at Burari Plant.

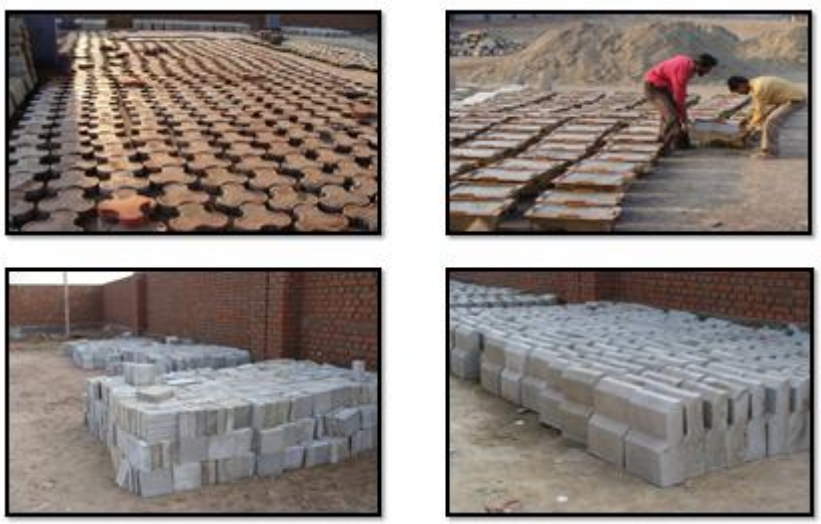

Fig 4 : C&D Products : Pavement Blocks and kerb stones

V. GLOBAL SCENARIO OF HANDLING C & D WASTE

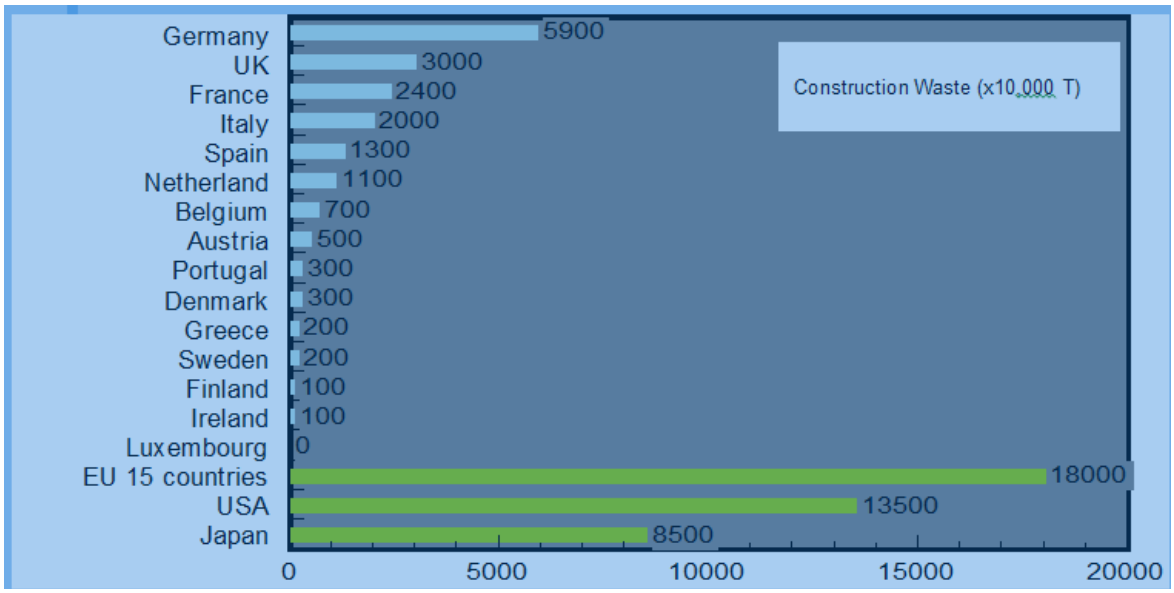

Fig. 5 Construction waste generated in different countries

ISSN: 2319-8753

International Journal of Innovative Research in Science, Engineering and Technology

(An ISO 3297: 2007 Certified Organization)

Vol. 3, Issue 2, February 2014

An assessment if constructed waste generated in different countries has been shown in Fig. 5. A brief study of processing of C& D waste in Korea and Japan has been covered in this section

5.1 C&D WASTE RECYCLING IN Korea

As per the objectives of the 1st National C&D Waste Management Plan (2007-2011) in Korea, it included C&D waste reduction by step-by-step demolition, C&D wastes generated in the field and those received by waste treatment companies to be registered in the national waste information management system (ALLBARO, www.allbaro.or.kr), an effective utilization of recycled aggregates and Safe treatment of hazardous waste (e.g. asbestos). As an achievement of the Plan, now, all C&D waste information by constructor and waste treatment companies are recorded on-line and the rate of use of demolished concrete (e.g. application of recycled aggregates) has drastically improved.

Further the Objectives of the 2nd National C&D Waste Management Plan (2012-2016), included improvement on the national waste information management, additional data input by the user of treated wastes, construction of life-cycle inventory data of C&D wastes and reduction on the amount of mixed wastes.

In 2009, total C&D waste generation was 67 million tons which was 51.2% of all wastes (131 million tons). C&D wastes are largely divided into 4 groups: (1) concrete, asphalt concrete, bricks, blocks, etc., (2) non-combustible wastes other than concrete and bricks, (3) combustible wastes and (4) mixed wastes.

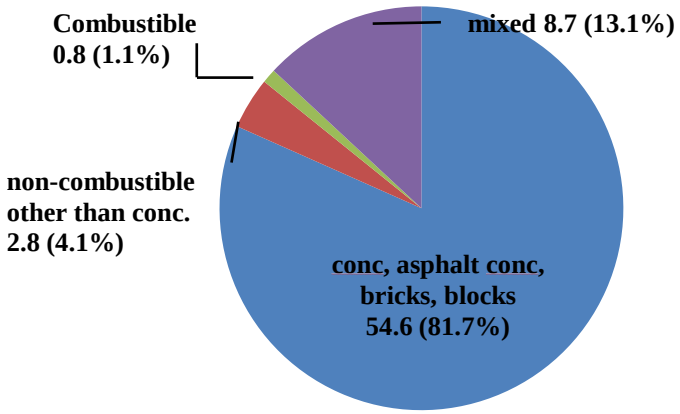

Fig. 6 Different components of C&D waste generation in Korea in 2009

In 2009, 42.1 million tons of demolished concrete was generated which is63% of all C&D wastes and effective recycling rate was 36% (definition of effective recycling: usage on road sub-base construction or equivalent, concrete blocks, and recycled aggregate for concrete). Concrete products such as concrete blocks were 6% and production of concrete as recycled aggregates was 1.5%.

Fig. 6 Recycled aggregates

ISSN: 2319-8753

International Journal of Innovative Research in Science, Engineering and Technology

(An ISO 3297: 2007 Certified Organization)

Vol. 3, Issue 2, February 2014

Method of application of recycled aggregates for concrete

Concrete having compressive strength of more than 21 MPa prepared with natural and partly RCA as coarse aggregates, but fineaggregates from natural source only were put into use as column, girders, slab, load bearing walls etc.. Where thecompressive strength was lesser than 21 MPa and fine aggregates also consistof partly RCA, its use was limited to concrete blocks, road base, filler material for concrete etc.

Impact crusher

Cone crusher **Roll crusher**

Fig. 7 Different types of crushers under operation

5.2 C&D WASTE RECYCLING IN JAPAN

As per the basic philosophy followed in Japan, viewpoint of environmental conservation must be added to price and quality, selection making is based on diverse viewpoints, including formation of socio-economic system withenvironmentally sound material cycle and combating global warming, consideration is given to reducing environmental impact throughout the product lifecycle, from manufacture to disposal and a commitment to long-term use, correct utilization, and sorted disposal of procured goods. Aggregate, 70% by volume of concrete, anticipated as a recipient of waste and by-products from other industries.

Fig. 8Advanced Technologies for Concrete Recycling Heated Scrubbing Method

ISSN: 2319-8753

International Journal of Innovative Research in Science, Engineering and Technology

(An ISO 3297: 2007 Certified Organization)

Vol. 3, Issue 2, February 2014

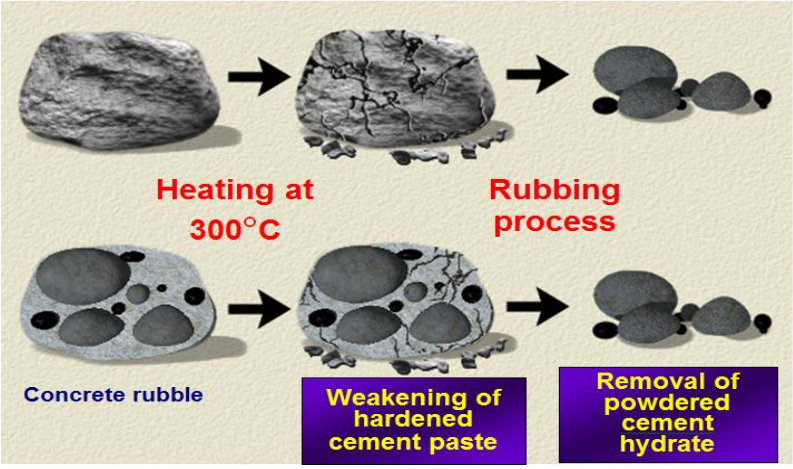

Fig. 9Mechanism of Heated Scrubbing

Japan Industrial Standards define three classes of concrete depending upon the properties of recycled Coarse and Fine aggregates

Class H : Having density of Coarse and Fine aggregates more than 2500 Kg/cum. Water absorption lesser than 3% for Coarse aggregates and lesser than 3.5 % for fine aggregates. Such products are put into use without any limitation for concrete strength upto 45 MPa

Class M : Having density of Coarse more than 2300 Kg/cum and of Fine aggregates more than 2200 Kg/cum. Water absorption lesser than 5% for Coarse aggregates and lesser than 7 % for fine aggregates. Such products are allowed to be used where members are not subjected to drying or freezing and thaw action like piles, underground beams and concrete filled in steel tubes.

Class L : Having Water absorption lesser than 7% for Coarse aggregates and lesser than 13 % for fine aggregates. Such products are used only as backfill concrete, blinding concrete and leveling concrete.

VI. CONCLUSION

Concrete has become a high tech material and its production is used by economists as a measure of a country's economic strength. Aggregates from natural sources are getting scarce over the years. The situation has forced us to explore aggregate from alternate sources. It is important to minimize C&D waste generation and maximize reuse/recycling as the construction industry is consumer of tremendous amount of natural resources.

In view of international developments and experiences, as well as shortage of aggregate from natural sources being experienced in many parts of the country, it is time that recycled aggregate are permitted for use in concrete constructions. The Municipal bye-laws are required to be reviewed and suitably modified. Establishment of effective strategies and enactment of laws and regulations are essential to achieve this. In addition, provisions of some incentives to users of the recycled products are necessary to promote the use.

Research & Development is to be promoted by Government.

There is lack of public awareness and it is required to spread the Information, Education and Communication in order to Garner Public Support and change the attitude of Public and Staff. Data and results should to be posted in Public Domain.

Material flow should be further optimised in cooperation with other industries as part of the resource recycling of society as a whole, reflecting back on the abundant resource consumption of concrete and the long service lives of buildings and civil structures.

ISSN: 2319-8753

International Journal of Innovative Research in Science, Engineering and Technology

(An ISO 3297: 2007 Certified Organization)

Vol. 3, Issue 2, February 2014

As a matter of Principle, recycling should be of high quality. Recycled products are not marketable unless they are of a quality that satisfies users. Recycling should be repeatable. If a recycled product has to be dumped in a landfill after use with no chance of recycling, then the recycling is no better than producing waste of the following generation.

REFERENCES

[1] Dhir, R. K., and Paine, K. A., "Value added sustainable use of recycled and secondary aggregates in concrete", Indian Concrete Journal, March 2010, pp. 7 – 26.

[2] IL&FS ECOSMART, "Construction & demolition (C&D) waste; Collection, transportation and disposal system", Project Report for MCD, Delhi Solid Waste Management Program, 38p.

[3] Noguchi, Takafumi, "Sustainable recycling of concrete structures", Indian Concrete Institute (ICI) Journal, April – June 2012, Vol. 13, No. 1, pp. 40 – 53.

[4] Mullick, A. K., "Green options for binder system and aggregate in sustainable concrete", Indian Concrete Journal, June 2012, pp. 9 – 17.

[5] Radonjanin, V., Malesev, M.,andMarinkovi, S. A., "Recycled concrete as aggregate for structural concrete production", The Masterbuilder, Chennai, May 2012, pp. 58 – 72.

[6] Choi, Dong-Uk, "Concrete and environment – a Korean perspective", Indian Concrete Institute (ICI) Journal, April – June 2012, Vol. 13, No. 1, pp.21 – 27.

[7] UdayModha, Preeti Dave, " Image Inpainting-Automatic Detection and Removal of Text From Images", International Journal of Engineering Research and Applications (IJERA), ISSN: 2248-9622 Vol. 2, Issue 2, 2012

[8] Muthukumar S, Dr.Krishnan .N, Pasupathi.P, Deepa. S, "Analysis of Image Inpainting Techniques with Exemplar, Poisson, Successive Elimination and 8 Pixel Neighborhood Methods", International Journal of Computer Applications (0975 – 8887), Volume 9, No.11, 2010.

Amine-Functionalized Poly(styrene) Microspheres as Thermoplastic Toughener for Epoxy Resin

S. Chaudhary,[1,2] P. Surekha,[1] D. Kumar,[2] C. Rajagopal,[1] P. K. Roy[1]
[1]*Centre for Fire, Explosive and Environment Safety, DRDO, Timarpur, Delhi 110054, India*

[2]*Department of Applied Chemistry and Polymer Technology, Delhi Technological University, Delhi 110042, India*

In this article, the potential of amine-functionalized poly(styrene) (PS) microspheres as toughening agent for epoxy resin has been explored. PS microspheres were prepared by suspension polymerization, where the monomer concentration and stirring speed was varied to control the microsphere dimensions (52–183 μm). The obtained microspheres were chemically functionalized with an aim to improve its dispersion within the epoxy matrix. The amine groups generated on the microsphere surface offer a potential site of covalent linkage with the epoxy matrix, thereby resulting in increased compatibility and improved properties. Epoxy composites containing varying amounts of microspheres (1–7% w/w) were prepared and their mechanical properties were evaluated under both quasi-static as well as dynamic conditions. The amination of poly(styrene) (APS) led to improved dispersion of the rigid microspheres in the epoxy matrix, which was evident from higher impact strength and fracture energies (G_{IC}) as compared to its neat analogs. The izod impact strength and G_{IC} increased by 33% and 150%, respectively, on introduction of 3% APS. This was accompanied with an increase in the tensile modulus and strength of the epoxy resin. Further increase in loading led to agglomeration of the microspheres, which in turn resulted in lowering of impact strength and toughness. Excellent agreement was found between the experimentally measured modulae and the predictions made on the basis of Halpin–Tsai and Lewis–Neilson models. Fracture surface morphology was studied to arrive at the principal toughening mechanisms behind the experimental findings. POLYM. COMPOS., 00:000–000, 2014. © 2014 Society of Plastics Engineers

INTRODUCTION

Physical blending and curing are fundamental tools, which can be employed to alter the structure–property relationship of polymeric materials. This technique has been used to improve the fracture properties of epoxies by shifting its mechanical response from "brittle" manner toward "ductile" mode. Most of the conventional epoxies are extremely vulnerable to impact-induced damage because of their inherently brittle nature, which limits their usage in more demanding applications. Physical toughening techniques include blending of epoxy–resin with elastomers [1–3], thermoplastics [4–6], rigid particulates [7–10], and nanomaterials [11]. In this context, the oldest approach being practiced involves blending with liquid reactive rubbers [12]; however, the resultant blends suffer from specific disadvantages including reduced elastic modulus, low glass transition temperatures and high water absorption. To address these issues, it has lately become more common to use thermoplastics as toughening agents [13–15]. However, these thermoplastic modifiers are rather difficult to process [16], and many a times require the use of solvents [17], which warrant a separate removal step, as the presence of even residual amounts can adversely affect the final properties of the blends.

It is to be noted that irrespective of the type of polymer used for epoxy toughening, it is the thermodynamically (location of the phase diagram) and kinetically controlled process (competition between phase separation and polymerization kinetics), which governs the morphology of the resultant blend, thereby determining its final properties and applications [18]. The curing phenomenon, in the presence of another polymer results in the formation of phase separated blends, a phenomenon more commonly known as "polymerization-induced phase separation" (PIPS). It becomes increasingly difficult to control this process in fast curing compositions, leading to minimal improvement in the properties. In view of the above, developing ways and means of controlling the morphology has attracted the attention of

Correspondence to: P. K. Roy; e-mail: pk_roy2000@yahoo.com; pkroy@cfees.drdo.in
Additional Supporting Information may be found in the online version of this article.
DOI 10.1002/pc.22927
Published online in Wiley Online Library (wileyonlinelibrary.com).

researchers worldwide [16, 19, 20]. An alternative route toward achieving increased toughness of epoxy is the inclusion of small quantities of preformed materials within the matrix [12, 21–23]. Here, the process of phase separation during curing is no longer dependent on the aforementioned factors, which permits proper control over the blend morphology, thereby leading to larger improvements at much lower loadings [24]. Although, this technique is widely used during the preparation of rubber-toughened compositions, the use of preformed thermoplastics as toughening agents is less common and definitely deserves more attention [25].

The key aim of this work was to develop preformed thermoplastic microspheres for use as effective toughening agent for brittle thermosets and to determine the fracture properties of the developed composites. In addition to toughening, epoxy-poly(styrene) blends have been reported to exhibit higher hygrothermal stability [26, 27]. However, due to the incompatible nature of preformed poly(styrene) (PS) microspheres and epoxy matrix, proper dispersion is an issue, which can be resolved by introducing reactive groups on the surface of the dispersed phase. We hypothesize that the functionalization of PS microspheres with amine groups would result in increased compatibility, stronger interfacial adhesion [4] and improved dispersion of the same within the epoxy matrix, which in turn would result in improved mechanical properties. In this article, we explore the potential of polystyrene microspheres as effective thermoplastic toughening agents for epoxy. Microspheres were prepared by suspension polymerization route and to aid their dispersion within the epoxy matrix, the surface of the microspheres were functionalized to generate pendant amino groups capable of forming covalent bonds with the epoxy resin.

EXPERIMENTAL

Materials

Epoxy resin (Ciba Geigy, Araldite CY 230; epoxy equivalent 200 equiv g^{-1}, Basel, Switzerland) and hardener (HY 951; amine content 32 equiv kg^{-1}, Basel, Switzerland) was used as received. Styrene (AR, E. Merck, Dermstadt, Germany) was washed with 10% aqueous sodium hydroxide to remove inhibitor, followed by washing with water till neutral. It was dried over anhydrous sodium sulfate and was further purified by vacuum distillation at 60°C. Poly(vinyl alcohol) (PVA; molecular weight 14,000, Central Dug House, Mumbai, India) and benzoyl peroxide (AR, Central Dug House, Mumbai, India) were used without any further purification. Double distilled water was used throughout the course of study.

Preparation of Amino-Poly(styrene) Microspheres

PS microspheres were prepared by suspension polymerization process in the presence of a suspending agent as per the procedure reported in the literature [28]. For this purpose, a feed solution of styrene in chloroform (30–60% v/v) and benzoyl peroxide (0.05% v/v styrene) was introduced into a reaction vessel containing aqueous solution of PVA (1.5% w/v) where the polymerization reaction was allowed to continue at 80 ± 2°C under inert atmosphere for 8 h under varying stirring speeds (500–700 rpm), after which the reaction mixture was cooled and filtered. The extent of conversion was measured gravimetrically as the ratio of mass of microspheres obtained to the amount of monomer used for its preparation.

About 5 g of PS microspheres were nitrated with 5:2 v/v mixture of sulfuric acid and nitric acid at 60°C on a controlled water bath for 1 h. The resulting nitro-PS microspheres (NPS) were washed repeatedly with distilled water till free from acid and dried in vacuum at 70°C for 24 h. It was reduced to amino-poly(styrene) (APS) with a mixture of tin(II) chloride (40 g), concentrated hydrochloric acid (45 ml) in 50 ml ethanol for 12 h at 90°C under nitrogen atmosphere [28]. The product was filtered, washed first with distilled water, and then with 2 M NaOH to recover the free amino polymer.

Preparation of Epoxy Composites

Microspheres were sieved through a 100–200 mesh to obtain a particle size range of 75–150 μm which was added to the epoxy prepolymer in requisite amounts (1–7% w/w) followed by ultrasonication of the resulting mixture for 30 min at 33 kHz. Requisite amount of triethylene tetra-amine hardener was added to the mixture (13 phr) to achieve an amine: epoxide stoichiometry of 1:1 and ultrasonicated for another 15 min to remove any entrapped air bubbles. The suspension was transferred to greased silicone molds, where the curing reaction was allowed to proceed for 24 h at 30°C. Neat epoxy specimens were also prepared in a similar manner and the details of all the compositions prepared are listed in Supporting Information Table S1. The samples have been designated as EP followed by its concentration and by the type of microsphere used for its preparation, i.e., "PS" denotes poly(styrene) microsphere and 'APS' denotes poly(styrene) beads functionalized with amino groups.

Characterization

The effect of stirring speed on the microsphere dimensions was determined by a particle size analyzer (DIPA 2000, Donner Technologies, Netherland). FTIR spectra of samples were recorded in the wavelength range 4000–600 cm^{-1} using a Thermo Fisher FTIR (NICOLET 8700, Madison) analyzer with an attenuated total reflectance crystal accessory. The thermal behavior was investigated using Perkin Elmer Diamond STG-DTA (Diamond SDTA, Shelton, CT), under N_2 atmosphere in the temperature range 50–800°C. A heating rate of 10°C min^{-1} and sample mass of 5.0 ± 0.5 mg was used for each experiment. The surface area of the microsphere was determined by N_2 adsorption on a Micromeritics (ASAP 2010, Novcross, Georgia) surface area analyzer. For

 DOI 10.1002/pc

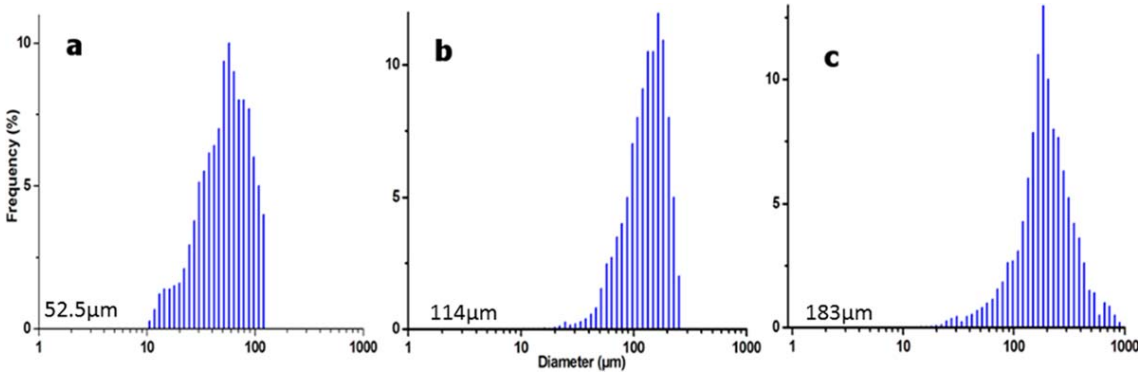

FIG. 1. Effect of increasing stirring speed (rpm) on particle size distribution (Feed concentration: 60% w/v). (a) 500, (b) 600 and (c) 700. [Color figure can be viewed in the online issue, which is available at wileyonlinelibrary.com.]

this purpose, the sample was initially outgassed under vacuum (10^{-6} Torr) at 90°C for 24 h and the nitrogen adsorbate was pulsed at 77 K. Surface area was calculated from the linear part of the BET plot. The C, H, and O content were determined by an elemental analyzer (Elementar, Vario EL, Germany). The amino content in the APS was determined by acetylation method as per the procedure reported previously [29].

The glass transition temperature (T_g) of the epoxy-based samples, as determined from the peak value of damping tan δ, was measured by dynamic-mechanical analyzer (DMA8000, Perkin Elmer,Walthan) on standard test specimens (40 × 10 × 5 mm^3). A double cantilever mode was employed and the sample was subjected to a heating rate of 3°C min^{-1} from 20 to 200°C at a frequency of 1 Hz. The quasi-static mechanical properties were determined as per ASTM method D638 using a Universal Testing System (International Equipments, Mumbai, India) at ambient temperature. The dog-bone shaped specimens used for tensile testing were 165 mm long, 3 mm thick, and 13 mm wide along the center of the casting for epoxy resin. The samples were subjected to a cross head speed of 50 mm min^{-1}. The notched Izod impact strength of the specimens was determined as per ASTM D256 using an impact strength testing machine (International Equipments, Mumbai, India). Notched flexural testing of the samples was performed under three-point single-edge notch bending mode using the same instrument. For this purpose, specimens with requisite dimensions (127 mm length × 12.5 mm width × 3.5 mm thickness and 3 mm notch) were prepared and the samples were subjected to a deformation rate of 2 mm min^{-1} while maintaining a span length of 60 mm. The mode I critical stress intensity factor (K_{IC}) of the samples was determined as per the following equation [30]:

$$K_{Ic} = \frac{3 \times P \times L \times a^{1/2}}{2 \times B \times w^2} Y\left(\frac{a}{w}\right) \quad (1)$$

where P, L, and B refer to the load at break, span length, and sample thickness, respectively. The geometry factor, $Y\left(\frac{a}{w}\right)$ is calculated as per the formula below, where a is the notch length, and w is the sample width.

$$Y\left(\frac{a}{w}\right) = 1.93 - 3.07 \times \left(\frac{a}{w}\right) + 14.53 \times \left(\frac{a}{w}\right)^2 - 25.11 \times \left(\frac{a}{w}\right)^3 + 25.8 \times \left(\frac{a}{w}\right)^4 \quad (2)$$

The K_{IC} was used to estimate the fracture energy (G_{IC}), which was calculated using the following equation:

$$G_{IC} = \frac{K_{IC}^2 (1 - v^2)}{E} \quad (3)$$

where E is the flexural modulus of the polymer, and v is the Poisson's ratio of epoxy (0.35) [31]. For each composition, at least five identical specimens were tested and the average results along with the standard deviation have been reported.

The surface morphology of samples was studied using a scanning electron microscope (Zeiss EVO MA15, Oberkochen, Germany) under an acceleration voltage of 20 kV. Samples were mounted on aluminum stubs and sputter-coated with gold and palladium (10 nm) using a sputter coater (Quorum- SC7620, Oberkochen, Germany) operating at 10–12 mA for 120 s.

RESULTS AND DISCUSSION

Suspension Polymerization of Styrene

PS microspheres were prepared by suspension polymerization process as per the procedure reported in the literature [32]. The effect of increasing stirring speed on the particle size distribution and mean particle diameter is presented in Fig. 1. As expected, with increase in the stirring speed, the particle size distribution shifts toward lower size, which could be attributed to the shearing of the large oily droplets into smaller microspheres, under the experimental conditions employed.

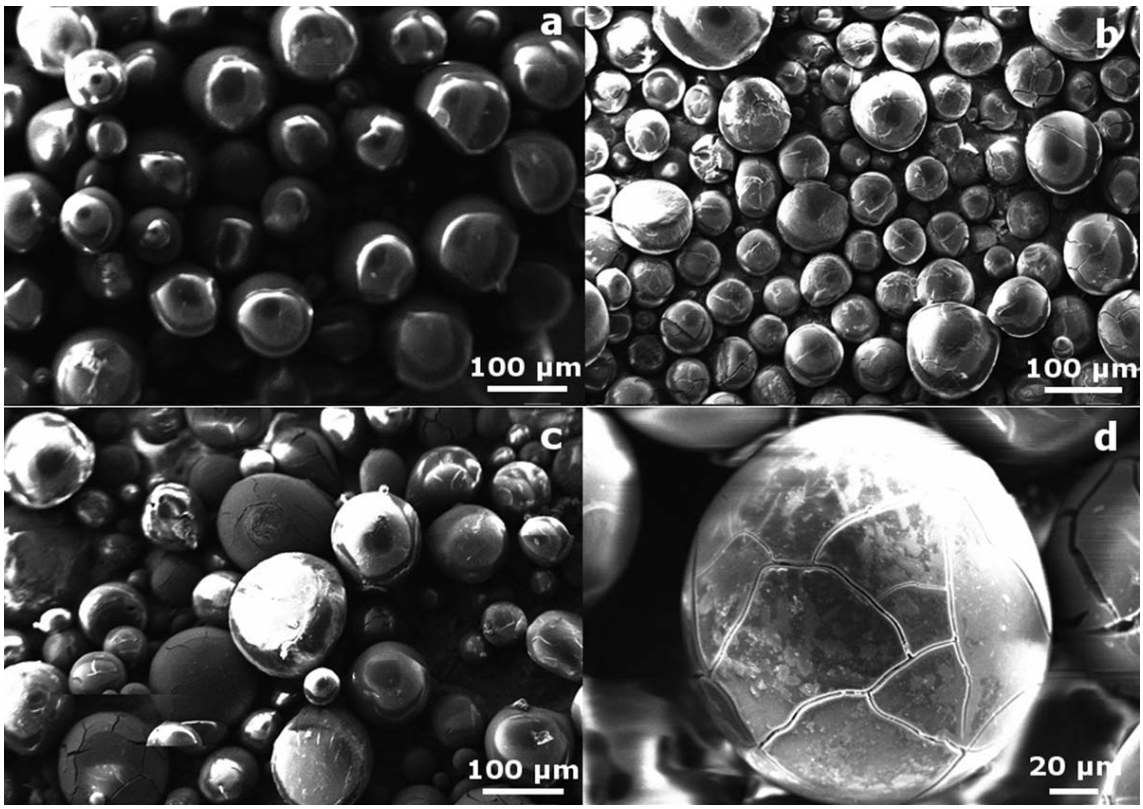

FIG. 2. Effect of functionalization on the morphology of poly(styrene) microspheres: (a) poly(styrene), (b) nitro-poly(styrene), (c) amino-poly(styrene) (100×), and (d) amino poly(styrene) (200×) revealing the presence of cracks.

Effect of Functionalization on Surface Morphology of Microspheres

PS microspheres were functionalized by nitration followed by reduction to improve their compatibility with the thermosetting epoxy matrix. The effect of nitration and amination on the morphology of PS microspheres is presented in Fig. 2. As is apparent, the surface of poly (styrene) is rather smooth and the morphology is affected appreciably due to nitration, which leads to formation of cracks on the surface. However, the presence of these surface aberrations did not lead to any substantial increase in the surface area (8.7 $m^2\ g^{-1}$ for neat poly(styrene) and 10.3 $m^2\ g^{-1}$ for APS).

The nitrogen content in NPS and APS was found to be 10.3 and 11.6%, respectively. Determination of amine content by acetylation technique revealed that ~8.1% of the total nitrogen exists as free amino groups in APS, indicating that the remaining ~3.5% exist as unconverted nitro groups. The effect of functionalization on the FTIR spectra is presented in Fig. 3. The absorption band appearing at 3107 and 2930 cm^{-1} can be attributed to the aromatic and aliphatic C-H stretching vibrations, respectively. Additional absorption bands at 1514 and 1341 cm^{-1} in the nitro derivative (NPS) appears due to the asymmetric and symmetric N=O stretching, respectively. In the amino derivative (APS), absorption due to asymmetrical N-H stretch was observed at 3357 cm^{-1} [33]. The C-N stretching vibration for aromatic amines (1335–1250 cm^{-1}) overlaps with the symmetric N=O stretching at ~1341 cm^{-1}, and the absorption band due to N-H bending vibration (1500–1640 cm^{-1}) overlaps with the asymmetric N=O stretching appearing at 1514 cm^{-1} [34].

The TG and DTG traces of poly(styrene) and its derivatives are presented in Fig. 4. Neat poly(styrene) exhibits a single step degradation, with a mass loss of ~98% at 500°C whereas 63% of weight loss was observed for nitro-poly(styrene). A small hump at lower temperature ($\sim T_{peak} = 327$°C) is perceptible in the DTG trace of functionalized poly(styrene), which is indicative of the cleavage of the labile C-N and N-O bonds. The char yield (at 500°C) of nitro and amino derivative was 36.6 and 38.4%, respectively. The pyrolytic degradation of poly (styrene) reportedly occurs via unzipping reaction [35], and our studies indicate that the presence of functional groups interfere with the unzipping of the main chain, which is accepted as the mechanism for pyrolytic degradation of poly(styrene) [35].

Epoxy-Microsphere Composites

Epoxy composites were prepared by dispersing requisite amounts of either PS or APS microspheres in the epoxy resin by ultrasonication followed by curing.

 DOI 10.1002/pc

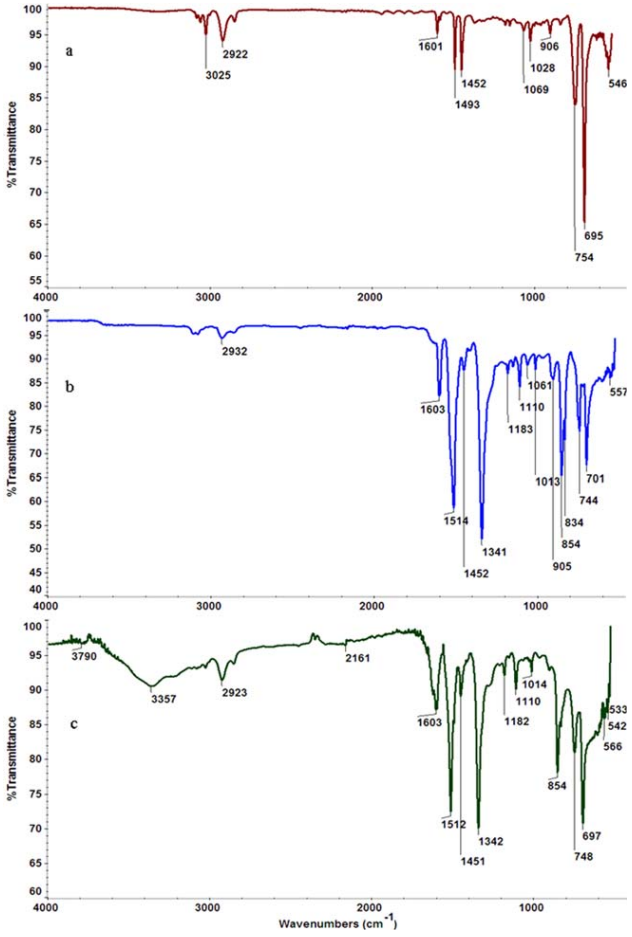

FIG. 3. FTIR spectra of (a) poly(styrene), (b) nitropoly(styrene), and (c) amino poly(styrene). [Color figure can be viewed in the online issue, which is available at wileyonlinelibrary.com.]

Detailed structural and thermal characterization of unmodified epoxy and the composites is presented in Supporting Information Figs. S1 and S2. The introduction

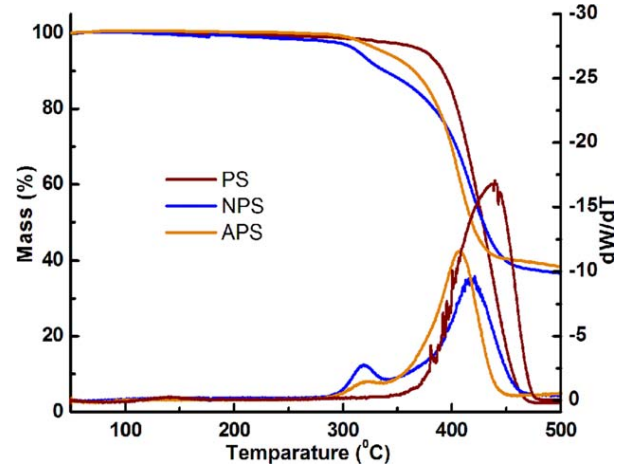

FIG. 4. Effect of functionalization on the TG and DTG traces. [Color figure can be viewed in the online issue, which is available at wileyonlinelibrary.com.]

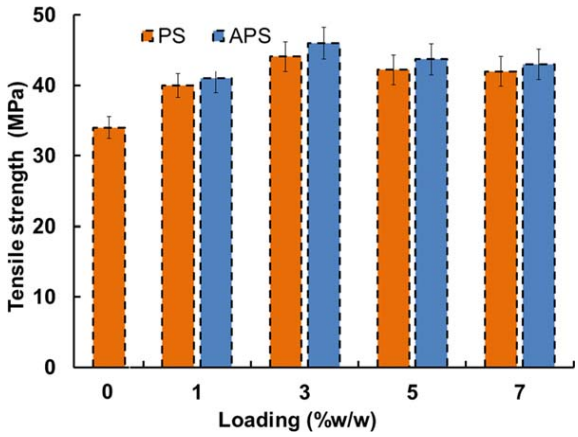

FIG. 5. Increase in tensile strength of epoxy due to introduction of poly(styrene) and its amino derivative. [Color figure can be viewed in the online issue, which is available at wileyonlinelibrary.com.]

of poly(styrene) in the studied concentration range did not affect the thermal decomposition behavior of the epoxy matrix and all the compositions can be used in service till 250°C, irrespective of the type of filler employed. Figure 5 presents the variation in mechanical properties of the epoxy composites due to introduction of neat poly(styrene) as well as its amino derivative. As expected, the introduction of PS microspheres led to an increase in the tensile strength and modulus, the extent of which was found to be proportional to the amount of loading. The values of the experimentally obtained modulae were compared with the predictions of two common theoretical models, namely "Halpin–Tsai" and "Lewis–Nielsen" [36, 37].

According to the Halpin–Tsai model [34], the modulus of the epoxy composite is computed as per the following equation:

$$E = \frac{1+\zeta\eta V_f}{1-\eta V_f} E_m \tag{4}$$

where ζ is the shape factor, V_f is the volume fraction of the microsphere, and

$$\eta = \frac{\left(\frac{E_f}{E_m}-1\right)}{\left(\frac{E_f}{E_m}+\zeta\right)} \tag{5}$$

The shape factor in the Halpin–Tsai model is a function of the aspect ratio of the filler particles, which is usually calculated as $\zeta = 2w/t$, where w and t are the length and thickness of the reinforcement, respectively [38]. In view of the spherical nature of the microspheres used in the present work, a shape factor of $\zeta = 2$ was used for the prediction of the modulus. The modulae of poly(styrene) (E_f) has been assumed to be 3000 MPa, based on previous studies [39].

The basic Lewis–Nielsen model [40], takes into account the effect of the adhesion between the polymer

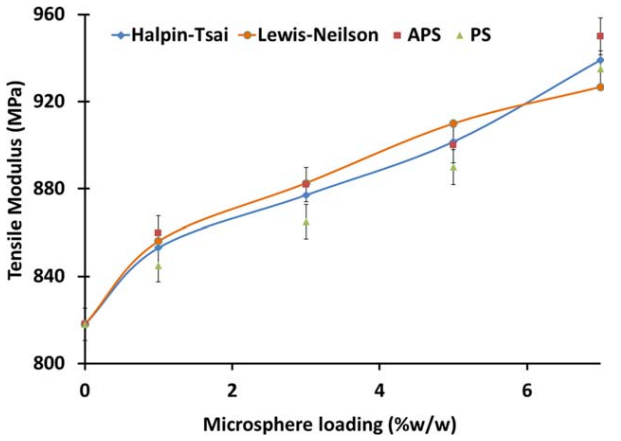

FIG. 6. Comparison of experimental modulae with Halpin–Tsai and Lewis–Nielsen predictions. [Color figure can be viewed in the online issue, which is available at wileyonlinelibrary.com.]

and the fillers by employing the following equation to predict the modulus of the composite:

$$E = \frac{1+(k_E-1)\beta V_f}{(1-\beta\mu V_f)} E_m \tag{6}$$

where k_E is the generalized Einstein coefficient. The constant β depends on the ratio of E_f and E_m and is given by:

$$\beta = \frac{(\frac{E_f}{E_m}-1)}{(\frac{E_f}{E_m}+(k_E-1))} \tag{7}$$

The constant μ being dependent on the maximum volume fraction of the filler (V_{max}) by:

$$\mu = 1+\frac{(1-V_f)}{(V_{max})}[V_{max}V_f+(1-V_{max})(1-V_f)] \tag{8}$$

The values of V_{max} for a range of particle shapes and types of packing have been tabulated by Nielsen and Landel [41]. The morphological studies indicated that all the microspheres were randomly dispersed; therefore, a figure of 0.632 for V_{max} was employed for the present studies, which is representative of random close-packed and nonagglomerated spheres [41]. The value of the generalized Einstein coefficient, k_E, reportedly varies with the Poisson's ratio of the polymeric matrix and the degree of the adhesion of the polymer to the particles. Since the present investigation deals with epoxy resin ($v = 0.35$), where no slippage at the interface between the polymeric matrix and the particles was evidenced from the morphological investigations, a value of $k_E = 2.167$ was used [31, 41].

The experimentally observed values were compared with the predictions based on the aforementioned models, the results of which are presented in Fig. 6. Substantial agreement is evident, with the modulus of composites containing APS microspheres being higher. However, for both the cases, the experimental data were found to generally lie close to the Halpin–Tsai and Lewis–Nielsen predictions.

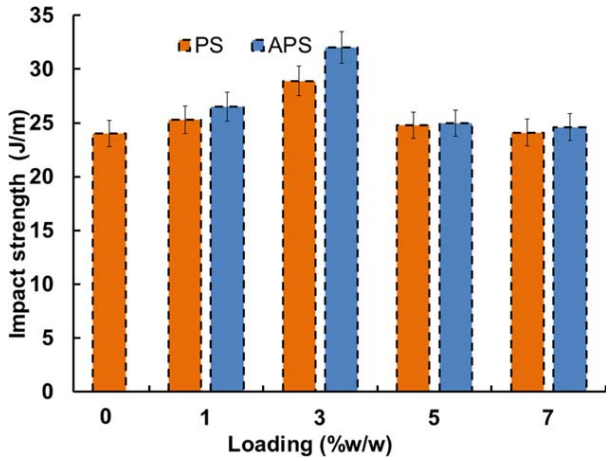

FIG. 7. Effect of functionalization on the impact strength of poly(styrene)–epoxy composites. [Color figure can be viewed in the online issue, which is available at wileyonlinelibrary.com.]

Interestingly, the introduction of PS and APS led to a remarkable improvement in the impact strength of epoxy, as is evident from data presented in Fig. 7. The impact strength increased from 24 J m^{-1} (unmodified epoxy) to 32 J m^{-1} on addition of 3% w/w APS (~33% increase). In comparison, the improvement in impact strength was less pronounced (~20% increase) when neat poly(styrene) was employed as a filler. This can be attributed to the increased compatibility resulting from the covalent interaction between the epoxy groups with the amine functionality of APS. The resultant morphology is more capable in bearing dynamic loads as compared to the inhomogeneous structure resulting from solution blending.

The flexural stress–strain response of the compositions prepared is presented in Fig. 8. As expected, the composites exhibited higher strength and lower flexural strain in comparison to the unmodified epoxy, which can be

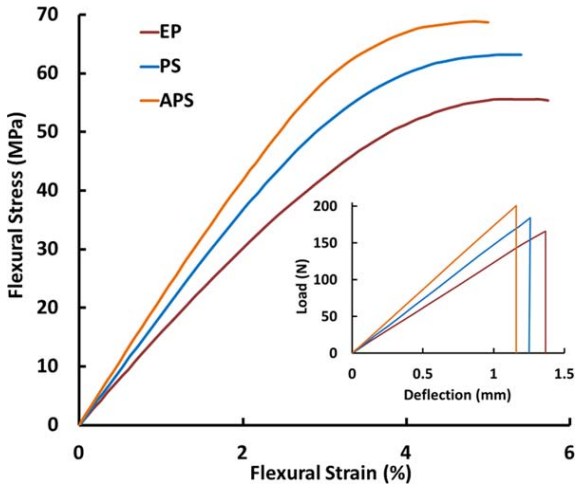

FIG. 8. Flexural stress–strain response of representative compositions. Inset shows the effect of notch on the load-deflection curve. [Color figure can be viewed in the online issue, which is available at wileyonlinelibrary.com.]

DOI 10.1002/pc

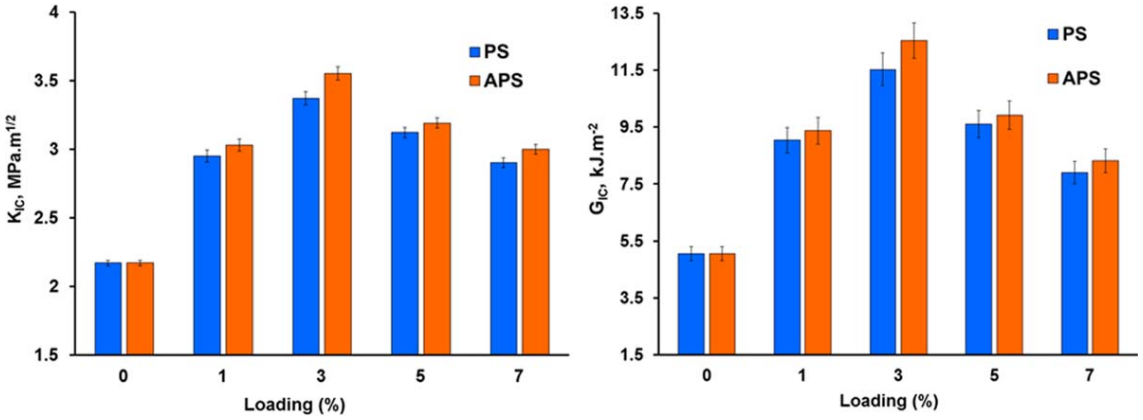

FIG. 9. Effect of introduction of polystyrene and amino poly(styrene) on the fracture toughness and fracture energy. [Color figure can be viewed in the online issue, which is available at wileyonlinelibrary.com.]

attributed to the higher modulus and low extensibility of the added fillers. The mechanical response of notched samples is also presented in Fig. 8 (Inset), which clearly reveal the detrimental effect of notch on the flexural strength, which in turn can be attributed to stress concentration due to lower cross-sectional area.

A comparison of critical stress intensity factor (K_{IC}) and fracture energy (G_{IC}) as a function of microsphere loading is presented in Fig. 9. It can be seen that the K_{IC} of epoxy increased due to introduction of microspheres, from an initial value of 2.17 MPa m$^{1/2}$ for the unmodified epoxy to 3.5 MPa m$^{1/2}$ for composites containing 3% w/w of the APS microspheres, which corresponds to an increase of ~30%. The K_{IC} value was used to calculate the fracture energy of the samples, which was found to increase substantially on introduction of the second phase. The mean fracture energy increased from 5.05 kJ m^{-2} for unmodified epoxy polymer, to 12.53 kJ m^{-2} for EP3APS (~70% increase).

Representative plots, exhibiting the variation of storage modulus and tan δ as a function of temperature for neat epoxy and its composites with microspheres (3% w/w) is presented in Fig. 10. The glass transition temperatures (T_g) and the storage modulus (G') of the unmodified cured epoxy resin was 66°C and 2.73 GPa at 20°C, respectively. The introduction of PS microspheres was found to have no effect on T_g of the base polymer, and the damping (tan δ) traces overlap. The second peak at 110°C corresponds to the T_g of amorphous PS chain, which suggests that both the polymers are completely phase-separated without any evidence of plasticizing action.

Toughening Mechanisms

The morphology of the cracked surface of impact tested samples was studied by SEM, the results of which are presented in Fig. 11a–h. The smooth and featureless surface of epoxy is characteristic of fracture in a brittle thermosetting polymer, which exhibits no signs of plastic deformation [42, 43]. In comparison, the fractured surface of the composites was found to be rather rough, with the extent of roughness being higher in compositions containing APS. Although, the dispersion of microspheres was uniform at lower loadings (≤3%), increasing the loading led to agglomeration of the microspheres, as is evident from the SEM image of EP7PS and EP7APS.

Several interesting features were observed during the fractographic analysis, on the basis of which the underlying toughening mechanisms were identified (Fig. 12). One of the most commonly cited mechanism toward toughening by thermoplastics is "crack pinning," according to which, the role of rigid thermoplastic particles is to act as impenetrable objects that cause the crack front to bow out, a process requiring larger amount of energy. Indirect evidence of the occurrence of this mechanism is the presence of "tails" associated with the PS microspheres in EP3PS (Fig. 12a). In certain cases, the crack front is forced to change its path as it approaches the rigid phase, a phenomenon more commonly known as

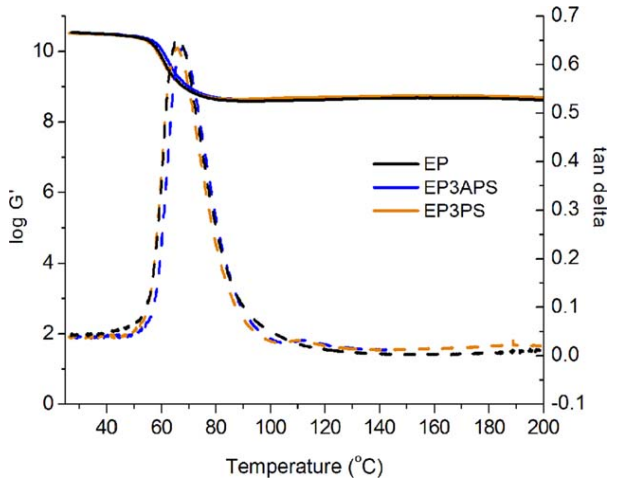

FIG. 10. Storage modulus and damping tan δ traces for representative epoxy composites. [Color figure can be viewed in the online issue, which is available at wileyonlinelibrary.com.]

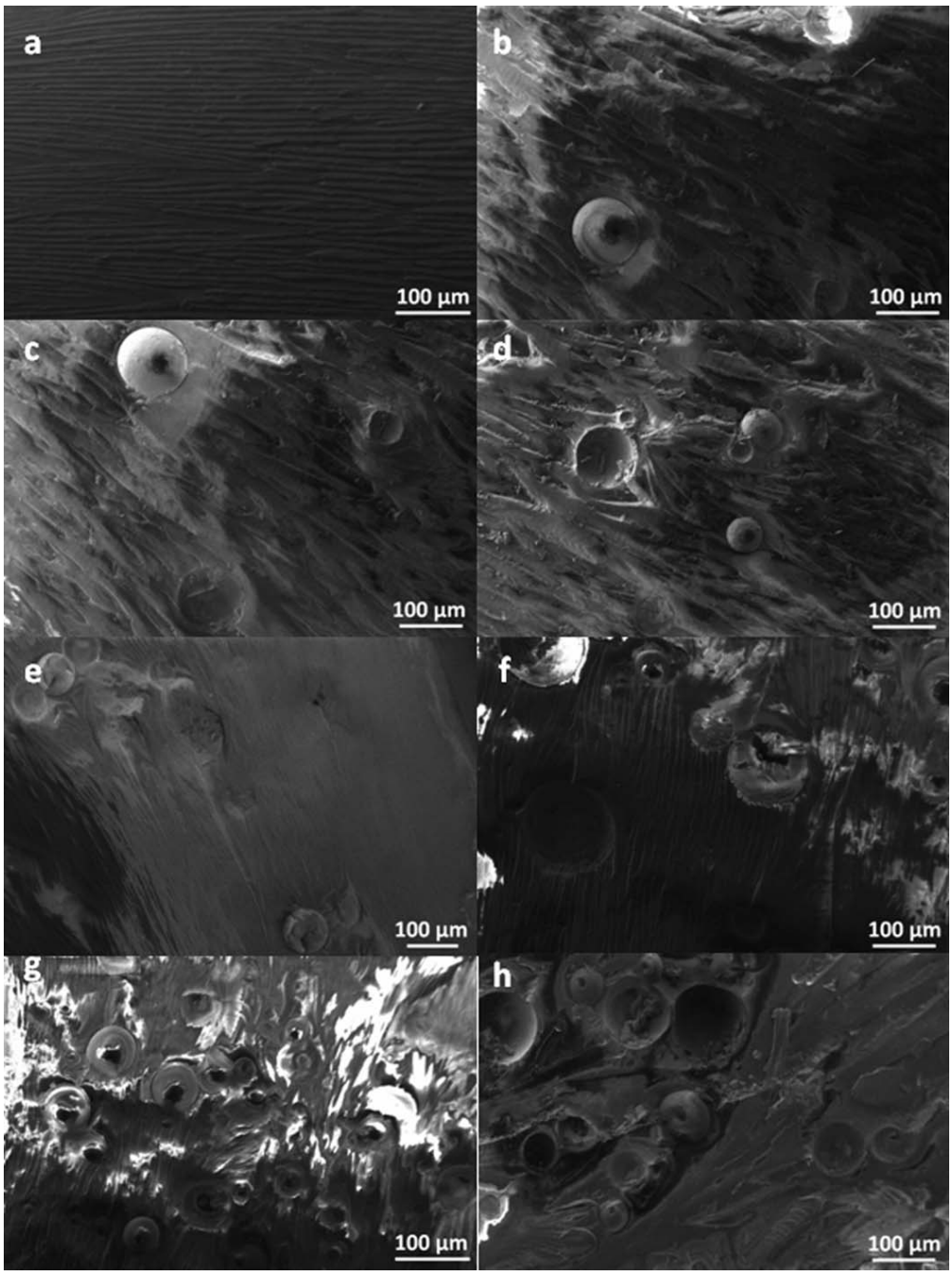

FIG. 11. SEM image of fracture surfaces (a) neat epoxy, (b) EP1APS, (c) EP3PS, (d) EP3APS, (e) EP5PS, (f) EP5APS, (g) EP7PS, and (h) EP7APS.

crack bowing, which can be seen in EP3APS (Fig. 12b). This result in increased surface area and reduction in the mode I character of the crack opening, which in turn requires larger amount of energy for its propagation. In addition, evidence of "Microcracking" in EP3APS (Fig. 12c) and "Crack path deflection" in EP5APS (Fig. 12d) could also be found during fractography [4].

Another commonly cited mechanism to explain the higher values of toughness in the blends is "Particle bridging" as can be seen in EP3APS (Fig. 12e). In this case, the rigid particles tend to span the fracture surfaces formed as a result of crack propagation, thereby forming tractions, which in turn reduces the local stress at the propagating crack tip. Substantial energy is expected to be consumed during the plastic deformation and subsequent fracture of the rigid PS microspheres (Fig. 12f) as can be seen in the fracture surface of EP5PS. It is to be noted that increase in particle dimensions, stiffness, and tearing energy, each would

 DOI 10.1002/pc

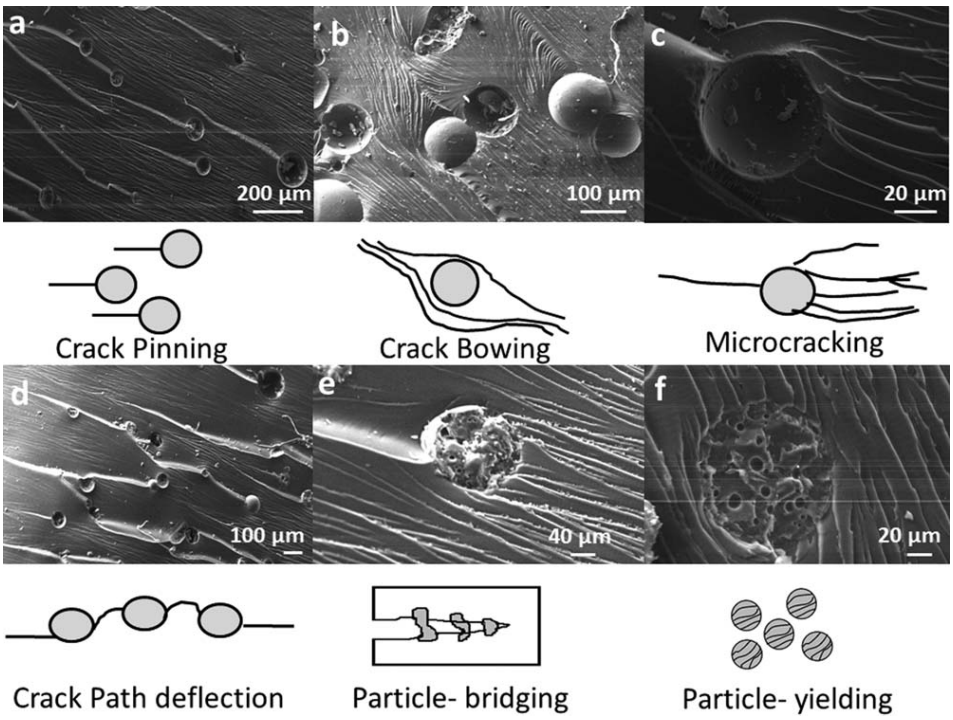

FIG. 12. Pictorial schematic of the underlying toughening mechanisms along with SEM images of fracture surface revealing (a) crack pinning, (b) crack bowing, (c) microcracking, (d) crack path deflection, (e) particle bridging, and (f) particle yielding.

individually contribute positively toward the toughness of the composite. It is essential to mention here that in view of the reduced stiffness of elastomeric modifiers, the contribution of crack bridging is almost negligible in rubber-modified epoxies. However, in the present work, a number of "broken" microspheres were observed on the fracture surface, which clearly point out the significant contribution of this route in rigid microsphere modified epoxy toughening.

It is to be noted that quantification of each route toward the overall toughening of the composite is almost impossible, but nonetheless the SEM studies clearly provide evidence for the same. It is well understood that one of the most important criteria which needs to be met by the fillers in order to exhibit their full potential as impact modifiers is their random dispersion within the matrix as a well-separated phase. The importance of interfacial adhesion between the two phases toward improvement of the mechanical properties has been emphasized previously [4]. Our studies indicate that the presence of amine functionalities in the APS leads to its better dispersion within the matrix, and the phenomenon of particle-matrix debonding is responsible for absorbing significant amount of energy during the fracture process, which in turn leads to improved mechanical behavior.

CONCLUSIONS

APS microspheres were prepared for use as impact modifier for thermosetting epoxy resin. PS microspheres were first prepared by suspension polymerization process and the effect of operating parameters like stirring speed and feed concentration on the particle size distribution of the resultant microspheres was quantified. The microspheres were subsequently functionalized to yield aminated derivatives, to improve their compatibility with the epoxy thermoset in the subsequent step of composite preparation. Both unmodified as well as aminated PS microspheres were dispersed in epoxy matrix to prepare toughened composites (1–7% w/w) and the effect of their addition on both quasi static and dynamic mechanical properties was studied. The presence of amino groups on the surface seems to play an important role in dispersion of the microspheres, as evident from the improved mechanical properties in APS-loaded compositions. Impact strength and fracture energy increased by 33% and 150%, respectively, on addition of 3% w/w APS. The increase in the experimentally observed tensile modulus was compared with two analytical models which revealed excellent agreement. Morphological investigation of the fracture surface was performed to gain insight into the underlying mechanisms. Evidence of particle yielding, crack pinning, particle bridging, crack bowing, microcracking, crack path deflection was observed during morphological investigations.

REFERENCES

1. R. Bagheri and R. A. Pearson, *Polymer*, **37**, 4529 (1996).
2. R. Bagheri and R. A. Pearson, *Polymer*, **41**, 269 (2000).

3. Y. L. Liang and R. A. Pearson, *Polymer*, **51**, 4880 (2010).
4. R. A. Pearson and A. F. Yee, *Polymer*, **34**, 3658 (1993).
5. J. Choi, S. Lim, J. Kim, and C.-R. Choe, *Polymer*, **38**, 4401 (1997).
6. G. Cicala, A. Mamo, G. Recca, and C. L. Restuccia, *Polym. Eng. Sci.*, **47**, 2027 (2007).
7. P. K. Roy, A. V. Ullas, S. Chaudhary, V. Mangla, P. Sharma, D. Kumar, and C. Rajagopal, *Iran. Polym. J.*, **22**, 709 (2013).
8. L.-C. Tang, H. Zhang, S. Sprenger, L. Ye, and Z. Zhang, *Compos. Sci. Technol.*, **72**, 558 (2012).
9. H. Zhang, L.-C. Tang, Z. Zhang, K. Friedrich, and S. Sprenger, *Polymer*, **49**, 3816 (2008).
10. S. C. Zunjarrao and R. P. Singh, *Compos. Sci. Technol.*, **66**, 2296 (2006).
11. B. Wetzel, P. Rosso, F. Haupert, and K. Friedrich, *Eng. Fract. Mech.*, **73**, 2375 (2006).
12. D. Ratna and A. Banthia, *Macromol. Res.*, **12**, 11 (2004).
13. J. H. Hodgkin, G. P. Simon, and R. J. Varley, *Polym. Adv. Technol.*, **9**, 3 (1998).
14. A. Asif, V. L. Rao, and K. N. Ninan, *Polym. Adv. Technol.*, **22**, 437 (2011).
15. B. B. Johnsen, A. J. Kinloch, and A. C. Taylor, *Polymer*, **46**, 7352 (2005).
16. I. A. Zucchi, M. J. Galante, and R. J. J. Williams, *Polymer*, **46**, 2603 (2005).
17. M. Rico, J. López, B. Montero, and R. Bellas, *Eur. Polym. J.*, **48**, 1660 (2012).
18. C. E. Hoppe, M. J. Galante, P. A. Oyanguren, R. J. J. Williams, E. Girard-Reydet, and J. P. Pascault, *Polym. Eng. Sci.*, **42**, 2361 (2002).
19. A. R. Bhattacharyya, A. K. Ghosh, A. Misra, and K. J. Eichhorn, *Polymer*, **46**, 1661 (2005).
20. J. W. Barlow and D. R. Paul, *Polym. Eng. Sci.*, **24**, 525 (1984).
21. B. S. Hayes and J. C. Seferis, *Polym. Compos.*, **22**, 451 (2001).
22. G. Levita, A. Marchetti, and A. Lazzeri, *Makromol. Chem. Macromol. Symp.*, **41**, 179 (1991).
23. P. Roy, N. Iqbal, D. Kumar, and C. Rajagopal, *J. Polym. Res.*, **21**, 1 (2014).
24. R. A. Pearson and A. F. Yee, *J. Mater. Sci.*, **26**, 3828 (1991).
25. H. Kishi, K. Uesawa, S. Matsuda, and A. Murakami, *J. Adhes. Sci. Technol.*, **19**, 1277 (2005).
26. A. Salazar, S. G. Prolongo, and J. Rodríguez, *Mater. Lett.*, **64**, 167 (2010).
27. A. Salazar, S. G. Prolongo, and J. Rodríguez, *J. Appl. Polym. Sci.*, **106**, 3227 (2007).
28. V. K. Jain, S. S. Sait, P. Shrivastav, and Y. K. Agrawal, *Talanta*, **45**, 397 (1997).
29. P. K. Roy, A. S. Rawat, and P. K. Rai, *Talanta*, **59**, 239 (2003).
30. J. F. Knott, *Fundamentals of Fracture Mechanics*, Butterworths, London (1976).
31. A. J. Kinloch, *Adhesion and Adhesives: Science and Technology*, Chapman & Hall, London (1987).
32. Siddaramaiah, *Practicals in Polymer Science: Synthesis and Qualitative & Quantitative Analysis of Macromolecules*, CBS Publishers and Distributers, Delhi (2005).
33. P. K. Roy, A. S. Rawat, V. Choudhary, and P. K. Rai, *Indian J. Chem. Technol.*, **11**, 51 (2004).
34. J. Coates, *Interpretation of Infrared Spectra, A Practical Approach*, Wiley, Chichester (2000).
35. J. D. Peterson, S. Vyazovkin, and C. A. Wight, *Macromol. Chem. Phys.*, **202**, 775 (2001).
36. G. Giannakopoulos, K. Masania, and A. C. Taylor, *J. Mater. Sci.*, **46**, 327 (2011).
37. B. B. Johnsen, A. J. Kinloch, R. D. Mohammed, A. C. Taylor, and S. Sprenger, *Polymer*, **48**, 530 (2007).
38. J. C. H. Affdl and J. L. Kardos, *Polym. Eng. Sci.*, **16**, 344 (1976).
39. D. R. Akeland, Ed. *The Science and Engineering of Materials*, Chapman and Hall, London (1996).
40. S. McGee and R. L. McGullough, *Polym. Compos.*, **2**, 149 (1981).
41. L. E. Nielsen and R. F. Landel *Mechanical Properties of Polymers and Composites*, Boca Raton, Marcel Dekker Inc., New York, (1994).
42. J. G. Williams, *Compos. Sci. Technol.*, **70**, 885 (2010).
43. R. Voo, M. Mariatti, and L. C. Sim, *Compos. B: Eng.*, **43**, 3037 (2012).

 DOI 10.1002/pc

International Journal of Trends in Computer Science *ISSN: 7462 – 8452*
Volume 2, Issue 11, 2013

Analyzing OFDM System Through MATLAB

Manu Singh, M.Tech Student, Delhi Technological University, New Delhi

Alka Verma, Electrical Electronics and Instrumentation department, Moradabad Institute of technology, Moradabad

Isha Singh, Electrical Electronics and Instrumentation department, Moradaba Institute of technology, Moradabad

Abstract *– In a single carrier communication system, the major hurdle are the inter-symbol interference (ISI) to avoid it an OFDM (Orthogonal Frequency Division Multiplexing) which is a multicarrier system is proposed .It combines a large number of flow data rate carriers to construct a composite high data rate communication system. In our paper we are studying the characteristics of an OFDM system and simulating it through MATLAB and thus analyzing its performance.*

Keywords *– OFDM, FFT, IFFT, Carrier*

I. INTRODUCTION

Now a days wireless applications demands high data rates and thus dealing with ever-unpredictable wireless channel at high data rate communications is not an easy task. The idea of multi-carrier transmission has surfaced recently to be used for combating the hostility of wireless channel and providing high data rate communications.OFDM is a special form of multi-carrier transmission where all the subcarriers are orthogonal to each other. OFDM promises a high user data rate transmission capability at a reasonable complexity and precision .At high data rates, the channel distortion to the data is very significant, and it is somewhat impossible to recover the transmitted data with a simple receiver. OFDM can drastically simplify the equalization problem by turning the frequency-selective channel into a flat channel. A simple one-tap equalizer is needed to estimate the channel and recover the data. OFDM uses the available spectrum very efficiently which is very useful for multimedia communications. For all of the above reasons, OFDM has already been accepted by many of the future generation systems [1]. To avoid ISI due to multipath, successive OFDM symbols are separated by guard band. This makes the OFDM system resistant to multi-path effects In this paper we are analyzing an OFDM system using matlab.

II. THEORETICAL OFDM SYSTEM ANALYSIS

A block diagram of the ofdm system is shown in Figure 1.

Fig 1: OFDM Model for Simulation

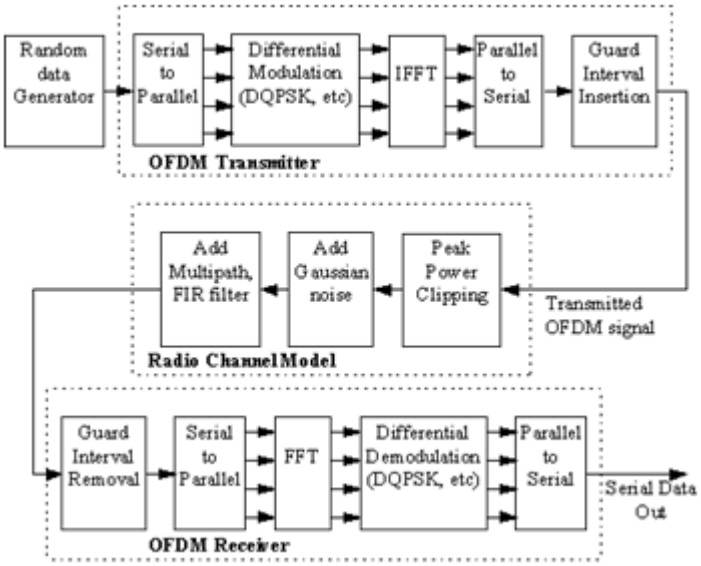

A. Serial to Parallel Conversion

The input serial data is converted into the word size which is essential for transmission and converted into a parallel format. Then data is transmitted in parallel form. [2]

B. Modulation of Data

The data which is to be transmitted on each carrier is converted into differential encoded with previous symbols, then converted into a Phase Shift Keying (PSK) format. An extra symbol is added at the start as differential encoding requires an initial phase reference. The data is then converted into a phase angle based on the modulation method. To reduce problems with amplitude fluctuations due to fading the phase shift keying is used.

C. Inverse Fourier Transform

To find the corresponding time waveform an inverse fourier transform is used. The guard period is then added to the start of each symbol. [3]

D. Guard Period

The guard period that we used was made up of two sections. The first section of the guard period time is a zero amplitude transmission. The other half of the guard period is a cyclic extension of the symbol to be transmitted. This done for symbol timing to be easily recovered by envelope detection. When the guard has been added, the symbols are then converted back to a serial time waveform. This is then the act as a base band signal for the OFDM transmission. [4]

E. Channel

Now channel model is then applied to the transmitted signal. Though this model signal to noise ratio, multipath, and peak power clipping can be controlled. White noise is added to the transmitted signal in order to set noise ratio. By simulating the delay spread multipath spread is added using an FIR filter .The reflected signal magnitude can be determined through coefficient amplitude while the maximum delay spread can be determined by computing the length of the FIR filter. [5]

F. Receiver

The receiver basically perform the reverse operation to the transmitter. The guard period is removed. To find the original transmitted spectrum the FFT is done. The phase angle of transmission carrier is then evaluated and converted into data word by demodulating.To receive original data the data word are combined back to same word size

III. OFDM SIMULATION AND RESULT

The simulation flow chart is shown in figure 2. The input data which is taken as 128 bits is converted by the transmitter from a serial stream to parallel sets. For each subcarrier there is one symbol for each set of data. An inverse Fourier transform converts the frequency domain data set into samples of the corresponding time domain representation of this data and the results are shown in figure 4. The channel simulation sees the effects of noise, multipath, and clipping. By

adding random data to the transmitted signal, simple noise can be simulated. Multipath simulation involves adding attenuated and delayed copies of the transmitted signal to the original Figure 5 shows the received signal with noise.

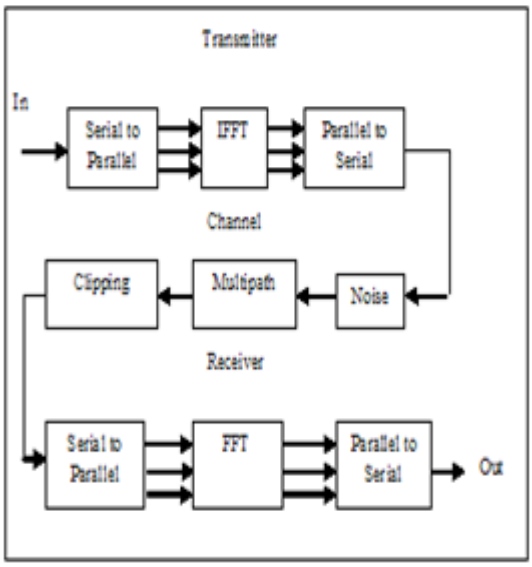

Fig.2: Simulaton flowchart

The receiver splits the OFDM data from a serial stream into parallel sets. The Fast Fourier Transform (FFT) converts the time domain samples back into a frequency domain representation. The magnitudes of the frequency components correspond to the original data. Lastly, the parallel to serial block converts this parallel data into a serial stream to recover the original input data which is indicated in figure 6.

Fig 4: OFDM Signal Transmitted

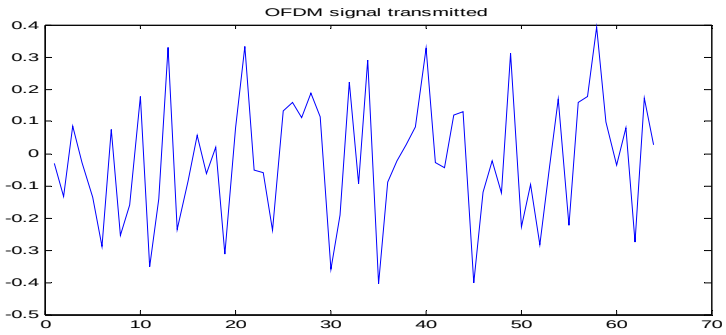

Fig 5: Received OFDM Signal with Noise

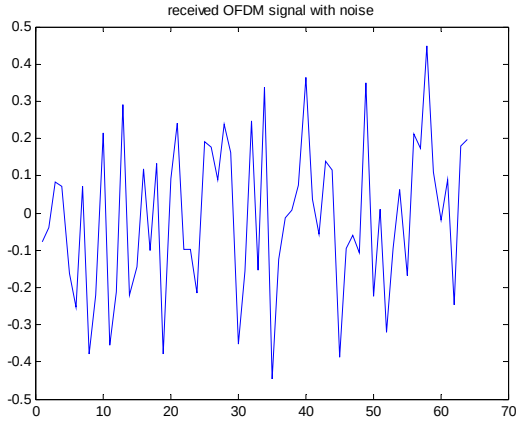

Figure 6: Original message and Recovered

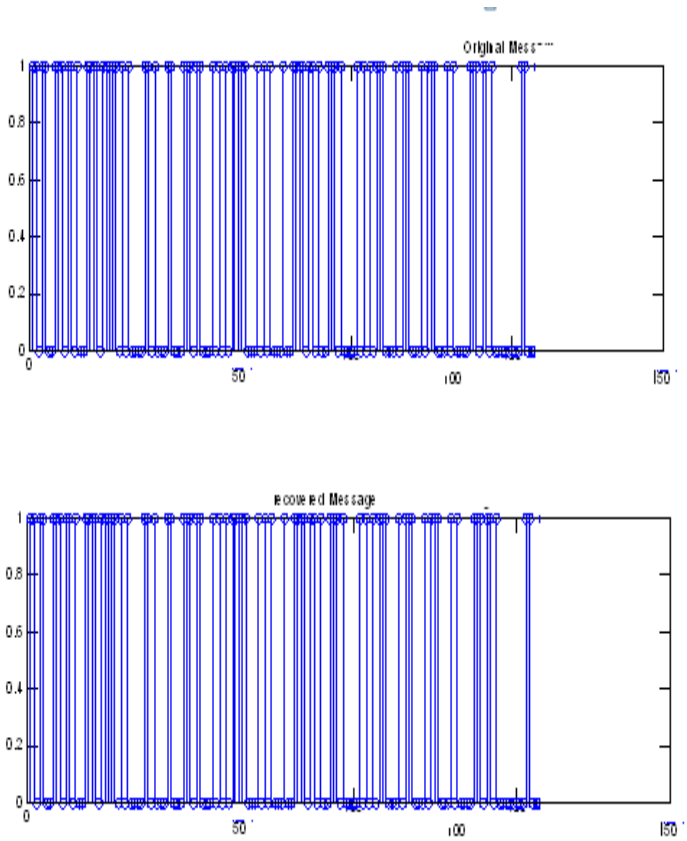

IV. CONCLUSIONS

The OFDM system was simulated using MATLAB and the results are as shown. The results are matching with expected results.. This is very basic implementation and has advantage of less processing time requirement and complexity.

REFERENCES

[1]R. V. Nee and R. Prasad, *OFDM Wireless Multimedia Communications*, Norwood, MA: Artech House, 2000.

[2] J. A. C. Bingham, "Multi-carrier modulation for data transmission: An idea whose time has come", *IEEE Communications Magazine*, vol.28, no. 5, pp. 5-14, May 1990.

[3] A. V. Oppenheim and R. W. Schafer, *Discrete-Time Signal Processing*, Englewood Cliffs, NJ: Prentice Hall, 1989

[4] K. Panta and J. Armstrong, “Spectral Analysis of OFDM Signals and its Improvement by Polynomial Cancellation Coding”, IEEE 2003

[5] Charan Langton, “Orthogonal Frequency Division Multiplexing”, Intuitive guide to Principles of Communications, www.complextoreal.com, 2004

Artificial Life and Cellular Automata Based Automated Test Case Generator

Harsh Bhasin
Delhi technological University
New Delhi
India
+919818730508
i_harsh_bhasin@yahoo.com

ABSTRACT
Manual test data generation is carried out by using the ability of neurons to recognize patterns. The nervous system and the brain coordinate to generate test cases, which are capable of finding potential faults. Automated test data generators lack the ability to produce efficient test cases because they do not imitate natural processes. This paper proposes using Artificial Life based systems for generating test cases. Cellular Automata and Langton's loop have been used to accomplish the above task. Cellular Automata are parallel distributed systems capable of reproducing using self generated patterns. These fascinating techniques have been amalgamated with standard test data generation techniques to give rise to a methodology, which generates test cases for white box testing. Langton's Loops have been used to generate test cases for Black Box Testing. The approach has been verified on a set of 20 programs. The programs have been selected on the basis of their Lines of Code and utility. The results obtained have been verified using Average Probability of Fault Detection. This paper also proposes a new framework capable of crafting test cases taking into account the oracle cost.

Categories and Subject Descriptors
D.2.5 [**Software Engineering**]: Testing and Debugging – *Testing Tools (e.g., data generators, coverage testing)*

General Terms
Algorithms, Design, Reliability, Human Factors.

Keywords
Automated test data generation, Cellular Automata, Artificial life, Testing.

1. INTRODUCTION
"To everything, there is a season, and a time to every purpose, under Heaven." The Byrds used these words from the book of Ecclesiastes in one of their most famous compositions. The relevance of these words in one's life is unquestionable. However, the concept is still not used in software testing. The crux of the above song is the premise of the following methodology henceforth called "the work." Test case generation also requires 'the right time' and 'the favorable environment.' It may be noted that, 'the right time' and 'the favorable environment' are a consequence of emerging patterns. These emerging patterns can be generated by fairly simple rules. Artificial Life (AL) is a discipline that deals with such emergent patterns. There are three types of AL namely Hard, Wet and Soft. Cellular Automata (CA) is a type of soft AL. The proposed technique uses a CA to produce test cases for white box testing and Langton's Loops for generating test cases for black box testing. The proposed system produces test cases that cover both the functional and structural aspects of the software. The system will henceforth be called Comprehensive Test Data Generation System (CTDGS).

Testing is an expensive process, which consumes more than 50% of the cost of developing software [1]. This calls for the automation of the process that would be beneficial both in terms of cost and time. Automatic test data generators can be classified into three categories namely random, static and dynamic [2-4]. It has been observed that manual test data generation leads to better test cases [4]. This is because of the fact that the human brain is capable of pattern matching. The paths that optimize the fault finding capacity of the test suites are conceptually grouped together by the brain. This process helps in deciding paths with maximum coverage. The process of choosing the optimal paths depends on many factors. The process is complicated and difficult to replicate. In order to tap this non-determinism many automatic test data generators use random numbers for accomplishing the task. The statistical aptness and goodness of the pseudo random number generator, therefore, becomes deciding factors for the robustness and efficiency of the test data generator. This paper proposes a framework for an automated test data generator. The proposed system examines the code of each module and generates test cases on the basis of the analysis. The system also analyzes the interactions between the modules. The proposed system uses CA and AL as its base. This paper is a continuation of our previous works [5, 6, 7]. It is novel in the sense that CA has seldom been used in the manner presented in this paper. Moreover, it produces better results as compared to the earlier works [8, 9]. This paper also analyzes the theoretical basis of the applicability of a CA in software testing. The work adds a blend of nature to the complex process of test data generation. The system uses the ability of cellular automata to imitate sociological behavior. Test data generation is important even in areas like regression testing as the amalgamation of the two would result in the generation of a system that is automatic in the true sense and is not dependent on counterfeit test cases. The testing methodology has been verified using an Enterprise Resource Planning system of about 8K lines of code. The results prove that the combination of CA and AL furnishes an alternative way for generating test data.

The emergent patterns generated in Langton's loop have "a time to be born, a time to die a time to plant, a time to reap a time to kill, a time to heal" and are therefore used as a substitute for nature in the "CTDGS."

The rest of the article is organized as follows. Section 2 presents the literature review, section 3 presents a brief description of automated test case generators, section 4 presents the proposed work, and section 5 discusses the theoretical basis of the proposed system, the conclusions and future scope.

2. LITERATURE REVIEW
Test data generation refers to the process of discovering a set of test data that fulfills a particular testing requirement. Test data generation is a complex task. It requires a large amount of resources, both in terms of time and manpower. In order to find gaps in the existing methodologies and to propose a new framework, an extensive literature review has been carried out. The present section focuses on

DOI: 10.1145/2557833.2557843 http://doi.acm.org/10.1145/2557833.2557843

the need of test data generation, the classification of the techniques and the premises on which the techniques are based.

The papers were selected from the following portals.

- IEEE explore
- Science Direct
- Springer
- ACM digital Library

This was done in order to ensure the quality of the selected papers. The keywords used for selecting the papers were "test data generation" and "automatic test data generation." The papers have been selected on the basis of their citation count and novelty. In order to select the papers a team of Assistant professors from different colleges was constituted as to keep the selection free from any bias.

Test Data Generation has always been a topic of interest for the computing fraternity. Numerous techniques have been proposed in order to accomplish the above task. C. V. Ramamoorthy et al. presented the concept of symbolic execution [10]. Webb Miller and David L. Spooner proposed the Numerical Maximization Method [11]. Lori A. Clarke refined Symbolic Execution [12]. Praveen Ranjan Srivastava and Tai-hoon Kim used Variable length Genetic Algorithms to generate test data [13]. James Miller et al. proposed a system named TDGen that uses Program Dependence Analysis Techniques and GAs [14]. Harmen - Hinrich Sthamer also used Genetic Algorithms (GAs) to generate test data [15]. Roy P. Pargas et al. developed a tool named TGen that uses Genetic Algorithms [16]. Joachim Wegener et al. used evolutionary testing [17]. A test environment that supported all common control-flow and data-flow oriented test methods was developed by Girgis [18]. Moheb R. Girgis used modified GAs to produce test data [19]. Dunwei Gong et al. also used GAs [20]. Anastasis A. Sofokleous and Andreas S. Andreou worked on dynamic test data generation using GAs [20]. Jin-Cherng Lin and Pu-Lin Yeh proposed GAs that used extended Hamming distance and a fitness function called SIMILARITY [21]. Raquel Blanco et al. used the scatter search metaheuristic technique [22]. Bruno T. de Abreu et al. used Generalized Extremal Optimization [23]. Neelam Gupta et al. proposed an algorithm based on the iterative relaxation method [24]. R. Landa Becerra et al. used differential evolution to generate test data [25]. Shaoying Liu and Yuting Chen harnessed the concept of a relation-based method, which combined functional and structural testing [26]. Eugenia Díaz et al. used the tabu search metaheuristic algorithm [27]. Dunwei Gong et al. made use of multi-population parallel genetic algorithms [28]. Jifeng Chen et al. proposed using a predicate constraint solving technique [29].

The techniques summarized in Table 1 have been also been studied.

Table 1. Techniques of test data Generation

Author	Type	Property
Offutt [4]	Static	Path analysis
Gotlieb [30]	Dynamic	Path analysis
Lin and Yeh [31]	Hybrid	Evolutionary
Chu et. al. [32]	Hybrid	Statistics based
Gupta et. al. [33]	Graph Based	
Korel et. al. [34]	Dynamic	Function Minimization
Liu et. al. [35]	Dynamic	Evolutionary
Diaz et. al. [36]	Hybrid	Path analysis

It was observed that the techniques based on AL and CA have seldom been used to generate test data.

3. AUTOMATED TEST DATA GENERATION

A good test data generator is essential. It can be used in all forms of testing: in black box, white box and even in regression testing, which is carried out when changes are made in the software.

An automated test data generator has a program analyzer, a path selector and a test data generator. The component of the test data generator that analyses the program is called the Program Analyzer. The program analyzer generates either a Control Flow Graph (CFG) or a Data Dependency Graph (DDG). The CFG, produced by the first component, helps the second component that is the Path Selector (PS) to choose an optimal path. A program may have many paths that are extracted from the graphs generated by the previous component. The main aim of the path selector is to select paths that have maximum bug finding capacity. Test paths are used to generate the test data by the third component called the Test Data generator (TDG). The generated data may also be used by the PS to enhance the process of path selection. This concept is similar to a feedback neural network. Like we learn from our past mistakes, a Test Data Generator may also be designed in such a way that it learns from its past mistakes. In order to do so a database can be developed that keeps track of the test data generated by the system and its gradation during the testing phase.

All three components are essential to produce adequate test data. Fig. 1 shows the architecture of an Automated Test Data Generator.

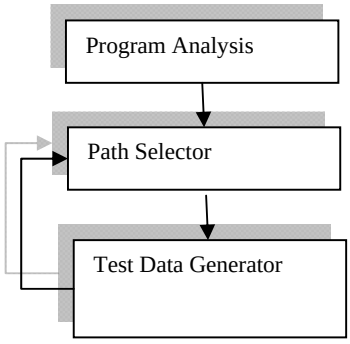

Figure 1: Automated Test Data Generator

Test data generators may be classified as either code based or specification based. The code based test data generators analyze the internal structure of the program. They can further be classified as random, path oriented or goal oriented. The path selector component of the automatic test data generator tries to achieve maximum coverage. The coverage in question can be statement coverage, path coverage, branch coverage or condition coverage. The test data generation may further be classified as static or dynamic. Static test data generation refers to generating test data without actually executing the code. The earlier implementations of static test data generators used symbolic execution. In symbolic execution each expression is written in terms of input variables. For example, one of the two roots of a quadratic equation $ax^2 + bx + c = 0$ is given by: $root1 = \frac{c+\sqrt{d}}{2*a}$, where $c = -1 * b$ and $d = b^2 - 4*a*c$. Symbolic execution requires the expression to be written as

$$root = \frac{-b + \sqrt{b^2 - 4ac}}{2a}$$

However, there is a problem in the above conversion. The conversion becomes very difficult for complex expressions. Moreover, the technique cannot be applied when the code is not available. Gupta et. al. [17] suggested a hybrid of the two techniques in order to achieve optimization both in terms of time and storage cost.

It has been observed that from amongst random and path oriented techniques, the path oriented technique gives better results as it does not leave any path of the program under test. However, the choice depends on the implementation. Figure 2 summarizes the classification of Automated Test Data Generation.

It may be stated here that the use of AL in test data generation has not been completely explored. Moreover, except for one attempt, which uses Langton's loop [7, 8], no other work was found on the application of AL to test data generation.

As stated earlier, test data generation is an intricate process. It requires the intellect of a human being in order to produce effective and efficient test cases. The various methods explained in sections 2 and 3 prove the fact that none of the algorithmic ways have been able to achieve the task of generating effective test cases completely. Therefore, there is a need of using nature-based approaches in the discipline. The ways followed by nature are fascinating. As is evident from the recent cloud burst in Uttarakhand, India, nature can even reclaim the riverbed and mountain occupied in the name of development in just a stroke. So, there is a strong reason; to give chance; to nature-based techniques in software testing.

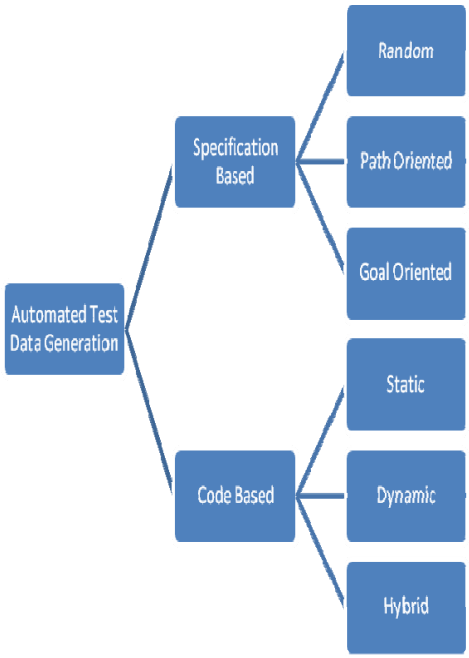

Figure 2: Classification of Automated Test Data Generator

4. PROPOSED METHOD

The proposed system consists of two Components: Module Analyzer (MA) and Module Interaction Analyzer (MIA). MA generates test cases on the basis of the code of a module and MIA generates test cases on the basis of the interaction between the modules. The MIA accomplishes the task using a Function Flow Graph (FFG) as per our earlier work [7].

The MA component uses a cellular automata based algorithm for generation of test cases [6]. The conditional statement in a program is depicted by a decision node that helps in deciding the direction. This decision is made by the cellular automata patterns. If there are 'n' decision nodes in the program under test (PUT), then 'n' values are required to generate the path. To extract 'n' values, a local region of a cellular automata pattern is selected. The task has been accomplished by using the coefficient of autocorrelation. The i^{th} value generated by the system corresponds to the value of i^{th} node of the graph of the PUT. If the value is 0, then the corresponding node evaluates to false, otherwise it evaluates to true. A path is generated using the above nodes. Many paths are needed for the generation of a comprehensive test suite. The number of paths depends on how much coverage is required. This is followed by the removal of repeated paths so as to minimize oracle cost.

Path selection is followed by the process of test case generation. So as to carry out this task, a path is selected from the paths whose test cases have not yet been generated. Variables defined and used in the selected path are extracted. This step is followed by the determination of legal values from the design specifications. A value from the legal set of values is chosen for each variable. This task is accomplished by the corpuscular random number generator [37]. The above values result in the generation of a test case for the selected path. The process is then repeated for each path.

The above process results in the crafting of a test case for each module. The next step is to analyze the interaction between the modules. This task is done by the second component.

The second component of the system uses a technique called Test Data Generation Using Artificial Life (TDGUAL). The technique was proposed in one of our earlier works. Modules are considered as the basic unit. The test cases are generated for all the modules of the program under test. This can be done using the calling sequence of the functions. Our earlier technique proposed a new state machine called the Function Flow Graph (FFG). The FFG covers all the modules and helps in generating the test suite [5]. The Artificial Life (AL) sub-component will select the appropriate value of each variable in question. The technique works as follows.

Algorithm: Module Interaction Component

1. The test case suite is initialized to a null set.
2. The process starts from the main module.
3. The calling sequence may be derived from the stack trace of PUT. So, the technique works either by using the stack trace or the design specifications.
4. $\forall module\ m_i$ stumbled upon, the following tasks are performed and the module is put onto the stack.
    a. For each module, the $inputs\ a_i$, are identified and stored.
    b. The types and constraints of the input are extracted from the design view. A test case is designed and added to the test case suite.
    c. Once all the modules have been processed repeatedly pop modules from the stack and store the test cases generated in the database.
    d. The feasibility of all $cases\ T_i$ as per the design phase is then checked. If the test case passes the feasibility test put it in the final suite.

The system is depicted in Figure 3.

5. RESLTS AND CONCLUSIONS

Utmost care has been taken to select the regions of the CA patterns that were used in the MA. In our earlier implementation the difference between the number of live and dead cells in a particular region was taken as the criteria for selecting the region. The premise had to be changed because even if the difference between them is zero, the patterns do not satisfy most of the statistical tests for PRNG. The criterion of selecting the region was, therefore, changed to the value of coefficient of correlation obtained from the selected region.

DOI: 10.1145/2557833.2557843 http://doi.acm.org/10.1145/2557833.2557843

Software was developed in C#, .NET 4.0 to select the regions from the 256 patterns and the patterns were stored in a repository. This repository was used in the path selector sub-component of MA. The corpuscular pseudo random number generator used in the system is based on the concept of hemoglobin content and the size of the Red Blood Cells. The CRNG has been tested using gap test, frequency test and the coefficient of correlation of the sequence of numbers produced.

The technique for generating test cases of modules has been tested on 20 programs. The programs have been selected on the basis of the lines of code and their importance. The programs are diverse both in terms of size and in terms of applicability. The complete system was also tested by analyzing an ERP system developed for a paint company. The technique based on interaction between the modules, has been tested on an ERP system developed by SahibSoft. The ERP system was around 8K lines of code and was developed in C#. The ERP system had 53 modules. The technique has also been applied on a large set of programs. The complete system has been developed and 2100 test cases have been generated. The aim is to use these cases in regression testing. To carry out the task a team of students, lecturers and Assistant professors was constituted from 5 colleges.

The system has shown encouraging results. The system produces test cases, both on the basis of the code of a module and on the basis of the interaction between the modules. The base of the system is cellular automata and Langton's loop. The combination has never been used in automatic test data generation and hence the technique is novel. The system is being developed into a full fledged software, which would be used in regression testing.

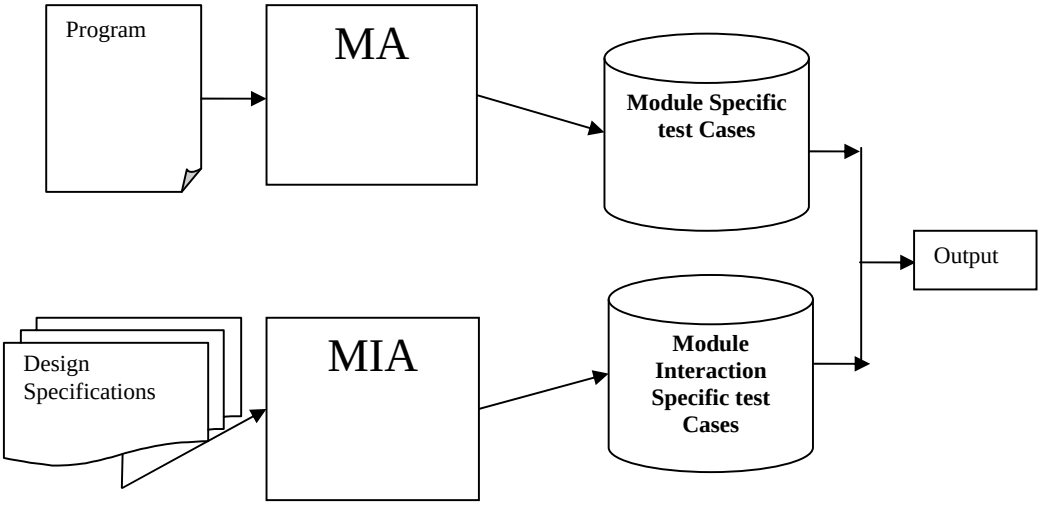

Figure 3: Comprehensive Test Data Generation System (CTDG)

6. REFERENCES

[1] Pan, J. 1999. Software Testing, Dependable Embedded Systems. *CARNEGIE Mellon University Spring*.

[2] S. Mahmod. 2007. A Systematic Review of Automated Test Data Generation Techniques. *Master Thesis, Blekinge Institute of Tech.*, Sweden.

[3] M. J. Gallagher & V. Lakshmi-Narasimhan. 1997. ADTEST: a test data generation suite for ada software systems. *IEEE Transactions on Software Engineering*. Vol. 23 (8), pp. 473-484.

[4] J. Offutt, Z. Jin & J. Pan. 1994. The Dynamic Domain Reduction Procedure for Test Data Generation: Design and Algorithms. *Technical Report ISSE*.

[5] Bhasin, H., Singla, N., & Sharma, S. 2013. Cellular Automata Based Test data Generation. *ACM Sigsoft, Software Engineering Notes*. 38 (4).

[6] Bhasin, H., & Singla, N. 2013. Cellular-Genetic Automata Based Test data Generation. *ACM Sigsoft, Software Engineering Notes*. 38 (5).

[7] Bhasin, H., Shewani, & Goyal, D. 2013. Test Data Generation using Artificial Life. *International Journal of Computer Applications*. Vol. 67, No.12, pp. 34-39.

[8] Shiba, T., Tsuchiya, T., & Kikuno, T. 2004. Using artificial life techniques to generate test cases for combinatorial testing. *Computer Software and Applications Conference, 2004. COMPSAC 2004. Proceedings of the 28th Annual International*. 72 - 77 vol.1, pp. 28-30.

[9] Ali M. Alakeel. 2010. A Framework for Concurrent Assertion – Based Automated Test Data Generation. *University of Tabuk. Saudi Arabia.*

[10] Ramamoorthy, C. 1976. On the automated generation of program test data. *Transactions on Software Engineering*. SE-2, 4, 293-300.

[11] Miller, W., & Spooner, D. 1976. Aytomatic generation of floating-point test data. *Transactions on Software Engineering.* SE-2, 3, 223-226.

[12] Clarke, L. A. 1976. A system to generate test data and symbolically execute programs. *IEEE Trans. Sofrware Eng.* SE-2, 3, 215-222.

[13] Srivastava, P. R., & Kim, T.-h. 2009. Application of Genetic Algorithm in Software Testing. International Journal of Software engineering and its Applications. 3, 4, 87-96.

DOI: 10.1145/2557833.2557843 http://doi.acm.org/10.1145/2557833.2557843

[14] Miller, J., Reformat, M., & Zhang, H. 2006. Automatic test data generation using genetic algorithm and program dependence graphs. *Information and Software Technology*. 48, 7, 586–605.

[15] Sthamer, H. 1996. The automatic generation of software test data using genetic algorithms. Ph.D. Thesis, University of Glamorgan, Pontypridd, Wales, UK.

[16] Pargas, R., Harrold, M., & Peck, R. 1999. Test data generation using genetic algorithms. *Journal of Software Testing, Verification and Reliability*. 9, 4, 263–282.

[17] Wegener, J., Baresel, A., & Sthamer, H. 2001. Evolutionary test environment for automatic structural testing. Journal of Information and Software Technology. 43, 14, 841–854.

[18] Girgis, M. 2005. Automatic test data generation for data flow testing using a genetic algorithm. *Journal of Universal Computer Science*. 11, 5, 898–915.

[19] Gong, D., Zhang, W., & Yao, X. 2011. Evolutionary generation of test data for many paths coverage based on groupings. *Journal of Systems and Software*. 84, 12, 2222-2233.

[20] Sofokleous, A. A., & Andreou, S. A. 2008. Automatic, evolutionary test data genereation for dynamic software testing. *Journal of Systems and Software*. 81, 11, 1883-1898.

[21] Lin, J.-C., & Yeh, P.-L. 2001. Automatic test data generation for path testing using GAs. *Information Sciences: an International Journal*. 131, 1-4, 47-64.

[22] Blanco, R., Tuya, J., Adenso-Díaz, B. 2009. Automated test data generation using a scatter search approach. *Information and Software Technology*, 51, 4, 708-720.

[23] Abreu, B. T., Martins, E., and Sousa, F. L. 2007. Generalized extremal optimization: an attractive alternative for test data generation. *GECCO* , 1138.

[24] Gupta, N., Mathur, A. P., & Soffa, M. L. 1998. Automated test data generation using an iterative relaxation method. *Proceedings of the 6th ACM SIGSOFT international symposium on Foundations of software engineering*. 231-244.

[25] Becerra, R. L., Sagarna, R., and Yao, X. 2009. An evalution of Differential Evolution in software test data generation. *IEEE Confress on Evolutionary Computation*. IEEE, Trondheim. 2850-2857.

[26] Liu, S., & Chen, Y. 2008. A relation-based method combining functional and structural testing for test case generation. *Journal of Systems and Software*. 81, 2, 234-248.

[27] Diaz, E., Tuya, J., Blanco, R., & Dolado, J. J. 2008. A tabu search algorithm for structural software testing. *Computers and Operations Research*. 35, 10, 3052-3072.

[28] Gong, D., Tian, T., & Yao, X. 2012. Grouping target paths for evolutionary generation of test data in parallel. *Journal of Systems and Softwares*. 85, 11, 2531-2540.

[29] Chen, J., Zhu, L., Shen, J., Wang, Z., and Wang, X. (2006). An Approach on Automatic Test Data generation with Predicate Constraint Solving Technique. *Internation Journal of Information Technology*. 12, 3, 132-141.

[30] A. Gotlieb, B. Botella and M. Reuher, "Automatic Test Data Generation using Constraint Solving Techniques", Proceeding of ISSTA 98, 1998, pp. 53-62.

[31] C. Lin and P. L. Yeh, "Automatic Test Data Generation for Path Testing Using GAs", Elsevier Information Sciences 131, 2001, pp. 47-64.

[32] H. D. Chu, J. E. Dobson and I. C. Liu, "FAST: A Framework for Automating Statistical-based Testing", Software Quality Journal, Vol.6, pp. 13-36, 1997.

[33] M. Gupta, F. Bastani, L. Khan and I. L. Yen, "Automated Test Data Generation using MEA-Graph Planning", Proceedings of the 16

[34] B. Korel and A. M. Al-Yami, "Assertion-oriented automated test data generation", Proceedings of the 18th international conference on Software engineering, Berlin, Germany, 1996, pp. 71 - 80.

[35] M. H. Liu, Y. G. Gao, J. H. Shan, J. H. Liu, L. Zhang and J. S. Sun, "An Approach to Test Data Generation for Killing Multiple Mutants", Proceedings of 22.

[36] E. Diaz, J. Tuya, and R. Blanco, "Automated Software Testing using a Metaheuristic technique Based on Tabu Search", Proceedings of the 18.

[37] Bhasin, H. 2012. Corpuscular Random Number Generator. *International Journal of Information and Electronics Engineering*, vol. 2, no. 2, pp. 197-199.

DOI: 10.1145/2557833.2557843 http://doi.acm.org/10.1145/2557833.2557843

International Journal of Computer Information Systems and Industrial Management Applications.
ISSN 2150-7988 Volume 6 (2014) pp. 603 -614

BBO Algorithms with Graded Emigration for Yagi-Uda Antenna Design Optimization for Maximal Gain

Shelja Tayal[1], Satvir Singh[2] and Gagan Sachdeva[3]

[1] SBS State Technical Campus,
Ferozepur, Punjab [INDIA]
sheljatayal18@gmail.com

[2] SBS State Technical Campus,
Ferozepur, Punjab [INDIA]
satvir15@gmail.com

[3] Rayat Bahra Group of Institutes,
Mohali, Punjab [INDIA]
gagan.sachdeva04@gmail.com

***Abstract*: Biogeography Based Optimization (BBO) is a swarm based optimization algorithm that has shown impressive performance over other Evolutionary Algorithms (EAs). Immigration Refusal Biogeography Based Optimization (IRBBO), Enhanced Biogeography Based Optimization (EBBO), Blended Migration are the most improved version of BBO and are known as migration variants of BBO. In this paper, a new concept of graded emigration for EBBO is proposed for furthur improved convergence performance. This graded emigration is also experimented on other BBO variants and found to be a competitive option. To validate the performance of Graded Emigration (GE-EBBO), experiments have been conducted on a testbed of unimodal, multimodal and deceptive benchmark test functions. Besides validation, GE-EBBO is also subjected to evolve solution to a real world problem of designing a Yagi-Uda antenna for maximal gain. Designing a Yagi-Uda antenna involves determination of wire-element lengths and their spacings in between them those bear highly complex and non-linear relationships with antenna gain, impedance, and Side Lobe Level (SLL), etc. at a particular frequency of operation. In this paper, a comparative study among BBO, EBBO, IRBBO, PSO (Particle Swarm Optimization) and GE-EBBO is conducted to analyze convergence performance while evolving the antenna designs for maximum gain, multiple times. The average of 10 monte-carlo simulations are plotted for fair quantitative comparative study of convergence performance of these stochastic algorithms.**

***Keywords*:** BBO and its variants, GE-EBBO, PSO, Benchmark Functions, Yagi-Uda Antenna, Antenna Gain, NEC2.

I. Introduction

Antenna is an electrical device which forms an interface between free-space radiations and transmitter or receiver. The choice of an antenna depends on various factors such as gain, impedance, bandwidth, frequency of operation, SLL, etc. A Yagi-Uda antenna is a widely used antenna design due to high forward gain capability, low cost and ease of construction. It is a parasitic linear array of parallel dipoles, one of which is energized directly by transmission-line while the others act as a parasitic radiators whose currents are induced by mutual coupling. The characteristics of Yagi-Uda antenna are affected by all of the geometric parameters of array.

A Yagi-Uda antenna was invented in 1926 by H. Yagi and S. Uda at Tohoku University [1] in Japan, however, published in English [2]. Since its invention, continuous efforts have been put in optimizing the antenna for gain, impedance, SLL and bandwidth using different optimization techniques based on manual, traditional mathematical approaches [3, 4, 5, 6, 7, 8, 9] and Artificial Intelligence (AI) based techniques [10, 11, 12, 13, 14, 15, 16].

Yagi aerials approximate design was proposed for maximum gain in 1949, [17]. Ehrenspeck and Poehler have given a manual approach to maximize the gain of the antenna by varying various lengths and spacings of its elements [18].

Later on, with the availability of improved computational facilities at affordable prices made it possible to optimize antennas numerically. A numerical optimization technique was proposed to calculate the maximum gain of Yagi-Uda antenna arrays with equal and unequal spacings between adjoining elements. Optimum design of Yagi-Uda antenna where antenna gain function is proved to bear a highly nonlinear relationship with its geometric parameters.

In 1975, John Holland introduced Genetic Algorithms (GAs) as a stochastic, swarm based AI technique, inspired from natural evolution of species, to optimize arbitrary systems for certain cost function. Then many researchers investigated GAs to evolve solutions to engineering problems including Yagi-Uda antenna for gain, impedance and bandwidth, separately [19, 10, 20] and collectively [11, 21, 22]. Baskar *et al.*, have optimized Yagi-Uda antenna using Comprehensive Learning Particle Swarm Optimization (CLPSO) and presented better results than other optimization techniques [13]. Li has used Differential Evolution (DE) to optimize geometrical parameters of a Yagi-Uda antenna and illustrated

the capabilities of the proposed method with several Yagi-Uda antenna designs in [14]. Singh *et al*. have explored another useful stochastic global search and optimization technique named as Simulated Annealing (SA) for the optimal design of Yagi-Uda antenna [15].

In 2008, Dan Simon introduced yet another swarm based stochastic optimization technique based on science of biogeography where features sharing among various habitats (potential solutions) is accomplished with migration operator and exploration of new features is done with mutation operator

[23]. Singh *et al*. have presented BBO as a better optimization technique for Yagi-Uda antenna designs [16]. In [10, 21, 13, 24, 25, 26, 27, 28, 29, 30, 31, 32, 33, 34], BBO have shown comparatively better performance as compared to EAs.

In 2009, Du *et al*. have proposed the immigration refusal in BBO, where immigration from poor habitat to better habitat tend to occur [35].

In 2010, Pattnaik *et al*. have proposed EBBO in which duplicate habitats created due to migration is modified with random mutation to increase the exploitation ability of BBO. Here, experiments have been conducted on unimodal and multimodal benchmark functions. EBBO gives excellent performance when compared with BBO and other versions of BBO [36].

Ma and Simon introduced new migration operator, i.e., Blended migration, to solve the constrained optimization problem and to make BBO convergence faster [37, 38]. Firstly, Blended Crossover operator of GA outperform standard BBO on a set of benchmark optimization problems. Then, Blended BBO algorithm is compared with solutions based on a Stud Genetic Algorithm (SGA) and PSO.

In this paper, a new variant for EBBO migration, i.e., GE-EBBO is proposed to improve the performance of EBBO and other BBO variants. The proposed algorithm of GE-EBBO is applied on a testbed of benchmark functions. The results of GE-EBBO when compared with Standard BBO, IRBBO, EBBO and Blended Migration, where GE-EBBO outperformed all of them. GE-EBBO is based upon grading of habitats for migration and EBBO itself prevents similar solutions and to increase the diversity in the population. Then the proposed algorithm GE-EBBO along with other BBO variant and PSO are subjected to evolve solution to real world problem of designing Yagi-Uda to study final results and convergence performance. A method of moments based freeware programme, NEC2 (Numerical Electromagnetics Code), is used to evaluate the antenna designs for gain, input impedance, bandwidth, beamwidth and SLL, etc.

After this brief historical background, the paper is outlined as follows: In the Section II, various stochastic algorithms like Standard BBO, IRBBO, EBBO, Blended migration and PSO algorithms are discussed. It is followed by, in Section III our newly proposed algorithm, i.e., GE-EBBO. Section IV discusses about the benchmark function. In the Section V, Yagi-Uda antenna design problems are discussed. Section VI contains the comparison of performance among GE-EBBO, BBO and its variants and PSO while tested on benchmark functions and evolved solution to Yagi-Uda antenna design problem. Finally, conclusions, work in progress and research agenda have been discussed in Section VII.

II. Stochastic Algorithms

Most of AI based EAs are stochastic in nature that uses multiple solutions at a time to evolve better solutions iteratively by imitating one or another natural phenomenon. BBO and PSO are similar EAs those have been developed by imitation of biogeography study and flocking behaviour of birds and fish, etc. These algorithms are discussed in detail as follows:

A. Biogeography Based Optimization

As the name suggest, BBO is a population based global optimization technique developed on the basis of the science of biogeography, i.e., study of the distribution of animals and plants among different habitats over time and space. Originally, biogeography was studied by Alfred Wallace and Charles Darwin mainly as descriptive study [39, 40, 41]. However, in 1967, the work was carried out by MacAurthur and Wilson changed this view point and proposed a mathematical model for biogeography and made it feasible to predict the number of species in a habitat [42] under arbitrary conditions. Mathematical models of biogeography describe migration, speciation, and extinction of species in various islands. BBO has certain features common with other swarm based algorithms. Like GAs and PSO, BBO has a way of sharing information (exploitation) among solutions. GA solutions die at the end of each generation, while in PSO and BBO, solutions survive forever although their characteristics change as the optimization process progresses. PSO solutions are more likely to clump together in similar groups, while GA and BBO solutions do not necessarily have any built-in tendency to cluster. The term *island* is used for any habitat that is geographically isolated from other habitats. Habitats that are well suited residences for biological species are referred to have high Habitat Suitability Index (HSI) value. HSI is analogues to fitness in other EAs whose value depends upon many factors such as rainfall, diversity of vegetation, diversity of topographic features, land area, and temperature, etc. The factors/variables that characterize habitability are termed as Suitability Index Variables (SIVs). *Immigration* is the arrival of new species into a habitat or population, while *emigration* is the act of leaving one's native region.The habitats with high HSI tend to have a large population of its resident species, that is responsible for more probability of emigration (emigration rate, μ) and less probability of immigration (immigration rate, λ) due to natural random behavior of species. On the other hand, habitats with low HSI tend to have low emigration rate, μ, due to sparse population, however, they will have high immigration rate, λ. Suitability of habitats with low HSI is likely to increase with influx of species from other habitats having high HSI. However, if HSI does not increase and remains low, species in that habitat go extinct that leads to additional immigration. For sake of simplicity, linear relationship between HSI (or population) and immigration (and emigration) rates are assumed, and maximum values of emigration and immigration rates are made equal, i.e., $E = I$, as depicted graphically in Figure 1.

For k-th habitat values of emigration rate, μ_k, and immigration rate, λ_k, are given by (1) and (2).

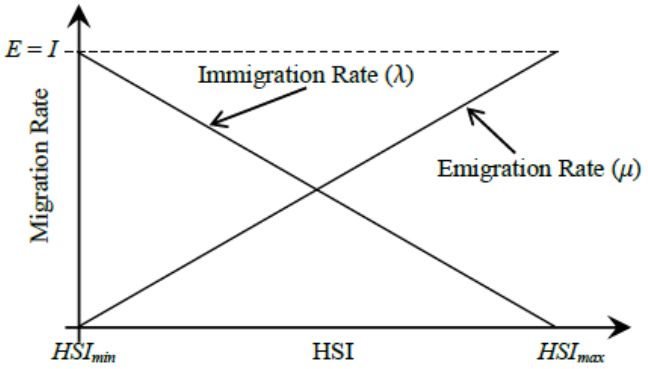

Figure 1. Migration Curves

$$\mu_k = E \cdot \frac{HSI_k}{HSI_{\max} - HSI_{\min}} \quad (1)$$

$$\lambda_k = I \cdot \left(1 - \frac{HSI_k}{HSI_{\max} - HSI_{\min}}\right) \quad (2)$$

The immigration of species from high HSI to low HSI habitats
may raise the HSI of poor habitats. Good solutions are more resistant to change than poor solutions whereas poor solutions are more dynamic and accept a lot of features from good solutions.

Each habitat, in a population of size *NP*, is represented by *M*-dimensional vector as $H = [SIV_1, SIV_2, \ldots . SIV_M]$ where *M* is the number of SIVs (features) to be evolved for optimal HSI. HSI is the degree of acceptability that is determined by evaluating the cost/objective function, i.e., *HSI = f(H)*. Algorithmic flow of BBO involves two mechanisms, i.e., migration and mutation, these are discussed in the following subsections.

1) Migration

Migration is a probabilistic operator that improves HSI of poor habitats by sharing features from good habitats. During migration, *i*-th habitat, H_i (where $i = 1, 2, \ldots, NP$) use its immigration rate, λ_i given by (2), to decide probabilistically whether to immigrate or not. In case immigration is selected, then the emigrating habitat, H_j , is found probabilistically based on emigration rate, μ_j given by (1). The process of migration takes place by copying values of SIVs from H_j to H_i at random chosen sites, i.e., H_i(SIV) ← H_j(SIV). The pseudo code of migration operator is depicted in Algorithm 1.

2) Mutation

Mutation is another probabilistic operator that modifies the values of some randomly selected SIVs of some habitats that are intended for exploration of search space for better solutions by increasing the biological diversity in the population. Here, higher mutation rates are investigated on habitats those are probabilistically participating less in migration process. The mutation rate, *mRate*, for *k*-th habitat is given as (3)

$$mRate_k = C \times \min(\mu_k, \lambda_k) \quad (3)$$

Algorithm 1 Standard Pseudo Code for Migration

```
for i=1 to NPdo
  Select H_i with probability based on λ_i
  if H_i is selected then
   for j=1 toNPdo
     Select H_j with probability based on μ_j
     if H_j is selected
       Randomly select a SIV(s) from H_j
       Copy SIV(s) to H_i
      end if
    end for
  end if
end for
```

where μ_k and λ_k are emigration and immigration rates, respectively, given by (1) and (2) corresponding to HSI_k. Here *C* is a constant and kept equal to 1, in this paper, i.e., mutation rate is much higher as compared to other EAs to maintain high diversity in the population. The pseudo code of mutation operator is depicted in Algorithm 2.

Algorithm 2 Standard Pseudo Code for Mutation

```
mRate = C × min(μ_k, λ_k) where C = 1
for i = 1 to NP do
   for j = 1 to length(H) do
       Select H_j(SIV) with mRate
       If H_j(SIV) is selected then
          Replace H_j(SIV) with randomly generated SIV
       end if
   end for
end for
```

3) BBO Algorithm

Algorithmic flow for BBO is depicted in Figure 2, and explained stepwise as follows:

1. In first step, identify SIVs and their universe of discourse (UODs).
2. In next step, create a habitat (string).
3. Then generate a random population.
4. Check for maximum iteration number arrived or not. If yes, select the best habitat and stop the BBO algorithm. If no, then evaluate fitness.
5. Check for fitness if achieved then select the best habitat and stop the BBO algorithm. If no, then apply migration.
6. After Migration, apply mutation.
7. If fitness is achieved then select the best habitat and stop the BBO algorithm. If no, then repeat the processes as shown in Figure 2.

B. BBO Variants

Simple migration may leads to same values of SIVs in all habitats. To increase the diversity in the population with the objective of improvement in evolutionary performance, in BBO, different variants are investigated here. These most popular variants are explained in the following subsections:

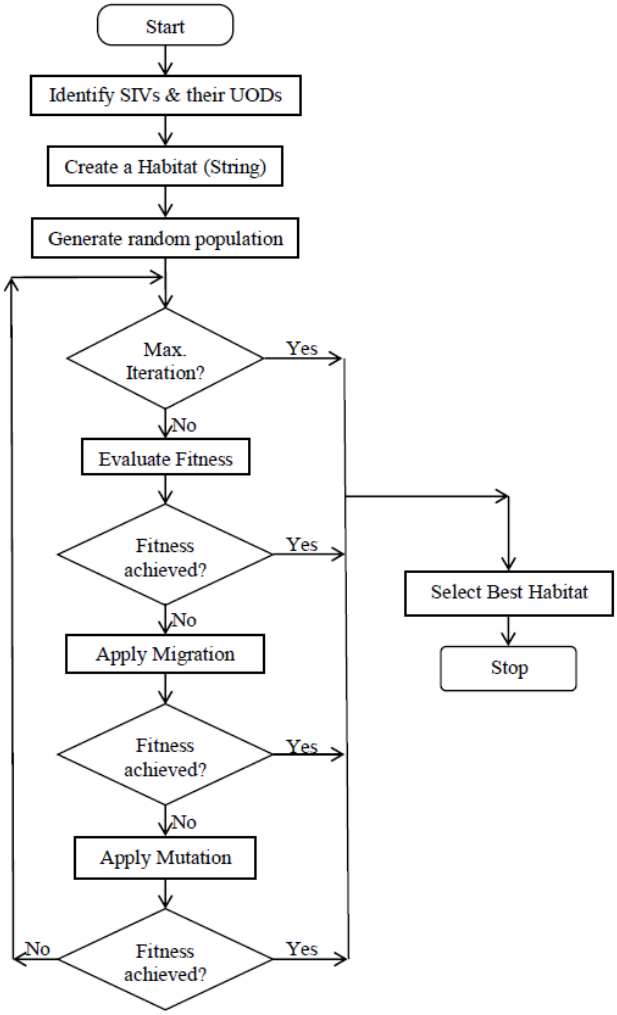

Figure 2. Flow Chart of BBO Algorithm

1) Immigration Refusal

In standard BBO, migration locations are decided on the basis of the emigration and immigration rates. If the habitat has a high emigration rate, then the probability of emigrating to other islands is high, whereas, the probability of immigration from other habitats is low. However, the low probability does not mean that immigration from low fit solution will never happen. Once in a while a high fit solution can tend to receive solution features from a low fitness solutions that may ruin the high HSI of the better habitat. So, when the SIVs from habitat which has low fitness try to emigrate to other habitats, the receiving habitats should carefully consider whether to accept these SIVs or not. If the emigration rate of the habitat is less than some threshold, and its fitness is also less than that of the immigrating habitat, then the immigrating island will refuse this migration. This idea of conditional migration is known as immigration refusal [35]. Immigration Refusal BBO variant is investigated, in this paper, for evolutionary performance here whose pseudo code is depicted in Algorithm 3.

Algorithm 3 Pseudo Code for Immigration Refusal

```
for i = 1 to NP do
  Select H_i with probability based on λ_i
  if H_i is selected then
    for j = 1 to NP do
      Select H_j with probability based on μ_j
      if H_j is selected
        if ((fitness(H_j)>fitness(H_i))
          apply migration
        end if
      end if
    end for
  end if
end for
```

2) Enhanced BBO

The exploitation ability of BBO is good as migration operator can efficiently share the SIVs between habitats. However, this creates similar habitats which decreases the diversity of the population. To increase diversity in the population so as to increase the exploration ability, clear duplicate operator is used. This variant is named as Enhanced BBO (EBBO) presented in [36], the same concept of standard migration and mutation is used. however, modified clear duplicate operator is incorporated to get better results and to make convergence faster. EBBO is investigated, in this paper, for convergence performance whose pseudo code is depicted in Algorithm 4.

Algorithm 4 Pseudo Code for Enhanced BBO

```
for i = 1 to NP do
  Select H_i with probability based on λ_i
  if H_i is selected then
    for j = 1 to NP do
      Select H_j with probability based on μ_j
      if H_j is selected
        if ((fitness(H_j) == fitness(H_i))
          eliminate duplicates
        end if
      end if
    end for
  end if
end for
```

3) Blended Migration

A new migration operator called blended migration [38], which is the modification of the standard BBO migration operator, and which is motivated from blended crossover operator of GAs. In blended crossover operator, new genes values are generated by combination of both parental gene values, instead of simple exchange of gene values. In blended migration, SIV of habitat H_i is not simply replaced by SIV of habitat H_j . However, a new SIV value in Blended Migration comprised of SIVs of both participating habitats, as given by 4. Blended Migration is also investigated here whose pseudo code is depicted in Algorithm 5.

$$H_i(SIV) \leftarrow \alpha.H_i(SIV) + (1-\alpha).H_j(SIV) \quad (4)$$

Algorithm 5 Pseudo Code for Blended Migration

```
for i = 1 to NP do
    Select H_i with probability based on λ_i
    if H_i is selected then
      for j = 1 to NP do
          Select H_j with probability based on μ_j
          if H_j is selected
              H_i (SIV) ← α.H_i + (1-α).H_j
          end if
      end for
    end if
end for
```

Here is a real number between 0 and 1. It could be random or deterministic. In Blended BBO, exploration of search space for better solution is in built, therefore, may require less mutation rates.

C. Particle Swarm Optimization

PSO also belongs to the category of swarm based EAs [43] useful in solving global optimization problems. It was originally proposed by James Kennedy, as improvement in flocking behavior of birds and was introduced later as an optimization method in [44,45]. PSO implementation is easy and computationally inexpensive, since its memory and CPU speed requirements are low [46]. Moreover, it does not require gradient information of the fitness function but only its values. PSO has been proved to be an efficient method for many global optimization problems and in some cases, it does not suffer from the difficulties experienced by other EAs.

Particle swarm algorithm originated from flocking behavior of birds for getting maximum protection from predators [47]. A simulation program was developed to generate a bird flock for a hollywood film [48]. In this simulation, a point on the screen was defined as food, called the cornfield vector, the idea was to allow birds to find food through social learning by observing the behavior of nearby birds, who seemed nearer to the food source. The optimization potential was realized in the initial experiments and the algorithm was modified to incorporate topological rather than Euclidean neighborhoods and multi-dimensional search was attempted successfully.

PSO usually initializes the population by assigning each particle an arbitrary random starting position in the solution space with a randomized velocity. GAs use selection, crossover and mutation to replace less fit individuals by combining the traits of high performing chromosomes/solutions. However, in PSO, members of the particle swarm persist over time, retaining their identities and improving through imitation and interactions of best performing particles/solutions in the swarm.

1) Flocks

There is something about the way they move, synchronize, fly-without colliding, and resulting in amazing choreography. In 1987, a very influential simulation of bird-flock was published by Craig Reynolds [48]. Reynolds assumed that flocking birds were driven by three concerns:

1. Avoid colliding with their neighbors.
2. Match with velocities of their neighbors.
3. Try to move towards the center of the flock.

These simple rules resulted in a very realistic flocking behavior that showed coherent clusters of boids (name of simulated birds) whirling through space, splitting to flock around obstacles and rejoining again. His simple non-centralized algorithm was used in many animated cinematic sequences of flocks and herds.

2) Schools and Social Behaviour

In their book [43], perfectly described the rationale behind the idea that originated PSO was perfectly described as "Whenever people interact, they become more similar, as they influence and imitate one another. Norms and cultures are the result. Human physical behavior is not flock-like or school-like; the trajectories of human thoughts through high-dimensional cognitive space just might be''. The particle swarm algorithm is really a simulation of the way minds think and of human social behavior.

Regarding concordance they state, "The social phenomenon behind thinking is more complex than the choreographed behaviors of fish and birds. First, thinking takes place in belief space, whose dimensionality is far greater than three. Second, when two minds converge on the same point in cognitive space, we call it agreement, not collision''. Each time it agrees, when travels to the same position in belief space (atleast in some of the coordinates). When it disagrees, the distance in belief space increases. Imitative behavior is characterized by a velocity vector whose direction aims at another person's place in belief space.

3) Global-Best PSO Model

The PSO algorithm is one of stochastic swarm intelligence based global search algorithms. The motivation behind the PSO algorithm is the social behavior of birds and fish [49]. In PSO, the particles have (1) adaptable *velocities* that determines their movement in the search space, (2) *memory* which enable them for remembering the best position in the search space ever visited. The position corresponding to the previous best fitness is known as past best, *pbest* and the overall best out of all *NP* the particles in the population is called global best, *gbest*. Consider that the search space is *M*-dimensional and *i*-th particle in the swarm can be represented by $X_i = [x_{i1}, x_{i2}, \ldots x_{id} \ldots, x_{iM}]$ and its velocity can be represented by another *M*-dimensional vector $V_i = [v_{i1}, v_{i2}, \ldots v_{id} .., v_{iM}]$. Let the best previously visited position of *i*-th particle be denoted by $P_i = [p_{i1}, p_{i2}, \ldots p_{id} .., p_{iM}]$, whereas, *g*-th particle, i.e., $P_g = [p_{g1}, p_{g2}, \ldots p_{gd} .., p_{gM}]$, is globally best particle. Figure 3 depicts the vector movement of particle element from location x_{id}^n to x_{id}^{n+1} in *(n + 1)*-th iteration that is being governed by past best, p_{id}^n, global best, p_{gd}^n, locations and current velocity v_{id}^n. Figure 4 depicts the flowchart of PSO Algorithm and discussed as follows:

1. Initialize the population of particles at random positions and velocities. Assign present location and fitness as p_{id} and *pbest* to every particle as starting position and fitness, respectively.

2. For each particle, evaluate its fitness at the present position, x_i.
3. Compare the particle's fitness with *pbest*. If the current fitness value is better, copy it to *pbest* and set p_{id} equal to the current position, x_{id}.
4. Identify the most successful particle in the swarm and store it as p_{gd}.
5. Update the velocity and position of the particle using equations 5 and 6 [44]:

$$v_{id}^{m+1} = \chi(wv_{id}^{m} + \psi_1 r_1(p_{id}^{m} - x_{id}^{m}) + \psi_2 r_2(p_{gd}^{m} - x_{id}^{m})) \quad (5)$$

$$x_{id}^{m+1} = x_{id}^{m} + v_{id}^{m+1} \quad (6)$$

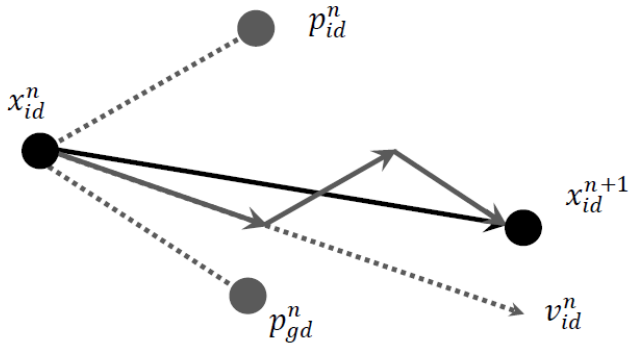

Figure 3. Movement of *i*-th particle in 2-dimensional search space

Here, *w* is inertia weight, ψ_1 is cognitive parameter, ψ_2 is social parameter and constriction factor χ are strategy parameters of PSO algorithm, while r_1, r_2 are random numbers uniformly distributed in the range [0,1]. Generally the inertia weight, *w*, is not kept fixed and is varied as the algorithm progresses. The particle movements is restricted with maximum velocity, $\pm V_{max}$, to avoid jump over the optimal location in the search space.

4) PSO Characterization

There are several parameters that need to be defined in order to successfully utilize PSO to solve a given problem [50]

Solution Encoding: It is a *M*-dimensional vector representation of collection problem feature to be evolved for desired fitness function. This usually involves a minimum and a maximum value allowed in each dimension, thus defining a hyperspace.

Fitness Function: This function is degree of suitability/accepatibility also problem dependent and represents a measurement of a given solution. The function should somehow create a total ranking in the solution.

Population Size: This parameter infuences the behavior of the algorithm. A very small population does not create enough interaction for the emergent behavior pertaining to PSO to occur. However, large population size may lead to more computational burden and consequently, take more evolutionary time. So the population size is to be decided as per the problem size and complexity.

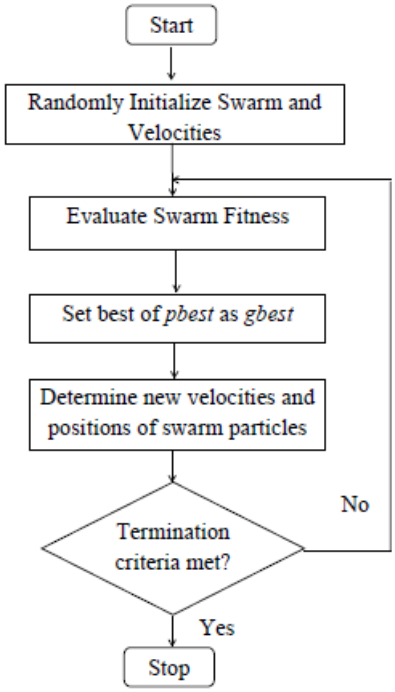

Figure 4. Flow Chart of PSO Algorithm

Acceleration Coefficients: The acceleration coefficients ψ_1 and ψ_2 are usually set to the same value. Infact, people usually talk about which sets the other two values $\psi_1 = \psi_2 = \psi/2$. If is too small, the maximum step size becomes quite small and so the algorithm will explore very slowly and degrade its performance. There is a consensus among the researchers that step size is generally optimal if $\psi = 4.1$, however, not for every problem and every time.

Constriction or Inertia coefficient: It is not necessary to guess its value as given by equation 7. If the value of ψ is set to 4.1, then $\chi \approx 0.729$.

$$\chi = \frac{2k}{2 - \psi - \sqrt{\psi^2 - 4\psi}} \quad (7)$$

$$where\ k = [0,1],\ \psi = \psi_1 + \psi_2,\ \psi > 4$$

Maximum Velocity: With the advent of the constriction coefficient, most researchers do not bother using this parameter. However, to avoid jump overs maximum velocity is fixed to some value less than unity.

Neighborhood Topology: If every particle is made to interact with every other in the swarm, then it becomes prone to fall into local optima. However, this may be avoided if swarm is divided into subgroups and every particle is made to interact with all members of its subgroup.

III. Graded Emigration

In standard migration and its other variants do decide emigrating and immigrating habitats and their SIVs probabilistically. Graded Emigration (GE) is a new migration variant introduced in this paper, where number of SIVs of each emigrating habitat and their SIV number are predecided where to migrate in accordance to with their fitness ranking. In GE the poorest habitat is completely replaced and the best habitat is preserved as it is, whereas the mediocre habitats are

partially modified by sharing fixed number of SIVs from better habitats. The number of migrating SIVs are fixed, however their location is decided randomly.

Example III.1 (Graded Emigration among 10 habitats having 10 SIVs in each habitat). *For Graded Emigration in a population of 10 habitats having 10 SIVs in each habitat following steps are required to be followed:*

1. *Sort habitats in ascending order to their fitness values.*
2. *The last poor habitat constitute a new habitat in the ratio of 4:3:2:1 to replace the poorest in the population.*
3. *Next to the poorest is contributed by 90% by first, second, third and fourth best habitats in the 4:3:2:0.*
4. *Subsequently, the other poorer habitats partially modified by the better habitats as per the matrix given in the Algorithm 6.*

For 20 or 30 habitats the algorithm may be extended by doubling or triplicating the rows of the matrix *X*. Furthur modified clear duplicate opertor is integrated here to increase the exploration ability and thereafter named as GE-EBBO.

IV. Benchmark Functions

There are many benchmark functions [50, 44] which are commonly used to critically test the performance of numeric optimization algorithms. These functions are chosen because of their particularities, which render their optimization difficulties. These comprise (a) multi-modality (b) deceptive gradient information (c) the curse of dimensionality. There are many benchmark test functions like a few of them listed in Table 1 and used in this paper to validate and compare the concept of GE with other variants.

Function Name	Function ($f(\mathbf{x})$)
Dejong/Sphere	$\sum_{i=1}^{n} x_i^2$
Ackley	$20 + e - 20e^{-0.2\sqrt{\frac{\sum_{i=1}^{n} x_i^2}{n}}} - e^{\frac{\sum_{i=1}^{n} \cos 2\pi x_i}{n}}$
Griewank	$1 + \frac{\sum_{i=1}^{n} (x_i - 100)^2}{4000} - \prod_{i=1}^{n} \frac{\cos(x_i - 100)}{\sqrt{i}}$
Rastrigin	$\sum_{i=1}^{n} x_i^2 - 10\cos 2\pi x_i + 10$
Rosenbrock	$\sum_{i=1}^{n-1} 100(x_{i+1} - x_i^2)^2 + (x_i - 1)^2$

Table 1. Benchmark Testbed for various Stochastic Algorithms.

Dejong/Sphere function is very simple and any algorithm capable of numeric optimization should solve it without any problem. It is unimodal function, with global minima located at $x = (0, \ldots, 0)$, with $f(x) = 0$.

Ackley is a multimodal function with many local optima, however global minimum is $f(x) = 0$, is located at $x = (0, \ldots, 0)$. This function is difficult because optimization algorithms can easily be trapped in a local minima on it's way to the global minimization.

Griewank function is strongly multimodal function with significant interaction among its variables, caused by the product term. This function has the interesting property that the number of local minima increases with dimensionality. The global minimum, $x = (100, 100, \ldots, 100)$, yields a function value $f(x) = 0$.

Rastrigin is a multimodal version of the spherical function, characterized by deep local minima arranged as sinusoidal bumps. The global minimum $f(x) = 0$, is located at $x = (0, \ldots, 0)$.

Rosenbrock function variables are strongly dependent and gradient information often misleads algorithms. It's global minimum of $f(x) = 0$ is located at $x = (1, \ldots, 1)$.

Algorithm 6 Standard Pseudo Code for GE-EBBO

$$X[i][j] = \begin{bmatrix} 4 & 3 & 2 & 1 \\ 4 & 3 & 2 & 0 \\ 4 & 3 & 1 & 0 \\ 4 & 3 & 0 & 0 \\ 4 & 2 & 0 & 0 \\ 4 & 1 & 0 & 0 \\ 4 & 0 & 0 & 0 \\ 3 & 0 & 0 & 0 \\ 2 & 0 & 0 & 0 \\ 1 & 0 & 0 & 0 \end{bmatrix}$$

Poor Habitat

Best Habitat

for *i to NP* **do**
for *j*=1 to *X*[*i*][1] **do**
Randomly Select SIV(s) from *NP-th* Habitat and copy to random SIV(*s*) in *i-th* Habitat
end for
for *j*=5 to *X*[*i*][1]+ *X*[*i*][2] **do**
Randomly Select SIV(s) from *(NP-1)-th* Habitat and copy to random SIV(*s*) in *i-th* Habitat
end for
for *j*=8 to *X*[*i*][1]+ *X*[*i*][2]+ *X*[*i*][3] **do**
Randomly Select SIV(s) from *(NP-2)-th* Habitat and copy to random SIV(*s*) in *i-th* Habitat
end for
for *j*=10 to *X*[*i*][1]+ *X*[*i*][2]+ *X*[*i*][3]+ *X*[*i*][4] **do**
Randomly Select SIV(s) from *(NP-3)-th* Habitat and copy to random SIV(*s*) in *i-th* Habitat
end for
end for

V. Antenna Design Parameters

Yagi-Uda antenna consists of three types of wire elements: (a) *Reflector*–biggest among all and is responsible for blocking radiations in one direction. The reflector element is about 5 percent is longer than the feeder element. There is typically only one reflector, adding more reflectors improves performance very slightly. This element is important in determining the front-to-back ratio of the antenna. (b) *Feeder*–which is fed with the signal from transmission line to be transmitted. There is usually just one driven element. A dipole driven element will be resonant when its electrical length is half of the wavelength of the frequency applied to its feed point. and (c) *Directors*–these are usually more then one in number and responsible for unidirectional radiations. The lengths of directors reduces in the direction of radiations and depends upon the director spacing, the number of directors used in the antenna, the desired pattern, pattern bandwidth and

element diameter. Figure 5 depicts a typical six-wire Yagi-Uda antenna where all wires are placed parallel to *x*-axis and along
y-axis. Middle segment of the reflector element is placed at origin, $x = y = z = 0$, and excitation is applied to the middle segment of the feeder element. An incoming field sets up resonant currents on all the antenna elements which reradiate signals. These re-radiated fields are then picked up by the feeder element, that leads to total current induced in the feeder equivalent to combination of the direct field input and the re-radiated contributions from the director and reflector elements.

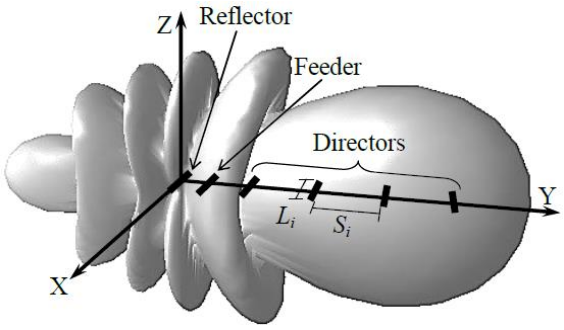

Figure 5. Radiation Pattern of atypical 6-wire Yagi-Uda Antenna

The radiation or antenna pattern describes the relative strength of radiated field in various directions from the antenna at a constant distance. The radiation pattern is also called reception pattern as well, since it also describes the receiving properties of the antenna. The radiation pattern is three-dimensional, however, usually the measured radiation patterns are a two dimensional slice of the three-dimensional pattern in the horizontal and vertical planes. These pattern measurements are presented in either a rectangular or a polar format. A polar format of the gain versus orientation (radiation pattern) is useful when characterizing antennas. Some other important features of antenna that appears on plot are:

1. Forward Gain: Forward gain is the ability of an antenna to focus energy in a particular direction while transmitting/receiving energy better to/from a particular direction. To determine the gain or directivity of an antenna, a reference antenna is used to compare antenna performance. Forward gain is expressed in decibel (dB) relative to an isotropic source or a standard dipole in direction of maximum gain. Typically, higher the gain, more the efficient antenna performance and longer the range of the antenna will operate. Radiation pattern of a typical six-elements Yagi-Uda antenna is depicted in Figure 5.
2. Front to Back ratio: The Front to Back ratio is used in describing directional radiation patterns for antennas. If an antenna radiates maximum in one direction, the F/B ratio is the ratio of the gain in the maximum direction to that in the opposite direction (180 degrees from the specified maximum direction) ans is also expressed in dB.
3. Beamwidth: Beamwidth is the angle between directions where the power is half the value at the direction of maximum gain which is -3dB. It gives the measure of directivity of antenna
4. Sidelobes: Antenna is not able to radiate all the energy in one preferred direction because some part of energy is inevitably radiated in other directions. Sidelobes are unwanted peaks in the gain at angles other than in forward direction, they reduce the amount of useful energy contained in the forward direction. The peaks are referred to as side lobes, as shown in Figure 5, and commonly specified in dB down from the main lobe.

Other characteristics that do not appear on the polar plot but which are equally important are:
1. Bandwidth: Bandwidth is the range of frequency over which the antenna exhibits acceptable characteristics.
2. Radiative impedance: For an efficient transfer of energy, the radiative impedance of the antenna and transmission cable connecting them must be the same. Transceivers and their transmission lines are typically designed for 50Ω resistive impedance. If the antenna has an impedance different from 50Ω then there is a mismatch and an impedance matching circuit is required to avoid signal loss.
Designing a Yagi-Uda antenna involves determination of wire-lengths and wire-spacings in between to get maximum gain, desired impedance and minimum SLL at an arbitrary frequency of operation. An antenna with N elements requires $2N - 1$ parameters, i.e., N wire lengths and $N - 1$ spacings, that are to be determined. These $2N - 1$ parameters, collectively, are represented as a string vector referred as a habitat in BBO or particle in PSO given as (8).

$$H = [L_1, L_2, \ldots, L_N, S_1, S_2, \ldots, S_{N-1}] \quad (8)$$

where L_s are the lengths and S_s are the spacing of antenna elements.

VI. Simulation Results and Discussions

Simulation results by testing with benchmark functions and its convergence performance on Yagi-Uda antenna is explained in the following subsections:

A. Testing with Benchmark Functions

A testbed of benchmark functions is used to test the proposed algorithm of GE-EBBO and compared with the results of other migration variants of BBO are tabulated in Table 2.

To provide similar platform for comparitive study parameters used are:

1. Population size: 20
2. Number of SIV's: 10
3. Search space of f(x) : $-2 \leq x \leq 2$
4. Number of Iterations: 10000
5. Number of Monte-Carlo simulations per experiment: 10

In Figure 6, 7 GE-EBBO optimizes faster as compared to other stochastic algorithms. EBBO gives poor results followed by IRBBO, BBO and Blended.
In Figure 8, GE-EBBO and EBBO gives almost same results. Initially, EBBO converges faster. But with increase in iterations, GE-EBBO performs almost equal to EBBO.

In Figure 9, Initially, GE-EBBO converges slowly than other algorithms. But with increase in number of iterations, GEEBBO performs better than all other algorithms.

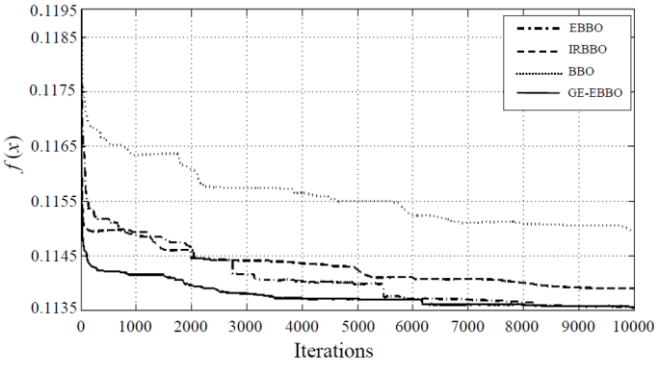

Figure 6. Performance of various Stochastic Algorithms using Ackley

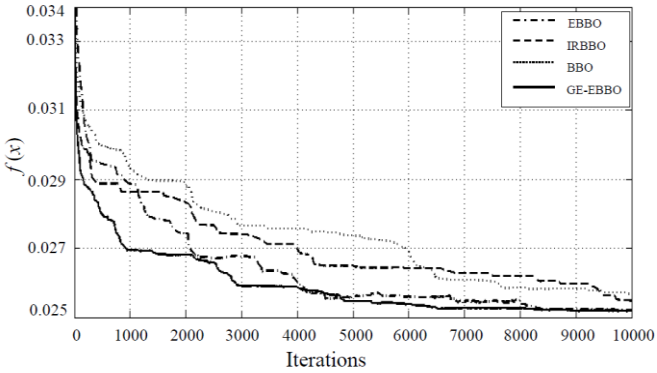

Figure 7. Performance of various Stochastic Algorithms using Dejong

In Figure 10, At initial stage GE-EBBO does not perform upto mark but with increase in iterations at 3000-4000 the performance increases and approaches almost to the performance of IRBBO which gives best results.
Figures 6, 7, 8, 9 concluded that GE-EBBO outperforms all other algorithms. Average of 10 Monte Carlo simulations runs is depicted in Table 2. Here the minimization approach has been taken by taking the overall average of all test functions.

B. Convergence Performance for Yagi-Uda Antenna

Six-wire Yagi-Uda antenna designs are optimized for gain using BBO, EBBO, PSO and GE-EBBO algorithms are investigated. Average of 10 monte-carlo evolutionary runs for each algorithm are plotted here for investigation in Figure 11. The C++ programming platform is used for coding of optimization algorithms, whereas, a method of moments based software named as Numerical Electromagnetics Code (NEC) [51] is used for evaluation of antenna designs. Each potential solution in BBO is encoded as vector with 11 SIVs as given by equation (8) and shown in Figure 5. The universe of discourse for the search of optimum values of wire lengths and wire spacings are fixed at 0.40λ - 0.50λ and 0.10λ - 0.45λ, respectively, however, cross sectional radius and segment sizes are kept same for all elements, i.e., 0.003397λ and 0.1λ respectively, where λ is the wavelength corresponding to frequency of operation, i.e, 300 MHz. Excitation is applied to the middle segment of driven element and location of middle segment of the reflector element is always kept at $x = 0$.

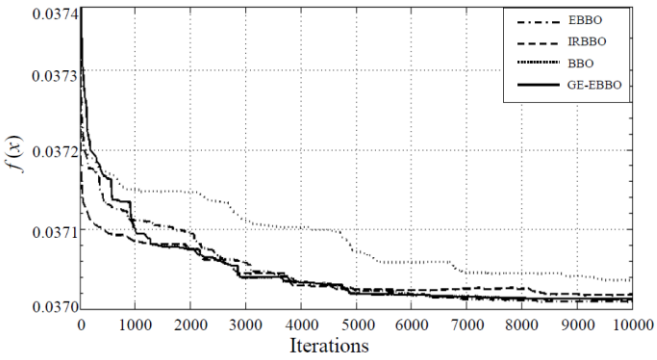

Figure 8. Performance of various Stochastic Algorithms using Griewank

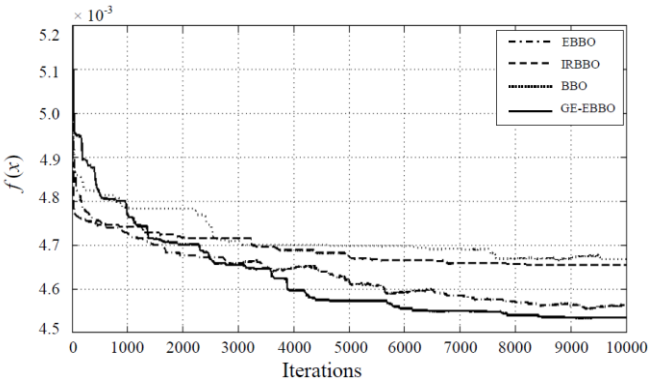

Figure 9. Performance of various Stochastic Algorithms using Rastrigin

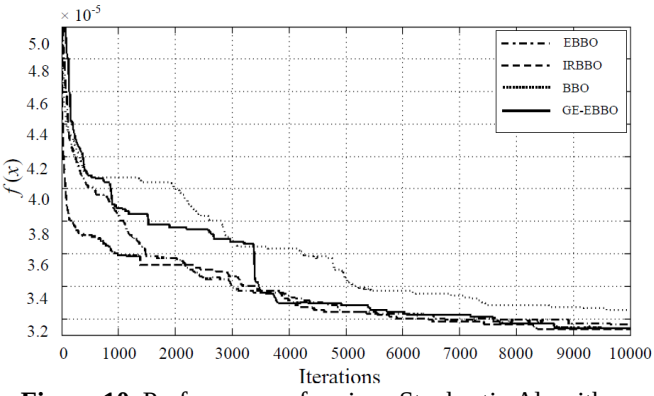

Figure 10. Performance of various Stochastic Algorithms using Rosenbrock

Test Functions	BBO	IRBBO	EBBO	Blended	GE-EBBO
Ackley	0.1149567	0.1139057	0.1135618	0.1211875	**0.1135563**
Dejong	0.0256786	0.0254857	0.0252104	0.0286977	**0.0251785**
Griewank	0.0370556	0.0370368	**0.0370287**	0.0371918	0.0370322
Rastrigin	0.0046668	0.0046538	0.0045540	0.0052622	**0.0045334**
Rosenbrock	0.0000325	**0.0000313**	0.0000316	0.0000414	0.0000314
Overall Average	**0.0364780**	**0.0362226**	**0.0360773**	**0.0384761**	**0.0360663**

Table 2. Result obtained by testing on Benchmark Testbed

The parameters used in experiments are:

1. No. of Habitats or population: *NP* = 30
2. Generations: 50
3. No. of SIVs per habitat: 11
4. Mutation range: ±1%
5. Maximum migration rates *E* = 1 and *I* = 1

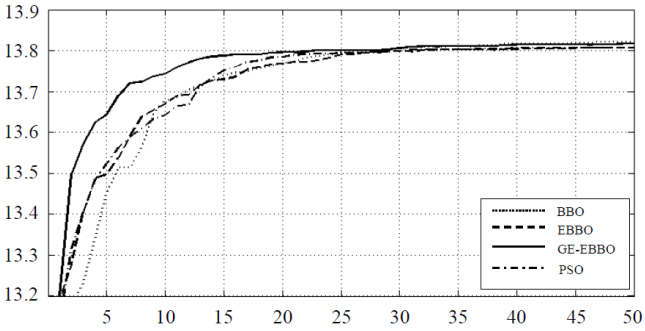

Figure 11. Convergence Performance of BBO, EBBO, GE-EBBO and PSO

Here, mutation range is the percentage of SIV's that adds to the randomly selected SIVs to increase the exploration of search space. Typically, the best antenna designs obtained during process of optimization are tabulated in Table 3. Figure 11 concludes that GE-EBBO is performing best among all optimization algorithms. Though EBBO converges faster than BBO, but performs in comparison to PSO.

The reason for GE-EBBO's best performance is the exploitation on less fit habitats, whereas less exploitation on high fit habitats and then the modified clear duplicate operator is furthur integrated to increase the diversity.

Stochastic algorithms	Element	1(λ)	2(λ)	3(λ)	4(λ)	5(λ)	6(λ)	Gain(dBi)	Z(Ω)
BBO	Length	0.4875	0.4884	0.4400	0.4233	0.4217	0.4233	**13.84**	**4.09+j54.53**
	Spacing	-	0.1503	0.2571	0.4087	0.3932	0.4095		
EBBO	Length	0.4827	0.4735	0.4424	0.4259	0.4201	0.4256	**13.83**	**5.23+j31.59**
	Spacing	-	0.2255	0.2160	0.3889	0.4181	0.3911		
GE-EBBO	Length	0.4842	0.4910	0.4425	0.4253	0.4181	0.4270	**13.84**	**4.47+j59.63**
	Spacing	-	0.1778	0.2381	0.3918	0.4212	0.3870		
PSO	Length	0.4872	0.4944	0.4423	0.4272	0.4194	0.4276	**13.85**	**3.83+j62.16**
	spacing	-	0.1597	0.2420	0.3857	0.4190	0.3841		

Table 3. The Best Results obtained during Gain Optimization

VII. Conclusions and Future Scope

In this paper, Experimental Analysis shows that GE-EBBO gives comparitively better results than various stochastic algorithms discussed here, when applied on testbed of benchmark functions and to optimize six-element Yagi-Uda antenna designs for gain maximization. GE-EBBO solves the global optimization problem with faster convergence rate because of high exploitation and performs better. Reasons for poor performance of PSO include use of global best PSO model where each particle learns from every other and *gbest*. This may lead to be trapped into local optima. Our future agenda is to apply GE-EBBO on various real time applications

and to investigate it's performance by influencing the population size and search space to get better results. It can also be explored for multi-objective optimization of different antenna as well.

References

[1] S. Uda and Y. Mushiake, *Yagi-Uda Antenna*. Research Institute of Electrical Communication, Tohoku University, 1954.

[2] H. Yagi, "Beam Transmission of Ultra Short Waves," *Proceedings of the Institute of Radio Engineers*, vol. 16, no. 6, pp. 715–740, 1928.

[3] D. G. Reid, "The Gain of an Idealized Yagi Array," *Journal of the Institution of Electrical Engineers-Part IIIA: Radiolocation*,, vol. 93, no. 3, pp. 564–566, 1946.

[4] J. Bojsen, H. Schjaer-Jacobsen, E. Nilsson, and J. Bach Andersen, "Maximum Gain of Yagi–Uda Arrays," *Electronics Letters*, vol. 7, no. 18, pp. 531–532, 1971.

[5] D. K. Cheng, "Optimization Techniques for Antenna Arrays," *Proceedings of the IEEE*, vol. 59, no. 12, pp. 1664–1674, 1971.

[6] L. C. Shen, "Directivity and Bandwidth of Single-band and Double-band Yagi Arrays," *IEEE Transactions on Antennas and Propagation*,, vol. 20, no. 6, pp. 778–780, 1972.

[7] D. Cheng and C. Chen, "Optimum Element Spacings for Yagi-Uda Arrays," *IEEE Transactions on Antennas and Propagation*,, vol. 21, no. 5, pp. 615–623, 1973.

[8] C. Chen and D. Cheng, "Optimum Element Lengths for Yagi-Uda Arrays," *IEEE Transactions on Antennas and Propagation*,, vol. 23, no. 1, pp. 8–15, 1975.

[9] D. K. Cheng, "Gain Optimization for Yagi-Uda Arrays," Antennas and Propagation Magazine, IEEE, vol. 33, no. 3, pp. 42–46, 1991.

[10] E. A. Jones and W. T. Joines, "Design of Yagi-Uda Antennas using Genetic Algorithms," *IEEE Transactions on Antennas and Propagation*,, vol. 45, no. 9, pp. 1386–1392, 1997.

[11] H. J. Wang, K. F. Man, C. H. Chan, and K. M. Luk, "Optimization of Yagi array by Hierarchical Genetic Algorithms," *IEEE*, vol. 1, pp. 91–94, 2003.

[12] N. Venkatarayalu and T. Ray, "Optimum Design of Yagi-Uda Antennas Using Computational Intelligence," *IEEE Transactions on Antennas and Propagation*,, vol. 52, no. 7, pp. 1811–1818, 2004.

[13] S. Baskar, A. Alphones, P. N. Suganthan, and J. J. Liang, "Design of Yagi-Uda Antennas using Comprehensive Learning Particle Swarm Optimisation," *IEEE*, vol. 152, no. 5, pp. 340–346, 2005.

[14] J. Y. Li, "Optimizing Design of Antenna using Differential Evolution," *IEEE*, vol. 1, pp. 1–4, 2007.

[15] U. Singh, M. Rattan, N. Singh, and M. S. Patterh, "Design of a Yagi-Uda Antenna by Simulated Annealing for Gain, Impedance and FBR," *IEEE*, vol. 1, pp. 974–979, 2007.

[16] U. Singh, H. Kumar, and T. S. Kamal, "Design of Yagi-Uda Antenna Using Biogeography Based Optimization," *IEEE Transactions on Antennas and Propagation*,, vol. 58, no. 10, pp. 3375–3379, 2010.

[17] R. M. Fishenden and E. R. Wiblin, "Design of Yagi Aerials," *Proceedings of the IEE-Part III: Radio and Communication Engineering*, vol. 96, no. 39, p. 5, 1949.

[18] H. Ehrenspeck and H. Poehler, "A New Method for Obtaining Maximum Gain from Yagi Antennas," *IRE*

Transactions on Antennas and Propagation,, vol. 7, no. 4, pp. 379–386, 1959.

[19] E. Altshuler and D. Linden, "Wire-antenna Designs using Genetic Algorithms," *Antennas and Propagation Magazine, IEEE*, vol. 39, no. 2, pp. 33–43, 1997.

[20] D. Correia, A. J. M. Soares, and M. A. B. Terada, "Optimization of gain, impedance and bandwidth in Yagi-Uda Antennas using Genetic Algorithm," *IEEE*, vol. 1, pp. 41–44, 1999.

[21] N. V. Venkatarayalu and T. Ray, "Single and Multi-Objective Design of Yagi-Uda Antennas using Computational Intelligence," *IEEE*, vol. 2, pp. 1237–1242, 2003.

[22] Y. Kuwahara, "Multiobjective Optimization Design of Yagi-Uda Antenna," *IEEE Transactions on Antennas and Propagation,*, vol. 53, no. 6, pp. 1984–1992, 2005.

[23] D. Simon, "Biogeography-based Optimization," *IEEE Transactions on Evolutionary Computation,*, vol. 12, no. 6, pp. 702–713, 2008.

[24] M. Rattan, M. S. Patterh, and B. S. Sohi, "Optimization of Yagi-Uda Antenna using Simulated Annealing," *Journal of Electromagnetic Waves and Applications*, 22, vol. 2, no. 3, pp. 291–299, 2008.

[25] S. Singh, S. Tayal, and G. Sachdeva, "Evolutionary performance of bbo and pso algorithms for yagi-uda antenna design optimization," *IEEE*, pp. 861–865, 2012.

[26] S. Singh and G. Sachdeva, "Mutation effects on bbo evolution in optimizing yagi-uda antenna design*," in Third International Conference on Emerging Applications of Information Technology (EAIT 2012)*, Kolkata, India, November-December 2012.

[27] ——, "Yagi-uda antenna design optimization for maximum gain using different bbo migration variants," International Journal of Computer Applications, vol. 58, no. 5, pp. 1–5, 2012.

[28] S. Singh, E. Mittal, and G. Sachdeva, "Nsbbo for gain impedance optimization of yagi-uda antenna design," *in Information and Communication Technologies (WICT)*, 2012 World Congress on. IEEE, 2012, pp. 856–860.

[29] S. Singh, Shivangna, and S. Tayal, "Analysis of different ranges for wireless sensor node localization using pso and bbo and its variants," *International Journal of Computer Applications*, vol. 63, no. 22, pp. 31–37, February 2013, published by Foundation of Computer Science, New York, USA.

[30] S. Singh, Shivangna, and E. Mittal, "Range based wireless sensor node localization using pso and bbo and its variants," 2013.

[31] S. Singh, E. Mittal, and S. Tayal, "Evolutionary performance comparison of bbo and pso variants for yagi-uda antenna gain maximization," in *National Conference on Contemporary Techniques & Technologies in Electronics Engineering*, 2013.

[32] S. Singh, Shivangna, and E. Mittal, "Performance of pso with different ranges for wireless sensor node localization," in *National Conference on Contemporary Techniques & Technologies in Electronics Engineering*, Murthal, Sonepat, India, March 2013.

[33] S. Singh, S. Tayal, E. Mittal, and Shivangna, "Evolutionary performance of graded emigration in bbo for yagi-uda antenna design optimization," *CiiT International Journal of Programmable Device Circuit and Systems*, April 2013, ciiT International Journal

[34] S. Singh, E. Mittal, and G. Sachdeva, "Multi-objective gain-impedance optimization of yagi-uda antenna using nsbbo and nspso," *International Journal of Computer Applications*, vol. 56, no. 15, pp. 1–6, October 2012, published by Foundation of Computer Science, New York, USA.

[35] D. Du, D. Simon, and M. Ergezer, "Biogeography based Optimization Combined with Evolutionary Strategy and Immigration Refusal," *IEEE*, vol. 1, pp. 997–1002, 2009.

[36] S. S. Pattnaik, M. R. Lohokare, and S. Devi, "Enhanced Biogeography-Based Optimization using Modified Clear Duplicate Operator," *IEEE*, vol. 1, pp. 715–720, 2010.

[37] H. Ma and D. Simon, "Biogeography-based optimization with blended migration for constrained optimization problems," *in Proceedings of the 12th annual conference on Genetic and evolutionary computation*. ACM, 2010, pp. 417–418.

[38] ——, "Blended Biogeography-based Optimization for Constrained Optimization," *Engineering Applications of Artificial Intelligence*, vol. 24, no. 3, pp. 517–525, 2011.

[39] C. Darwin, "On the origins of species by means of natural selection," *London: Murray*, 1859.

[40] A. R. Wallace, *The geographical distribution of animals: With a study of the relations of living and extinct faunas as elucidating the past changes of the earth's surface*. Cambridge University Press, 1876, vol. 1.

[41] C. Darwin, *On the Origin of Species: A Facsimile.* Harvard University Press, 1964.

[42] R. MacArthur and E.Wilson, *The Theory of Island Biogeography*. Princeton Univ Pr, 1967.

[43] R. Eberhart, Y. Shi, and J. Kennedy, *Swarm Intelligence*. Morgan Kaufmann Publisher, 2001.

[44] Y. Shi and R. Eberhart, "Empirical Study of Particle Swarm Optimization," in *Evolutionary Computation, 1999. CEC 99. Proceedings of the 1999 Congress on*, vol. 3. IEEE, 1999.

[45] J. Kennedy and R. Eberhart, "Particle swarm optimization," in *Neural Networks, 1995. Proceedings., IEEE International Conference on*, vol. 4. IEEE, 1995, pp. 1942–1948.

[46] Y. Shi et al., "Particle Swarm Optimization: Developments, Applications and Resources," *in Evolutionary Computation, 2001. Proceedings of the 2001 Congress on*, vol. 1. IEEE, 2001, pp. 81–86.

[47] F. Heppner and U. Grenander, "A stochastic nonlinear model for coordinated bird flocks." *AMERICAN ASSOCIATION FOR THE ADVANCEMENT OF SCIENCE, WASHINGTON, DC(USA)*. 1990., 1990.

[48] C. W. Reynolds, "Flocks, herds and schools: *A distributed behavioral model*," vol. 21, no. 4, pp. 25–34, 1987.

[49] K. Parsopoulos and M. Vrahatis, "Recent Approaches to Global Optimization Problems through Particle Swarm Optimization," *Natural computing*, vol. 1, no. 2, pp. 235–306, 2002.

[50] R. Mendes, "Population topologies and their influence in particle swarm performance," 2004.

[51] G. J. Burke and A. J. Poggio, "Numerical Electromagnetics Code (NEC) method of moments," *NOSC Tech. DocLawrence Livermore National*

Laboratory, Livermore, Calif, USA, vol. 116, pp. 1–131, 1981.

Author Biographies

Shelja Tayal was born on Oct 14, 1989. She received her Bachelor's degree (B.Tech.) from Lala Lajpat Rai Institute of Engineering & Technology (Moga) in year 2011 and presently she is a research scholar in Shaheed Bhagat Singh State Technical Campus (formerly, SBS College of Engineering & Technology), Ferozepur, Punjab (India) with specialization in Electronics & Communication Engineering. She has published and communicated many papers in International/National Journals and Conferences. Her research interests include Artificial Intelligence, Evolutionary Algorithms and Antenna design optimization.

Dr. Satvir Singh was born on Dec 7, 1975. He received his Bachelors degree (B.Tech.) from Dr. B. R. Ambedkar National Institute of Technology, Jalandhar, Punjab (India) with specialization in Electronics & Communication Engineering in year 1998, Masters degree (M.E.) from Delhi Technological University (Formerly, Delhi College of Engineering), Delhi (India) with distinction in Electronics & Communication Engineering in year 2000 and Doctoral degree (Ph.D.) from Maharshi Dayanand University, Rohtak, Haryana (India) in year 2011. During his 13 years of teaching experience he served as Assistant Professor and Head, Department of Electronics & Communication Engineering at BRCM College of Engineering & Technology, Bahal, (Bhiwani) Haryana, India and as Associate Professor & Head, Department of Electronics & Communication Engineering at Shaheed Bhagat Singh State Technical Campus (Formerly, SBS College of Engineering & Technology), Ferozepur Punjab, India.
His fields of special interest include Evolutionary Algorithms, High Performance Computing, Type-1 & Type-2 Fuzzy Logic Systems, Wireless Sensor Networks and Artificial Neural Networks for solving engineering problems. He is active member of an editorial board of International Journal of Electronics Engineering and published nearly 30 research papers in International Journals and Conferences. He has delivered nearly 20 Invited Talks during National and International Conferences, Seminar, Short Term Courses and Workshops. He completed two AICTE funded projects under MODROB Scheme worth 15 Lacs. He has also conducted four Faculty Development Programmes, of total duration of six weeks, around Soft Computing techniques under various schemes of AICTE and TEQIP.

Gagan Sachdeva was born on Oct 4, 1988. He received his Bachelors degree (B.Tech.) and Masters degree (M.Tech.) from Shaheed Bhagat Singh State Technical Campus (formerly, SBS College of Engineering & Technology), Ferozepur, Punjab (India) with specialization in Electronics & Communication Engineering in year 2010 and 2012, respectively. He is presently with Rayat Bahra Group of Institutes, Mohali Campus as Assistant Professor in the department of ECE. His research interests include Evolutionary Algorithms, Antenna design optimization, and Wireless Sensor Networks.

CMS Tool: Calculating Defect and Change Data from Software Project Repositories

Ruchika Malhotra
Department of Software Engineering
Delhi Technological University, Delhi, India
+91-9910290445
ruchikamalhotra2004@yahoo.com

Anushree Agrawal
Department of Software Engineering
Delhi Technological University, Delhi, India
+91-7827858115
anushreeagrawal.iet@gmail.com

ABSTRACT
Defect and change prediction is a very important activity in software development. Predicting erroneous classes of the system early in the software development life cycle will enable early identification of risky classes in the initial phases. This will assist software practitioners in designing and developing software systems of better quality with focused resources and hence take necessary corrective design actions. In this work we describe a framework to develop and calculate the defect fixes and changes made during various versions of a software system. We develop a tool, Configuration Management System (CMS), which uses log files obtained from a Concurrent Versioning System (CVS) repository in order to collect the number of defects from each class. The tool also calculates the number of changes made during each version of the software. This tool will also assist software practitioners and researchers in collecting defect and change data for software systems.

Categories and Subject Descriptors
D.2 [Software Engineering]: D.2.8 Metrics, D.4.8 Performance

General Terms
Measurement, performance, reliability.

Keywords
Change prediction, defect prediction, Software project repositories, CVS.

1. INTRODUCTION
Software Quality is defined as "The problem inherent in attempts to define the quality of a product, almost any product. The difficulty in defining quality is to translate future needs of the user into measurable characteristics, so that a product can be designed and turned out to give satisfaction at a price that the user will pay. This is not easy, and as soon as one feels fairly successful in the endeavor, he finds that the needs of the consumer have changed, competitors have moved in, etc. [19]". Changes are inherent in a software system and hence development processes should be well managed to accommodate those changes as and when needed to compete in the industry. Hence it is important to be correct in all kinds of estimates related to the software development life cycle and continuously improve the development process. In order to improve, we must be familiar with the current process, and continuously analyze, measure and monitor it. This helps in identifying and measuring the weaknesses as well as in process improvement by giving a better understanding of the solution. This approach is appropriate for iterative software development, where the analysis results of previous releases can be applied to subsequent releases in order to optimize the development and testing of upcoming releases. The cost estimation and project planning accuracy highly depends on the accuracy of prediction results. Thus early change and defect prediction helps the project team to develop good quality products with fewer defects and less effort. The quality of software is directly related to the number of defects and changes in the software product. Hence change and defect prediction is very important in this field [7].

For a quality prediction model, we need metric data as well as defect data as input to the model. We need tools to calculate this data. A lot of testing tools are available freely on the internet for researchers to calculate metric data, but calculating defect data is tedious due to lack of appropriate tools for defect data collection and most of defect data needs to be calculated manually. In this work, we describe a tool CMS for defect prediction which calculates the defect data from the logs obtained via various CVS commands from the CVS repository of the project under study. Here we have considered an object oriented approach and calculated the defect data for each class separately. CMS compares every pair of comparable classes in two versions and produces a change report. Both the generated reports i.e. change report as well as defect report are quantitative measures of the number of changes and number of defects in each class. This data will be used to predict the defect and change prone classes of the software and hence further change and maintenance of the software can be done more efficiently by handling all defect prone classes with care.

The rest of the paper is organized as follows: section 2 presents the related work in this field, section 3 describes in detail our proposed tool, section 4 shows the change and defect results of the software under study and section 5 presents our conclusions from the study.

2. RELATED WORK
A lot of research has been carried out in the area of change data collection and defect data collection. Chidamber and Kimerer initially proposed object-oriented metrics, which measure software quality attributes [9]. Pooley et al. developed a web based project metric system for collecting and analyzing web based project metrics [10]. Zimmermann et al. collected defects for open source software, eclipse in their work "Predicting Defects for Eclipse" [11]. A tool named Duo Tracker presented by Akinwale et al. also allows collecting defect information [12]. Research has been done in searching and analyzing defect tracking data from the web using semantic techniques [13]. Support Vector Machines are also proposed for early defect prediction in software systems [14].

Change data helps in the efficient maintenance of software systems. Calculation of change data also helps in predicting software quality models. A lot of research has been carried out to calculate change data. A change oriented framework for software configuration management in "A Change-Oriented Conceptual Framework Of Software Configuration Management" [15] is a study that can be applied to various development approaches for improving service management. Faults in software can also be predicted by studying the change history as numerous new faults arise when changes are made in software [16]. Complexity of software systems is increasing and user needs change frequently, hence change control is important in software quality management [17]. The object oriented approach is followed in most of

DOI: 10.1145/2557833.2557849 http://doi.acm.org/10.1145/2557833.2557849

the software systems now a days. Hence change data should also be collected in a similar manner [18]. Defect and change data should be collected accurately to maintain quality in software systems.

3. CMS PROCESS

A lot of researches has been done in the past and are still going in the area of software quality and defect prediction and solutions provided in these researches require past data for learning. These solutions need project specific metric data and defect data, which is obtained from the source code and environment. In this work we have used "diff" to differentiate between source files and CVS commands to obtain logs from CVS repositories. Figure 1 gives an overview of the CMS process.

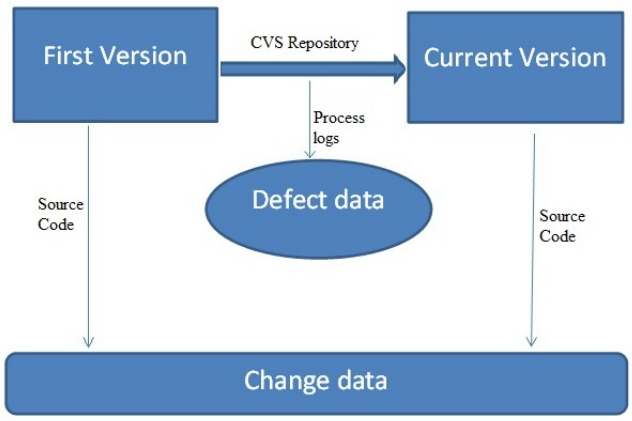

Figure 1: Change data and defect data collection process

3.1 About the diff command

The diff command takes two files as input for comparison and attempts to change the first file such that it appears identical to the second file. For this, it changes (c) or deletes (d) the lines of the first file. It may also append (a) lines from second file to the first file [3]. It follows the steps listed below to produce the difference

- The first line of both files is checked. If they do not match then it keeps on travelling down the first file, until a similar line in the second file is encountered. If the first line of second file is absent in the first file it marks this as change or append. If the line is found then intermediate lines are marked as deleted.
- If the two lines match, then it does nothing.

3.2 About CVS

Concurrent Versioning System or CVS is a central repository where code and associated metadata is kept. CVS is used in the software development lifecycle to maintain code consistency and co-ordination in development teams [5].

A CVS client program is needed to access the CVS repository. We used the CVS client tortoiseCVS that runs on the Microsoft Windows platform. The source code is freely available at http://www.sourceforge.net.

3.3 Calculation of Defects

Step 1 CVS checkout: first we need to check out the code from the CVS repository and make a local working copy of the software under study. This is done using the following CVS command:

CVS -z3 -d:pserver:username@CVS-url co -P module-name"

Step 2 Fetching logs: logs are fetched from the repository, once the checkout is made. These logs contain information about all the versions of each file, comments made by developers during check in of code and hence the defects and defect fixing information. Log files can be obtained using the below CVS command:

CVS -d:pserver:username@CVS-url log filename

Step 3 Processing logs: the log files contain all the meta-data of the source code. This is useful in extraction of defect information. The keywords "bug" and "fix" are used by developers in logs to indicate defects that are found or fixed. Counting the frequency of these keywords gives an estimate of the number of defects in each class. This also means that only the defects which were found and fixed are being considered.

After studying various projects, we observed the following difficulties and we have tackled them with the following assumption:
For software developed in the java language, each file may contain one or more classes, but it contains one class with same name as the filename. Defects are counted for each file of the software and we have assigned a defect count to the class with same name as filename [6].

3.4 Calculation of Change prone classes

Step 1 Preprocessing of source files: the source files contain executable statements and comments. To obtain the correct number of changes in files, we need to identify useful statements of the source file. Hence some preprocessing is required in order to obtain the correct results i.e count of added, deleted and modified lines. Rules for counting and preprocessing are as follows:

- Comment lines and blank lines are not considered for comparing changes.
- Changes or additions of import statements are not taken into account.
- Class names should not contain "?", "(", ")" or "/".
- Rules for counting the added, deleted and changed lines are the standard rules of the diff command for counting the added, deleted and changed lines.

Step 2 Applying diff: after application of above rules, preprocessing of all source files is done. We consider only those files with the same name in both versions. Then diff command is run for same files of both the versions. For two files file1.java in version 1 and file2.java in version 2, we run the diff command as:

"diff [options] file1.java file2.java"

The diff command compares the contents of the two files and returns the results back to the calling function. The results are calculated by counting the added, deleted and changed lines for each class [8]. The total change in a class is calculated as:

Total change= added lines + deleted lines + (2 * modified lines)

Here the change for modified lines is twice that of added and deleted lines because each modification requires a deletion followed by an addition.

Figure 2 shows the diagrammatic representation of the steps involved in the CMS process.

DOI: 10.1145/2557833.2557849 http://doi.acm.org/10.1145/2557833.2557849

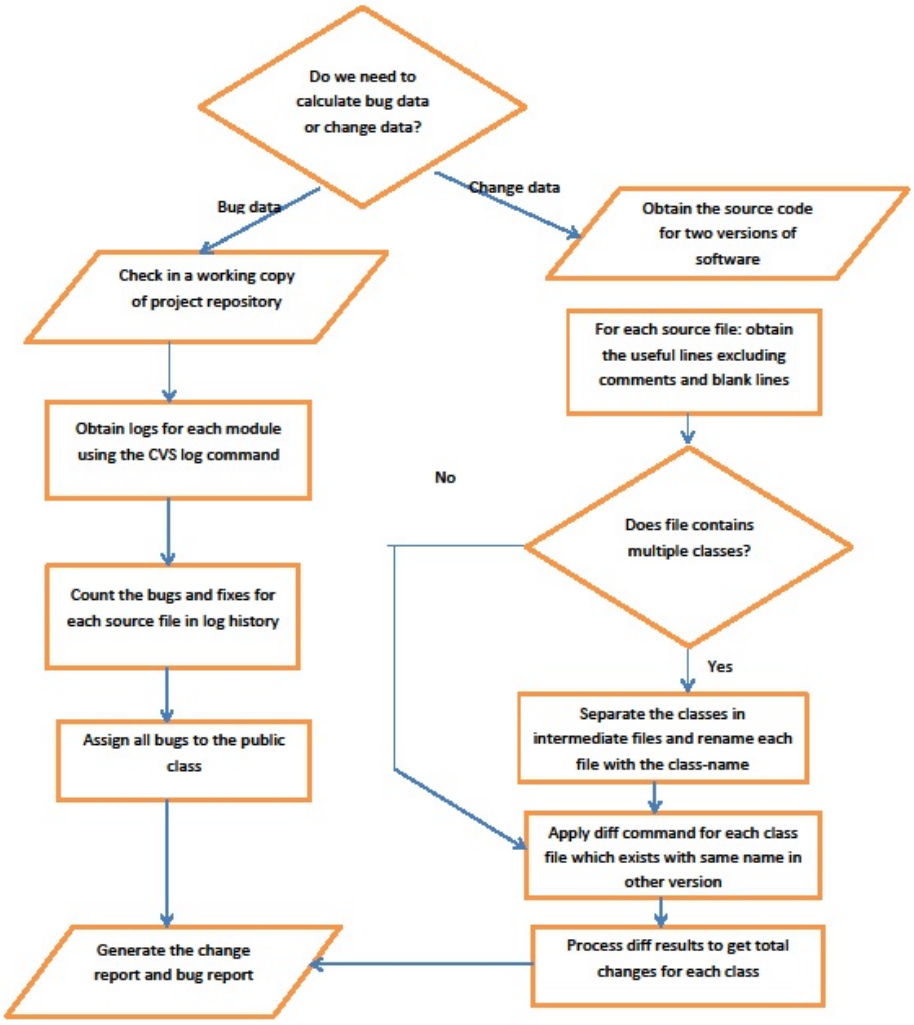

Figure 2: Steps to calculate defect and change data

4. RESULTS

We have computed the defect and change prone classes for the application "Jtreeview". For this purpose, we have taken two versions of jtreeview, whose source code is freely available at http://www.sourceforge.net. Jtreeview is an open source, cross platform Gene Expression Visualization Tool developed in Java which renders gene expression data into several interactive views. The main treeview application considers these views interchangeable, and it is possible to define additional views. This capability will be exploited to speed development of new programs [1].

We have used two releases of the software for evaluation:

First Version : Jtreeview v 1.0.0 (15-10-2003)

Current version : Jtreeview v 1.1.6r2 (30-8-2011)

Table 1 shows the characteristics of the project under study.

Version	Programming language	Developed in	Number of files
1.0.0	Java	2003	229
1.1.6r2	Java	2011	235

Table 1 : Characteristics of used project

4.1 Change analysis

CMS takes two versions of software as input and computes the number of added, deleted and modified lines for all the comparable classes. CMS provides a graphical user interface to give inputs and obtain the output. While considering the Java program files, one file may contain more than one class. CMS considers all these classes individually and computes the result for each class separately. It also counts the total number of added and deleted classes . Table 2 shows the distribution of change for jtreeview. Total Number of added classes: 308 and total Number of deleted classes: 234. Figure 3 is screenshot of the CMS tool for change calculation. Figure 4 shows the page of the CMS tool which provides the change report to be saved. Figure 5 shows the distribution of change count where different colors are used to represent the percentage distribution of change count in classes. Here 42% of the classes have no change and 37% of the classes have change counts ranging from 1 to 50, 6% of classes have change count from 50 to 100, 9% from 100 to 200 and 5% of total classes have change count greater than 200.

DOI: 10.1145/2557833.2557849 http://doi.acm.org/10.1145/2557833.2557849

Changes	0	1-50	50-100	100-200	200-inf
No of classes	41	36	6	9	5

Table 2: Distribution of change count

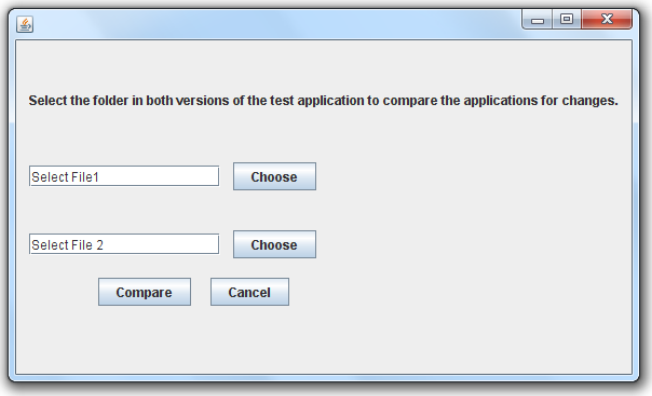

Figure 3: Change calculation

4.2 Defect Analysis

We use log files from the CVS repository of the project, which is fetched via the TortoiseCVS client program. The log file is then analyzed for defects and fixes during the particular release. Figure 4 is a screenshot of the CMS dialog used to obtain logs from the CVS repository. Table 3 shows the distribution of defect counts. Figure 6 shows the defect distribution, where different colors are used to represent the percentage distribution of defect counts in classes. Here 8% of the classes are defect free with zero defects. The major share is of the classes which have a defect count between 1 and 5 which is 84 % of the total classes. 5 % of the classes contain a defect count from 6 to 10 while the percentage of classes with the highest number of defects (in this case greater than 11) is 3% of the total number of classes.

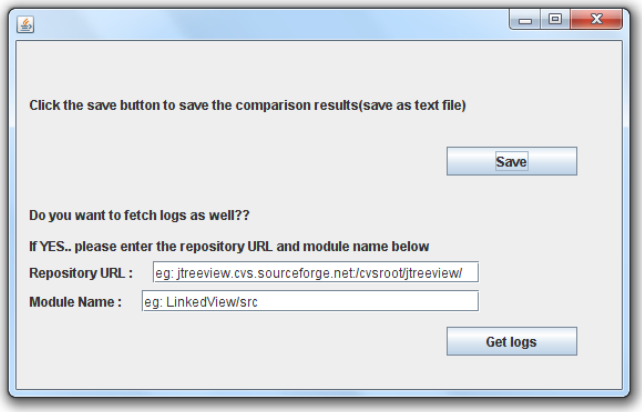

Figure 4: Save change report and defect calculation in CMS

Defect Count	0	1-5	6-10	11-inf
No. of Classes	22	222	14	7

Table 3: Distribution of defect count

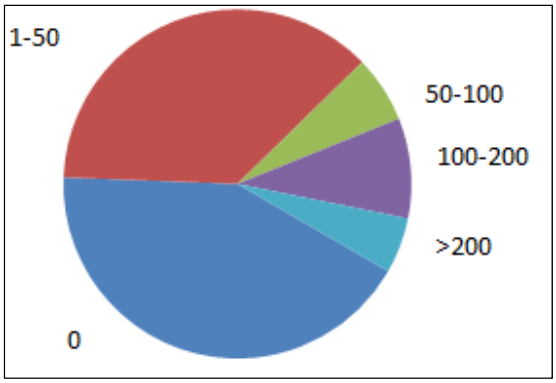

Figure 5: Change distribution

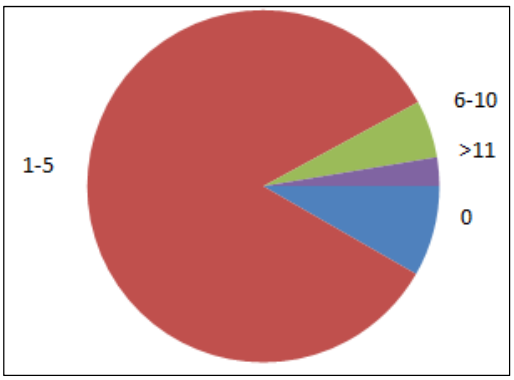

Figure 6: Defect Distribution

CMS works only for software developed in Java and whose repository is maintained in CVS.

5. CONCLUSION

In this work we have described a framework for collection of defects and change data from software repositories. We have developed the CMS tool for estimating defects and changes in software systems. The working of CMS has been demonstrated using jtreeview. The developed tool can be used by software practitioners and researchers to collect defect and change data for object oriented software. Data collected through the tool can be used for defect trend analysis and change count and for developing models for prediction of defects and changes. These models can be used in the early phases of software development to predict defect and change prone classes. This will help software practitioners to plan testing resources and correct design and implementation issues in early phases of software development. In future we may develop models using machine learning techniques for predicting defects.

6. REFERENCES

[1] http://jtreeview.sourceforge.net/docs/overview.html.

[2] http://linux.about.com/library/cmd/blcmdl1_diff.htm.

[3] http://unix.worldiswelcome.com/understanding-the-diff-command-in-unix.

[4] http://sourceforge.net/apps/trac/sourceforge/wiki/TortoiseCVS%20instructions#ConfiguringTortoiseCVSforAnonymouspserverAuthentication.

[5] TortoiseCVS user's guide.

[6] Shinya Watanabe, Haruhiko Kaiya and Kenji Kaijiri. Adapting a Fault Prediction Model to Allow Inter Language Reuse. PROMISE'08, May 12–13, 2008, Leipzig, Germany, 2008.

[7] Naheed Azeem, Shazia Usmani, Defect Prediction Leads to High Quality Product, Journal of Software Engineering and Applications, 4, 639-645, 2011.

[8] Yuming Zhou, Hareton Leung and Baowen Xu, Examining the Potentially Confounding Effect of Class Size on the Associations between Object-Oriented Metrics and Change-Proneness, IEEE Transactions on Software Engineering, Vol. 35, No. 5, September/October 2009.

[9] Chidamber, S.R., Kemerer, C.F., A Metrics Suite for Object Oriented Design. IEEE Transactions on Software Engineering 20(6), 476–493, 1994.

[10] Rob Pooley, Dave Senior and Duncan Christie, Collecting and Analyzing Web-Based Project Metrics, IEEE SOFTWARE, J a n u a r y / F e b r u a r y 2 0 0 2.

[11] Thomas Zimmermann, Rahul Premraj and Andreas Zeller , Predicting Defects for Eclipse, PROMISE, Third International Workshop on Predictor Models in Software Engineering, 2007.

[12] Olusegun Akinwale, Sergiu Dascalu and Marcel Karam, DuoTracker: Tool Support for Software Defect Data Collection and Analysis, ICSEA, Proceedings of the International Conference on Software Engineering Advances ,2006.

[13] Ha Manh Tran, Christoph Lange, Georgi Chulkov, Ju¨rgen Scho¨nwa¨lder, Michael Kohlhase, Applying Semantic Techniques to Search and Analyze Bug Tracking Data, Springer 2009.

[14] Saeed Parsa, Somaye Arabi, and Mojtaba Vahidi-Asl, A Learning Approach to Early Bug Prediction in Deployed Software.

[15] Liang Ping, Li JianYang, A Change-Oriented Conceptual Framework Of Software Configuration Management, IEEE, 2007.

[16] Todd L. Graves, Alan F. Karr, J.S. Marron, and Harvey Siy , Predicting Fault Incidence Using Software Change History IEEE Transactions on Software Engineering, Vol. 26, No. 7, July 2000.

[17] Tao Xing, Software Configuration Management of Change Control Study Based on Baseline, International Conference on Intelligent Control and Information Processing August 13-15, 2010 - Dalian, China.

[18] R. Malhotra and M. Khanna, Investigation of relationship between object-oriented metrics and change proneness, Springer-Verlag 2012.

[19] W. E. Deming, Out of the crisis: quality, productivity and competitive position, Cambridge University Press, 1988

DOI: 10.1145/2557833.2557849 http://doi.acm.org/10.1145/2557833.2557849

International Journal of Advanced Science and Technology
Vol.62, (2014), pp.103-112
http://dx.doi.org/10.14257/ijast.2014.62.08

Design of A Novel Reconfigurable Fractal Antenna for Multi-Band Application

Preet Kaur[1], Asok De[2] and S. K. Aggarwal[3]

[1]*YMCAUST, Electronics Dep't., Faridabad, India*
[2]*Director, NIT Patna, Bihar, India*
[3]*Professor, YMCAUST, Faridabad, India*

preetmoar@gmail.com

Abstract

With advancement in communication technology over the past decade, there is an increasing demand for miniaturization, cost effective, multiband and wideband antennas. Fractal antenna designs can support in meeting these requirements. Though these antennas provide several advantages but at the same time miniaturization and performance of the fractal antennas can be further enhanced using reconfiguration concept. This paper proposes a novel hybrid reconfigurable fractal antenna that combines the advantage of both the categories. A reconfigurable fractal antenna is designed, simulated and optimized using Ansoft-High Frequency Structure Simulator (HFSS). The optimized antenna is fabricated and tested using Vector Network Analyzer. The fabricated antenna results are in good agreement with simulated results. The proposed antenna can be used for satellite communication, medical imaging and microwave imaging application, Vehicular radar applications and wireless industry application.

Keywords: *Fractal antenna, planar antenna, reconfigurable*

1. Introduction

The rapid expansion of wireless technology during the last years has led to increase in demand for small size, low-cost and multiband antennas for use in commercial communications systems. Fractal antenna [1] is one such category that provides miniaturization and have multi-band characteristic. These are composed of multiple iterations of a single elementary shape and are used to describe a family of complex shapes that possess an inherent self-similarity and self-affinity in their geometrical structure. Various researchers [2-8] have proposed fractal antennas of different shapes such as Sierpinski fractal antenna [2-4], tree-shaped fractal antenna [5-6], and some other types including snowflake fractal antenna [7] and Koch fractal antenna [8]. Though these antennas reduce the size and cost, but in case of communication system many applications are used that works at different frequency band hence a single fractal antenna cannot be used to serve the purpose of the whole communication system.

To resolve this issue researchers have proposed reconfigurable antennas [9-13]. These antennas resonate at different frequencies at different time by using switches therefore reduces the cost and overall size of the system. In comparison to fractal antennas the reconfigurable antennas have the following advantages [12] as follows:

- Compact size

ISSN: 2005-4238 IJAST

- Effective use of electromagnetic spectrum
- Similar radiation pattern and gain at all desired frequency bands

We are of the opinion that reconfiguration concept when applied to fractal can be a great asset for future wireless communication industries since it provides enhanced miniaturization in size of the overall communication system as well as provides frequency selectivity. Therefore this paper presents a hybrid reconfigurable fractal antenna that tries to incorporate the merits of both the antennas.

The rest of the paper has been organized into following sections. Section 2 provides the design and simulation results of reference antenna. Section 3 provides the design of the proposed novel hybrid reconfigurable rectangular fractal antenna. Section 4 provides the simulation and measured results of the proposed antennas in all optimized reconfigurable modes and section 5 provide the conclusion followed by references.

2. Design & Simulation Results of Reference Antenna

Reference Antenna is a rectangular patch antenna designed on FR4 epoxy substrate having dielectric constant $\mathcal{E}r = 4.4$, loss tangent δ=.0025 and thickness $h = 1.6$ mm as shown in Figure 1. This antenna is fed using coaxial cable.

Antenna design parameter for f =5.6 GHz resonant frequency is calculated using transmission line model equations[14] given below.For an efficient radiator, practical width W that leads to good radiation efficiencies is calculated by

$$W = \frac{C}{2f\sqrt{\frac{\varepsilon r+1}{2}}}$$

The effective dielectric constant is obtained by referring to equation:

$$\mathcal{E}_{reff} = \frac{\mathcal{E}r+1}{2} + \frac{\mathcal{E}r-1}{2}\left[1 + 12\frac{h}{w}\right]^{-\frac{1}{2}}$$

The effective length is calculated using equation

$$\boldsymbol{L_{eff} = \frac{c}{2f\sqrt{\varepsilon reff}}}$$

The value of ΔL can be obtained by using equation

$$\Delta L = 0.412h\left(\frac{(\varepsilon reff + 0.3)\left(\frac{W}{h} + 0.264\right)}{((\varepsilon reff - 0.258)\left(\frac{W}{h} + 0.8\right)}\right)$$

The actual length of radiating patch is obtained by: $L_{eff} = L + 2\Delta L$

The transmission line model is applicable to infinite ground planes only. However, for practical considerations, it is essential to have a finite ground plane. It has been shown by that similar results for finite and infinite ground plane can be obtained if the size of the ground plane is greater than the patch dimensions by approximately six times the substrate thickness all around the periphery. Hence, for this design, the ground plane dimensions would be given as: $L_g = 6h$+W , $W_g = 6h+ W$

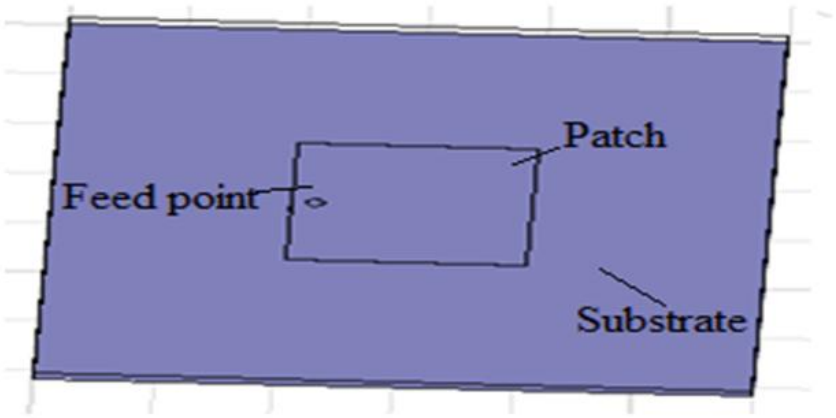

Figure 1. Top view of Reference antenna

After calculating the antenna design parameters it is modeled and optimized using HFSS software. After optimization it resonates at 5.61 GHz and 8.6 GHz as shown in Figure 2.

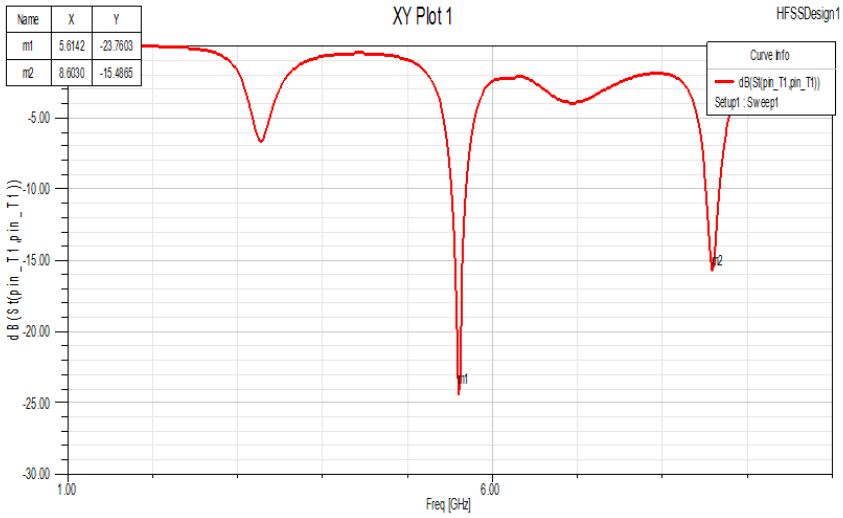

Figure 2. Return loss of Reference antenna

3. Design of Proposed Reconfigurable Fractal Antenna

The proposed reconfigurable fractal geometry is shown in Figure 3 and its design parameter is given in Table 1. For the purpose of reconfiguration, four RF switches D1-D4 are used. Antenna is fed with a 50Ω coaxial cable. Figure 4 shows the side view of the proposed antenna. The prototype of antenna is fabricated using lithography process. The top and bottom view of fabricated antenna is shown in Figure 5 and Figure 6.

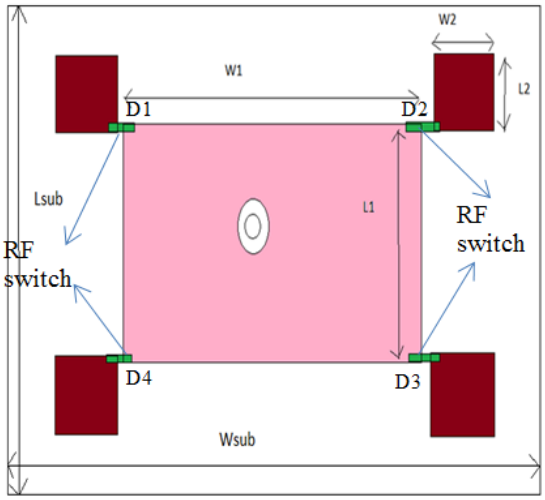

Figure 3. Geometry of proposed reconfigurable fractal antenna

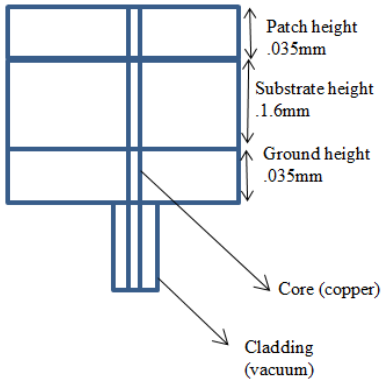

Figure 4. Side view of proposed re-configurable fractal antenna

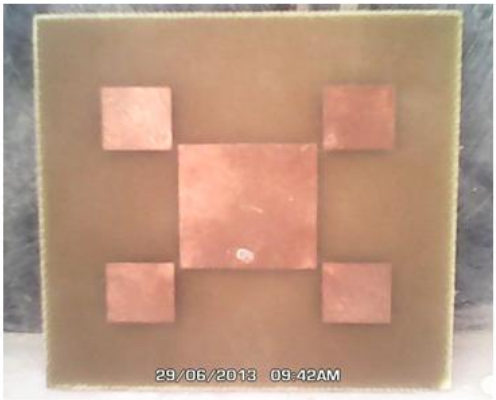

Figure 5. Top view of fabricated reconfigurable fractal antenna

Figure 6. Bottom view of fabricated re-configurable fractal antenna

Table 1. Critical antenna dimension of proposed reconfigurable fractal antenna

Antenna parameter	Dimension(mm)	Antenna parameter	Dimension(mm)
W1	23.7	ε_r	4.4
L1	20.02	H	1.6
W2	11.85	L2	9.87
Wsub	71.7	Lsub	60.02

4. Simulated and Measured Results of Proposed Reconfigurable Fractal Antenna

Simulated results presented here are obtained using HFSS software. This antenna is optimized for four modes using different switch position. Relationship between the operation modes and the states of switches for the 1nd iteration of antenna are shown in Table 2.

Table 2. Relationship between various modes and switch positions

S.NO.	MODES	Switch Position
1	Mode 1	D1=OFF,D2=OFF D3=OFF,D4=OFF
2	Mode 2	D1=ON,D2=ON, D3=ON, D4=ON
3	Mode 3	D1=ON,D2=OFF D3=ON,D4=OFF
4	Mode 4	D1=OFF,D2=OFF, D3=OFF,D4=ON

For modeling of RF switch, a common way is that when switch is on, it is represented by copper strip ($1\times1mm^2$) and when switch is off, no copper strip is used. In simulation and measurement this modeling is used to get the results. The results of fabricated antenna are measured using Agilent Technologies VNA N5230A: A.07.50.13

and compared with the simulated ones. This section presents details of the various reconfigurable modes of proposed antenna.

Modes of Proposed Antenna

4.1. Mode 1

In this mode, all switches are off. Figure 7 shows the simulated and measured return loss of optimized reconfigurable antenna. Following points can be concluded for above mode.

- The antenna resonates nearly at same frequency of 5.74GHz & 8.82GHz as that of reference antenna since all the switches are in the off position.

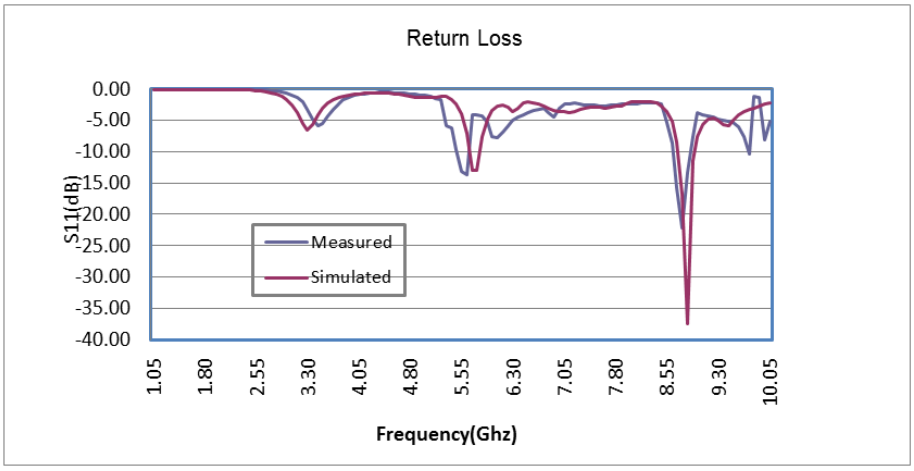

Figure 7. Return loss of proposed reconfigurable antenna in mode 1

- The maximum gain of antenna is 2.488dB & 4.93 dB for the above mentioned frequencies.
- The radiation efficiency of antenna at two resonant frequencies is 36% and 38% respectively.
- The maximum gain of antenna is 2.488dB & 4.93 dB for the above mentioned frequencies.
- The radiation efficiency of antenna at two resonant frequencies is 36% and 38% respectively.

4.2. Mode 2

Figure 8 shows the return loss of the antenna in mode 2 when all the diodes are in the on position. Following points can be concluded for this mode.

- The resonant frequencies for the antenna in this mode are 5.76GHz, 6.35GHz, 7.54GHz and 9.80GHz.
- The gain of antenna above mentioned resonant frequencies are 4.8 dB, 4.6dB, 2.20dB and 5.46dB respectively.
- Radiation efficiency of antenna at above frequencies is 87%, 43%, 45% and 62%.

- For non-reconfigurable fractal antenna only this mode will exist for 1st iteration.

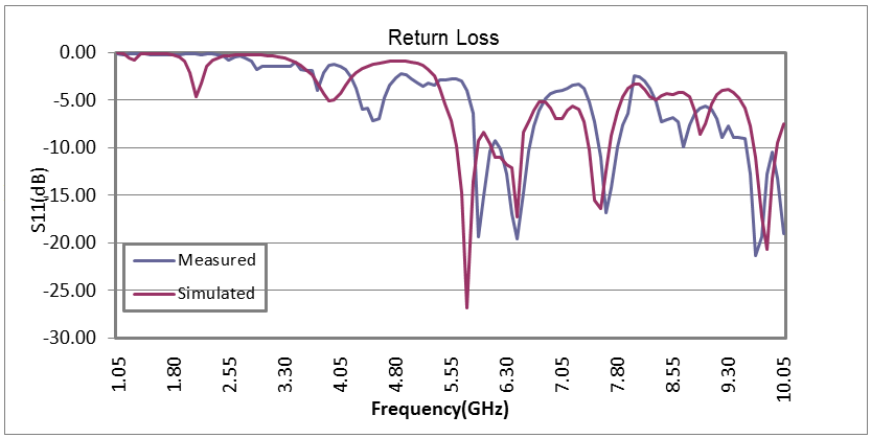

Figure 8. Return loss of proposed reconfigurable antenna in mode 2

4.3. Mode 3

The switches D1 and D3 are turned on while D2 and D4 are turned off in this mode. Following point can concluded for above mode

- Figure 9 shows that the antenna resonates at 5.70 GHz, 7.23GHz and 9.52GHz with a good return loss of -25.43, -28.05 and -21.74 dB respectively.
- Antenna has a gain of 3.62,5 and 5.02dB at above mentioned resonant frequencies respectively.

4.3. Mode 3

The switches D1 and D3 are turned on, while D2 and D4 are turned off in this mode. Following point can concluded for above mode

- Figure 9 shows that the antenna resonates at 5.70 GHz, 7.23GHz and 9.52GHz with a good return loss of -25.43dB, -28.05dB and -21.74 dB respectively.

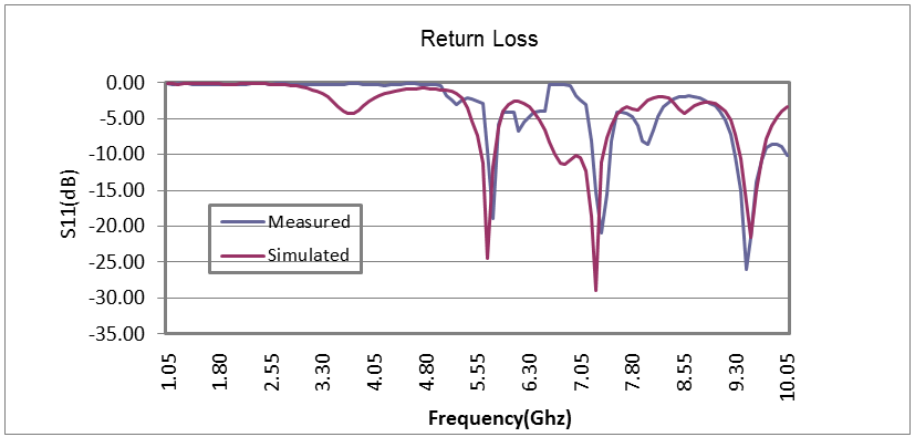

Figure 9. Return loss of proposed reconfigurable antenna in mode 3

- Antenna has a gain of 3.62dB, 5dB and 5.02dB at above mentioned resonant frequencies respectively.
- Radiation efficiency of antenna at resonant frequencies is 56%, 47% and 52% respectively.
- Measured results are in good agreement with simulated results.

4.4. Mode 4

In this mode switch position D1, D2 and D3 are turned off and D4 is on. Following points can be concluded for above mode.

- Figure 10 show that antenna resonates at 3.436GHz, 5.811GHz, 6.51GHz, 7.363GHz and 8.915GHz.

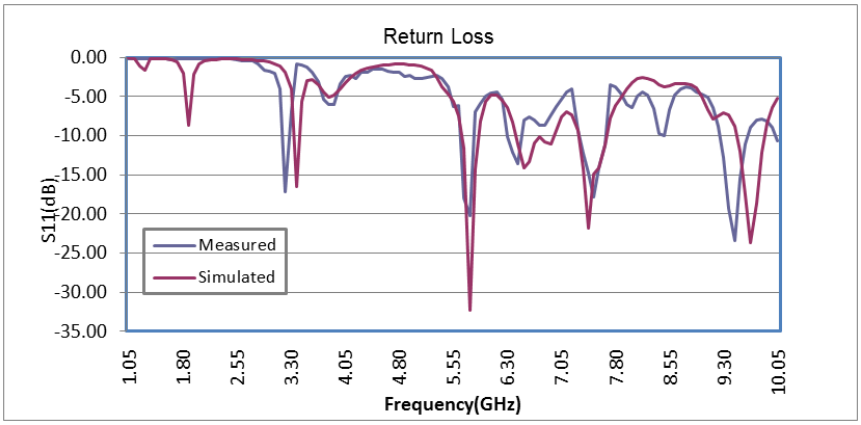

Figure 10. Return loss of proposed reconfigurable antenna in mode 4

- Simulated resonant frequencies 3.436GHz and 8.915 GHz shifted slightly to lower side in measurement results due to fabrication errors.
- At 3.436GHz antenna has very good radiation efficiency of 80%.

The antenna parameters for various reconfigurable modes for the 1nd iteration of reconfigurable fractal antenna are shown in Table 3.

Table 3. Various modes of reconfigurable antenna and its parameters

	Resonant Frequency(GHz)	Return - loss(dB)	Gain (dB)	Radiation Efficiency (magnitude)
Mode 1	5.74 8.822	-14.97 -37.69	2.488 4.93	.36 .38
Mode 2	5.76 6.35 7.54 9.800	-26.59 -12.35 -17.42 -22.35	4.8 4.6 2.20 5.46	.87 .43 .45 .62

Mode 3	5.70 7.23 9.52	-25.43 -28.05 -21.74	3.62 5 5.02	.56 .47 .52
Mode 4	3.436 5.811 6.51 7.363 8.91	-16.03 -22.84 -27.00 -12.36 -14.60	5 3.60 3.03 2.24 3.02	.80 .60 .55 .39 .54

5. Conclusion

The proposed hybrid reconfigurable fractal antenna is novel compact, simple, multiband and reconfigurable. The presented antenna is multiband in each reconfigurable mode due to self-similarity of fractal structure. The antenna presents only three resonant frequencies if non-reconfigurable fractal configuration is used in which central patch is permanently connected to all small patches (MODE 2), but by using reconfiguration concept this antenna can resonates at approximately ten different resonant frequencies in all the modes. Also by using reconfiguration concept power interference issues can be avoided by switching between different modes. The proposed multi-band reconfigurable antenna can be used for satellite communication, medical imaging and microwave imaging application, Vehicular radar applications and wireless industry application.

References

[1] D. H. Werner and S. Ganguly, "An Overview of Fractal Antenna Engineering Research", IEEE Antenna and wave Propagation Magazine, vol. 45, no. 1, **(2003)** February.
[2] K. C. Hwang, "A Modified Sierpinski Fractal Antenna for Multiband Application", Antennas and Wireless Propagation Letters, IEEE, vol. 6, **(2007)**, pp. 357-360.
[3] N. Kingsley, D. E. Anagnostou, M. Tentzeris and J. Papapolymerou, "RF MEMS Sequentially Reconfigurable Sierpinski Antenna on a Flexible Organic Substrate With Novel DC-Biasing Technique", Microelectromechanical Systems, vol. 16, **(2007)** October, pp. 1185-1192.
[4] J. Vemagiri, M. Balachandran, M. Agarwal, *et al.*, "Development of compact half-Sierpinski fractal antenna for RFID applications", Electronics Letters, vol. 43, no. 22, **(2007)** October 25.
[5] H.-W. Song, H.-S. An, J.-N. Lee, *et al.*, "Design of the Tree-Shaped UWB Antenna Using Fractal Concept", Korea-Japan Microwave Conference, **(2007)**, pp. 73-76.
[6] H. Rmili, O. E. Mrabet, J. -M. Floc'h and J. -L. Miane, "Study of an Electrochemically-Deposited 3-D Random Fractal Tree-Monopole Antenna", IEEE Transactions on Antennas and Propagation, vol. 55, **(2007)** April, pp. 1045-1050.
[7] B. Mirzapour and H. R. Hassani, "Size reduction and bandwidth enhancement of snowflake fractal antenna", IET Microwaves, Antennas& Propagation, vol. 2, **(2008)** March, pp.180-187.
[8] A. Sundaram, M. Maddela and R. Ramadoss, "Koch-Fractal Folded-S.lot Antenna Characteristics", IEEE Antennas and Wireless Propagation Letters, vol. 6, **(2007)**, pp.219-222.
[9] J. cho, C. W. Jung and K. Kim, "Frequency reconfigurable two-port antenna for mobile phone operating over multiple service bands", Electronics letters, vol. 45, no. 20, **(2009)** September, pp. 1009-1011.
[10] H. F. A. Tarboush, R. Nilavalan, K. M. Nasr, H. S. Al-Raweshidy and D. Budimir, "A reconfigurable H-shape antenna for wireless applications", Proceedings of the Fourth European Conference on Antennas and Propagation, **(2010)** April, pp. 1-4, 12-16.
[11] M. Adhikari and K. F. Warnick, "Miniature radiation pattern reconfigurable antenna for 2.4 GHz band", Antenna and propagation society international symposium (APSURSI), IEEE, **(2010)** July 11-17, pp. 1-4.
[12] P. kaur, "A reconfigurable square ring slot antenna for operation in GSM and WLAN frequency bands", International journal of microwave and optical technology, vol. 7, no. 1, **(2012)** January, pp. 49-54.

[13] Y. Zhang, B. -Z. Wang, X. -S. Yang and W. Wu, "A fractal Hilbert microstrip antenna with reconfigurable radiation patterns", Proceedings of IEEE Antennas and Propagation Society International Symposium (APS-URSI 2005), ,Washington DC, USA, **(2005)** July, pp. 254–257.
[14] C. A. Balanis, "Antenna Theory: Analysis and Design", New York: Wiley, **(1997)**.

Authors

Preet Kaur is B.tech (Electronics & communication Engg.) from DCRUST, Murthal and M.tech (RF& Microwave Engg.) from IIT Roorkee and currently pursuing her Ph.D from YMCA University of Science and Technology, Faridabad. Her academic interests include metamaterials, antenna design and electromagnetic wave theory. She is working as Assistant professor (Electronics Engg.) with YMCA University, Faridabad since 2008.

Dr. Asok De received the B.E and M.E degree from Jadavpur university, Kolkata and Ph.D. degrees from IIT Kharagpur in 1986. He is currently the Director of National Institute of Technology, Patna (Bihar). His research interest includes microwave Engg., metamaterials, EM-wave propagation, and antenna miniaturization.

Dr. S. K. Aggarwal is B.tech (Electrical Engg.) from NIT, Calicut (Kerala) and M.tech from Delhi College of Engineering and Ph.D from Jamia Milla Islamiya University, Delhi. He is currently the Professor and Chairman of electronics department with YMCA University of Science and Technology.

American International Journal of Research in Science, Technology, Engineering & Mathematics

Available online at http://www.iasir.net

ISSN (Print): 2328-3491, ISSN (Online): 2328-3580, ISSN (CD-ROM): 2328-3629

AIJRSTEM is a refereed, indexed, peer-reviewed, multidisciplinary and open access journal published by International Association of Scientific Innovation and Research (IASIR), USA

(An Association Unifying the Sciences, Engineering, and Applied Research)

Direct Current Control of Grid connected Photovoltaic Distributed Generation system

Dr Rachana Garg[1], Dr. Alka Singh[2], Ms Shikha Gupta[3]

[123]Electrical Engineering Department

Delhi Technological University (formerly DCE)

Delhi-42, India

Abstract*: Grid connected Photo voltaic system is emerging as reliable and sustainable solution in future renewable energy segment. Conventional grid connected photovoltaic (PV) system consists of PV array, DC-DC boost converter with maximum power point tracking (MPPT) controller and a current controlled full bridge IGBT inverter with L-C-L filter. This paper proposes and demonstrates control architecture and technique for medium and large scale PV arrays connected to the power system grid. The array is interfaced to the grid through power conditioning unit to change output voltages and currents from DC to AC quantities. A DC-DC boost converter is used to step up the output voltage of the array and extract maximum power under a given temperature and solar irradiation via incremental conductance(IC) method. A voltage source inverter (VSI) under current control mode is connected to the DC converter through a DC link capacitor. The inverter is controlled in the rotating (dq) frame to inject AC power into the grid. A PI controller is used to regulate the DC link capacitor voltage and to keep it constant by balancing its input and output powers. MATLAB/SIMULINK software is used to simulate the proposed system and confirm the performance and effectiveness of the proposed technique.*

Keywords*: MPPT; Direct control; Photovoltaic (PV); Inverter; Hysteresis.*

I. Introduction

Limited reserves of fossil fuels along with their environmental impact has encouraged gradual growth and drift towards green energy sources. Costly transmission infrastructure for suburban and rural market is another barrier for sustainability of conventional power system and shifted renewed focus on distributed generation. Among the available green energy sources, photovoltaic (PV) systems are becoming popular due to technological advancement, decreasing cost and acceptability of stakeholders. In past times, PV systems were used as power supplies only for special applications like communication and satellite fields. But with advancement of power electronic devices, application of photovoltaic source has entered into electricity market along with commercial fields. Intermittent nature of solar radiations is major concern and hence reliability, stability and quality of output power supply are areas where there is significant research scope for integration of PV systems with conventional power system. Grid connected Photo voltaic generation system involves two major issues. The first issue is to track and regulate output power at the Maximum Power point (MPP) with change in irradiation level. The second important issue to be considered is that inverter should inject sinusoidal current into utility grid with low total harmonic distortion (THD).

The paper contains design of a grid connected Photovoltaic generation system (PVGS) of 8 KW with direct current control strategy of inverter unit using two stages approach. The proposed control strategy is also validated under different environmental and load conditions. Owing to the fact that DC bus voltage of the boost converter will vary due to irradiation change, a DC bus voltage controller is designed to generate the injected current command. DC bus voltage controller is designed using PI controller. For direct current control of VSI, synchronous-reference-frame (SRF)-based control technique is used. In SRF, a synchronous frame regulator is required to transform a measured stationary frame ac current (or error) to rotating frame dc quantities, and transforming the resultant control action back to the stationary frame for execution. The simulation results show the load sharing between PV generation system and utility grid based on the generation of PV and load requirement of system.

II. PV Solar Array

This paper is based on solar cell model using a single diode, as given by equations (1-3) is used for simulation of PV module for datasheet KC200GT[1].This model can be changed by user for any configuration of array by just multiplying required number of series and parallel cell given in equation (4).

$$I = I_{ph} - I_{s1}\left[e^{\frac{q(V+IR_{se})}{kT}} - 1\right] - I_{s2}\left[e^{\frac{q(V+IR_{se})}{AkT}} - 1\right] - \frac{(V + IR_{se})}{R_{sh}} \quad (1)$$

$$I = I_{ph} - I_{s}\left[e^{\frac{q(V+IR_{se})}{AkT}} - 1\right] - \frac{(V + IR_{se})}{R_{sh}} \quad (2)$$

$$I_{ph} = I_{sc^*}\frac{I_{rr}}{1000^*}\left[1 + \left(T_{cell} - T_{ref}\right)^* K\right] \quad (3)$$

$$I = I_{pv}N_{par} - I_O N_{par}\left[e^{\left(\frac{V+R_s\left(\frac{N_{ser}}{N_{par}}\right)I}{V_t a N_{ser}}\right)} - 1\right] - \frac{V + R_s\left(\frac{N_{ser}}{N_{par}}\right)I}{R_p\left(\frac{N_{ser}}{N_{par}}\right)} \quad (4)$$

III. Integration of PV panel with DC-DC converter

The designed PV array is integrated with dc-dc Boost converter for system requirement. A controller based on IC algorithm is built to keep the output voltage of the PV panel at the maximum power point [2-3]. The function of the DC-DC converter is realized by using the energy storage devices such as inductor, capacitor and fast switching devices such as transistor and diodes. The values of inductor and capacitor are calculated using Equation (5,6) according to desired output levels of system [4].

$$L = \frac{(DV_{pv})}{(2f_{sh}\,\Delta i_1)} \quad (5)$$

$$C = \frac{(DI_d)}{(f_{sh}\,\Delta V)} \quad (6)$$

Where V_{pv} = Output voltage on PV side; D = Duty cycle of converter;i_1 = Input current (PV side) ripple; I_d = Output current on load side; V = Output voltage (load side) ripple; f_{sh} = Switching frequency.

Boost DC-DC converter steps-up a DC input voltage by a ratio which can be calculated as given by equation(7).

$$M = 1/\,(1 - D) \quad (7)$$

From (7)it can be seen that boost converter is electronically adjustable by changing the switch duty ratio D . The output power flow is controlled by adjusting the ON\OFF duty cycle of the switch. The current and voltage is changed at the load side but the power remains constant at a required level even for the variation in load.

IV. Inverter Control

There are direct current control and indirect current control methods for grid side converter. The former need to detect the AC side current through the current regulator to keep the actual value of AC current followed the reference value in order to control the power factor. The latter control the reactive power and active power system by controlling the voltage amplitude and the phase deviation with the supply voltage at the AC side [5].
Possibility of compensating power without energy storage element is possible with the help of pq theory and this theory deals with all three phases simultaneously as a unity system. The SRF algorithm is also known as d–q method, and it is based on a–b–c to d–q–0 transformation (park transformation). In nonlinear power systems, the i_d and i_q components of the current include both oscillating components and average components, The reference current generated for d component of grid current is given as[6]:

$$i_d^* = I_{ddc} + I_{loss} \quad (8)$$

The oscillating components of the current correspond to harmonic currents, and the average components of the current correspond to the active and reactive currents [7]. Here the objective is to provide independent control on feeding of active and reactive power. The transformation equation used for abc to dq0 conversion is:

$$\begin{bmatrix} i_{Lq} \\ i_{Ld} \\ i_{L0} \end{bmatrix} = 2/3 \begin{bmatrix} cos\theta & cos\left(\theta - \frac{2\pi}{3}\right) & cos\left(\theta + \frac{2\pi}{3}\right) \\ sin\theta & sin\left(\theta - \frac{2\pi}{3}\right) & sin\left(\theta + \frac{2\pi}{3}\right) \\ 1/2 & 1/2 & 1/2 \end{bmatrix} \begin{bmatrix} i_{La} \\ i_{Lb} \\ i_{Lc} \end{bmatrix} \quad (9)$$

The reference for the ac mains grid in terms of abc components from the references in terms of dq0 component can be obtained using inverse Park's transformation given as:

$$\begin{bmatrix} i_a^* \\ i_b^* \\ i_c^* \end{bmatrix} = 2/3 \begin{bmatrix} cos\theta & sin\theta & 1 \\ cos(\theta - 2\pi/3) & sin(\theta - 2\pi/3) & 1 \\ cos(\theta + 2\pi/3) & sin(\theta + 2\pi/3) & 1 \end{bmatrix} \begin{bmatrix} i_d^* \\ i_q^* \\ i_0^* \end{bmatrix} \quad (10)$$

Here, Phase Locked Loop (PLL) is used to generate angle theta which provides grid synchronization. PLL is a control system that generates an output signal whose phase is synchronized with the input 50 Hz signal. It is an electronic circuit consisting variable frequency oscillator and phase detector, to generate periodic signal and to o compare the signal for the phase matching respectively.

In inverter control system, outer voltage loop generates error by comparing the reference DC link voltage and actual DC link voltage which is then given to the Proportional-Integral (PI) controller which generates reference current I_d and I_q kept zero. Values of these generated current references decide the amount of flow of active and reactive power in the system. Firing pulses are generated by hysteresis current controller (HCC). Control scheme block diagram is shown in figure 1.

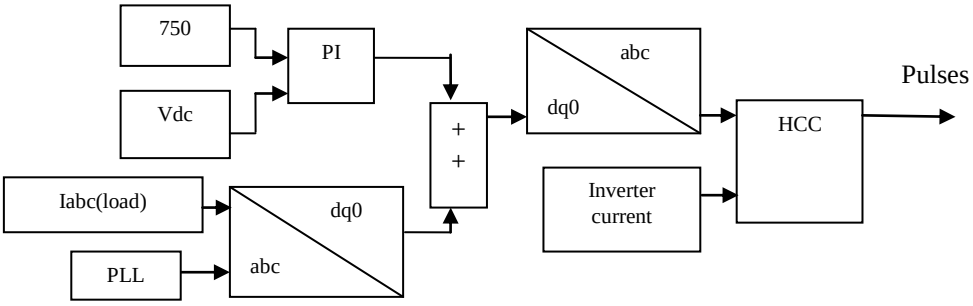

Figure1: Direct Current Control Scheme

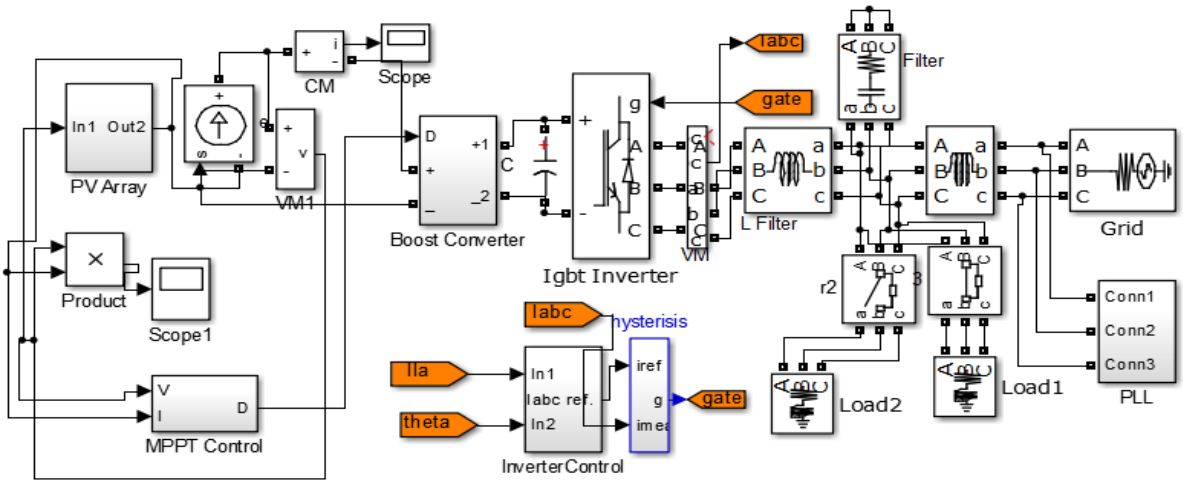

Figure2: MATLAB implementation of proposed PVGS

V. Result And Discussions

A simulation program is conducted by using MATLAB software to demonstrate the effectiveness of proposed control methodology for grid connected PVGS. Simulation has been carried for (i) Change in load. (ii) Change in irradiation level. Results for load voltage (Vload), load current (Iload) , inverter voltage(Vi), inverter current(Ii), Active Reactive Power Provided by Grid(Pg) and PV source Power

(Ppv), DC link voltage(Vdc) and maximum powerobtained from MPPT control (Pm) has been studied to verify the significance of Grid connected system behavior.

(i)Change in load

The simulation results as shown in figure 3 have been obtained under standard climatic conditions (T=25°C and G=1000W/m^2 and can be clearly conclude that, for standard condition the PV system provides maximum power i.e. 8kW. Simulation is run for 0.5 seconds initially a load of 24 kW, 9kVAR is connected up to 0.3 second, at 0.3 second 12kW,5kVAR is disconnected. It can be seen from the Figure 3b that PV is giving 8kW, power and grid is providing rest 16kW, 9kVAR for first 0.3 seconds, for further 0.2 second PV power is same as before and grid is now providing rest 4kW, 9kVAR with maintained THD level. Figure 3a shows the 8kW Maximum power provided by the PV array, regulated dc link voltage which is maintained at a constant level (750 V), inverter voltage, inverter current respectively and figure 3b shows load current, load voltage, source active reactive power, grid active reactive power respectively.

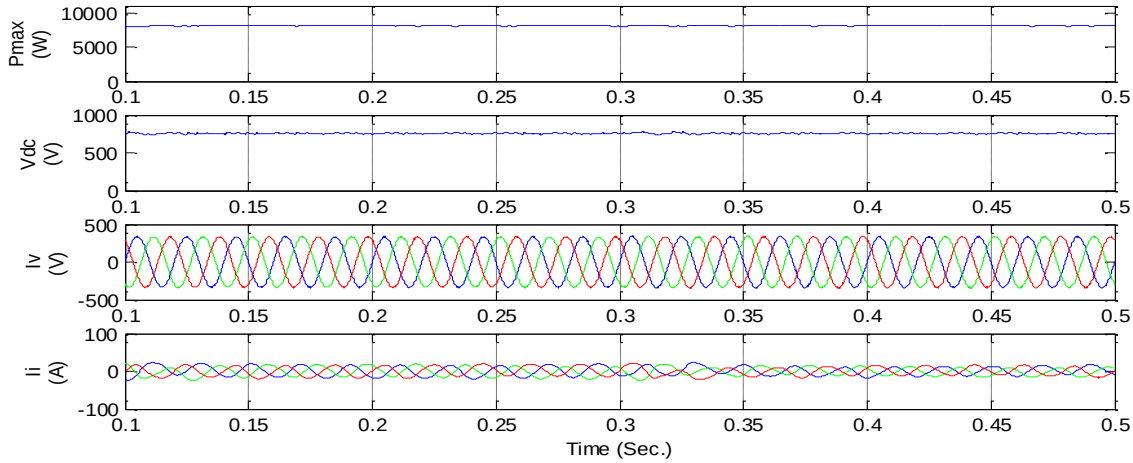

Figure: 3(a) Performance of the system for change of load

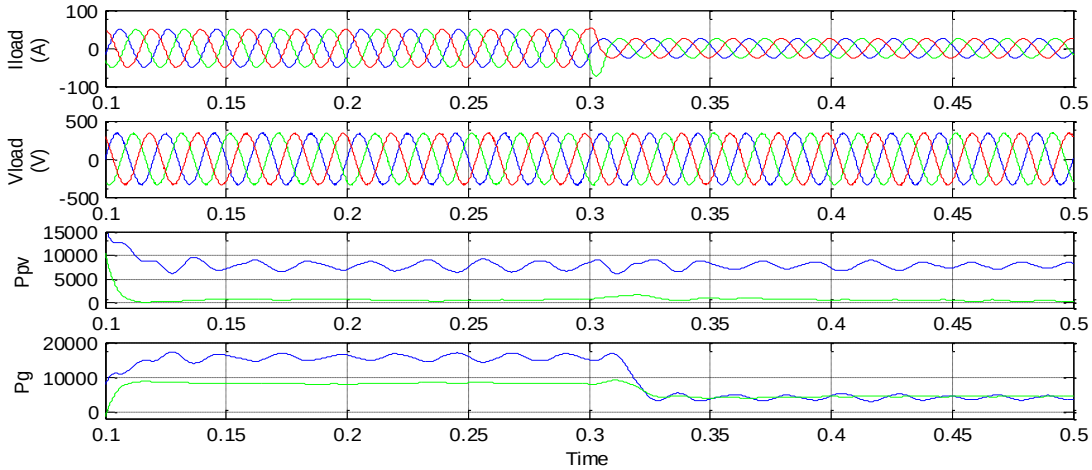

Figure: 3(b) Performance of the system for change of load

Change of climatic conditions

Figure 4 presents the evolution of the grid-connected PV system during a variation in solar radiation. It can be seen that the system is tracking the new operating point quickly. The maximum power point is tracked when the radiance changes between t=0.2s to t=0.4s for G=300W/m^2. Figure 4a represents Maximum power tracking with the change in irradiation, dc link voltage i.e. maintained at a constant level V_{ref}=750V, grid side converter voltage, grid side converter current respectively. Figure 4b depicts load current, load voltage active & reactive power provided by the inverter, active reactive power provided by the grid respectively.

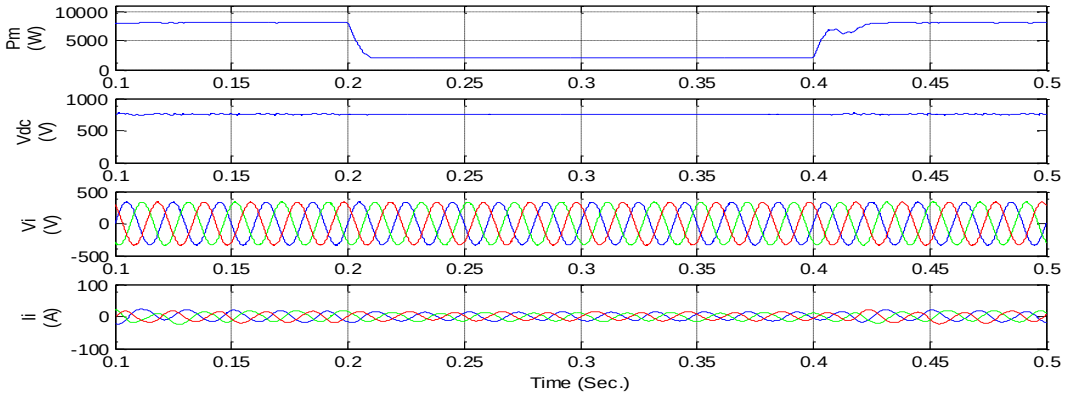

Figure:4(a) Performance of the system for change of irradiation level

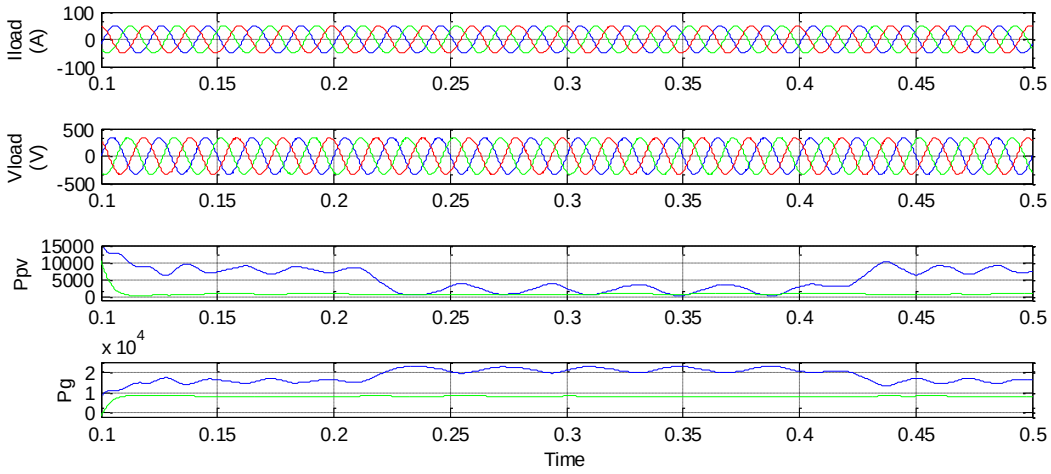

Figure:4(b) Performance of the system for change of irradiation level

VI. CONCLUSION

The grid interconnected PVGS performance is investigated and analyzed under different environmental conditions and load variation. The DC bus voltage and PCC voltage maintained at desired level for different conditions with maintained THD level under 5%. Results verify the satisfactory performance of proposed system.

References

.

[1] Bhuvaneswari, G., and R. Annamalai. "Development of a solar cell model in MATLAB for PV based generation system." In proceedings of INDICON), 2011 Annual IEEE. IEEE, 2011

[2] Ali, Ali Nasr Allah, Mohamed H. Saied, M. Z. Mostafa, and T. M. Abdel-Moneim. "A Survey of MPPT techniques of PV Systems." InEnergytech, 2012 IEEE, pp. 1-17. IEEE, 2012.

[3] Wang NianCHun, Sun Zuo Kazuto Yukita, Yasuyuki Goto, Katsuhiro Ichiyanagi "Research of PV Model and MPPT Methods in Matlab"978-1-4244-4813-5/10/$25.00 ©2010 Crown

[4] Ned Mohan, Tore M. Undeland and William P. Robbins, "Power electronics converters, applications, and design", Wiley India Press Pvt. Ltd. Third Edition, Reprint 2009 J. Joe-Air, "Maximum power tracking for photovoltaic power systems," Tamkang Journal of Science and Engineering, vol. 8, no 2, 2005, pp. 147-153.

[5] S. Bhattacharya, D. M. Divan, and B. Banerjee, "Synchronous reference frame harmonic isolator using series active filter," in Proc. 4th EPE,Florence, Italy, 1991, vol. 3, pp. 030–035.

[6] Arun Verma, Bhim Singh, D.T.Sahani, " Grid Interfaced Photovoltaic power generating system with Power Quality Improvedmennt at AC mains," IEEE ICSET,2012,Nepal.

[7] S. Bhattacharya, T. M. Frank, D. M. Divan, and B. Banerjee, "Active filter system implementation," IEEE Ind. Appl. Mag., vol. 4, no. 5, pp. 47–63, Sep./Oct. 1998.

2012 IEEE Global Humanitarian Technology Conference

Fuzzy-Genetic Algorithm For Patient Data Processing In Telemedicine

Richa Gupta
Department of Information Technology
Delhi Technological University
Delhi, India
(e-mail: guptaricha_it@yahoo.co.in)

Dr. Parmod Kumar
Department of Electrical Engg.
Delhi Technological University
Delhi, India
(e- mail:pramodk2003@yahoo.co.in)

Abstract—Uncertainties and vagueness are always present in the patient data received from far distance. It is, therefore, not possible to extract the information about the patient condition properly, and the patient data need processing before presenting to the physician. In this paper, it has been demonstrated that processing the patient data with a fuzzy-genetic algorithm at physician / expert doctor end will reduce the uncertainties and vagueness in the patient data. The physician is able to diagnose the patient disease with better reliability and prescribe the medicine accordingly.. Initial population for the genetic algorithm is randomly generated with assumed fuzzy functions. These functions are optimized using the theory of reproduction, crossover, and mutation. The result shows that the fuzzy-genetic algorithm gives satisfactory result for processing the patient data for the purpose.

.Keywords-component; Fuzzy logic, Genetic algorithm, blood pressure,, cholesterol .

I. INTRODUCTION

Telemedicine is the information exchange between a patient and a doctor or between a physician and specialist located at far distance. It involves the information technology and telecommunication to receive the data/information of patient, radiologist, pathologist etc. geographically at far distance. Many times the patient is not able to communicate with expert due to language or data may be corrupted due to various reasons. Thus, there is vagueness and uncertainty involved in the two way communication. This needs processing the data and information received at the doctor/specialist end to diagnose the possible disease/s. Accordingly, the physician prescribes the medicine. Till now, the processing of information at physician end is done by conventional Fourier series which has fixed resolution at all the frequencies. The various techniques such as wavelet method have replaced the Fourier series method, which take into account the variation of resolutions at different frequencies. However, these methods do not meet the requirements related to uncertainty and vagueness in the raw data/ information of patient. Fuzzy logic is a convenient method of processing information with uncertainty [1]-[3]. It is based on a rule based algorithm and expert's knowledge that can handle noise and vagueness in information. Fuzzy logic algorithm can also construct a decision where no mathematical model is possible to develop. However, a qualitative understanding of the system is required in order to develop a reliable fuzzy logic algorithm as the knowledge base degrades. The time response of processing the patient data at physician / specialist end reduce with fuzzy logic algorithm. This requires tuning of fuzzy functions. Traditionally, the tuning of fuzzy function is done manually by adjusting the support of the functions. Fig.1 shows the sample universe of discourse and OA, OB and OC represent support of fuzzy functions for low(L), medium(M), and High (H) membership functions, respectively. These fuzzy functions can be optimized by hit and trial method. However, this is a time consuming process and can result in local

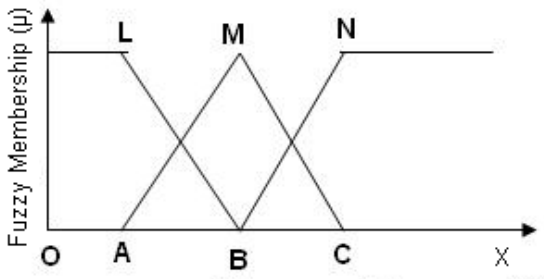

Fig.1 Sample Universe of discourse(X)

optimum solution. This difficulty of the fuzzy logic algorithm has been overcome by integrating genetic algorithm with fuzzy functions. The authors in this paper have optimized the fuzzy functions assumed using a genetic algorithm for processing the data at doctor's/specialist end. The genetic algorithm is a stochastic optimization method, it applies the principle of fitness, reproduction and mutation to produce successively better fuzzy functions leading to the optimum decision with fuzzy logic algorithm[4]-[5]. The optimized fuzzy functions have been used for the blood pressure and blood cholesterol computation from a raw data. The simulation studies are useful for understanding the feasibility in implementation for the patient residing in rural and remote areas.

978-0-7695-4849-4/12 $26.00 © 2012 IEEE
DOI 10.1109/GHTC.2012.45

II.ESSENTIAL PARAMETER S

Telemedicine is based on the concept of storage and forwarding of information related to audio, video images and clips, ECG, etc. The digital information is sent to the expert for reviewing, interpretation and advice at his convenience. The expert opinion is transmitted back, suggesting the required medicine/ treatment to be started. Telemedicine can also be a real time exchange of information between two doctors and/ or doctor/expert interviewing the patient. It is essential to create the following detailed electronic patient record so that the needful information can be accessed whenever required:

i) Primary patient data: Name, age , occupation, sex, address , telephone no etc.

ii) Patient history: personal and family history and diagnostic reports

iii) Investigation: complete analysis of various tests done on the patient

iv) Data report: radiographs, MRI, CT, ultrasound and nuclear medicine etc.

III. FUZZY LOGIC SYSTEM

A fuzzy logic system is an expert system which can process the fuzzy information using a collection of fuzzy membership functions and rules. The rules in a fuzzy system are usually of form similar to the following:

If A is low and B is high then C is medium

Where, A and B are patient input variables (data values) , and C is diagnosed output variable (data value of symptom). Low is membership function (fuzzy subset) defined on A, high is membership function defined on B and medium is membership function defined on C. A general fuzzy inference processing system is shown in fig. 2.

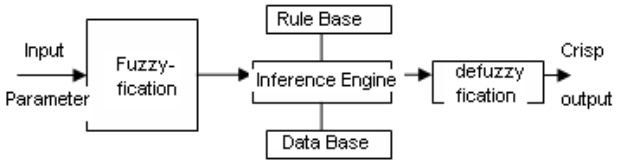

Fig.2 Fuzzy Inferencing system

IV. GENETIC ALGORITHM

A genetic algorithm is an evolutionary algorithm used to optimize the fuzzy functions shape or rules. The evolution starts from random generated populations. In each generation, the fitness of whole population is evaluated based on their fitness value. The population is modified using crossover or mutation operators to form a new population, which becomes current generation in the next iterations of the algorithm. The iterations are repeated until better and better fitness is achieved. It is stopped if fitness value is poor compared to last value. The major components of genetic algorithm are encoding scheme, fitness function , parents selection, crossover and mutations operators [4], [12].

(i) Encoding scheme: This transforms points in parameters space into bit string representations, for example, a point (11,4,8,5) in four dimensional space can be represented as concatenated binary string (1011 0100 1000 01001) in which each coordinate value is encoded as a gene composed of four binary bits using binary coding.

(ii) Fitness function : The first step after creating a generation is to calculate the fitness value of the each member in the population.

(iii) Selection operator: After evaluation, a new population is created from the current generation. Selection operator determines which parents participate in producing offspring for the next generation, and it is analogous to survival of the fittest in natural selection.

(iv) Crossover : To exploit the potential of the current population, the crossover operator generates new chromosomes. Crossover is usually applied to select pairs of parent with a probability equal to a given crossover rate. In one point crossover, the genetic code is selected at random and two parent chromosomes are interchanged at this point. In two-point crossover, two crossover points are selected and the part of the chromosome string between these two points is then swapped to generate two children.

(v) Mutation: While crossover exploits current gene potentials, mutation operators are capable of spontaneously generating new chromosomes. A mutation operator can prevent any single bit from converging to a value throughout the entire population, and more important, it can prevent the population from stagnating

V. FUZZY- GENETIC ALGORITHM [1]

The main problem in fuzzy function selection is the difficulty in defining the host parameters, such as number and shape of fuzzy sets for the patient data and the output decision parameters, the form of inference mechanism , and the de-fuzzy mechanism. The selection of fuzzy functions have considerable influence on the overall performance of the data processing. The authors in this paper have assumed three triangular functions as shown fig. 3.The three parameters a_1,a_2,and a_3 uniquely define the fuzzy sets. If μ_1,μ_2, μ_3 are the membership values belonging to patient data at a1,a2, and a3, respectively, then the discrete fuzzy sets can be represented by eqn.(1).

$$A = [\ \mu_1/a_1 + \mu_2/a_2 + \mu_3/a_3 + \text{--------}\ ] \quad (1)$$

The parameters of different fuzzy sets are encoded into binary strings of sufficient length, to give the desired precision. The genetic algorithm is applied to the string and decoded back to evaluate the objective function. The de-fuzzy value can be calculated by using eqn.(2).

$$Df = \frac{\mu 1a1 + \mu 2a2 + \mu 3a3 + \cdots}{\mu 1 + \mu 2 + \mu 3} \quad (2)$$

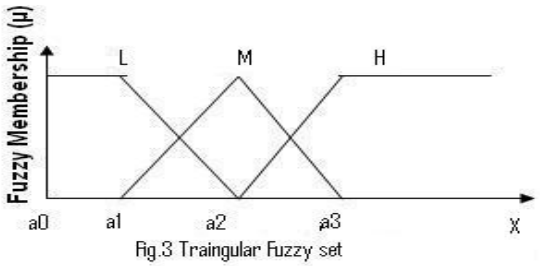

Fig.3 Traingular Fuzzy set

VI. PROBLEM FORMULATION [7]-[9].

The normal blood pressure (B.P.) for an adult is 120/80, where 120 is called Systolic Pressure and 80 is called Diastolic Pressure. If B.P. of a person does not lie around this standard value then further investigations are required and needful medicines have to be started. The cholesterol measurement provides the information regarding health of arteries, supply of blood to heart,. There are two types of cholesterol: (i) HDL cholesterol, its value shall be more than 40 mg/dl indicates the good , and higher the value it is better, and (ii) LDL cholesterol , it should be less than 130 mg/dl for good health and LDL to HDL ratio should be 3 for minimum risk. Decreased HDL cholesterol and/ or increased LDL cholesterol are associated with increased risk of coronary artery disease. Fuzzy functions for systolic BP, diastolic BP , LDL cholesterol, and HDL cholesterol are considered similar to functions shown in fig.3, respectively. These can be represented by the following fuzzy sets eqns. (3)-(17) :

For Diastolic Pressure, eqns. are

$$\mu(L) = 1, \quad BP \le 70$$
$$= (80-BP)/10, \quad 70 \le BP \le 80$$
$$= 0, \quad \text{otherwise} \qquad (3)$$
$$\mu(M) = (80 - BP)/10, \quad 70 \le BP \le 80$$
$$= 1, \quad BP = 80$$
$$= (BP - 90)/10, \quad 80 \le BP \le 90$$
$$= 0, \quad \text{otherwise} \qquad (4)$$
$$\mu(H) = (BP - 90)/10, \quad 80 \le BP \le 90$$
$$= 1, \quad BP \ge 90 \qquad (5)$$

For Systolic Pressure, eqns. are:

$$\mu(L) = 1, \quad BP \le 110$$
$$= (120 - BP)/10, \quad 110 \le BP \le 120$$
$$= 0, \quad \text{otherwise} \qquad (6)$$
$$\mu(M) = (120 - BP)/10, \quad 110 \le BP \le 120$$
$$= 1, \quad BP = 120$$
$$= (BP-130)/10, \quad 120 \le BP \le 130$$
$$= 0, \quad \text{Otherwise} \qquad (7)$$
$$\mu(H) = (BP-130)/10, \quad 120 \le BP \le 130$$
$$= 1, \quad BP \ge 130 \qquad (8)$$

LDL Cholesterol eqns. are:

$$\mu(G) = 1, \quad \text{LDL Cholesterol} \le 120$$
$$= (130-chol)/10, \quad 120 \le cholesterol \le 130$$
$$= 0, \quad \text{otherwise} \qquad (9)$$
$$\mu(M) = (130-chol)/10, \quad 120 \le cholesterol \le 130$$
$$= 1, \quad cholesterol = 130$$
$$= (chol-140)/10, \quad 130 \le cholesterol \le 140$$
$$= 0, \quad \text{otherwise} \qquad (10)$$
$$\mu(B) = (chol-130)/10, \quad 130 \le cholesterol \le 140$$
$$= 1, \quad \text{Otherwise} \ge 14 \qquad (11)$$

HDL Cholesterol eqns. are:

$$\mu(B) = 1, \quad \text{HDL Cholesterol} \le 30$$
$$= (40-chol)/10, \quad 30 \le cholesterol \le 40$$
$$= 0, \quad \text{otherwise} \qquad (12)$$
$$\mu(M) = (40-chol)/10, \quad 30 \le cholesterol \le 40$$
$$= 1, \quad cholesterol = 40$$
$$= (chol-50)/10, \quad 40 \le cholesterol \le 50$$
$$= 0, \quad \text{otherwise} \qquad (13)$$
$$\mu(G) = (chol-40)/10, \quad 40 \le cholesterol \le 50$$
$$= 1, \quad \text{Otherwise} \ge 50 \qquad (14)$$

For Disease eqns. are :

Range (1-5): Severe = 1, Medium = 3, Low = 5

$$\mu(L) = 1, \quad D \le 2$$
$$= (3-D)/1, \quad 2 \le D \le 3$$
$$= 0, \quad \text{otherwise} \qquad (15)$$
$$\mu(M) = (3-D)/1, \quad 2 \le D \le 3$$
$$= 1, \quad D = 3$$
$$= (D-4)/1, \quad 3 \le D \le 4$$
$$= 0, \quad \text{Otherwise} \qquad (16)$$
$$\mu(H) = (D-4)/1, \quad 3 \le D \le 4$$
$$= 1, \quad D \ge 4 \qquad (17)$$

VII. APPLICATION OF GENETIC ALGORITHM TO FUZZY SETS

The universe of discourse for blood pressure and cholesterol are similar to fig.(3), however, value of a0,a1,a2 and ,a3 for systolic pressure, diastolic pressure, LDL Cholesterol, HDL Cholesterol, and disease are (100,60,100,20,1), (110,70,120, 30,2), (120,80,130,40,3), and (130,90,140,50,4), respectively , are perfectly triangular in shape .The tuning of this fuzzy function has been done with the help of genetic algorithm. Initially the ideal shape of fuzzy function has been assumed. The fuzzy sets are given below, eqns.(18)- (32).

For Systolic Pressure,

$$\mu(L) = 1.0/100+1.0/105+1.0/110+0.5/115+0/120+0/125+0/130 +0/135 + 0/140 \qquad (18)$$
$$\mu(M) = 0/100+0/105+0/110+0.5/115+1.0/120+0.5/125+0/130 +0/135 + 0/140 \qquad (19)$$
$$\mu(H) = 0/100+0/105+0/110+0/115+0/120+0.5/125+1.0/130 +1.0/135 + 1.0/140 \qquad (20)$$

For Diastolic Pressure,

$$\mu(L) = 1.0/60+1.0/65+1.0/70+0.5/75+0/80+0/85+0/90 +0/95+0/100 \qquad (21)$$
$$\mu(M) = 0/60+0/65+0/70+0.5/75+1.0/80+0.5/85+0/90 +0/95 + 0/100 \qquad (22)$$
$$\mu(H) = 0/60+0/65+0/70+0/75+0/80+0.5/85+1.0/90 +1.0/95 + 1.0/140 \qquad (23)$$

For LDL Cholesterol,

$$\mu(G) = 1.0/110+1.0/115+1.0/120+0.5/125+0/130+0/135$$

+0/140+0/145+0/150 (24)

μ (M) = 0/110+0/115+0/120+0.5/125+1.0/130+0.5/135 +0/140+0/145+0/150 (25)

μ (B) =0/110+0/115+0/120+0/125+0/130+0.5/135 +1.0/140+1.0/145+1.0/150 (26)

For HDL Cholesterol,

μ (B) =1.0/20+1.0/25+1.0/30+0.5/35+0/40+0/45+0/50 +0/55+0/ 60 (27)

μ (M) =0/20+0/25+0/30+0.5/35+1.0/40+0.5/45+0/50 +0/55+0/ 60 (28)

μ (G) = 0/20+0/25+0/30+0/35+0/40+0.5/45+1.0/50 + 1.0/55+1.0/ 60 (29)

For Disease,

μ (L) =1.0/1+1.0/1.5+1.0/2+0.5/2.5+0/3+0/3.5+0/4 (30)

μ (M) =0/1+0/1.5+0/2+0.5/2.5+1.0/3+0.5/3.5+0/4 (31)

μ (H) =0/1+0/1.5+0/2+0/2.5+0/3+0.5/3.5+1.0/4 (32)

Thus, the encoded strings for Diastolic Pressure are given by:

μ (L) =1010 1010 1010 0101 0000 0000 0000 0000 0000(33)

μ (M) =0000 0000 0000 0101 1010 0101 0000 0000 0000(34)

μ (H) =0000 0000 0000 0000 0000 01011010 10101010 (35)

The encoded strings for Systolic Pressure are given by:

μ (L) =1010 1010 1010 0101 0000 0000 0000 0000 0000(36)

μ (M) =0000 0000 0000 0101 1010 0101 0000 0000 0000(37)

μ (H) =0000 0000 0000 0000 0000 0101 1010 1010 1010(38)

The encoded strings for LDL Cholesterol are given by:

μ (G) =1010 1010 1010 0101 0000 0000 0000 0000 0000(39)

μ (M =0000 0000 0000 0101 1010 0101 0000 0000 0000(40)

μ (B)= 0000 0000 0000 0000 0101 0101 1010 1010 1010(41)

The encoded strings for HDL Cholesterol are given by:

μ (B) =1010 1010 1010 0101 0000 0000 0000 0000 0000(42)

μ (M)=0000 0000 0000 0101 1010 0101 0000 0000 0000(43)

μ (M)=0000 0000 0000 0000 0101 0101 1010 1010 1010(44)

The encoded strings for Disease are given by:

μ (L) =1010 1010 1010 0101 0101 0000 0000 (45)

μ (M) =0000 0000 0000 0101 1010 0101 0000 (46)

μ (H) = 0000 0000 0000 0000 0000 0101 1010 (47)

In order to apply crossover operator to the diastolic fuzzy function μ (L) following random string is considered.

1000 0000 000010000 0000 0000 0000 0000 0000 0000 (48)

Two point crossover is applied between diastolic pressure string and random string. Thus, two output strings are again obtained as below.

1000 1010 1000 0101 0000 0000 0000 0000 0000 (49)

1010 0000 1010 0000 0000 0000 0000 0000 0000 (50)

The fitness value of strings (49), and (50) is 63.8 and 65, respectively. In order to get the best fitness value, cross over operator and mutation operator are applied to strings given by eqn. (49) and (50) again . This process is repeated until the best value of fitness is obtained. The final fuzzy function for μ(L)is given by .:

0.0 1.0 1.0 0.5 0.0 0.0 0.0 0.0 0.0 (51)

This fuzzy function has maximum value of fitness function. Similarly, the fuzzy function for μ (M), and μ (H) are optimized using genetic algorithm and optimized fuzzy function for diastolic pressure is given by fig.4.

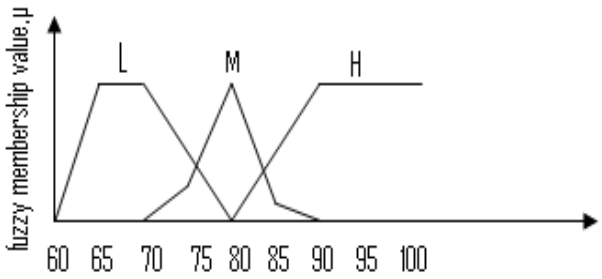

Fig.4 Optimised fuzzy function

The new fuzzy function (universe of discourse) is shown in fig.4, when the genetic algorithm is applied to the fuzzy functions related to diastolic pressure. The optimized fuzzy functions for systolic pressure, LDL cholesterol, HDL cholesterol , and disease are shown in fig.5-8.

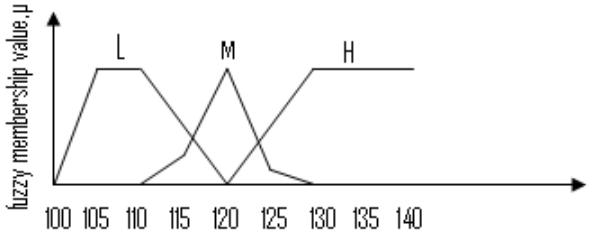

Fig.5 optimised fuzzy function for systolic pressure

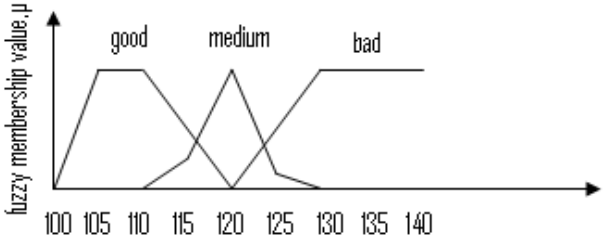

Fig. 6 Optimised fuzzy function for LDL cholesterol

VIII. CASE STUDY [10]-[11]

In order to show the utility of optimize design fuzzy functions for patient data processing in telemedicine, two case studies have considered. In first case, the blood pressure data (85/135) of a patient, 35 years of age with no blood pressure history, at 120 km is communicated using BSNL trunk lines TCP/IP protocol. The blood pressure data, received at physician / doctor expert end is processed using Fourier

method and fuzzy logic tool. The reliability of information

Fig.7 optimised fuzzy function for HDL cholesterol

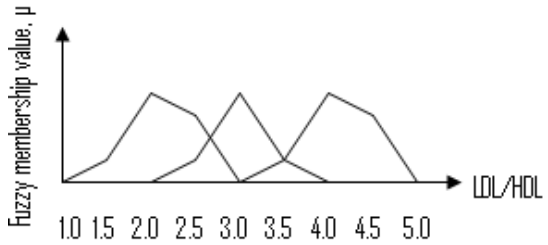

Fig.8 Optimised fuzzy function for disease

extraction from received data is 82% and 96%, respectively for the two methods when compared with the measurement at patient end. From fig.4, it is noted that the pressure related to diastolic fuzzy set is (0.0, 0.2, 0.5) whereas from fig.5 the systolic pressure fuzzy set is (0.0,0.0,1.0). This clearly shows from fig (4) and fig.(5) that the blood pressure is high. Thus, the doctor prescribes the medicine corresponding to high blood pressure to the patient at 120km.

For case-II, the cholesterol data (115-LDL, 25-HDL)of a patient, 78 years of age with no family history of heart problem, at 120 km is also communicated on same channel. Reliability of information extraction from cholesterol data received at physician end, by processing with two methods, is again the same as that of blood pressure case. Measurement of LDL cholesterol and HDL cholesterol are taken as 115 and 25, respectively. The ratio of LDL/HDL ratio = 115/25. The corresponding fuzzy value for LDL, and HDL, are (0 0 1), (0.2, 0.75, 0.0), (0.8,0.0,0.0), and (0.0 0.0 0.8). Now applying Mamdani [1]-[2] rule for extracting the severity of disease, the risk factor is high and need further investigations.

IX. CONCLUSION

In this paper, the fuzzy-genetic algorithm has been applied for processing the patient data received from 120km distance. From the optimized fuzzy function, it is noted that S-shaped fuzzy function is more appropriate to triangular function when processing related to biological data is carried out. The results show that uncertainties and ambiguities present in the patient data/ information due to any cause can be taken into account by fuzzy logic method, wherein the genetic algorithm optimizes the fuzzy functions. The authors in this paper have applied the developed algorithm in two case studies. Similarly for other symptoms, it can be applied to other patient data/ information communicated to radiologist, pathologist etc. which deal with uncertainties and the vagueness. Validation of the proposed algorithm is to be further carried out on more patients data communicated from tribal areas/ rural areas under different environment conditions.

REFERENCES

[1] J. Harris, An introduction to Fuzzy Logic Applications, Norwell, MA: Kluwer, 2000, pp: 1-10, 198-208.

[2] R.R.Yoger and D.P. Filev, Essential of fuzzy Modeling and Control, New York: Wiley, pp1-25, 123-129.

[3] L.A. Zadeh," Outline of a new approach to the analysis of complex systems and decision processes", IEEE Trans. System, Man, Cybernatic, SMC-1,PP28-44, 1973.

[4] M. Mitchell, An Introduction to genetic Algorithm, pp: 1-25, 90-115, 2002..

[5] A. Homaifar and E. McCormic," Simultaneous design of membership functions and rule sets for fuzzy controller using genetic algorithm, IEEE Trans Fuzzy system, vol.3, pp129-139, May 1995.

[6] Y. shi, R. Eberhart, and Y. Chen," IEEE Trans Fuzzy System, Vol.7, pp: 109-119, Apr.1999.

[7] G.P. Bansal, A.K.Tiwari, and P.K. Chande,"Genetic algorithm based fuzzy expert systems", IETE Tech. Rev., Vol. 19, no. 3, pp 111-118, May-June 2002.

[8] M.Setnes and H. Robos," GA – Fuzzy modeling and classification: complexity and performance", IEEE Trans Fuzzy Syst., Vol.8, pp 509-522, Oct. 2000.

[9] H. Ishibuchi, K. Nozaki, N.Yamamoto, and H. Tanak," Selecting fuzzy if- than rules for classification problems using genetic algorithm", IEEE Trans, Fuzzy Syst. Vol.3, pp.260-270, Aug.1995.

[10] David L. Paul, Keri E. Pearlson and Reuben R," Assessing technological barriers to telemedicine: Technology- Management implications.,IEEE Trans on engineering Management, Vol. 46, No,3, pp: 279-288, Aug. 19999..

[11] A. Rovetta, A. Cuce, C. Solenghi, and M.Bisogni," Remote house call" , IEEE Robotics & Automation Magazine, Vol.10, Issue 1, pp: 65-71, 2007.

[12] Parmod Kumar, V.K.Chandna,Mini S Thomas," Fuzzy Genetic Algorithm For Preprocessing Data At RTU ," IEEE Transaction On Power Systems, No.19, Vol.2,May-2004,Pp 718-723.

JOURNAL OF Applied Polymer SCIENCE

Graft-Interpenetrating Polymer Networks of Epoxy with Polyurethanes Derived from Poly(ethyleneterephthalate) Waste

Saurabh Chaudhary,[1,2] Surekha Parthasarathy,[1] Devendra Kumar,[2] Chitra Rajagopal,[1] Prasun Kumar Roy[1]

[1]Centre for Fire, Explosive and Environment Safety, DRDO, Timarpur, Delhi 110054, India

[2]Department of Applied Chemistry and Polymer Technology, Delhi Technological University, Delhi 110042, India

Correspondence to: P. K. Roy (E-mail: pk_roy2000@yahoo.com or pkroy@cfees.drdo.in)

ABSTRACT: Polyester polyurethanes derived from poly(ethyleneterephthalate) (PET) glycolysates were blended with epoxy to form graft-interpenetrating networks (IPNs) with improved mechanical properties. Microwave-assisted glycolytic depolymerization of PET was performed in the presence of polyethylene glycols of different molecular weights (600–1500). The resultant hydroxyl terminated polyester was used for synthesis of polyurethane prepolymer which was subsequently reacted with epoxy resin to generate grafted structures. The epoxy-polyurethane blend was cured with triethylene tetramine under ambient conditions to result in graft IPNs. Blending resulted in an improvement in the mechanical properties, the extent of which was found to be dependant both on the amount as well as molecular weight of PET-based polyurethane employed. Maximum improvement was observed in epoxy blends prepared with polyurethane (PU1000) at a loading of 10% w/w which resulted in 61% increase in tensile strength and 212% increase in impact strength. The extent of toughening was quantified by flexural studies under single edge notch bending (SENB) mode. In comparison to the unmodified epoxy, the Mode I fracture toughness (K_{IC}) and fracture energy (G_{IC}) increased by ~45% and ~184%, respectively. The underlying toughening mechanisms were identified by fractographic analysis, which generated evidence of rubber cavitation, microcracking, and crack path deflection. © 2014 Wiley Periodicals, Inc. J. Appl. Polym. Sci. **2014**, *131*, 40490.

KEYWORDS: blends; grafting; mechanical properties; polyesters; polyurethanes

Received 25 October 2013; accepted 21 January 2014

DOI: 10.1002/app.40490

INTRODUCTION

The last few decades have seen an enormous increase in the usage Poly(ethyleneterephthalate) (PET) as packaging material, primarily because of its excellent mechanical and barrier properties, low cost, and high energy effectiveness. The largest consumption of this thermoplastic is by the textile sector for production of synthetic fibers, followed by bottling industry for packaging beverages, particularly carbonated drinks.[1] Unfortunately, the large scale usage of PET, in conjunction with irresponsible methods of disposal has led to its accumulation in the environment, for which it has received much criticism by environmentalists.[2]

Several strategies have evolved for effective management of PET wastes, the most common being the "primary" and "secondary" recycling techniques.[3] Although, the last two decades have seen huge advancements in "bottle to fiber and bottle to bottle" recycling technologies,[1] only a fraction of PET is practically recycled, the primary reason being the high cost of the recycled product.[4] It is thus highly desirous to adopt technically and economically feasible routes towards recycling of PET into industrially important products. In this context, tertiary recycling of PET offers interesting possibilities.[5–7] This process refers to the chemical depolymerization of PET, leading to the production of fuels or basic chemicals. The ester linkages which form the backbone of PET can be chemically transformed by processes like glycolysis, aminolysis, hydrolysis, acidolysis, alkalolysis, and alcoholysis, out of which the former two have reached the level of commercial maturity.[5,7] The polyester polyols formed as a result of glycolytic depolymerization of PET have further been used for preparation of industrially important polymers including polyurethanes,[8,9] unsaturated polyesters,[10] and UV curable films.[11]

In our previous papers,[6,12–14] we have demonstrated the potential of microwave-assisted glycolytic process towards reducing the time and energy requirements towards PET depolymerization. The aromatic polyester polyols obtained by PET glycolysis

Additional Supporting Information may be found in the online version of this article.

were used to prepare polyurethane foams with superior mechanical properties as compared with its aliphatic analogs. This was attributed to the presence of aromatic functionalities in the polyurethane main chain.[14] We hypothesize that introduction of PET-derived polyurethanes can result in substantial improvements in mechanical properties of brittle polymers, provided optimized blends are formulated.

In this context, blending of epoxy with elastomeric polyurethanes has been attempted to improve the fracture toughness of the base brittle thermoset.[15–20] Epoxy-polyurethane blends offer interesting properties, as polyurethanes are associated with excellent elasticity, abrasion resistance, and damping properties, while the epoxy resins possess excellent mechanical properties along with strong adhesion to metals. Polyurethanes are particularly attractive elastomers for toughening purpose, because of the possibility of tailoring its mechanical properties by altering the chemical structure.[16,21–25] Several attempts in this direction have been made where the polyurethane is derived from poly(oxyethylene),[19] poly(oxytetramethylene),[26] poly(caprolactone),[27] poly (oxypropylene),[18] castor oil,[16,20] and polyester polyols.[16] However, the potential of PET glycolysate-based polyurethane has not yet been explored.

In this article, we report the preparation of an epoxy network with aromatic polyester polyurethanes derived from PET wastes by microwave-assisted glycolysis. The reaction of terminal NCO in polyurethane with the hydroxyl groups available with the epoxy resin leads to grafting and subsequent curing of the epoxy resin leads to the formation of graft-interpenetrating networks, with enhanced mechanical properties.[28] The primary aim of this work is to improve the energy absorption characteristics of the base epoxy resin by blending with PET-based polyurethanes, and to gain insight into the underlying toughening mechanisms.

EXPERIMENTAL

Materials

Disposed PET bottles were collected, washed, dried, and used after removal of the polyethylene caps and the polypropylene label. The bottles were shredded into small pieces (6 mm × 6 mm) and glycolytic experiments were performed with polyethylene glycol (PEG) of varying molecular weights for which PEG 600, PEG 1000, and PEG 1500 (E. Merck) were used. Zinc acetate dihydrate [Zn $(CH3COO)_2$. $2H_2O$, Merck] with a purity of 99% was employed as the trans-esterification catalyst. Metallic carboxylate-based catalyst, Di-butyltinlaurate (DBTL), Diphenylmethane 4,4'-diisocyanate: a mixture of di- and triisocyanates (MDI) was obtained from E. Merck were used without any further purification. Di-glycidyl ether of bis-phenol A epoxy resin (DGEBA) (Huntsman, Araldite GY 250; epoxy equivalent 190 g/eq) and triethylene tetramine (TETA) hardener (HY 951; amine content 32 eq/kg) were used as received.

Microwave-Assisted Glycolysis

Microwave-assisted glycolysis of PET was performed in the presence of glycols of varying molecular weight as per the procedure reported previously.[13] A domestic microwave oven (LG) with a magnetron source for microwave generation (2.45 GHz, maximum power: 900 W) was used for this purpose. PET pieces (10 g) together with requisite amount of glycol and zinc acetate (0.5%, w/w, PET) were introduced into a loosely stoppered reaction flask which was placed in the microwave reactor. PET glycolysis was performed at PET : glycol: 1 : 2, and the reaction was allowed to proceed at 450 W for extended time periods. After predetermined periods, the reaction mixture was filtered through a copper wire mesh (0.5 × 0.5 mm^2 pore size), and the remaining unreacted PET flakes were weighed to quantify the extent of PET conversion, as the ratio of mass of PET reacted to the initial mass of the flakes taken. To obtain the polyol, the reaction mixture was cooled to room temperature, dissolved in a suitable amount of $CHCl_3$, and shaken vigorously with an equal amount of distilled water in a separating funnel to get rid of the unreacted glycol and zinc acetate catalyst. The organic layer was subsequently collected, and the residual water was removed in a rotary evaporator. The obtained glycolysates were dried over molecular sieve (5A) and stored under desiccation. The obtained polyols will be referred to as PY-*x*, where *x* refers to the molecular weight of glycol used for its preparation. For example, PY-1000 refers to the polyester polyol formed after glycolysis of PET with PEG 1000.

Synthesis of Polyurethane Prepolymer

PET glycolysate-based NCO terminated polyurethanes was prepared by adding requisite amount of diphenylmethane-4,4′-diisocyanate (PET glycolysate : MDI :: 1: 2) in a round bottom flask in the presence of DBTL as a catalyst. The reaction was performed under inert atmosphere at 15°C, which was maintained using an ice bath. The polyurethane prepolymer obtained will be designated as PU *x*, where *x* refer to the molar mass of glycol used for glycolysis.

Preparation of Epoxy Blends

The polyurethane prepolymer was added to epoxy resin in varying amounts (5, 10, and 15% w/w) and stirred for 10 min (700 rpm) on a magnetic stirrer under ambient temperature to aid homogenization. TETA hardener was subsequently added and the mixture was degassed to remove entrapped air bubbles and poured into silicone molds for specimen preparation. For comparison purposes, neat epoxy samples were also prepared, which will be referred to as EP. All grafted IPNs prepared in the presence of polyurethanes will be referred to as E*y*PU*x*, where *x* refers to the molecular weight of glycol used for its preparation and *y* refers to the amount of polyurethane in the formulation (% w/w). For example, E10PU600 refers to a blend of epoxy with PU 600 (10% w/w).

CHARACTERIZATION TECHNIQUES

Viscometric Studies

The viscosity-average molecular weight of PET was determined by solution viscometry. Samples were dissolved in a mixture of phenol and 1,1,2,2-tetrachloroethane (60/40 w/w) under heating, and the intrinsic viscosity [η] was measured using Ubbelohde suspension level viscometer at 25°C. The viscosity average molecular weight of PET was calculated using the following equation[29]:

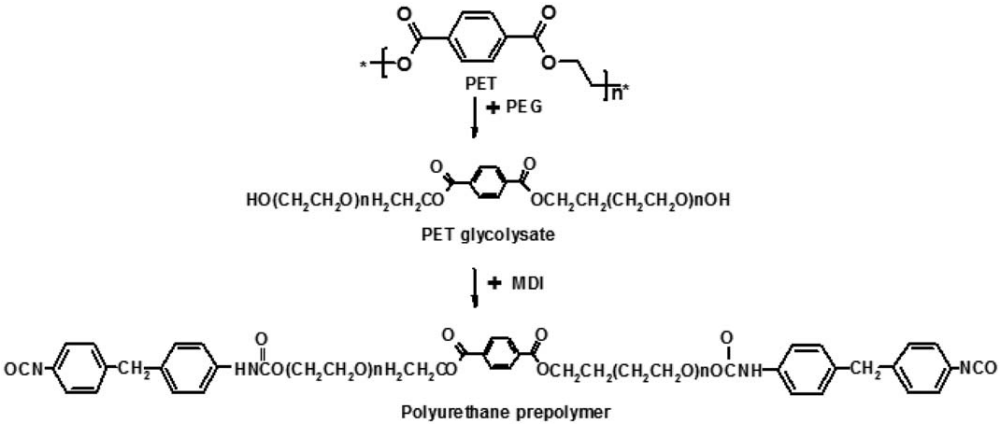

Scheme 1. Reaction schematic illustrating the formation of PET-derived polyurethane.

$$[\eta] = 75.5 \times 10^{-3}\text{mL}/\text{g}M_v^{0.685} \quad (1)$$

The intrinsic viscosity of the glycolysed polyols was determined in methanol at 25°C.

Hydroxyl Number Estimation

The hydroxyl number (HN) was determined using acetic anhydride, as per test method A, described in ASTM D 4274–99. For the purpose of acid number determination, the solution was titrated against standard methanolic KOH solution in acetone medium, as per the procedure reported previously.

Isocyanate Content

The NCO content was determined by nonaqueous titrimetry as per the established procedure, where the polyurethane was allowed to react with excess dibutylamine under reflux. The amount of unreacted dibutylamine was quantified by titrating against standard hydrocholoric acid, which was used to estimate the NCO content in the prepolymer.

Structural Characterization

The FTIR spectra of samples were recorded in the wavelength range 4000–600 cm^{-1} using Fourier Transform Infrared (FTIR) spectroscopy on a Thermo Fisher FTIR (NICOLET 8700) with an attenuated total reflectance (ATR) crystal accessory.

Thermal Characterization

The changes in the thermal properties of the samples were investigated using DSC (TA instruments, Q 20 module) under nitrogen atmosphere. Approximately 4–6 mg of the sample was placed in a 40 μL aluminum cap without pin and sealed with a lid. After erasing the thermal history of samples, they subjected to a heating program from −60 to 250°C at 10°C min^{-1}. Thermogravimetric studies were performed using Perkin Elmer Diamond STG-DTA-DSC in N_2 atmosphere in the temperature range of 50–800°C. A heating rate of 10°C min^{-1} and sample mass of 5.0 ± 0.5 mg was used for each experiment. Percentage crystallinity was calculated from the DSC traces as follows.

$$\%\,\text{Crystallinity} = \frac{\Delta H_{f\,(\text{observed})}}{\Delta H_{f\,(100\%\,\text{crystalline})}} \times 100 \quad (2)$$

where $\Delta H_{f(\text{observed})}$ is the enthalpy associated with melting of the material and $\Delta H_{f(100\%\ \text{crystalline})}$ is the enthalpy of 100% crystalline PET reported in the literature to be 135.8 J g^{-1} (Ref. 30).

Evaluation of Mechanical Properties

Quasi-static mechanical properties were determined according to ASTM method D638 using a Universal Testing System (International equipments) at ambient temperature. The samples were subjected to a cross head speed of 50 mm min^{-1}. The notched Izod impact strength of the specimens was determined according to ASTM D 256 using an impact strength testing machine (International Equipments, India) at a striking velocity of 3.5 m s^{-1}. Six identical specimens were tested for each composition and the average results along with the standard deviation values have been reported.

Notched flexural testing of the samples was performed under three point single edge notch bending mode according to ASTM D 5045. For this purpose, specimens of requisite dimensions (127 mm length × 12.5 mm width × 3.5 mm thickness and 3 mm notch) were prepared and subjected to a deformation rate of 2 mm min^{-1} while maintaining 60 mm span length. The data obtained was analyzed to determine the mode I fracture toughness (K_{IC}) and fracture energy (G_{IC}),[31] by assuming the Poisson's ratio of epoxy to be 0.35.[32]

Morphological Studies

The surface morphology of samples was studied using a Scanning Electron Microscope (Zeiss EVO MA15) under an acceleration voltage of 20 kV. Samples were mounted on metal stubs and sputter-coated with gold and palladium (10 nm) using a sputter coater (Quorum-SC7620) operating at 10–12 mA for 60 s.

RESULTS AND DISCUSSION

Polyester Polyols from PET by Microwave-Assisted Glycolysis

A schematic of the PET glycolytic process, followed by its reaction with isocyanate is presented in Scheme 1. The conditions employed for glycolysis have been discussed in our previous papers.[12,13] The TG and DSC trace of the PET used for this study is presented in the Supporting Information Figure S1. The PET samples exhibit a sharp melting point peaking at 246°C and undergoes a single step decomposition commencing at 400°C. The DSC crystallinity as determined from the area

Table I. Characteristics of the Glycolysed Polyols

Polyol	HN (mg KOH/g)	[η] (dL/g)	M_n	M_w	M_z	PDI
PL 600	110.3 ± 5	0.045	1114	2025	3074	1.8
PL 1000	86.4 ± 4	0.051	1745	3078	4436	1.7
PL 1500	32 ± 3	0.056	2776	4080	5508	1.5

under the endotherm is ~27.2% and the molecular weight (M_v) of PET, as determined from viscometric studies is 27,431. Transesterification of PET resulted in the formation of a viscous liquid, which was soluble in nonpolar organic solvents like $CHCl_3$, CH_2Cl_2, CCl_4, benzene, toluene, etc. and could be separated from the water soluble reactants and catalyst by water extraction. The maximum level of PET conversion could be achieved within 30 min of irradiation, while under the same PET : glycol concentrations; the reaction takes ~9 h to reach the same level of depolymerization.

Physical Properties of Polyols

The HN of the glycolyzed products obtained after the reaction of PET with increasing molecular weight glycols after microwave irradiation for 30 min is listed in Table I. The intrinsic viscosities as determined in methanol at 25°C, along with the M_n, M_w, and M_z values, as obtained by GPC are also presented. It is to be noted that prior to determination of the HN, the liquid sample was extracted with chloroform, to eliminate the contribution of water soluble reactants i.e. PEG and side products, i.e. ethylene glycol, to the HN. As expected, with increasing molecular mass of glycol employed for the transesterification purpose, the intrinsic viscosity and the molecular mass of the resulting polyol increases, while the hydroxyl number decreased.

PET-Derived Polyurethane

The resulting polyester polyols were subsequently reacted with MDI to prepare NCO terminated polyurethane prepolymer (PET glycolysate : MDI :: 1 : 2). The FTIR spectra of PET, a representative glycolysate (PY 1000) and the polyurethane prepolymer obtained there from (PU 1000) is presented in Figure 1. Both PET as well as its glycolysed derivative exhibit absorption band peaking at 1715 cm^{-1} due to carbonyl stretching ($\nu_{C=O}$). The appearance of a broad absorption band (~3200–3600 cm^{-1}) in the spectra of glycolysed PET can be attributed to the presence of terminal hydroxyl groups. An absorption peak at 2200 cm^{-1} can be seen in the FTIR spectra of PU prepolymer, which can be attributed to the NCO

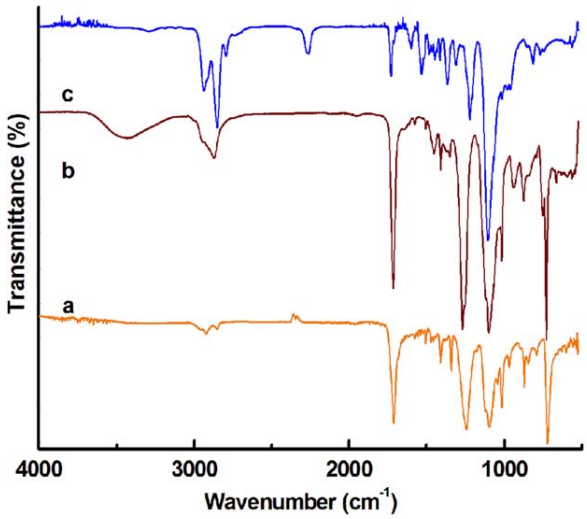

Figure 1. FTIR spectra (a) PET, (b) PY 1000, (c) PU 1000. [Color figure can be viewed in the online issue, which is available at wileyonlinelibrary.com.]

stretching (ν_{NCO}). The intensity of the hydroxyl band (~3200–3600 cm^{-1}) was substantially lower in the PU prepolymer, which is expected on the basis of its reaction with isocyanates.

Epoxy-Polyurethane Blends

Graft interpenetrating network of epoxy with polyurethane prepolymer was prepared by reacting the terminal NCO functionalities with the pendant hydroxyl groups available with the DGEBA-based epoxy resin to form polyurethane linkages (Scheme 2). In addition to increased interpenetration due to grafting, the possibility of hydrogen bonding between the hydroxyl groups in cured epoxy with the >C═O groups of both carbamate and ester groups in polyurethane is expected to render improved mechanical strength to these blends.

It is to be noted that the uncured epoxy resin and polyurethane prepolymer were completely miscible under the experimental conditions employed, thereby forming a clear solution. The progress of this reaction was monitored by following the decrease in the intensity of the absorption band peaking at 2200 cm^{-1} (Figure 2). The NCO content was also determined by titrimetry and the decrease in the NCO indices is also presented in the figure. As expected, the intensity of the epoxide group stretching vibrations at 920 cm^{-1} remained unaltered, which clearly reveals the availability of these groups for subsequent curing

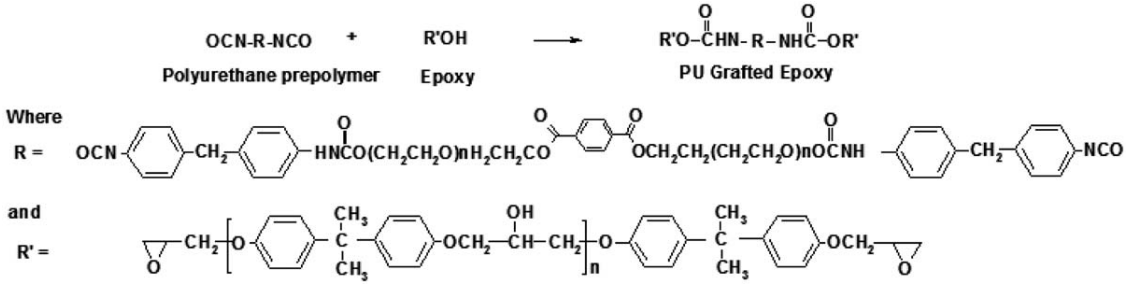

Scheme 2. Schematic representing the formation of epoxy-polyurethane graft interpenetrating networks.

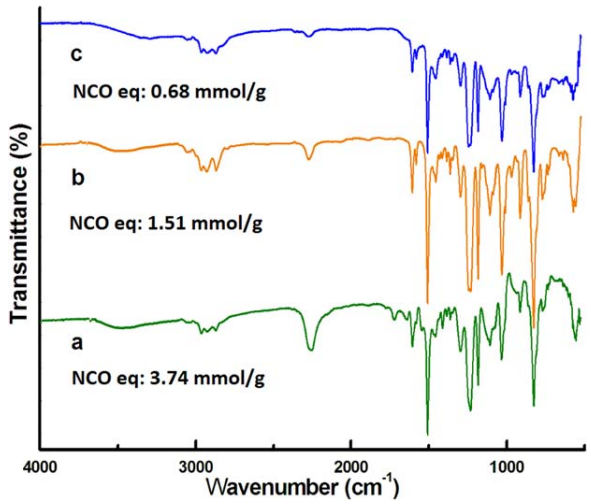

Figure 2. Changes in the FTIR spectra and NCO index due to grafting reaction of polyurethane with epoxy (E5PU1000) (a) 2 min, (b) 6 min, and (c) 10 min. [Color figure can be viewed in the online issue, which is available at wileyonlinelibrary.com.]

reaction. The resin was cured with TETA hardener after leveling of the isocyanate index (~10 min), which was allowed to continue for 24 h under ambient conditions.

The gel content of cured compositions was determined in order to quantify the extent of insolubility, which in turn is dependent on the extent of grafting and crosslinking. All the samples exhibited complete insolubility, as evidenced by high gel content ~98.5 ± 1%, irrespective of the amount and type of polyurethane used in the formulation, which confirms the formation of completely insoluble graft-interpenetrating networks.

Mechanical Properties

The effect of increasing the extent of polyurethane loading and chain length on the mechanical properties of the graft IPNs is presented in Figure 3 and the data is also tabulated in the Supporting Information Table S1. It can be seen that both tensile strength and impact toughness increased significantly due to introduction of polyurethane, which can be attributed to the increased level of interpenetration occurring as a consequence of grafting reaction.[20] In addition, the intermolecular hydrogen bonds between the hydroxy groups available in cured epoxy with the carbonyl group of urethane and ester, are also expected to contribute significantly to the energy absorption characteristics of the polymer. Of all the formulations studied, maximum improvement was observed in blends prepared with polyurethane loading of 10% w/w (E10PU1000) which resulted in 61% increase in tensile strength and 212% increase in impact strength.

Earlier studies have revealed that blending of epoxy with poly(oxyethylene) (PEG 400)-based polyurethane led to 60% improvement in the impact strength,[15] while in a separate study introduction of polyurethane (40% w/w) reportedly increased the impact toughness by 46%.[33] In comparison, the improvement in impact strength is larger (190%) when poly(oxypropylene)-based polyurethanes are blended with epoxy. Interestingly, blending of epoxy with polyester polyurethanes leads to larger improvements in impact strength (200%),[17] as compared with polyether polyurethanes[15] which may be attributed to the additional sites of hydrogen bonding available with the former. However, irrespective of the type of polyurethane being blended, the main cause behind the toughened nature of blends is the elastomeric nature of the polymer. The introduction of this rubbery phase hinders the process of crack propagation in the brittle epoxy matrix.[15] The decrease in properties at higher loadings (>10%), can be attributed to the formation of large separated phase domains at higher loadings.[17]

The flexural stress–strain response of neat epoxy has been compared with that of its blends with polyurethane in Figure 4. As expected, the graft IPNs exhibited higher flexural strength and high level of extensibility as compared with unmodified epoxy. More importantly, the graft-IPNs could be flexed to a higher extent and results in the yielding of the matrix prior to fracture, which in turn reflected in larger values of fracture toughness (K_{IC}). The load-deflection curve for notched specimens is also presented in Figure 4 (Inset), which clearly reveal the detrimental effect of notch on the flexural strength, which in turn can be attributed to stress concentration resulting from the reduced cross-sectional area.

A comparison of critical stress intensity factor (K_{IC}) and fracture energy (G_{IC}) as a function of polyurethane loading is presented in Figure 5. The stress intensity factor K_{IC} of epoxy

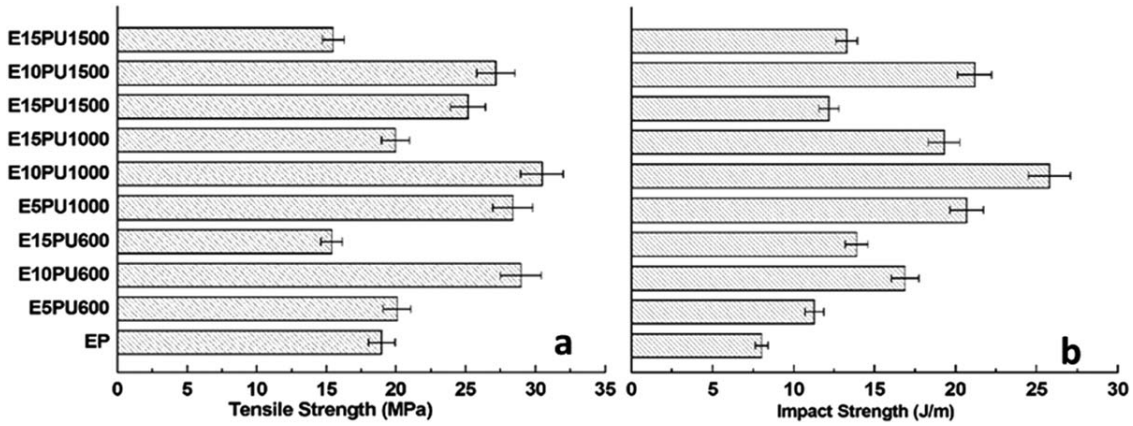

Figure 3. Improvement in mechanical properties of epoxy due to formation of graft IPN (a) Tensile Strength (b) Impact toughness.

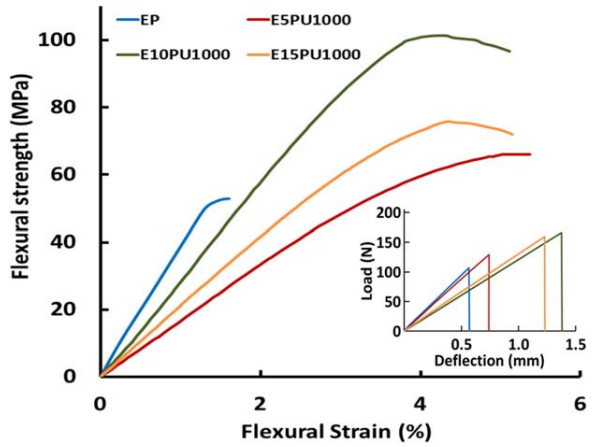

Figure 4. Representative stress–strain curves of epoxy and its blends with graft IPN with polyurethanes (flexural mode). Inset shows the effect of notch on the flexural response of specimens. [Color figure can be viewed in the online issue, which is available at wileyonlinelibrary.com.]

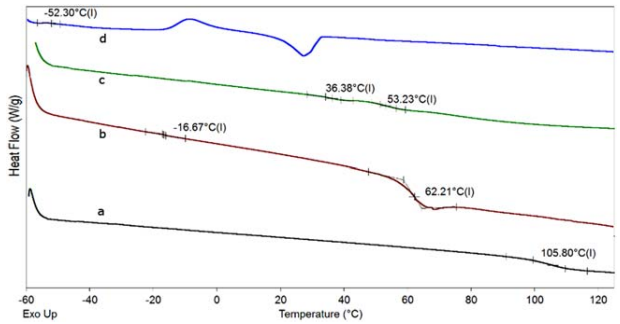

Figure 6. DSC traces of cured samples (a) neat epoxy, (b) E10PU1000, (c) E15PU 1000, and (d) PU 1000. [Color figure can be viewed in the online issue, which is available at wileyonlinelibrary.com.]

increased on blending, from an initial value of 2.18 MPa $m^{1/2}$ (unmodified) to 3.18 MPa $m^{1/2}$ for E10PU1000, which corresponds to an increase of ~45.8%. The K_{IC} values were further used to calculate the fracture energy, which too was found to increase substantially, from a mean value of 4.29 ± 0.4 kJ m^{-2} (unmodified epoxy) to 12.2 ± 0.4 kJ m^{-2} after blending with 10% PU 1000 (184% increase). Our studies clearly bring out the potential of PET glycolysate-based polyurethane in the field of epoxy toughening.

Thermal Properties

The DSC traces of the cured epoxy and the graft networks formed with PU1000 are presented in Figure 6. The change in the baseline of the DSC trace of cured epoxy resin at ~106°C is associated with the reversible glass-rubber like transition of the amorphous epoxy structure, corresponding to the glass transition temperature (T_g) of the neat resin. It is to be noted that the reported T_g is just a convenient numerical representation of the entire glass transition region. For comparison purposes, DSC analysis of cured polyurethane (PET glycolysate : NCO::1 : 1) was also performed, which revealed that the neat polyurethane exhibits elastomeric nature with a glass transition at −53°C followed by cold crystallization and melting. It is apparent from the figure that the glass transition region corresponding to the PU in the graft IPN shifts towards higher temperature, while that of epoxy is lowered, with the extent of shift being proportional to the amount of polyurethane blended, a feature characteristic of a partially miscible blends. Interestingly, epoxy-PEG graft IPNs have been reported to exhibit a single T_g characteristic of completely miscible blends.[34] The partial miscibility observed in this study can be attributed to the aromatic groups present in the PU segment, which results in phase separation.

The TG trace of epoxy and its graft IPN with polyurethane (PU 1000) is presented in Figure 7 and the data is tabulated in Supporting Information Table S2. The degradation behavior of epoxy resins have been extensively studied by several researchers,[35] and a two-step degradation process is generally reported. The first step is associated with evolution of water at $T > 100$°C, followed by the pyrolytic decomposition of the main chain at ~350°C, leading to the formation of condensable like acetone,

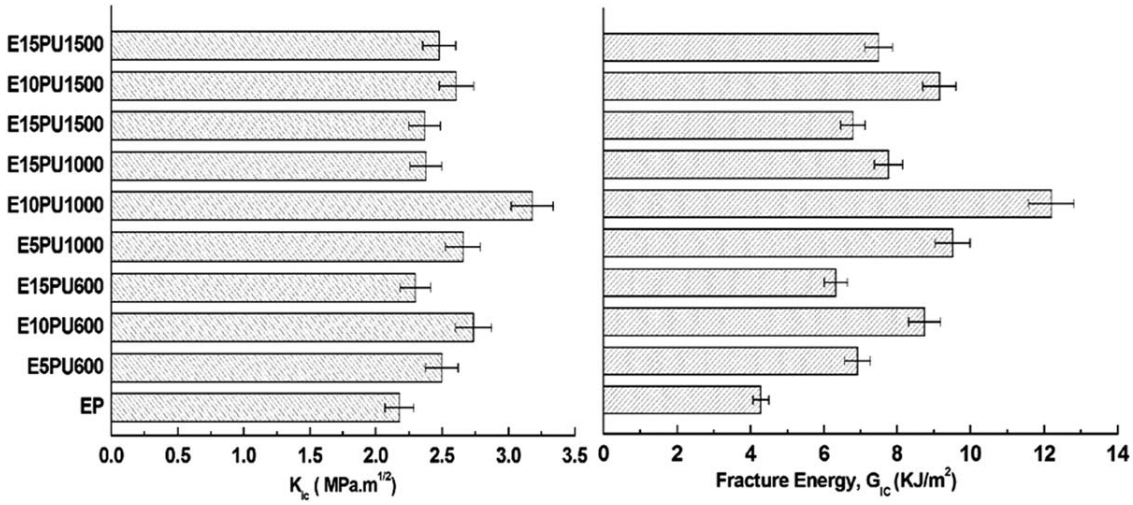

Figure 5. Improvement in fracture toughness (K_{IC}) and fracture energy (G_{IC}) of epoxy due to formation of graft IPNs.

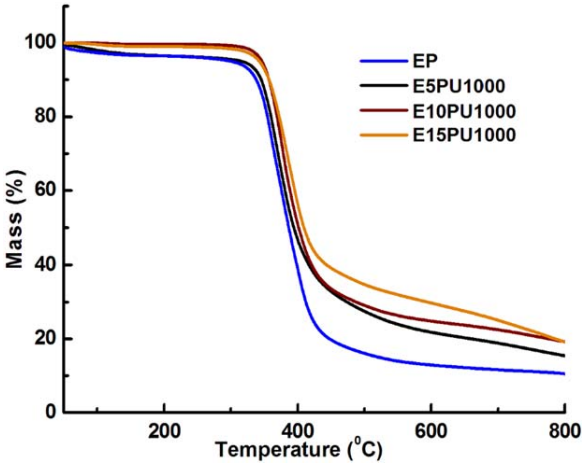

Figure 7. TGA trace of epoxy and its graft IPNs with polyurethane. [Color figure can be viewed in the online issue, which is available at wileyonlinelibrary.com.]

carbon dioxide, hydrogen cyanide, aliphatic hydrocarbons, etc.[35] The graft IPNS exhibit higher thermal stability in comparison to epoxy, which can be attributed to the presence of intermolecular hydrogen bonds between the hydroxyl group of epoxy and the carbamate group in polyurethane chain.[33] The IPNs also exhibited slightly higher char content as compared with the neat resin. However, the studies clearly established that all the compositions can safely be employed in service till 250°C, without any appreciable thermal degradation.

Morphological Studies

Fractographic analysis on the cracked surfaces was performed to gain an insight into the underlying micro-mechanisms behind the toughened nature of the graft IPNs. For this purpose, the fracture surface of both pristine epoxy and the interpenetrating networks were examined by SEM and the images are presented in Figure 8. As can be seen, the fracture surface of neat epoxy is almost featureless, indicative of uninterrupted crack propagation. Feather-like hackle markings could be observed on the surface of pristine epoxy, which changed into striations [Figure 8(a)] and finally transition to a mirror-like fracture surface.[14] These surface features are characteristic of brittle failure, which in turn accounts for the low fracture toughness of neat epoxy.[36] Figure 8(b–d) presents the micrographs of fracture surfaces of the interpenetrating networks, which appear to be comparatively rough. The surface aberrations are clearly indicative of the significant amount of plastic deformation which occurs in the material prior to its ductile failure. Interesting features could be observed on the surface of IPNs at higher magnification. Evidence of rubber cavitation is presented in Figure 8(b–d), a mechanism which is most commonly cited to explain the toughened nature of rubber-epoxy blends. Tensile loading results in dilation of the plastic region surrounding the rubbery polyurethane phase, leading to its cavitation from within. The role of the cavitation process, therefore, is to relieve the plane strain constraint from the surrounding matrix which permits significant amount of plastic deformation.[37]

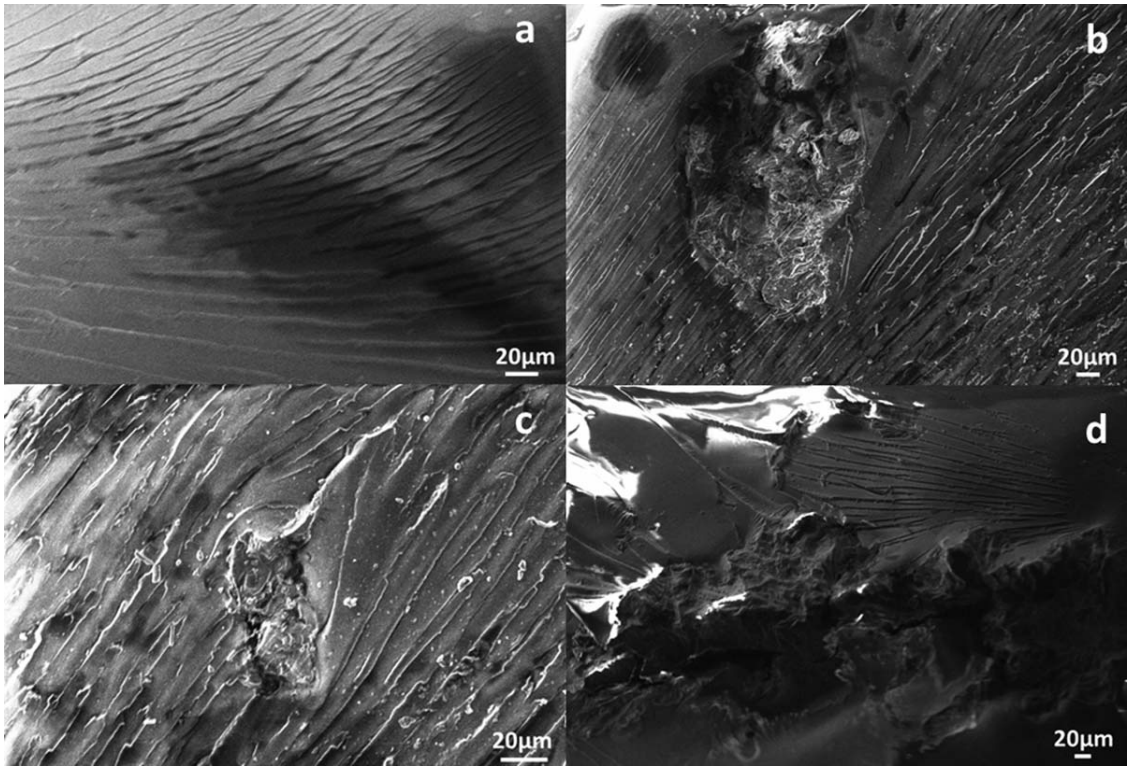

Figure 8. SEM images of fractured surface (a) neat epoxy, (b) E5PU1000, (c) E10PU 1000, and (d) E15PU 1000.

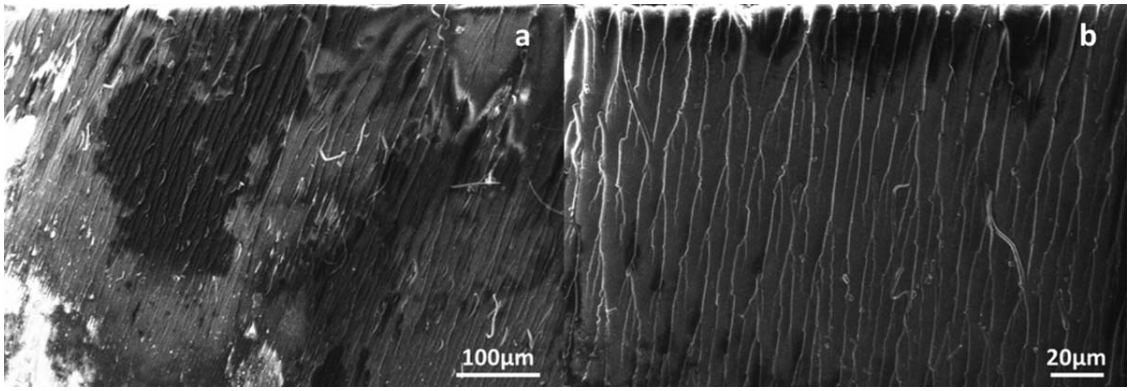

Figure 9. SEM images of fractured surface of E10PU1000 at different magnifications.

Another mechanism which can be used to explain the toughening in these toughened composites is that of particle yielding induced shear banding.[38] The process starts with the yielding of the polyurethane, thereby producing significant stress concentration, which in turn initiates shear banding in the matrix.

The rough texture of the fracture surface can also be attributed to crack path deflection and microcracking.[39] As a result of these phenomena, the surface area of the crack increases substantially and the mode I character of the crack opening is reduced, thereby resulting in increased energy for crack propagation. SEM micrographs at different magnifications are clearly indicative of this phenomenon (Figure 9).

CONCLUSIONS

PET was catalytically glycolysed with aliphatic polyethyleneglycols of varying molecular weight (600–1500) under microwave-assisted conditions. The resulting polyester polyols were reacted with MDI to form isocyanate terminated polyurethane prepolymer, which was subsequently blended with epoxy resin to form graft interpenetrating networks. The blends exhibited partially miscible nature, as indicated by two glass transition temperature with the shift in T_g being proportional to the amount of polyurethane being blended. The mechanical properties of the graft IPNs were studied under both quasi-static and dynamic conditions. In comparison to the neat resin, significant improvements in both tensile as well as impact strength were observed, the extent of which was dependant on the molecular weight of the polyurethane being introduced. Blending of epoxy with PU 1000 resulted in maximum improvement in the mechanical properties, with the improvement in impact properties being more pronounced (221% increase). As expected, the introduction of elastomeric polyurethane led to significant improvement in the fracture toughness, as indicated by flexure testing under single edge notch bending mode. The K_{IC} and G_{IC} values were found to increase by 46% and 184%, respectively as compared with neat resin. Morphological studies on the fracture surfaces was performed to gain an insight into the underlying toughening mechanisms. The unmodified epoxy fracture surface was featureless indicating brittle failure, while clear evidence of microcracking and rubber cavitation was observed on the fracture surface of the IPNs.

ACKNOWLEDGMENTS

The authors are thankful to Director, Centre for Fire, Explosive and Environment Safety, Delhi, India, for his keen interest in the work and providing logistic support to perform the study.

REFERENCES

1. Welle, F. *Resour. Conserv. Recycl.* **2011**, *55*, 865.
2. Bartolome, L.; Imran, M.; Cho, B. G.; Al-Masry, W. A.; Kim, D. H., Eds. Recent Developments in the Chemical Recycling of PET; InTech: Rijeka, Croatia, **2012**.
3. Shen, L.; Worrell, E.; Patel, M. K. *Resour. Conserv. Recycl.* **2010**, *55*, 34.
4. Lin, C. C. *Macromol. Symp.* **1998**, *135*, 129.
5. Nikles, D. E.; Farahat, M. S. *Macromol. Mater. Eng.* **2005**, *290*, 13.
6. Manju, P. K. R.; Ramanan, A.; Rajagopal, C. *Mater. Lett.* **2013**, *106*, 390.
7. Awaja, F.; Pavel, D. *Eur. Polym. J.* **2005**, *41*, 1453.
8. Vaidya, U. R.; Nadkarni, V. M. *J. Appl. Polym. Sci.* **1998**, *35*, 775.
9. Vitkauskiene, I.; Makuska, R.; Stirna, U.; Cabulis, U. *J. Cell. Plast.* **2011**, *47*, 467.
10. Abu Bakar, D. R.; Ahmad, I.; Ramli, A. *Malaysian J. Chem.* **2006**, *8*, 022.
11. Kao, C. Y.; Cheng, W. H.; Wan, B. Z. *Thermochim. Acta* **1997**, *292*, 95.
12. Chaudhary, S.; Parthasarathy, S.; Kumar, D.; Rajagopal, C.; Roy, P. K. *J. Appl. Polym. Sci.*, *131*, DOI:10.1002/app.39941 (2013).
13. Chaudhary, S.; Surekha, P.; Kumar, D.; Rajagopal, C.; Roy, P. K. *J. Appl. Polym. Sci.* **2013**, *129*, 2779.
14. Roy, P. K.; Mathur, R.; Kumar, D.; Rajagopal, C. *J. Env. Chem. Eng.* **2013**, *1*, 1062.
15. Bakar, M.; Hausnerova, B.; Kostrzewa, M. *J. Thermoplast. Compos. Mater.* **2013**, *26*, 1364.
16. Harani, H.; Fellahi, S.; Bakar, M. *J. Appl. Polym. Sci.* **1998**, *70*, 2603.
17. Harani, H.; Fellahi, S.; Bakar, M. *J. Appl. Polym. Sci.* **1999**, *71*, 29.

18. Kostrzewa, M.; Hausnerova, B.; Bakar, M.; Dalka, M. *J. Appl. Polym. Sci.* **2011**, *122*, 1722.
19. Ong, S.; Ismail, J.; Bakar, M. A.; Rahman, I. A.; Sipaut, C. S.; Chee, C. K. *J. Appl. Polym. Sci.* **2009**, *111*, 3094.
20. Raymond, M. P.; Bui, V. T. *J. Appl. Polym. Sci.* **1998**, *70*, 1649.
21. Yeganeh, H.; Hojati-Talemi, P. *Polym. Degrad. Stab.* **2007**, *92*, 480.
22. Klinedinst, D. B.; Yilgör, I.; Yilgör, E.; Zhang, M.; Wilkes, G. L. *Polymer* **2012**, *53*, 5358.
23. Desai, S.; Thakore, I. M.; Sarawade, B. D.; Devi, S. *Eur. Polym. J.* **2000**, *36*, 711.
24. Huang, J.; Zhang, L. *Polymer* **2002**, *43*, 2287.
25. Rosu, D.; Rosu, L.; Varganici, C.-D. *J. Anal. Appl. Pyrolysis* **2013**, *100*, 103.
26. Wang, H.-H.; Chen, J.-C. *J. Appl. Polym. Sci.* **1995**, *57*, 671.
27. Yeganeh, H.; Lakouraj, M. M.; Jamshidi, S. *Eur. Polym. J.* **2005**, *41*, 2370.
28. Kostrzewa, M.; Hausnerova, B.; Bakar, M.; Siwek, E. *J. Appl. Polym. Sci.* **2011**, *119*, 2925.
29. Wang, H.; Liu, Y.; Li, Z.; Zhang, X.; Zhang, S.; Zhang, Y. *Eur. Polym. J.* **2009**, *45*, 1535.
30. Jog, J. P. *J. Macromol. Sci. Part C* **1995**, *35*, 531.
31. Knott, J. F. *Fundamentals of Fracture Mechanics*; Butterworths: London, **1976**.
32. Chen, J.; Kinloch, A. J.; Sprenger, S.; Taylor, A. C. *Polymer* **2013**, *54*, 4276.
33. Park, S.-J.; Jin, J.-S. *J. Appl. Polym. Sci.* **2001**, *82*, 775.
34. Varganici, C.-D.; Rosu, L.; Rosu, D.; Simionescu, B. C. *Compos. Part B: Eng.* **2013**, *50*, 273.
35. Vogt, J. *Thermochim. Acta* **1985**, *85*, 411.
36. Roy, P. K.; Ullas, A. V.; Chaudhary, S.; Mangla, V.; Sharma, P.; Kumar, D.; Rajagopal, C. *Iran. Polym. J.* **2013**, *22*, 709.
37. Bagheri, R.; Pearson, R. A. *Polymer* **2000**, *41*, 269.
38. Chen, T.; Jan, Y. *J. Mater. Sci.* **1991**, *26*, 5848.
39. Pearson, R. A.; Yee, A. F. *Polymer* **1993**, *34*, 3658.

ISSN NO. 2320-5407

Journal homepage: http://www.journalijar.com

INTERNATIONAL JOURNAL OF ADVANCED RESEARCH

RESEARCH ARTICLE

GUAR GUM AND THEIR DERIVATIVES: A RESEARCH PROFILE

Anek Pal Gupta[1] and Devendra Kumar Verma[1*]

[1]Department of Applied Chemistry and Polymer Technology, Delhi Technological University (Formerly Delhi College of Engineering), Shahabad, Daulatpur, Bawana road, Delhi-110042, India.

*Corresponding author email: vermadev148@gmail.com

Manuscript Info

Manuscript History:

Received: 10 November 2013
Final Accepted: 25 December 2013
Published Online: January 2014

Key words:

Guar gum, Research profile, Guar gum derivatives.

Abstract

It is fact that Polymers and their products have changed the face of the world in all the field of the technology. They are the future of the coming up generation of the research of the world. But this is also fact that these synthetic non biodegradable polymers have created a tough situation for the living being for a healthy life. So now this is our priority to change the flow of our research from non-biodegradable polymeric product to the biodegradable polymeric products. Guar gum and their derivatives are fully biodegradable natural polymers. In this review we have described the huge research on guar gum and their derivatives and their application in different areas in last ten years. The aim of this review is also to find out the new area of research where guar gum and their derivatives can be used.

Introduction

Guar gum also called Guaran, Clusterbean, Calcutta lucern, Gum cyamposis, Cyamopsis gum, Guarina, Glucotard and Guyan is a natural non-ionic, water soluble polysaccharide exhausted from the refined endosperm of cluster bean seeds. Guar gum is a galactomannan [7, 8] similar to locust bean gum consisting of α (1, 4)-linked β- D-mannopyranose backbone with branch points from their 6- positions linked to α-D-galactose (i.e. 1, 6-linked-α-D-galactopyranose) (Dodi, 2011; Singh, 2011).

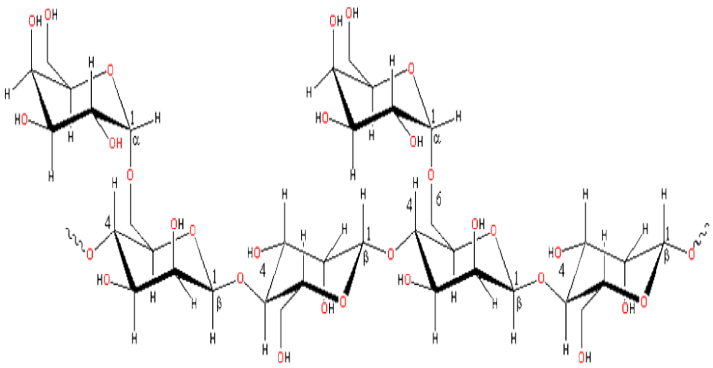

Fig.1.Chemical structure of guar gum

This polysaccharide has been extensively used in a wide range of applications because of its unique ability to alter the rheological properties [4, 15], the thickening and the viscosity of aqueous solution.

Qualities and Properties of Guar Gum

1. Guar gum has excellent property of high viscosity i.e. the result of its large hydrodynamic volume in solution and the nature of its specific intermolecular interactions (entanglements).

2. Guar gum products show a pronounced temperature thinning effect when their solutions are heated [5]. This is caused by loss of water of hydration around the polymer molecule which makes the guar gum most applicable natural polymer.

Application of Guar Gum and Its Derivatives: Guar gum and its derivatives have a long chain [6] of applications in all fields of sciences. Some of them are as:

1. Guar Gum as Dietary Fibers [1]

High viscosity of guar gum decreases the protein efficacy and lipid utilization during interfering with the digestion and absorption of nutrient (when it dissolved into water), results in slower, gastric problems. To solve this problem, PHGG (Partially Hydrolysed Guar Gum) named as Sun fibre is now being used in various beverages, food products and medicinal foods as a safe, natural and functional dietary fibre in all over the world.

2. Guar Gum as Sensor and Semiconductor

Recently J. I. Kadowaka [2] from Kagoshima University has developed a Semiconducting Guar Gum film and Temperature Sensing film [12] from an ionic liquid, 1-butyl-3-methyl-imidazolium chloride. D. B. Kestwal [3] have developed dip- strip sucrose sensor by the help of guar gum, chitosan and polyacrylamide hydrogels.

3. Guar Gum as in Drug Delivery [9, 10]

Guar gum is used for colon delivery [11] because it can be degraded by specific enzymes. The gum protects the drug during passing through the stomach and in small intestine environment and delivers the drug to the colon where it undergoes assimilation by specific microorganism

4. Guar Gum in Pharmaceutical and Pharmacological Profile.[14]

Guar gum has wide applications in pharmaceutical like cosmetic, food, textile, paper, explosive and toiletries industries etc. Therapeutically it is used as hypoglycaemic, hypolipidemic, antimicrobial, antiproliferative, bulk forming etc. Guar gum c-glycosylated derivative obtained by chemical modification of guar gum were found to have anti-inflammatory and anti-proliferative activity. The metabolic profile suggests that guar gum consumption contributes to better long term control in several diabetic, non –insulin dependent.

Need of derivatives of guar gum?

Although guar gum is abundantly available at low cost but its uncontrolled rate of hydration decreases its viscosity upon storage and further microbial contamination limits its long term applications. So guar gum has been chemically derived to modify into various properties for broaden its industrial applications such as in food, paint and pigments, oil field, mining, paper, water treatment, personal care, pharmaceutical and new types of superabsorbent. Some of the derivatives of the guar gum are listed below:

1. Carboxymethyl guar gum [13].
2. Hydroxymethyl guar gum[28].
3. Hydroxypropyl guar gum [29].
4. O- carboxymethyl- O-hydroxypropyl guar gum (CMHPG) [30].
5. O-2hydroxy-3- (trimethylammonia propyl) guar gum (HTPG).
6. O-carboyxymethyl-O-2 hydroxy-3-(trimethylammonia propyl) guar gum (CMHTPG) [34].
7. Ammonium hydroxyl propyl trimethyl chloride of guar gum [33].
8. Acryloyloxy guar gum [31].
9. Methacryloyl guar gum.[32].
10. Methylated guar gum.
11. Sulfated guar gum.[55]
12. Guar gum esters.[54]

The most specific property of the guar gum and their derivatives is that they have hydroxyl groups, which makes them suitable for making changes in their structure formula and functionalization. A lot of research has been done

on guar gum for the changing their physical and chemical properties by grafting, blending and compositing with synthetic and natural polymers.

Grafting:

Graft copolymerization of methyl methacrylate onto guar gum was carried out by Brij Raj Sharma et al [16] in an aqueous medium using a Ceric ammonium nitrate–nitric acid initiation system. The percent grafting (%G) and percent grafting efficiency (%GE) were determined as functions of the concentrations of Ceric ammonium nitrate, nitric acid, methyl methacrylate, guar gum, polymerization temperature and time. The optimum reaction conditions obtained for grafting of MMA onto GG were: amount of GG = 0:1g/L, CAN= 0:02 mol/L,MMA= 0:35 mol/L, HNO3=0:2M, reaction time =3 h and temperature of reaction = 308^{o}C

As a natural biopolymer, guar gum (GG) was covalently grafted [17] on the surfaces of multiwall carbon nanotube (MWCNT) to obtain GG–MWCNT composite. Then iron oxide nanoparticles were synthesized on the GG–MWCNT to prepare the magnetic GG–MWCNT–Fe3O4. GG–MWCNT was composed of about 21.6 wt% GG components, which enhanced the dispersion of GG–MWCNT in aqueous solution and also acted as a template for growth of iron oxide nanoparticles. GG–MWCNT–Fe3O4 exhibited superparamagnetic with a saturation magnetization (13.3 emu g−1), and good adsorption on neutral red and methylene blue. GG–MWCNT–Fe3O4 could be easily separated from the aqueous solution in a magnetic field.

A novel polymeric flocculant based on polyacrylamide grafted carboxymethyl guar gum (CMG-g-PAM) [18] had been synthesised by grafting polyacrylamide chains onto CMG backbone using conventional redox grafting and microwave assisted grafting methods. The flocculation characteristics of grafted and ungrafted polysaccharides had been evaluated in kaolin suspension, municipal sewage wastewater and decolourization efficiency of a dye solution (methylene blue). It was evident from results that CMG-g-PAM synthesised by microwave assisted grafting method was showing best flocculation characteristics.

Guaran was transformed into Guaran Grafted Polystyrene (G-G-Ps) Copolymer using vinyl monomer [19]. The grafting was initiated through the formation of free radical centres on the polymer backbone by oxidation of guaran with cerium (IV) in nitric acid medium. It was concluded that the guaran offers a very regular linear matrix suitable for incorporating the desired physical and chemical properties through appropriate grafting and crosslinkage. The viscosity, hydrophilic-hydrophobic nature of the graft, degree of grafting and chain length of the graft was found of great significance in mineral processing and petroleum industries.

A new sorbent material[20] based on guar gum (GG) was prepared by the polymerization grafting of acrylamide (Aam) onto guar gum, using potassium bromate/thiourea dioxide redox system for initiating the polymerization reaction. The so prepared polyacrylamide/guar gum graft copolymer (PAamGG) was further crosslinked with glutaraldehyde (GA) to obtain the sorbent material in the form of hydrogel. The so-obtained hydrogel was used for removal of hexavalent chromium ion (Cr (VI)) from its aqueous solution. It was found from the study that the sorption of Cr (VI) by the hydrogel was pH-dependent and maximum sorption was obtained at pH 3. The sorption data obeyed Langmuir and Freundlich sorption isotherms. The Langmuir sorption capacity (Qmax) was found to be 588.24 mg/g. Freundlish constants, KF and n, were found to be 55.03 and 2.835, respectively.

Modification [21] of either guar gum or hydroxyopropyl guar was achieved in a three-step process: carboxymethylation with sodium chloroacetate, esterification with dimethyl sulfate (DMS) and amidation with a series of polyalkoxyalkyleneamines by Ahmad Bahamdan. It was concluded that the solutions of the new derivatives possessed viscosities of approximately ten times less than the viscosities of the parent materials.

The graft copolymerization of 4-vinyl pyridine [22] onto guar gum initiated by potassium peroxymonosulphate/ascorbic acid redox pair in an aqueous medium was studied gravimetrically under a nitrogen atmosphere. The thermal analysis data showed that the synthesized graft-copolymer was more thermally stable than the un-grafted guar gum by considering the value of FDT and char yield. It was concluded that the synthesized graft-copolymer can be used as a coating material when protection from excessive heat is needed.

p-toluenesulfonate esters hydroxypropyl guar gum[23]- A new guar gum derivative containing amino group was synthesized through nucleophilic substitution of p-toluenesulfonate activated hydroxypropyl guar gum with ethanolamine.

Guar gum/polyacrylamide graft copolymer [24] was prepared in the presence of potassium bromate/thiourea dioxide as initiation system. The so-prepared and separated guar gum/polyacrylamide graft copolymer was used for preparation of silver nanoparticles through reduction of silver nitrate under certain conditions. For comparison, guar gum, polyacrylamide and guar gum/polyacrylamide composite were used individually for the preparation of silver nanoparticles under the same conditions. It was concluded that TEM images showed that 85% of silver nanoparticles prepared using the separated graft copolymer fall within the narrow range of 15–20 nm, while in case of using the composite for silver nanoparticles preparation, the histogram showed wide range of particle size distribution.

Graft copolymers of carboxymethyl guar gum (CMGG) and polyacrylamide (PAM) had been synthesized by grafting polyacrylamide [25] chains onto carboxymethyl guar gum backbone using a ceric-ion-induced solution polymerization technique. It was found that flocculation efficiency of CMGG graft copolymer shows better flocculation performance.

Guar gum (GG) was chemically modified with polyaniline (PANI) using ammonium persulfate (APS) as oxidant/initiator in acidic condition [57]. The solubility of copolymer in water was not obtained up to 230 %G. The maximum bulk electrical conductivity of the copolymer was 1.63×10^{-2} S/cm at pH 1. The grafted materials had hybrid properties of GG biopolymer and PANI both. It was concluded that Cyanaposis tetragonolobus could be usefully exploited for making environmental-friendly semiconductor devices by grafting with PANI, and would be novel materials for the fabrication of various electronic sensors.

Table 1. Guar gum modified by grafting and their different uses.

S. no.	Guar gum graft copolymer	Initiated by	Applications	References
1.	Methyl methacrylate onto guar gum	Ceric ammonium nitrate–nitric acid	---	Brij Raj Sharma et al. 2003 [16]
2.	Polyacrylamide grafted carboxymethyl guar gum	Potassium persulphate solution	Treatment of wastewater.	Sagar Pala, et al.2011. [18]
3.	Guaran Grafted Polystyrene (G-G-Ps) Copolymer	Cerium (IV) in nitric acid medium	In mineral processing and petroleum industries.	A.V. Singh et al.2010. [19]
4.	Acrylamide (Aam) onto guar gum	Potassium bromate/thiourea dioxide redox system	Removal of hexavalent chromium ion (Cr (VI)) from its aqueous solution.	E.S. Abdel-Halim, 2011. [20].
5.	copolymerization of 4-vinyl pyridine onto guar gum	Potassium peroxymonosulphate/ascorbic acid redox pair	As a coating material, when protection from excessive heat is needed.	Abhishek Srivastava et al. 2007.[22]
6.	p-toluenesulfonate esters hydroxypropyl guar gum	Tosyl chloride in pyridine,	----	Yongchao Zhao, et al. 2012 [23]
7.	Guar gum/polyacrylamide graft copolymer	Potassium bromate/thiourea dioxide	Used for synthesis of silver nanoparticles.	E.S. Abdel-Halima et al,2011. [24]
8.	carboxymethyl guar gum (CMGG) and polyacrylamide (PAM)	Ceric-ion-induced solution	polymeric flocculant material	P. Adhikary et al. 2011. [25]
9.	Magnetic guar gum grafted carbon nanotube.	-----	For removal of dye from the water	Li Yana et al.2012. [17].
10.	Guar gum graft polyaniline	APS (ammonium persulphate) in acidic medium	For making environmental-friendly	Tiwari,A., et al.2008. [57]

			semiconductor devices	

Blends:

Cationic guar gum (GG) and sodium carboxymethylcellulose (NaCMC) blend film [26] was synthesised by casting method. Differential scanning calorimetry (DSC), FTIR, X-ray diffraction (XRD), and viscosity methods were used to examine the miscibility, interaction, and degradability of cationic guar gum (GG) and sodium carboxymethylcellulose (NaCMC) in their blend films. Blend films was **degradable quicker** than pure GG or NaCMC film. It was concluded that GG/NaCMC blend films have good sustained release performance.

Polymer dispersions of Ethylcellulose (EC)/ inulin (IN), Ethylcellulose (EC)/Guar Gum (GG) or Ethylcellulose (EC)/ levan (LEV) blends[27], containing up 30% of the oligo-polysaccharide, were used for film casting on a Teflon" plate. All the films were tested for the thermal analysis. It was observed that Tmax1 (temperature at which a thermal degradation rate goes up to a maximum) and (OH (wavenumber at which the OH absorption band are centralised) show similar trends in the composition range of the studied blends.

Films from waterborne polyurethane (WPU) and carboxymethylated guar gum (CMGG) [35] with different contents (20–80 wt %) were prepared through solution casting method, and then were crosslinked with calcium chloride. The effect of CMGG content on the miscibility, morphology and physical properties of the blend films was investigated. The results revealed that the blend film had higher thermal stability and tensile strength than that of the WPU film, suggesting good miscibility between WPU and CMGG.

The rheological behavior and synergistic character of mixed polysaccharide systems were examined for blends of xanthan with enzymatically modified guar [36]. Blends of xanthan with enzymatically modified guar gum samples were examined in terms of their dynamic rheological properties and compared to those of xanthan locust bean gum blends. It was found that at constant ionic strength the enzymatically modified guar gum - xanthan blend was more elastic as the temperature of mixing was increased.

A new polymeric film based on blends of cellulose acetate and guar gum [37] blend was synthesized for **coating for colon targeting**. It was found that the blend had good film forming properties. It was resulted that guar gum cellulose acetate blends were highly promising film coating material for targeting the colonic site.

Aqueous polysaccharide blends, formed from 2.5% (w/v) solution of hydroxypropyl guar gum (HPG) and 2.5% (w/v) solution of carboxymethyl cellulose (CMC) [38] according to different blending ratios, were investigated at 20 °C in terms of their shear-dependent viscosity and thixotropic properties. It was found that aqueous HPG/CMC blends behaved as non-Newtonian shear-thinning fluids. Their shear-dependent viscosity behavior could be described using Cross viscosity model with reasonable accuracy.

Novel blends from quaternized polysulfone (QPSF) and benzoyl guar gum (BGG) [39] coded as QB with different contents (10-80 wt %) were prepared through solution casting method. Simultaneously, other kinds of blends were prepared from chloromethylated polysulfone (ClPSF) and BGG coded as ClB to compare the effects of the substituted groups on the miscibility and properties of the composite materials. The results revealed that QB blends had good or certain miscibility over the entire composition ratio of BGG to QPSF under study. It was found that the composite properties changed considerably with moisture content, which attributed that water molecules had a great effect on the hydrogen bonding between the two polymers.

Guar gum, a polymeric galactomannan, was intrinsically modified to a new guar gum benzamide [40]. Benzoylation was carried out by benzoyl chloride reaction in water medium and a propyl amine spacer was used to impart a high degree of hydrophobicity. The ability of GGBA film to **limit bacterial growth** was assessed in qualitative and quantitative experiments. Large inhibitory halo was observed against both gram positive and gram negative organisms.

A comparative study of the rheological properties of guar [GG], methyl guar [MG], hydroxypropyl guar [HPG] and hydroxypropyl-methyl guar [MHPG] [41] polymers aqueous solutions in semidilute (both unentangled and entangled) and concentrated regimes, using oscillatory and steady shear techniques was reported by Daniela Risica et al. The storage and loss moduli of guar and guar derivatives aqueous solutions had been measured using angular frequencies in the range between 10^{-3} and 10 rad/s. The data had been analyzed using the "blob" model for semidilute solutions and the scaling approach proposed by Rubinstein, Dobrynin and Colby for concentrated solutions.

Blend films of chitosan (CH) and hydroxypropyl guar gum (HGG) [42] were prepared using a conventional solvent-casting technique and were dried at room temperature. A good intermolecular interaction was found because of hydrogen bonding between CH and HGG occurred in the blend films. The blend film containing 60% HGG had greater thermal stability than did the other blend and pure CH films. In addition, **the best optical transparency** was observed from 500 to 800 nm in the blend film containing 60% HGG.

Films were prepared by the casting method using sodium alginate (SA) and methacryloyl guar gum (MAG) [43] in different ratios. Water vapor transmission rate and oxygen permeability of the films were investigated. Films were evaluated for mechanical and antibacterial properties. The film prepared with the blend containing 85% MAG and 15% MAG (v/v) was found to be the best as it had lower oxygen permeability, better mechanical properties while retaining the similar **antibacterial properties of MAG,** when compared with MAG film not containing SA.

A study on The swelling/degradation behavior of Ba2+ ions-crosslinked sodium alginate/carboxymethyl guar gum [44] bipolymeric beads which were intended to exhibit greater stability in the environment of changing pH along the gastrointestinal (GI) tract were reported by S.K. Bajpai. Finally, it was concluded that barium ion-crosslinked bipolymeric beads demonstrate **pH-sensitive swelling** and are quite stable in the environment of changing pH, thus offering their strong candidature for possible use in oral delivery of drugs along the GI tract.

The synergistic interaction between the cationic guar gum (the ammonium hydroxyl propyl trimethyl chloride of guar gum) [45] and sodium alginate was studied. The effect of the mass ratio, mixed temperature, balks salt ion concentration, incubation time and pH value on gelation were investigated. It was concluded that the gel strength was maximum at mass ratio 0.6, temperature 70^{o}, balk salt ion concentration 1.0 mol/L, incubation time 30 min and pH 8.

Composites/ nanocomposites:

A guar gum- silver nanocomposite was synthesised for **optical sensor for ammonia detection**. Aqueous ammonia sensing study of polymer/silver nanoparticles nanocomposite (GG/AgNPs NC) [46] was performed by optical method based on surface plasmon resonance (SPR). It was concluded that in the near future we could use our room temperature optical ammonia sensor for clinical and medical diagnosis for detecting low ammonia level in human.

A low cost eco-friendly method for the synthesis of gold nanoparticles (AuNPs) using guar gum (GG) as a reducing agent was reported. GG/AuNPs nanocomposite (GG/AuNPs NC) [47] was exploited **for optical sensor for detection of aqueous ammonia** based on surface plasmon resonance (SPR). It was found to have good reproducibility, response times of ~10 s and excellent sensitivity with a detection limit of 1 ppb (parts-per-billion). It was concluded that, this system could be used for the rapid production of an ultra-low-cost GG/AuNPs NC-based aqueous ammonia sensor.

GG/Ag nanocomposite [48] was synthesized for making a **ammonia gas sensor for chemical reaction** studies. It was concluded that the nanocomposite could detect ammonia as low as 500 parts-per-trillion at room temperature in a minute time. It was demonstrated by results that such made nanocomposite can be used in several applications including homeland security, environmental pollution and leak detection in research laboratories and many others.

Novel montmorillonite nanocomposites were prepared using neutral guar gum and cationic guar gum [49]. It was observed that morphology and structure of the guar-montmorillonite nanocomposites was dependence on the relative amounts of guar and montmorillonite used for their preparation. This was responsible for necessary flexibility for the potential applications of such nanocomposites.

Guar gum–nano zinc oxide (GG/nZnO) biocomposite [50] was used as **an adsorbent for enhanced removal of Cr(VI) from aqueous solution.** The maximum adsorption was achieved at 50 min contact time, 25 mg/L Cr(VI) conc., 1.0 g/L adsorbent dose and 7.0 pH. Langmuir, Freundlich, Dubinin–Kaganer–Radushkevich and Temkin isotherm models were used to interpret the experimental data. It was found that GG/nZnO biocomposite adsorbent showed an improved adsorption capacity for Cr (VI) (q_m = 55.56 mg/g) as compared to other adsorbents reported in the literature. The results suggested that GG/nZnO biocomposite is **economical, eco-friendly** and capable to remove Cr(VI) from natural water resources.

AgNPs were synthesized using a thermo-associating polymer namely, carboxymethyl guar grafted poly(ethylene oxide-co-propylene oxide) [CMG-g-PEPO][51]. It was found that the polymer was acting as both reducing agent as well as **stabilizing/capping agent**. The use of these nanoparticles in the controlled release of Doxorubicin hydrochloride (Dox), an anticancer drug was also demonstrated. The binding of Dox onto the polymer and AgNPs was investigated by XPS and Raman spectroscopy which indicated that a charge-transfer mechanism was operative between the Dox and polymer holding both the entities together.

The effect of acetylation of guar gum [52] on its properties as a filler in an unsaturated polyester matrix was studied. The rheology of the uncured composition indicated increased polymer-filler interaction with increased ester content. It was found that the tensile and flexural properties increased with the acetylation degree of guar gum; however the impact resistance of the composites was reduced. it was concluded that the treatment of GG particles was not restricted to the particle surface as in the case of natural fibres and changed the nature of the filler itself. Polysaccharides could thus be **used as fillers in unsaturated polyester** composites as a replacement to mineral fillers making the composites **more eco-friendly**.

Silver (Ag) nanoparticles were synthesized in aqueous GG solution by using gamma radiation [53]. The nanoparticles in solution were prepared by exposing aqueous solution of GG containing AgNO3 and isopropyl alcohol to 60 Co gamma radiation. The aim of this study was to investigate the optical and structural properties of silver nanoparticles as well as the influence of capping agent concentration, precuessor concentration along with effect of other parameters on nanoparticle size and size distribution.

Silver nanocomposite of carboxymethyl guar grafted poly (ethylene oxide-co-propylene oxide) [CMG-g-PEPO] was synthesized by Nivika R Gupta, et al 2013.[56]. It was found that the polymer acts as both **reducing agent** as well as **stabilizing/capping agent**. The binding of Dox onto the polymer and AgNPs was investigated by XPS and Raman spectroscopy which indicated that a charge-transfer mechanism was operative between the Dox and polymer holding both the entities together.

New cationic biopolymer guar gum alkylamine (GGAA) Silver Nanocomposites [58] was synthesized for Wound healing Applications. In wound healing experiments, faster healing and improved cosmetic appearance were observed in the new nanobiomaterial treated group compared to commercially available silver alginate cream. The nanobiomaterial was observed to promote wound closure by inducing proliferation and migration of the keratinocytes at the wound site.

Gamma ray induced synthesis of Ag clusters in the aqueous medium had been carried out using natural polysaccharide guar gum as a stabilizer.[59] The results showed that guar gum was very effective in binding the Ag clusters and restrict their size in the nano region. From thermogravimetric analysis it had been demonstrated that incorporation of nano sized Ag clusters within guar gum improved the thermal properties of irradiated guar gum.

Guar-gum stabilized copper Nanoparticles catalyst for cycloaddition reaction were synthesised by Ajeet kumar et al.2012. [60] To confirm the morphology of the synthesized nanoparticles, selected area electron diffraction (SAED) analysis of the samples was carried out and it was found that the particles were crystalline in nature which was further confirmed by X-ray diffraction study.

Conclusion

Guar gum and their derivatives have a hues research profile. They have a lot of applications in all fields of sciences. The main reason of easy derivatization of guar gum is the presence of hydroxyl groups which are capable of easy functionalization. Grafting of the guar gum is good technique for getting different materials which can be used in different applications as in treatment of waste water, in mineral processing and petroleum industry, in removal of heavy metals, in coating material for heat and chemicals, in removal of dye from water, synthesis of different nanoparticles and hydrogels. Blending of guar gum with different synthetic and natural polymers has given an extensive uses of guar gum. Good adsorbents, quick biodegradable films, coating material for colon targeting, optically transparent and antimicrobial film (MAG) with pH sensing(with respect to swelling) properties are some of the properties of guar gum blends, which can be obtained by very easy methods. The composite of the guar gum with different nanoparticles have also added a series of application. Guar gum based nanocomposite Gas sensor (quick response in 10 sec.) can be used for homeland security, gases leak detection in research lab and heavy metals removal from waste water.

But even of being such hues research in guar gum, there has been done a little work for nanocomposite. Even now very little work has been done for the affect of guar gum on conducting polymers and their blends, grafting and composite. If we use such natural polymer with conducting polymers, then we can also improve their processing problems and biodegradability. We can synthesize biomaterial based conductive, antimicrobial, pH sensitive nanocomposites and blends which can be used in bare paints, nanopaints, coating material, and sensing devices. A new field for researcher is the use of guar gum and their derivatives as filler in unsaturated polymers composites as a replacement to mineral fillers making the composites more eco-friendly.

So guar gum and their derivatives are even now a big interest of research. New areas are also there where researchers have a great space for research.

References

1. **Yoon, S.J., Chu, D. C., Juneja, L.R. (2008):** Chemical and physical properties, Safety and Application of Partially Hydrolized Guar Gum as Dietary Fiber. *J. Clin. Biochem. Nutr.,* 42:1–7.

2. **Kadowaka, J. I. (2009):** 101 uses for guar gum. *CSHCBM / www.rsc.org/chemicalscience Chemical Science*. 6(7).

3. **Bagal-Kestwala, D., Kestwala, R. M., Chianga, B.M., Karveb M.S.(2011):** Development of dip-strip sucrose sensors: Application of plant invertase immobilized in chitosan–guar gum, gelatin and poly-acrylamide films.*Sensors and Actuators B* 160:1026–1033.

4. **Venugopal, K.N., Abhilash M.(2010):** Study of Hydration Kinetics and Rheological Behaviour of Guar Gum. *International Journal of Pharma Sciences and Research (IJPSR),*1(1):28-39.

5. **Reddy,T.T., Tammishetti,S.(2004):** Free radical degradation of guar gum. *Polymer Degradation and Stability* 86:455-459.

6. **Chudzikowski.R.J.(1971):** Guar gum and its applications. *J Soc.½ osmt,. Gh•m*. 22:43-60.

7. **Abdallah, *M*.(2004.):** Guar Gum as Corrosion Inhibitor for Carbon Steel in Sulfuric Acid Solutions *Portugaliae Electrochimica Acta* 22: 161-175.

8. **Silveira, J.L.M., Bresolin, T.M.B. (2011):** Pharmaceutical Use of Galactomannans. *Quim. Nova,* 34(2), 292-299.

9. **Badmapriya D, Rajalakshmi A.N. (2011):** Guar Gum Based Colon Targeted Drug Delivery System: *In-Vitro* Release Investigation. *Research Journal of Pharmaceutical, Biological and Chemical Sciences.* 2(3): 899.

10. **Mohaptra, Santosh K, Kshirsagar Sanjay J, Bhalekar Magesh R, Shukla Gajendra N, Patil Amol V.(2011):**Development and Evaluation of enzymaticaly triggeded multiparticulate colon targated drug delivery system. *International Journal of Research in Ayurveda and Pharmacy*. 2(1):211-215.

11. **Abhishek Kumar Jain, C. P. Jain.(2011):**Naturally occurring biodegradable polymers for controlled release of ciprofloxacin for treatment of inflammatory bowel disease. *Asian Journal of Pharmaceutical and Clinical Research,* 4(2):16-22.

12. **Prasad. K., Izawa,H., Kaneko,Y., Kadokawa, J-I.(2009).** Preparation of temperature-induced shapeable film material from guar gum-based gel with an ionic liquid. Journal of Materials Chemistry,19: 4088-4090.

13. **Dodi, G., Hritcu, D., Popa, M.I. (2011):** Carboxymethylation of Guar Gum: Synthesis and Characterization. *Cellulose Chem. Technol*., 45 (3-4), 171-176.

14. **Shaikh,T., Kumar, S.S.(2011):** PHARMACEUTICAL AND PHARMACOLOGICAL PROFILE OF GUAR GUM AN OVERVIEW. *International Journal of Pharmacy and Pharmaceutical Sciences*, 3(5):38-40.

15. **Oblonsˇek, M., .Sonja S ˇostar-Turk, Lapasin, R. (2003):** Rheological studies of concentrated guar gum. *Rheol Acta*., 42: 491–499.

16. **Sharma,B.R., Kumar,V., Soni, P.L.(2003):** Ce(IV)-Ion Initiated Graft Copolymerization of Methyl Methacrylate onto Guar Gum. *Journal of Macromolecular Science Part A—Pure and Applied Chemistry*, 40(1):49–60.

17. **Li Y., Peter R.C., Pengwu Z, Xiaofei M.(2012):** Characterization of magnetic guar gum-grafted carbon nanotubes and the adsorption of the dyes. *Carbohydrate Polymers,* 87:1919– 1924.

18. **Pala,S., Ghoraia,S., Dasha,M.K., Ghoshb, S., Udayabhanu, G.(2011):** Flocculation properties of polyacrylamide grafted carboxymethyl guar gum (CMG-g-PAM) synthesised by conventional and microwave assisted method. *Journal of Hazardous Materials,* 192:1580– 1588.

19. **Singh, A.V., Singh, R.(2010):** Synthesis, Characterization and Rheological Properties of Guaran Grafted Polystyrene (G-G-Ps) Copolymer. *Journal of Engineering, Science and Management Education,* 3:47-51.

20. **Abdel-Halim,E.S., Al-Deyab,S.S.(2011):** Hydrogel from crosslinked polyacrylamide/guar gum graft copolymer for sorption of hexavalent chromium ion. *Carbohydrate Polymers* 86:1306– 1312.

21. **Bahamdan.A., William H. D.(2007):** Hydrophobic guar gum derivatives prepared by controlled grafting processes. *Polymers for Advanced Technologies*.18: 652–659.

22. **Srivastava,A., Tripathy,J., Mishra, M.M., Behari, K.(2007):** Modification of Guar Gum through Grafting of 4-Vinyl Pyridine using Potassium Peroxymonosulphate/Ascorbic Acid Redox Pair. *Journal of Applied Polymer Science.*106:1353–1358.

23. **Zhao,Y., He, J., Hana,X., Tian, X., Deng, M., Chen, W., Jiang, B.(2012):** Modification of hydroxypropyl guar gum with ethanolamine. *Carbohydrate Polymers*, 90:988– 992.

24. **Abdel-Halima,E.S., El-Rafieb, Al-Deyab, S.S.(2011):** Polyacrylamide/guar gum graft copolymer for preparation of silver nanoparticles. *Carbohydrate Polymers* 85:692–697.

25. **Adhikary, P., Krishnamoorthi, S., Singh, R.P. (2011):** Synthesis and Characterization of Grafted Carboxymethyl Guar Gum. *Journal of Applied Polymer Science*, 120:2621–2626.

26. **Yi, J.Z., Zhang, L.M.(2007):** Biodegradable Blend Films Based on Two Polysaccharide Derivatives and Their Use as Ibuprofen-Releasing Matrices. *Journal of Applied Polymer Science*, 103:3553–3559.

27. **Osvaldo A. C., Bruno P.I., Alessander C.B., Edgardo Alfonso G.P., Ana Adelina W.H.(2004):** Characterisation of Ethylcellulose Films containing Natural Polysaccharides by Thermal Analysis and FTIR Spectroscopy. *Acta Farm. Bonaerense*, 23(1): 53-7.

28. **Lapasin, R., Pric, S., Tracanelli, P. (1991):** Rheology of hydroxyethyl guar gum derivatives. *Carbohydrate Polymers* .14(4):411–427.

29. **Lapasin, R., Lorenzi, L.D., Pricl, S., Torrian, G.(1995):** Flow properties of hydroxypropyl guar gum and its long-chain hydrophobic derivatives. Carbohydrate polymers, 28(3):195-202.

30. **Shi,H-Y., Li, M.Z.(2007):** New grafted polysaccharide based on O-carboxymethyl- O-hydroxypropyl guar gum and N- isopropylacrylamide: synthesis and phase transition behaviour in aqueous media. *Carbohydrate polymer,*. 67:337-342.

31. **Shenoy,M. A., Dawid J. D'Melo.(2010):** Synthesis and Characterization of Acryloyloxy Guar Gum. *Journal of Applied Polymer Science*, 117:148–154.

32. **Xiao, W., Dong, L.(2011):** Novel excellent property film Prepared from Methacryloyl chloride -graft-Guar Gum Matrixes. Conference Location: XianNing, Date of Conference: 16-18 April, 1442 – 1445.

33. **Wilma F. Bergfeld.(2012):** On the Safety Assessment of Galactomannans As Used in Cosmetics-The 2012 Cosmetic Ingredient Review. http://www.cir-safety.org/sites/default/files/Galact032012FR.pdf.

34. **Li-Ming Z., Jian-Fang Z. and Peter S. H.(2005):** A comparative study on viscosity behavior of water-soluble chemically modified guar gum derivatives with different functional lateral groups. *Journal of the Science of Food and Agriculture,* 85:2638–2644.

35. **Huang,Y., Yu,H., Xiao,C.(2006):** Effects of Ca2+ crosslinking on structure and properties of waterborne polyurethane-carboxymethylated guar gum films. *Carbohydrate Polymers*, 66:500–513.

36. **Pai, V. B., Khan, S.A.(2002):** Gelation and rheology of xanthan enzyme modified guar blends. Carbohydate polymers, 49:207-216.

37. **Badmapriya D., Rajalakshmi A.N.(2011):** New polymeric film coating for colon targeting and its evaluation. *International Research Journal of pharmacy*, 2(7):136-140.

38. **Zhang, L-M., Kong, T.(2006):** Aqueous polysaccharide blends based on hydroxypropyl guar gum and carboxymethyl cellulose: synergistic viscosity and thixotropic properties. *Colloid Polym Sci*, 285: 145–151.

39. **Huang,Y.H., Xiao,C. (2007):** Miscibility and mechanical properties of quaternized polysulfone/benzoyl guar gum blends. *Polymer,* 48:371-381.

40. **Das,D., Ara,T., Dutta,S., Mukherjee.A.(2011):** New water resistant biomaterial biocide film based on guar gum. *Bioresource Technology* 102:5878–5883.

41. **Risica,D., Barbetta ,A., Vischetti ,L., Cametti ,C., Dentini,M.(2010):** Rheological properties of guar and its methyl, hydroxypropyl and hydroxypropyl-methyl derivatives in semi dilute and concentrated aqueous solutions. *Polymer* 51:1972-1982.

42. **Xiao,C., Zhang, J., Zhang,Z., Zhang,L.(2003):** Study of Blend Films from Chitosan and Hydroxypropyl Guar Gum. *Journal of Applied Polymer Science,* 90:1991–1995.

43. **Xiao,W., Dong,L. (2011):** Study of Blend Films from Methacryloyl Guar Gum and SodiumAlginate. Ieeexplore, 1639-1642.

44. **Bajpai, S.K., Saxena,S.K., Sharma,S.(2006):** Swelling behavior of barium ions-crosslinked bipolymeric sodium alginate–Carboxymethyl guar gum blend beads. *Reactive & Functional Polymers* 66:659–666.

45. **Dong, H., Li-hua L., Qing, L., Xiao-Zhen Y.(2004):** Synergistic interaction and gelation in cationic guar gum – sokium alginate system. *Wuhan university journal of natural sciences*. 9(3):371-374.

46. **Pandey,S., Goswami,G.K., Nanda, K.K.(2012):** Green synthesis of biopolymer–silver nanoparticle nanocomposite: An optical sensor for ammonia detection. *International Journal of Biological Macromolecules*, 51:583– 589.

47. **Pandey,S., Goswami,G.K., Nanda, K.K.(2013):** Green synthesis of polysaccharide/gold nanoparticle nanocomposite: An efficient ammonia sensor. *Carbohydrate Polymers,* 94:229– 234.

48. **Pandey,S., Goswami,G.K., Nanda, K.K.(2013):**Nanocomposite based flexible ultrasensitive resistive gas sensor for chemical reactions studies. Scientific Reports. www.nature.com/scientific reports.

49. **Mansa,R., Detellier,C.(2013):**Preparation and Characterization of Guar-Montmorillonite Nanocomposites. *Materials,* 6:5199-5216.

50. **Khan, T.A., Nazir,M., Ali,I., Kumar,A. (2013):** Removal of Chromium (VI) from aqueous solution using guar gum–nano zinc oxide biocomposite adsorbent. Arabian Journal of Chemistry. 1878-5352.

51. **Gupta,N.R., Bhagavatula,P., Chinnakonda, G.S., Badiger.M.V. (2013):** A Nanocomposite of Silver and Thermo-associating Polymer by Green Route: A Potential Soft-Hard Material for Controlled Drug Release. Accepted Manuscript DOI: 10.1039 /C3RA45022H.

52. **Shenoy,M., D'Melo, D.J.(2007):** Guar gum as filler in unsaturated polyester composites. *E-Polymers,* 111:1618-7229.

53. **Chapter 3:** Synthesis of spherical silver nanoparticles in guar gum by gamma irradiation. http://shodhganga.inflibnet.ac.in/bitstream/10603/11458/8/08_chapter%203.pdf.

54. **Dong, C., Tian, B.(1995):** Studies on Preparation and Emulsifying Properties of Guar Galactomannan Ester of Palmitic Acid, *J Appl Polym Sci*, 72:639–645.

55. **Mestechkina, N. M., Egorov, A. V., and Shcherbukhin, V. D.(2006):** Synthesis of Galactomannan Sulfates, *Applied Biochemistry and Microbiology*, 42:326–330.

56. **Gupta, N.R., Prasad, B., Chinnakonda, G.S., Badiger, M.V. (2013):** A Nanocomposite of Silver and Thermo-associating Polymer by Green Route: A Potential Soft-Hard Material for Controlled Drug Release. http://pubs.rsc.org/en/content/articlelanding/2013/ra/c3ra45022h#!divAbstract

57. **Tiwari, A., Singh, S.P.(2008):** Synthesis and Characterization of Biopolymer-Based Electrical Conducting Graft Copolymers. *Journal of Applied Polymer Science*, 108:1169–1177.

58. **Auddy, R.G., Abdullah, M.F., Das, S., Roy, P., Datta, S., Mukherjee, A.(2013):** New Guar Biopolymer Silver Nanocomposites for Wound Healing Applications. *Hindawi Publishing Corporation, BioMed Research International*, 1-9.

59. **Biswal, J., Ramnani, S.P., Shirolikar, S., Sabharwal, S.(2009):** Synthesis of Guar-Gum-Stabilized Nanosized Silver Clusters with *c* Radiation. *Journal of Applied Polymer Science*, 114:2348–2355.

60. **Kumar, A., Aerry, S., Saxena, A., De, A., Mozumdar, S.(2012):** Copper nanoparticulates in guar-gum: a recyclable catalytic system for the Huisgen[3+2]-Cycloaddition of Azides and Alkynes without additives under ambient conditions. Electronic Supplementary Material (ESI) for Green Chemistry, 1-11.

Universal Journal of Physics and Application 2(3): 171-181, 2014
DOI: 10.13189/ujpa.2014.020305 http://www.hrpub.org

Magnetized Viscous Fluid Anisotropic Models in String Cosmology

C.P.Singh[1,*], **A. Beesham**[2]

[1]Department of Applied Mathematics, Delhi Technological University (Formerly Delhi College of Engineering), Bawana Road, Delhi-110 042, India

[2]Department of Mathematical Sciences, University of Zululand, Private Box. X1001, Kwa-Dlangezwa 3886, South Africa

*Corresponding Author: cpsphd@rediffmail.com

Abstract We study the evolution of a homogeneous and anisotropic Bianchi type VI_0 cosmological model in the presence of magnetic field and viscous fluid together with a cloud of cosmic strings in general relativity. Since Viscous fluid and magnetic field have cosmological origin, it is interesting to discuss the effects of viscous fluid and magnetic field on the expansion history of the universe in early and later stages of evolution in string cosmology. Exact solutions of the field equations are obtained using the equation of state for a cloud of strings. The bulk viscous coefficient is assumed to be inversely proportional to the expansion scalar. The two string models, namely, geometrical(Nambu string) and Takabayasi (p-string) string models are discussed with magnetized and non-magnetized viscous fluid by taking certain physical conditions. We also examine numerically the effects of bulk viscosity and magnetic field on potential in each string model. We find that magnetic field and viscous fluid play important role during the early evolution of the universe. We observe that the viscous term affects the evolution much rapid as compare to magnetic field. The presence of viscous term prevents the universe to be empty. The other physical and geometrical aspects of each string model are also discussed in detail.

Keywords cosmology; Magnetic field; Bulk Viscosity

PACS number(s): 98.80-k, 98.80-cq, 04.20-q

1 Introduction

In recent years cosmic strings have been studied to describe the early evolution of the universe. Kibble [1], Zeldovich [2] and Vilenkin [3] believed that cosmic strings might be the source of density perturbations which are required for the formation of large scale structures in the universe. In the early stages of evolution of the universe it is expected that topological defects could have formed naturally during the phase transitions followed by spontaneous broken symmetries. Cosmic strings are linear topological defects, have very interesting properties which play an important role in the structure formation. These cosmic strings have stress energy and couple to the gravitational field. The gravitational effect of string in general relativity have been studied by Letelier [4] and Stachel [5]. Letelier[6] studied relativistic cosmological solutions of cloud formed by massive strings in Bianchi type-I and Kantowski-Sachs space-times. In these models each massive string is formed by a geometric string with particles attached along its extension. Letelier [4] pointed out that the universe could be represented by a collection of objects (galaxies), so a string dust cosmology gives a model to investigate properties related with this fact. Zeldovich [2] also explained that the string dust model could be used as a source of the gravitational field. In geometrical string model, the strings dominate and the tension along the string is equal to its energy density per unit length as we call it string dust model. Since the presence of strings in the early universe can be explained using grand unified theories, there must be different kinds of vacuum structures depending on the structure and topology of the gauge group. Letelier [6] studied a model of a cloud formed by massive strings instead of geometrical strings. Each massive string is formed by a geometrical strings with particles attached along its extension. Hence, the strings that form the cloud are the generalization of Takabayasi's realistic model of strings (p-strings). Therefore, p-string is the direct consequence of Takabayasi's string model. In principle we can eliminate the strings and end up with a cloud of particles. This is a desirable property of a model of a string cloud to be used in cosmology. The different string models can be represented by an equation of state of a cloud of strings. Matraverse [7] presented a class of exact solutions of

Einstein field equations with a two parameter family of classical strings as the source of the gravitational field.

The role of viscosity as a dissipative mechanism may be important in cosmology for a number of reasons. The dissipative mechanism not only modifies the nature of singularity usually occurring for perfect fluid but also successfully accounts for the large entropy per baryon in the present universe. Misner [8,9], while discussing the electron -neutrinos scattering and the subsequent decoupling of neutrinos in Bianchi type -I models, came to the conclusion that the viscosity of neutrinos could essentially reduce the initial anisotropy of the universe. Matzner [10] came to the similar conclusion for the Bianchi type -V models. A critical analysis to Misner's method were raised by Doroskevich et al. [11], Stewart [12], and Collins and Stewart [13]. They found that the isotropization by decoupling neutrinos could have lead to the isotropy level now observed only if at the end of the lepton era the degree of anisotropy was already small.

It is interesting to note that magnetic field present in galactic and inter galactic spaces play a significant role at cosmological scale. The study of magnetic field in the matter distribution is of considerable interest as it provides an effective way to understand the initial phases of cosmic evolution. The inclusion of the magnetic field is motivated by the observational cosmology and astrophysics indicating that many subsystems of the universe possess magnetic fields. It is reasonable to consider magnetic fields in the energy momentum tensor of the early universe. A cosmological model containing a global magnetic field is necessarily anisotropic. An understanding of the effect of a magnetic field upon the dynamics of the universe is necessary during early and late time evolution of the universe. Melvin [14] suggested that during the evolution of the universe, the matter was in a highly ionized state and was smoothly coupled to the gravitational field and subsequently forming neutral matter during expansion of the universe . Primordial magnetic field of cosmological origin have been discussed by Asseo and Sol [15], and Madsen[16]. Wolfe et al. [17], Kulsrud et al. [18], Barrow [19], Matravers and Tsagas [20] are some of the authors who have studied the cosmological models with magnetic field and have pointed out its important in the early evolution of the universe. Therefore, in string dust universe the presence of magnetic field is not unrealistic.

The recent observational data from Cosmic Background Explorer (COBE) and Wilkinson Microwave Anisotropy Probe (WMAP) support the existence of an anisotropic phase in the evolution of the universe. These studies lead many cosmologists to consider the anisotropic models to describe the early phase of the evolution of the universe which decay into isotropic in late time. Homogeneous and anisotropic cosmological models have been widely studied in the framework of general relativity to describe the early and late phases of the evolution of the universe. These models have a significant role in the description of the universe at early stages of the evolution. Therefore, it is interesting to study anisotropic cosmological models that decay into isotropic in later stages of evolution of the universe. Bianchi type -VI_0 (BVI_0) space times are of particular interest since they are sufficiently complex, while at the same time, they are simple generalizations of Bianchi type spaces. Barrow [21] pointed out that BVI_0 cosmological model give a better explanation of some of the cosmological problems like primordial helium abundance and isotropization in a special sense. Some of the authors [22−32] have discussed BVI_0 cosmological models with matter distribution in general relativity and scalar tensor theory.

Weaver [33] has studied dynamics of magnetic BVI_0 cosmologies whereas Sharif and Zubair [34,35] have discussed the dynamics of BVI_0 with and without magnetic field in the presence of anisotropic fluid. In recent past, many authors [36−38] have studied cosmic strings in Bianchi type VI_0 space time in general relativity. Ribeiro and Sanyal [39], Banerjee and Sanyal [40], Bali and Jain [41] have studied BVI_0 model with bulk viscosity and magnetic field in general relativity. Wang [42,43], Yadav et al.[44], Bali et al. [45,46], Tripathy et al.[47,48], Tripathy and Behera [49] have studied BVI_0 string cosmological models with magnetic field and viscous fluid in general relativity. Pradhan and Bali [50] have studied BVI_0 massive string cosmological models with decaying vacuum energy density. Sharif and Waheed [51] have discussed the dynamics of magnetized bulk viscous strings in Brans-Dicke gravity. Saha and Visinescu [52] have investigated the effect of magnetic field on classical potential in string cosmology. Saha et al.[53] and Rikhvitsky et al.[54] have studied Bianchi I string cosmological models in the presence of magnetic field and have examined the quantum effects in loop quantum cosmology. Saha and Visinescu [55] have extended their work to study the effect of magnetic field in string cosmology for Bianchi VI cosmological model. Recently Singh [56,57] has studied Bianchi I with viscous fluid and Bianchi V string cosmological models in the presence of magnetic field.

The presently observed universe is almost isotropic at large as we have discussed above, therefore, the isotropization problem appears inevitably in any study of anisotropic cosmologies. The presence of such a field demands the use of a class of space -times more general than the Friedmann - Roberstion-Walker ones, since the isotropy is broken. The most natural extension is the study of homogeneous and anisotropic models. String cosmological model have been used in attempts to describe the early universe and to investigate anisotropic behavior. On the other hand, bulk viscosity lead to negative energy field and hence have a significant impact on the dynamics of the universe. The motivation of this paper comes from the above discussion. It would be worthwhile to discuss the early and late phases of the universe in BVI_0 magnetized bulk viscous string cosmological model in general relativity. The main purpose of this work is to examine the effects of bulk viscosity on the dynamics of the universe with and without magnetic field in BVI_0. Assuming certain assumptions, some exact solutions of the field equations are presented for different string models. It is also resealable to study the string model in late time evolution.

The paper is organized as follows: In Section 2 we present spatially homogeneous and anisotropic BVI_0 space time and derive the field equations for cosmic string with magnetic field and viscous fluid. Section 3 deals with the exact solutions for different string models and discuss the physical behavior of bulk viscosity on the evolution of the universe with and without magnetic field. Finally, Section 4 concludes the results.

2 Model and Field Equations

The spatially homogeneous and anisotropic Bianchi type VI_0 model is described by the line element

$$ds^2 = dt^2 - A^2dx^2 - e^{2mx}B^2dy^2 - e^{-2mx}C^2dz^2, \tag{1}$$

where A, B, and C are functions of cosmic time t only and are the scale factors in anisotropic background, and $m \neq 0$ is a constant.
It is useful to define the volume scale factor τ

$$\tau = ABC. \tag{2}$$

The mean expansion rate as an average Hubble rate H is given by

$$H = \frac{1}{3}\left(\frac{\dot{A}}{A} + \frac{\dot{B}}{B} + \frac{\dot{C}}{C}\right) = \frac{1}{3}\frac{\dot{\tau}}{\tau}, \tag{3}$$

where an overdot means derivative with respect to time t. The expansion scalar θ is defined by

$$\theta = u^l{}_{;l} = \left(\frac{\dot{A}}{A} + \frac{\dot{B}}{B} + \frac{\dot{C}}{C}\right) = \frac{\dot{\tau}}{\tau}. \tag{4}$$

We also define the two relative shear anisotropy parameters R and S, i.e., the differences of the expansion rates as the Hubble normalized shear [58] as

$$R = \frac{1}{H}\left(\frac{\dot{A}}{A} - \frac{\dot{B}}{B}\right), \qquad S = \frac{1}{H}\left(\frac{\dot{A}}{A} - \frac{\dot{C}}{C}\right). \tag{5}$$

When $R = 0 = S$ and $m = 0$, the line element (1) reduces to Friedmann -Robertson - Walker (FRW) model. The energy momentum tensor of a cloud of strings in presence of bulk viscosity and magnetic field is given as [18,59,60]

$$T_i^j = \rho u_i u^j - \lambda x_i x^j - \xi u^l{}_{;l}\left(g_i^j + u_i u^j\right) + E_i{}^j, \tag{6}$$

where ρ is the rest energy density for a cloud of strings with particles attached to them and λ is the string tensor density which may be negative, zero or positive and is related by $\rho = \rho_p + \lambda$, where ρ_p is the particle energy density. The unit time-like vector u^i describes the particle's four velocity and unit space-like vector x^i denotes the direction of the string which can be taken along any of the three directions x, y and z axes. Thus, without loss of generality let us choose $x-$ direction as the direction of the string along which the magnetic field is assumed to be present, i.e.,

$$x^i = (A^{-1}, 0, 0, 0) \tag{7}$$

In a co-moving coordinate system, we have $u^i = (0, 0, 0, 1)$. Therefore, u_i and x_i satisfy the conditions

$$u_i u^i = -x_i x^i = -1, \;\; u_i x^i = 0. \tag{8}$$

In Eq. (6), ξ is the coefficient of bulk viscosity and $E_i{}^j$ is the electromagnetic field tensor which is given by (see, ref.[60])

$$E_i{}^j = \bar{\mu}\left[|h|^2\left(u_i u^j + \frac{1}{2}g_i{}^j\right) - h_i h^j\right], \tag{9}$$

where $\bar{\mu}$ is the magnetic permeability, and h_i, the magnetic flux vector defined by

$$h_i = \frac{\sqrt{-g}}{2\bar{\mu}}\epsilon_{ijkl}F^{kl}u^j. \tag{10}$$

Here F^{kl} is the electromagnetic field tensor and ϵ_{ijkl} is the Levi-Civita tensor density.

We assume that there is a magnetic field along $x-$ direction, that is, along the direction of string. The Maxwell's equations

$$F_{ij;k} + F_{jk;i} + F_{ki;j} = 0, \;\; \text{and} \;\; F^{ij}_{;k} = 0, \tag{11}$$

lead to

$$F_{23} = I, \tag{12}$$

where I is a constant characterizing the magnetic field intensity. It is to be noted that the semicolon stands for covariant derivative. All other components of F^{kl} are zero.
It follows from Eq.(10) that the non-zero component of magnetic flux vector is

$$h_1 = \frac{IA}{\bar{\mu}BC}. \tag{13}$$

Using (13) into (9), the non-trivial components of E_i^j are given by

$$E^1_{\ 1} = -\frac{I^2}{2\bar{\mu}^2 B^2 C^2} = -E^2_{\ 2} = -E^3_{\ 3} = E^4_{\ 4}. \tag{14}$$

The Einstein's field equations (in gravitational units $c = 8\pi G = 1$) read as

$$R_i^{\ j} - \frac{1}{2} g_i^{\ j} R = -T_i^{\ j}. \tag{15}$$

where R_i^j is the Ricci tensor and $R = g^{ij} R_{ij}$ is the Ricci scalar.

The field equations (15) with (1) and (6) lead to the following system of equations

$$\frac{\dot{A}\dot{B}}{AB} + \frac{\dot{B}\dot{C}}{BC} + \frac{\dot{C}\dot{A}}{CA} - \frac{m^2}{A^{\,2}} = \rho + \frac{I^2}{2\bar{\mu}B^{\,2}C^{\,2}}, \tag{16}$$

$$\frac{\ddot{A}}{A} + \frac{\ddot{C}}{C} + \frac{\dot{A}\dot{C}}{AC} - \frac{m^2}{A^2} = -\frac{I^2}{2\bar{\mu}B^{\,2}C^{\,2}} + \xi\theta, \tag{17}$$

$$\frac{\ddot{A}}{A} + \frac{\ddot{B}}{B} + \frac{\dot{A}\dot{B}}{AB} - \frac{m^2}{A^2} = -\frac{I^2}{2\bar{\mu}B^{\,2}C^{\,2}} + \xi\theta, \tag{18}$$

$$\frac{\ddot{B}}{B} + \frac{\ddot{C}}{C} + \frac{\dot{B}\dot{C}}{BC} + \frac{m^2}{A^2} = \lambda + \frac{I^2}{2\bar{\mu}B^{\,2}C^{\,2}} + \xi\theta, \tag{19}$$

$$m\left(\frac{\dot{C}}{C} - \frac{\dot{B}}{B}\right) = 0, \tag{20}$$

Equation (20) immediately gives

$$C = nB, \tag{21}$$

where n is a positive integration constant. Summation of field equations (17), (18), (19) and three times (16) gives

$$\frac{\ddot{\tau}}{\tau} = \frac{1}{2}\left[(3\rho + \lambda) + \frac{A^2 I^2}{\bar{\mu}\tau^2}\right] + \frac{3}{2}\xi\theta + \frac{2m^2}{A^2}. \tag{22}$$

The energy conservation equation $T_{i\ ;j}^{\ j} = 0$ takes the form

$$\dot{\rho} + \frac{\dot{\tau}}{\tau}\rho - \frac{\dot{A}}{A}\lambda = \xi\theta^2. \tag{23}$$

Now, we consider the following equation of state for a cloud of string models[6] to solve Eqs. (22) and (23).

$$\rho = \alpha\lambda, \tag{24}$$

where the constant α is defined by

$$\begin{aligned} \alpha &= 1 \quad (\textit{geometric or Nambu string}), \\ &= (1+\omega) \quad (p- \ \textit{string or Takabayasi string}), \\ &= -1 \quad (\textit{Reddy string}), \end{aligned} \tag{25}$$

where ω is a constant such that $\omega > 0$.

Letelier [4] pointed out that the universe could be represented by a collection of objects (galaxies), so a string dust cosmology ($\rho = \lambda$) gives a model to investigate properties related with this fact. Zeldovich [2] also explained that the string dust model could be used as a source of the gravitational field. In geometrical string model, the strings dominate and the tension along the string is equal to its energy density per unit length as we call it string dust model. Since the presence of strings in the early universe can be explained using grand unified theories, there must be different kinds of vacuum structures depending on the structure and topology of the gauge group. Letelier [6] studied a model of a cloud formed by massive strings instead of geometrical strings. Each massive string is formed by a geometrical strings with particles attached along its extension. Hence, the strings that form the cloud are the generalization of Takabayasi's realistic model of strings (p-strings). Therefore, p-string is the direct consequence of Takabayasi's string model. In principle we can eliminate the strings and end up with a cloud of particles. This is a desirable property of a model of a string cloud to be used in cosmology. The above equation of state are restricted by the energy conditions [61].

If we set R =constant in Eq.(5), then in view of (3), we get

$$A = d_0 B\, \tau^{R/3}, \tag{26}$$

where d_0 is a constant. From (2), (21) and (26), we find the following expression for metric functions in terms of τ.

$$A = \left(d_0^2 n^{-1}\right)^{1/3} \ \tau^{(3+2R)/9}, \tag{27}$$

$$B = (d_0 n)^{-1/3} \ \tau^{(3-R)/9}, \tag{28}$$

$$C = \left(d_0^{-1} n^2\right)^{1/3} \ \tau^{(3-R)/9}. \tag{29}$$

Using (24), Eq. (22) can be rewritten as

$$\frac{\ddot{\tau}}{\tau} = \frac{1}{2}\left[\left(\frac{3\alpha+1}{\alpha}\right)\rho + \frac{A^2 I^2}{\bar{\mu}\tau^2}\right] + \frac{3}{2}\xi\theta + \frac{2m^2}{A^2}. \tag{30}$$

From (27) and (23) we get

$$\dot{\rho} + \left(\rho - \frac{3+2R}{9}\lambda\right)\frac{\dot{\tau}}{\tau} = \xi\theta\frac{\dot{\tau}}{\tau}. \tag{31}$$

We further assume that the bulk viscosity is inversely proportional to the expansion scalar [62] which means that the rate of cosmic expansion decreases as the viscosity increases ,i.e.,

$$\xi\theta = \xi_0, \tag{32}$$

where ξ_0 is a positive constant. Using (24) and (32) into (31) and simplifying we get the energy density in terms of τ as

$$\rho = \frac{9\alpha}{9\alpha - (3+2R)}\left[\xi_0 + \rho_0 \tau^{-\left(\frac{9\alpha-(3+2R)}{9\alpha}\right)}\right], \tag{33}$$

where ρ_0 is a constant of integration. The string tension density is given by

$$\lambda = \frac{9}{9\alpha - (3+2R)}\left[\xi_0 + \rho_0 \tau^{-\left(\frac{9\alpha-(3+2R)}{9\alpha}\right)}\right], \tag{34}$$

which may be positive for $\alpha > (3+2R)/9$, or negative as $0 < \alpha < (3+2R)/9$. The rest energy density of particles, ρ_p is given by

$$\rho_p = \rho - \lambda = \frac{9(\alpha-1)}{9\alpha - (3+2R)}\left[\xi_0 + \rho_0 \tau^{-\left(\frac{9\alpha-(3+2R)}{9\alpha}\right)}\right], \tag{35}$$

For ρ and ρ_p to be positive we must have $\alpha > \frac{3+2R}{9}$. It is to be noted that $\frac{3+2R}{9}$ is always positive, therefore, the equation of state parameter α must be considered as a positive. Hence, we find that the Reddy string model ($\alpha = -1$) is not possible in this case. Specially, for the choice of $R = 0$, where the model isotropizes at late time, we find $\alpha > 1/3$. Therefore, this model is suitable to describe the geometrical and p-string models. The energy density, string tension density and particle energy density are decreasing functions of τ and tend to a constant as $\tau \to \infty$. It is observed that ρ_p vanishes for geometrical string model ($\alpha = 1$) and therefore it behaves as a cloud of geometric string ($\rho = \lambda$).

Using (27), (32) and (33), Eq. (30) now read as

$$\ddot{\tau} = \frac{9}{2}\frac{(3\alpha+1)\,\rho_0}{[9\alpha-(3+2R)]}\tau^{\frac{3+2R}{9\alpha}} + \frac{\left(d_0^2 n^{-1}\right)^{2/3} I^2}{2\mu}\tau^{\frac{4R-3}{9}} + \frac{3}{2}\left(\frac{18\alpha-2R}{9\alpha-3-2R}\right)\xi_0\tau + \frac{2m^2}{\left(d_0^2 n^{-1}\right)^{2/3}}\tau^{\frac{3-4R}{9}}, \tag{36}$$

This equation allows the following first integral

$$\dot{\tau} = \sqrt{C_1\tau^{\frac{3+2R+9\alpha}{9\alpha}} + C_2\tau^{\frac{4R+6}{9}} + C_3\tau^2 + C_4\tau^{\frac{12-4R}{9}} + C_5}, \tag{37}$$

where $C_1 = \left(\frac{81\alpha(3\alpha+1)\rho_0}{[9\alpha-(3+2R)][9\alpha+(3+2R)]}\right)$, $C_2 = \frac{9(d_0^2 n^{-1})^{2/3}k}{(4R+6)}$, $k = \frac{I^2}{\mu}$, $C_3 = \frac{3}{2}\frac{(18\alpha-2R)\xi_0}{[9\alpha-(3+2R)]}$, $C_4 = \frac{36m^2}{(d_0^2 n^{-1})^{2/3}(12-4R)}$, and $C_5 =$ constant.

We observe that Eq.(36) is a function of τ only, i.e.,

$$\ddot{\tau} = F(\tau). \tag{38}$$

From the mechanical point of view, Eq. (38) can be interpreted as equation of motion of a single particle with unit mass under the force $F(\tau)$. Then, the following first integral exists

$$\dot{\tau} = \sqrt{2[\epsilon - u(\tau)]}, \tag{39}$$

where ϵ can be viewed as energy level and $u(\tau) = -\int F(\tau)d\tau$ is the potential of the force F. A comprehensive description concerning potential may be found in ref. [63]. Comparing (37) and (39), we find $\epsilon = C_5/2$, and hence the potential is given by

$$u(\tau) = -\frac{1}{2}\left(C_1\tau^{\frac{3+2R+9\alpha}{9\alpha}} + C_2\tau^{\frac{4R+6}{9}} + C_3\tau^2 + C_4\tau^{\frac{12-4R}{9}}\right). \tag{40}$$

Equation (37) admits the following solution in quadrature form as

$$\int \frac{d\tau}{\sqrt{C_1\tau^{\frac{3+2R+9\alpha}{9\alpha}} + C_2\tau^{\frac{4R+6}{9}} + C_3\tau^2 + C_4\tau^{\frac{12-4R}{9}} + C_5}} = t + t_0, \tag{41}$$

where t_0 is a constant of integration and we take it as a zero for simplicity.

3 Solution for String Models

We observe that it is too difficult to solve (41), in general. Therefore, we limit ourselves to investigate the behavior of the solutions for large t, i.e., to investigate the possibility of the isotropic solutions where all the scale factors have a similar behavior. For this we consider $R = 0$ in the above solutions which we discuss for the various string models in the following subsections.

3.1 Geometric string model ($\alpha = 1$)

Let us find the solution for viscous fluid with and without magnetic field in the following subsections.

3.1.1 Viscous fluid solution with magnetic field

For $R = 0$ and $\alpha = 1$, Eq. (41) reduces to

$$\int \frac{d\tau}{\sqrt{(C_1 + C_4)\tau^{\frac{4}{3}} + C_2\tau^{\frac{2}{3}} + C_3\tau^2}} = t. \tag{42}$$

For $(C_1 + C_4)^2 < 4C_2C_3$, integrating (42), we get

$$\tau = \left[\frac{1}{2C_3}\left(\sqrt{4C_2C_3 - (C_1 + C_4)^2}\,\sinh\left(\frac{2}{3}\sqrt{C_3}\,t\right) - (C_1 + C_4)\right)\right]^{\frac{3}{2}}, \quad C_3 \neq 0, \tag{43}$$

For small t, we have $\sinh\left(\frac{2}{3}\sqrt{C_3}\,t\right) \approx \frac{2}{3}\sqrt{C_3}\,t$. Therefore, Eq. (43) gives

$$\tau = (k_1t - k_2)^{3/2}, \tag{44}$$

where $k_1 = \sqrt{\frac{4C_2C_3-(C_1+C_4)^2}{9C_3}}$ and $k_2 = \frac{(C_1+C_4)}{2C_3}$. We observe that τ becomes imaginary at $t = 0$. Thus, for reality of the model, we must have $t \geq \frac{k_2}{k_1}$.

The metric coefficients for isotropic regime have the form

$$A \sim B \sim C \sim (k_1t - k_2)^{\frac{1}{2}}, \tag{45}$$

and consequently the Hubble parameter is given by

$$H = \frac{k_1}{2(k_1t - k_2)}. \tag{46}$$

For this isotropic regime the density of strings is given by

$$\rho = \frac{3}{2}\left[\xi_0 + \frac{\rho_0}{k_1t - k_2}\right] = \lambda. \tag{47}$$

We observe that ρ and λ remains positive throughout the evolution and become infinite at the initial epoch at $t = \frac{k_2}{k_1}$. However, ρ and λ decrease with time for $t > \frac{k_2}{k_1}$ and approach to a constant value, $\frac{3}{2}\xi_0$ as $t \to \infty$. We observe that this constant value of ρ is due to the viscous term, ξ_0. It means that the bulk viscosity prevents the universe to be empty at late times of its evolution.

The potential (40) in terms of t takes the form

$$u(t) = -\frac{1}{2}\left[C_3(k_1t - k_2)^3 + (C_1 + C_4)(k_1t - k_2)^2 + C_3(k_1t - k_2)\right]. \tag{48}$$

The behavior of potential for viscous fluid (bold line) is shown in figure 1.

3.1.2 Viscous fluid solution without magnetic field

For $\alpha = 1$ and in the absence of magnetic field ($k = 0$), Eq.(41) becomes

$$\int \frac{d\tau}{\sqrt{(C_1 + C_4)\,\tau^{\frac{4}{3}} + C_3\tau^2}} = t, \tag{49}$$

which on integration it gives

$$\tau = \left(\frac{C_1 + C_4}{2C_3}\right)\left[\cosh\left(\frac{2\sqrt{C_3}}{3}\,t\right) - 1\right]^{\frac{3}{2}}, \quad C_3 \neq 0, \tag{50}$$

For small t, Eq.(50) gives

$$\tau = \left[\frac{2(C_1 + C_4)}{9}\right]^{\frac{3}{2}}\, t^3. \tag{51}$$

The metric coefficients for isotropic regime have the form

$$A \sim B \sim C \sim t, \tag{52}$$

and consequently the Hubble parameter is given by

$$H = \frac{1}{t}. \tag{53}$$

For this isotropic regime the density of strings is given by

$$\rho = \frac{3}{2}\left[\xi_0 + \frac{9\rho_0}{2(C_1 + C_4)}\,\frac{1}{t^2}\right] = \lambda. \tag{54}$$

We find that the energy density remains positive through out the evolution of the universe. It is infinite at initial epoch $t = 0$ and decreases with time, and ultimately attains a constant value, $\frac{3\xi_0}{2}$ in late time expansion of the universe. Therefore, the bulk viscosity prevents the universe to be empty during late time of evolution. We also find that the energy density attains the same constant value with and without magnetic field in late time of evolution which shows that the magnetic field has no effect in late time epoch.

The potential (40) in terms of t takes the form

$$u(t) = -\frac{2(C_1 + C_4)^3}{81}\left(1 + \frac{2C_3}{9}\,t^2\right)\, t^4. \tag{55}$$

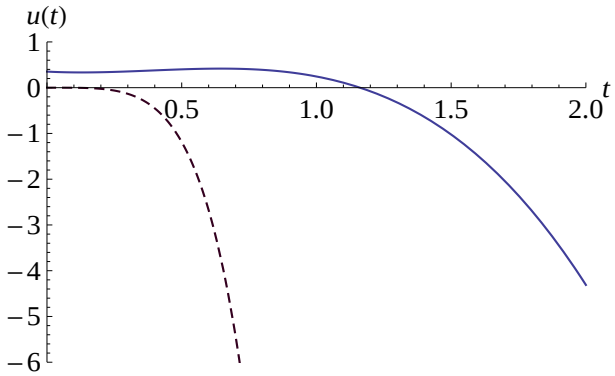

Figure 1. Potential versus time for viscous fluid with (bold line) and without (dashed line) magnetic field

Figure 1 plots the potential with respect to time in the presence of viscous fluid and magnetic field (bold line) and with viscous fluid only (dashed line). We have used the numerical value of various constants such as $\rho_0 = 1$, $d_0 = 1$, $n = 1$, $m = 1$, $\xi_0 = 1$, $I = 2$ or 0 and $\bar{\mu} = 1.00001$. We observe that $\mu(t)$ starts from origin and goes to negative through out the evolution in the presence of viscous without magnetic field where as it starts from some positive value and remains positive for finite time of interval and then becomes negative nature with respect to time t in magnetized viscous fluid. Therefore, we can say that viscous and magnetic field have the effects on the early evolution of the universe. However, the effects become negligible during late time evolution. The string model with viscous fluid may be described as an acceptable model.

3.2 Takabayashi string model ($\alpha = 1 + \omega$)

In this case, Eq.(41) reduces to

$$\int \frac{d\tau}{\sqrt{C_1\tau^{\frac{3\omega+4}{3\omega+3}} + C_2\tau^{\frac{2}{3}} + C_3\tau^2 + C_4\tau^{\frac{4}{3}}}} = t. \tag{56}$$

One can observe that it is very difficult to find a general solution of τ in terms of t. Therefore, we express ρ, λ and ρ_p in terms of τ as

$$\rho = \frac{3(1+\omega)}{3\omega+2}\left[\xi_0 + \rho_0\tau^{-\frac{2+3\omega}{3(1+\omega)}}\right], \tag{57}$$

$$\lambda = \frac{3}{3\omega+2}\left[\xi_0 + \rho_0\tau^{-\frac{2+3\omega}{3(1+\omega)}}\right], \tag{58}$$

$$\rho_p = \frac{3\omega}{3\omega+2}\left[\xi_0 + \rho_0\tau^{-\frac{2+3\omega}{3(1+\omega)}}\right], \tag{59}$$

As $\omega > 0$, we find that ρ, λ and ρ_p remain positive through out the evolution of the universe. These physical parameters are decreasing function of τ and become constant for large t due to the bulk viscosity. The geometrical string model may be recovered for $\omega = 0$ as discussed in Sect. 3.1. The potential in this is given by

$$u(\tau) = -\frac{1}{2}\left[C_1\tau^{\frac{4+3\omega}{3(1+\omega)}} + C_2\tau^{\frac{2}{3}} + C_3\tau^2 + C_4\tau^{\frac{4}{3}}\right]. \tag{60}$$

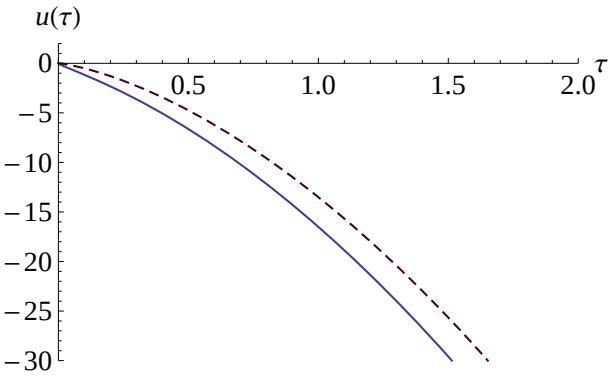

Figure 2. Potential versus time for viscous fluid solution with (bold lines) and without (dashed lines) magnetic field.

Figure 2 illustrates the behavior of potential $\mu(t)$ with respect to τ for $\rho_0 = 1$, $d_0 = 1$, $n = 1$, $m = 1$, $\xi_0 = 1$, $I = 2$, or 0, $\bar{\mu} = 1.00001$ and $\omega = 1$. It is clear that potential remains negative and decreases rapidly throughout the evolution of the universe for viscous fluid with and without magnetic field. It decreases rapidly due to the viscous fluid only.

4 Conclusion

We have studied anisotropic Bianchi VI_0 string cosmological model with viscous fluid and magnetic field in general relativity by taking certain physical assumptions. Since viscous fluid and magnetic field have cosmological origin, it is interesting to discuss the viscous and magnetic field effects on the expansion history of the universe in early and late stages of evolution in string cosmology. The Einstein's field equations have been solved exactly for geometrical string model for viscous fluid with and without magnetic field whereas a general quadrature form of average scale factor has been found in Takabayashi string model. The solutions present interesting features in the presence of magnetized viscous fluid and in the presence of viscous fluid only. We have found that the viscous term affects the solutions much rapid as compare to magnetic field. We have also analyzed the behavior of various physical parameters graphically in the presence of magnetized viscous fluid and bulk viscous fluid without magnetic field.

In geometrical string model we have observed that proper energy density remains positive through out the evolution and attains the same constant value during late time for viscous fluid with and without magnetic field. Hence, the presence of viscous term prevents to be empty in its future evolution. The classical potential changes its behavior rapidly due to the bulk viscous term. It is negative through out the evolution in the absence of magnetic field but it is positive for some finite time and after that it shows the negative nature during late time.

In Takabayashi model we have found a quadrature form of average volume which is too difficult to solve, in general. The solution for the proper energy density, string tension density and particle energy density in terms of

average scale factor have been represented. These physical parameters approach to a constant value asymptotically as $t \to \infty$ due to the bulk viscosity.

We have also discussed the potential with respect to time in each string model and have observed that the classical potential changes its behavior rapidly due to the bulk viscous term. In geometrical string model it remains negative and decreases rapidly in viscous fluid solution without magnetic field. In Takabayashi string model it remains negative in both cases but the effect of viscous fluid with and without magnetic field vary rapidly. Thus, we conclude that the bulk viscous fluid with and without magnetic field plays an important role in the evolution of the universe in anisotropic models as analyzed in this paper.

REFERENCES

[1] T.W.B. Kibble, J. Phys. A **9**, 1387 (1976)

[2] Y.B. Zel'dovich, Mon. Not. R. Astron. Soc. **192**, 663 (1980).

[3] A. Vilenkin, Phys. Rev. D **24**, 2082 (1981).

[4] P.S. Letelier, Phys. Rev. D **20**, 1294 (1979)

[5] J. Stachel, Phys. Rev. D **21**, 2171 (1980)

[6] P.S. Letelier, Phys. Rev. D **28**, 2414 (1983)

[7] D.R. Matraverse, Gen. Relativ. Grav. **20**, 279 (1988)

[8] C.W. Misner, Nature **214**, 40 (1967)

[9] C.W. Misner, Astrophys. J. **151**, 431 (1968)

[10] R.A. Matzner, Astrophys. J. **157**, 1085 (1969)

[11] A.G. Doroshkevich, Y.B. Zeldovich, I.D. Nivokov, Zh. Eksp. Theor. Fiz. **53**, 644 (1967)

[12] J.M. Stewart, Mon. Not. Roy. Soc. **145**, 347 (1969)

[13] C.B. Collins, J.M. Stewart, Mon. Not. Roy. Soc. **153**, 419 (1971)

[14] M.A. Melvin, Ann. N.Y. Acad. Sci. **262**, 253 1975.

[15] E. Asseo, H. Sol, Phys. Rep. **6**, 148 (1987)

[16] M.S. Madsen, MNRAS **237**, 109 (1989)

[17] A.M. Wolfe, K. Lanzetta, A.L. Oren, Astrophys. J. **388**, 17 (1992)

[18] R. Kulsrud, R. Cen, J.P. Ostriker, D. Ryu, Astrophys. J. **380**, 481 (1997)

[19] J.D. Barrow, Phys. Rev. D **55**,7451 (1997)

[20] D.R. Matravers, C.G. Tsagas, Phys. Rev. D **62**, 103519 (2000)

[21] J.D. Barrow, Mon. Not. R. Astron. Soc. **211**, 221 (1984).

[22] D. Lorentz, Astrophys. Space Sci. **85**, 69 (1982).

[23] S.R. Roy and J.P. Singh, Acta Physic Austriaca **5**, 57 (1983).

[24] S.R. Roy, J.P. Singh, S. Narain, Astrophys. Space Sci. **111**, 389 (1985).

[25] ShriRam: J. Math. Phys. **27**, 650 (1986).

[26] C. Uggla and K. Rosquist, Class. Quantum Gravity **5**, 767 (1988).

[27] ShriRam: Int. J. Theor. Phys. **28**, 917 (1989).

[28] A.A. Coley and K. Dunn, Astrophs. J. **348**, 26 (1990).

[29] S.R. Roy and S.K. Banerjee, Gen Relativ. Gravit. **24**, 1117 (1992).

[30] S.R. Roy and S.K. Banerjee, Gen Relativ. Gravit. **28**, 27 (1992).

[31] ShriRam and P. Singh, Astrophys. Space Sci. **200**, 35 (1993).

[32] G. Mohanthy, S.K. Sahu, Astrophys. Space Sci. **288**, 611 (2003).

[33] M. Weaver, Class. Quantum Gravity **17**, 421 (2000).

[34] M. Sharif and M. Zubair, Int. J. Mod. Phys. D **19**, 1957 (2010).

[35] M. Sharif and M. Zubair, Astrophys. Space Sci. **339**, 45 (2012).

[36] K.D. Krori, T. Chaudhury, C.R. Mahanta, A. Mazumdar, Gen. Relativ. Grav. **22**, 123 (1990)

[37] S. Chakraborty, Indian J. Pure Appl. Phys. **29**, 31 (1991).

[38] R. Tikekar, L.K. Patel, Pramana J-Phys **42**, 483 (1994).

[39] M.B. Ribeiro, A.K. Sanyal, J. Math. Phys. **28**, 657 (1987).

[40] A.K. Banerjee, A.K. Sanyal, Gen. Relativ. Gravit. **18**, 1251 (1986).

[41] R. Bali, D.R. Jain, Int. J. Theor. Phys. **28**, 903 (1989).

[42] X.X. Wang, Astrophys. Space Sci. **293**, 433 (2004).

[43] X.X. Wang, Chin. Phys. Lett. **23**, 1702 (2006).

[44] M.K. Yadav, A. Pradhan, S.K. Singh, Astrophys. Space Sci. **311**, 423 (2007).

[45] R. Bali, A. Pradhan, H. Amirhashchi, Int. J. Theor. Phys. **47**, 2594 (2008).

[46] R. Bali, R. Banerjee, S.K. Banerjee, Astrophys. Space Sci. **317**, 21 (2008).

[47] S.K. Tripathy, S.K. Nayak, S.K. Sahu, T.R. Toutray, Astrophys. Space Sci. **323**, 91 (2009).

[48] S.K. Tripathy, S.K. Nayak, S.K. Sahu, T.R. Toutray, Astrophys. Space Sci. **323**, 281 (2009).

[49] S.K. Tripathy , D. Behera, Astrophys. Space Sci. **330**, 191 (2010).

[50] A. Pradhan, R. Bali, Eect. J. Theor. Phys. **19**, 91 (2008).

[51] M. Sharif, S. Waheed, Int. J. Mod. Phys. D **55**, 21500 (2012).

[52] B. Saha, M. Visinescu, Astrophys. Space Sci. **315**, 99 (2008)

[53] B. Saha, V. Rikhvitsky, M. Visinescu, Cent. Eur. J. Phys. **8**, 113 (2010)

[54] V. Rikhvitsky, B. Saha, M. Visinescu, Astrophys. Sapce. Sci. **339**, 371, (2012)

[55] B. Saha, M. Visinescu, Rom. J. Phys. **55**, 1064 (2010)

[56] C.P. Singh, Astrophys. Space Sci. **343**, 773 (2013)

[57] C.P.Singh, Int. J. Theor. Phys. DOI:10.1007/s 10773-013-1952-1, (2013).

[58] J.D. Barrow, Phys. Rev. D **55**, 7451 (1997).

[59] L.D. Landau, E.M. Lifshitz, Fluid Mechanics, Pergamon Press, Oxford,p.505. (1936)

[60] A. Linchnerowicz, Relativistic Hydrodynamics and Magneto Hydrodynam ics, Benjamin, New York, p.13 (1967)

[61] A. Banerjee, A.K. Sanyal and S. Chakraborty, Pramana-J. Phys. **34**, 1 (1990).

[62] B. Saha, Mod. Phys. Lett. A **20**, 2127 (2005)

[63] B. Saha, T. Boyadjiev, Phys. Rev. D **69**, 124010 (2004).

Prasad Gajula et al., J Appl Bioinform Comput Biol 2013, 2:1
http://dx.doi.org/10.4172/2329-9533.1000103

Journal of Applied Bioinformatics & Computational Biology

Research Article

A SCITECHNOL JOURNAL

Molecular Interaction Studies of Shrimp Antiviral Protein, PmAV with WSSV RING Finger Domain *in silico*

MNV Prasad Gajula[1*], Garima Soni[1,2], Babu G[3], Rai A[1] and Bharadvaja N[2]

Abstract

Background: White spot disease (WSD) is an overwhelming syndrome of shrimp *Penaeus monodon* in which receptor protein of *P. monodon* interacts with viral envelops protein, and causes commencement of the disease. PmAV is the first and only anti-viral protein found in shrimp. It was isolated from a virus unaffected shrimp, *P. monodon* and identified to be up-regulated at the time of viral infection.

Methods: In the present study, we applied molecular modeling and molecular docking to determine the interaction pattern of amino acid residues between PmAV protein and WSSV RING finger domain.

Results and conclusion: Our result showed that PmAV interacts with WSSV RING finger domain and prevents their activity thus inhibiting the establishment of viral infection. Further studies like molecular dynamics simulation of the complex might be applied to open new possibilities for preventing WSD. The quantifiable calculations offer an opportunity for experimental analysis in future as well as provide with an upfront evidence to understand cellular mechanisms underlying the syndrome.

Keywords: Docking; Molecular dynamics simulation; Shrimp; White spot disease

Introduction

Black tiger shrimp, *Penaeus monodon* is one of the most widely cultured shrimp species in the world. However, the major setback to shrimp farming industry worldwide is white spot disease (WSD) caused by white spot syndrome virus (WSSV). Several efforts have been made in preventing and controlling the disease in recent years [1-4]. However, development of an effective therapy against this deadly disease has been a great challenge due to lack of specific immune system in shrimp. The shrimp defense system is believed to rely largely on innate immunity, which is little understood. In this context, it is important to understand the host-virus interaction at molecular level to develop effective therapies. Several authors have reported the effect of WSSV on host gene expression profiles to determine their role in pathogenesis [5,6].

PmAV is the first and the only antiviral protein identified in shrimp. It was cloned from a virus-resistant shrimp, P. monodon by differential display (DD) and found to be up-regulated in response to viral infection [7]. *PmAV* is a Calcium-dependent (C-type) lectin containing a single characteristic carbohydrate recognition domain (CRD). C-type lectins contain a prototypic lectin fold, consisting of two antiparallel β-strands and two α-helices. C-type lectins are regarded as primary candidates for pattern recognition receptors (PRRs) in innate immunity and play an important role in the clearance of pathogens [8-11].

The *PmAV* protein was found to be located mainly in the cytoplasm and showed no interaction with intact WSSV particles [7]. It implies that the antiviral mechanism of *PmAV* protein is not by inhibiting the attachment of virus to target host cell. Instead it may counteract the virus molecular strategies that establish the infection in a cell. It is implicit that many viruses including WSSV have evolved the ability to utilize the host protease machinery to direct cellular protein degradation for their survival and replication. Four proteins of WSSV, namely WSSV199, WSSV222, WSSV249 and WSSV403 contain RING-H2 domain, which is involved in specific ubiquitination events by acting as the E3 ubiquitin protein ligase [5].

Therefore, in this study we attempted *in silico* studies to explore the possible interaction between shrimp antiviral protein, *PmAV* and RING finger domain proteins of WSSV. Here we present 3D modeling and molecular docking of *PmAV* with RING finger domain of WSSV.

Material and Methods

Sequence retrieval proteins

The protein sequences of *Penaeus monodon PmAV* (Accession No. AAQ75589.1) and wsv199 of white spot syndrome virus (Accession No. NP_477666.1) were taken from National Centre for Biotechnology Information (NCBI) (www.ncbi.nlm.nih.gov) in Fasta format.

In order to obtain the RING domain fragment, sequence of wsv199 was subjected to domain analysis using EBI-SMART program (smart.embl-heidelberg.de).

Molecular modeling of the proteins

Each of the FASTA sequences was subjected to Protein-BLAST (www.blast.ncbi.nlm.nih.gov) against PDB (www.rcsb.org) database to select the suitable templates. The best template was selected on the basis of proportion of similarity and identity, E-value, bit scores and query coverage region. After the search, the multiple sequence alignment between the templates and the query sequences was performed using Clustal X 2.1 [12].

The three dimensional coordinates of *PmAV* was created using Modeller 9v10 [13]. It computes a model based on the alignment of the sequence to be modeled with known related 3D structures. 5-5 models for both of the proteins were generated through modeler and consequently the good 3D model was obtained. Another modeling method using I-TASSER server [14] was applied, in order to compare the results obtained by Modeller 9v10. I-TASSER is based on model building using multiple-template fragment alignments. The predicted models having minimum molecular probability density function (Molpdf) and Dope score were preferred for further study.

***Corresponding author:** MNV Prasad Gajula, Indian Agricultural Statistics Research Institute, Pusa Road, New Delhi, India-110012, Tel: 011-25847121-24 extn. 4337; E-mail: varaprasad22@yahoo.com

Received: June 24, 2013 **Accepted:** November 15, 2013 **Published:** November 20, 2013

Minimization and validation

Energy minimization of both the models was performed using steepest descent method by SwissPDB Viewer [15]. Models were applied for validation. Stereo-chemistry of all the models was evaluated by PROCHECK [16] and ProSA (www.prosa.services.came.sbg.ac.at/prosa.php) analyses.

Protein-protein interaction study by docking

Shape Complementarity Principle based docking was performed using PatchDOCK and FireDock servers [17-19]. The output files were subjected to FiberDock server for flexible induced-fit backbone and side chain refinement of the protein complexes [20,21]. The molecular interaction plots between *PmAV* and RING domain of wsv199 were generated using Dimplot in LIGPLOT software [22,23]. The 3D structure and detailed interaction of all protein complexes were visualized using Accelrys Viewerlite software.

Results and Discussion

Knowledge of the shrimp defense at the molecular level has focused mainly on antimicrobial factors [24] while little is known about the possible antiviral factors. So far, only one antiviral protein, *PmAV* has been identified from shrimp [7]. However, the molecular mechanism of this protein in controlling WSSV infection is still unknown. WSSV RING finger domain proteins, WSSV199, WSSV222, WSSV249 and WSSV403 functions as E3 ubiquitin ligases and mediates the degradation of important host immune proteins for disease manifestation [4]. Therefore, an attempt was made in this study to determine molecular interaction between *PmAV* and RING finger domain of WSSV proteins using *in silico* approach.

Domain analysis

Wsv199 protein was subjected for domain analysis. SMART program has predicted a RING finger domain lies from 743 to 795 amino acid residues in wssv199. The RING domain is found to exhibit affinity towards protein/protein complex non-covalently.

Comparative modeling of the proteins

In order to generate the 3 dimensional coordinates of protein, BLASTp was performed. Table 2 shows the templates chosen for the modeling process. The expectation value (E-value) characterizes several different alignments with scores equivalent to, else enhanced than the scores that are estimated to come about in an arbitrary database search. Usually, a lesser E-value specifies that alignment is tangible and does not occur by fortuitous.

The more important step in the modeling method is to find an adequate alignment of the target with the template sequences. Multiple sequence alignment was implemented and the alignment obtained using Clustal X 2.1 is shown in Figure 1. Alignments are showing significant identities and similarities between the sequences. Asterisk show identity and colon shows similarity between amino acid residues of the sequences.

The modeling of the 3D structure of *PmAV* and RING finger domain (Figure 2) was performed by modeller 9v10. Multiple template modeling was performed using modeler 9v10. In order to compare the modeling results threading alignment based server I-TASSER was used. It uses 10 most appropriate templates to generate the 3D coordinates. Finally, a model with a lesser MolPdf score and the one that exhibited a lower dope value was chosen for additional computational analysis.

Validation

The selected models were further validated stereo-chemically using PROCHECK. Ramachandran plot for the both models showed that most of the residues are in mostly favored and additionally allowed region. The Ramachandran plots for the *PmAV* and RING Domain models are depicted in Figure 3. It confirms the reliability and excellence of the generated models, by evaluating the backbone conformation, angles and bond lengths. The statistical parameters obtained for both the models are summarized in Table 1.

Furthermore, we also confirmed our models using ProSA which estimates the energy of the 3D structure by distance pair potential.

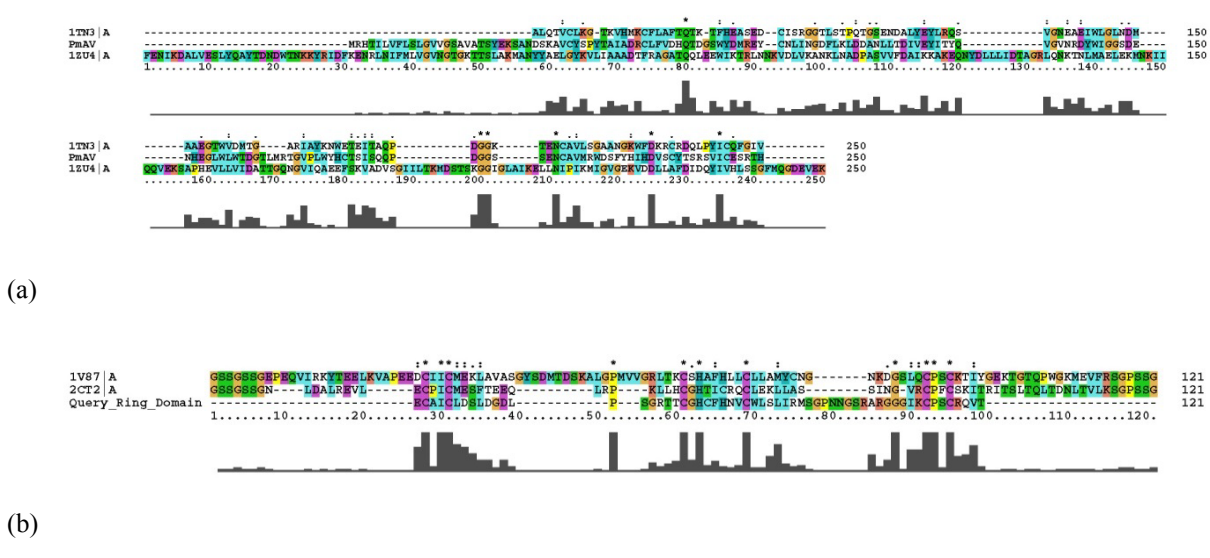

Figure 1: (a) and (b) represent multiple sequence alignments between the query and template sequences.

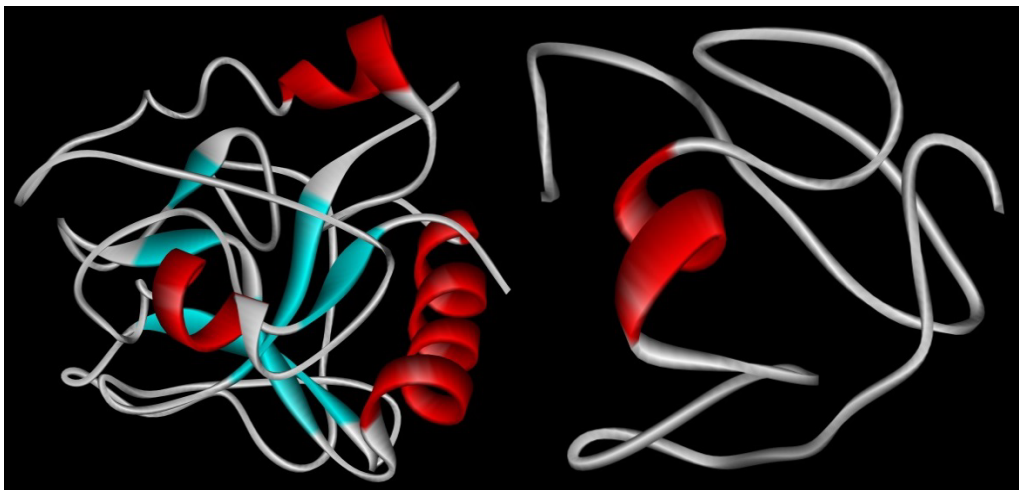

Figure 2: Modeled structure of (a) PMAV (b) RING domain of wsv199. Visualization by Accelrys Viewer Lite: All the validating parameters were assuring the quality and reliability of models.

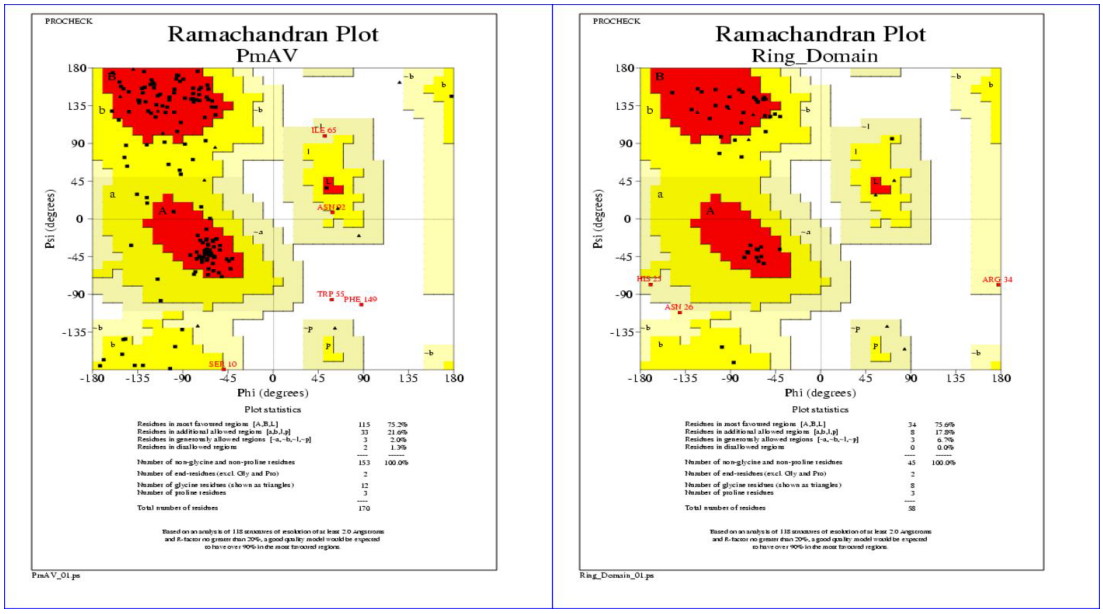

Figure 3: (a) and (b) shows the Ramachandran plots for the PmAV and RING domain of wsv199, respectively.

Table 1: Details of Ramachandran plot for both the models.

	Core region	Allowed	Generously allowed region	Disallowed region
PmAV	75.2	21.6	2.0	1.3
Ring domain	75.6	17.8	6.7	0.0

Residues with negative ProSA value ractify the stability of the model. The ProSA energy score for *PmAV* and RING domain models were found to be -2.68 and -2.54.It indicates overall model quality and measures the deviation of the total energy of the structure with respect to an energy distribution derived from random conformations.

Results determine the selected models are satisfactory. The quality of the predicted model was marked by ProSA energy scores. In contrast, PROCHECK outcome showed somewhat deteriorated values of the models, as no better templates are available. Though, from the outcomes we can summarize that almost all the residues are in most favored and additionally allowed regions except some. These refined models of were further used for docking analyses.

Protein-protein interaction study by docking

The molecular mechanism, the dynamic behavior of proteins and its interactions in this shrimp disease is still unknown. In the present

study, we applied molecular modelling and docking to study the nature and interaction between *PmAV* and wssv199 proteins (Figure 4). Docking study was performed using PatchDock online server (cluster RMSD 4.0). 20 different solutions with their score, area and transformation file were obtained. The output file is applied to another online server i.e. FireDock. This server was used to refinement the docking interaction. FireDock gave the 10 best results on the basis of minimum Global, Attractive and Repulsive van-der Wall, Atomic contact and Hydrogen bond energies as shown in Table 3. In order to analyze the backbone induced-fit refinement of docking interactions, FiberDock server was used. Rigid body protein-protein solutions, in the form of protein files and transformations file, were taken as an input and 1 refined solution file was obtained as a result.

This result file was used to generate molecular interaction plots certifying the protein-protein interaction between protein complexes, using DIMPLOT tool. Figure 5 illustrates the interaction between the two proteins. Residues with red circle belong to *PmAV* protein and residues with pink circle belong to RING domain.

In conclusion, the *in silico* study suggested that *PmAV* might interact with WSSV RING finger domain containing proteins and inhibits their activity thus preventing the establishment of viral

Table 2: List of the selected templates.

Name of the protein	AA	Template_chain	Name of the template
PMAV	170	1TN3_A	The c-type lectin carbohydrate recognition domain of human tetranectin
		1ZU4_A	Crystal structure of FtsY from Mycoplasma mycoides- space group P21212.
RING domain of wsv199	133	1V87_A	Solution Structure of the Ring-H2 Finger Domain of Mouse Deltex Protein 2.
		2CT2_A	Solution Structure of the RING domain of the Tripartite motif protein 32

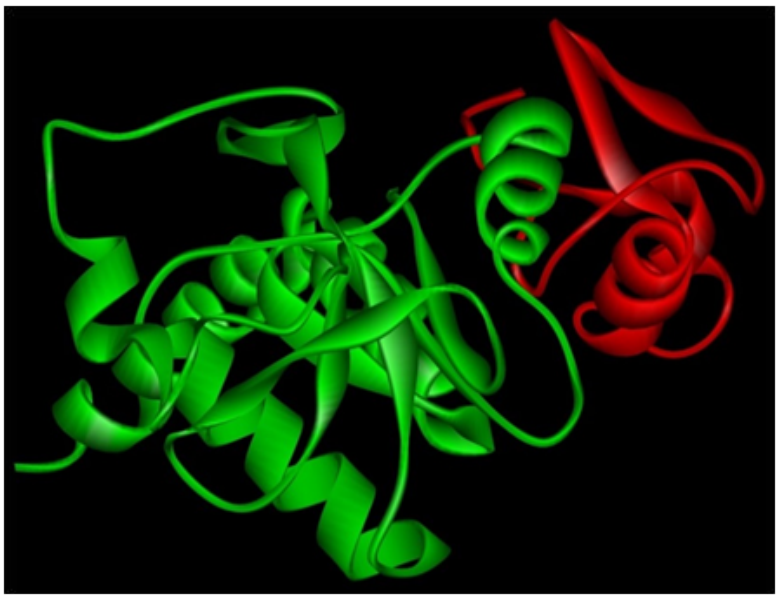

Figure 4: Globular view of interaction between PmAV (green) and RING domain of wsv199 (red).

Table 3: Fire dock results.

Rank	Sol. Number	glob	aVdW	rVdW	ACE	HB
		↓				
1	10	0.00	0.00	0.00	0.00	0.00
2	3	0.00	0.00	0.00	0.00	0.00
3	4	0.00	0.00	0.00	0.00	0.00
4	5	0.00	0.00	0.00	0.00	0.00
5	7	0.00	0.00	0.00	0.00	0.00
6	8	0.00	0.00	0.00	0.00	0.00
7	9	0.00	0.00	0.00	0.00	0.00
8	6	3.41	-9.83	3.15	3.88	0.00
9	1	3.90	-9.26	15.03	1.51	-2.77
10	2	2799.19	-22.64	3558.90	-8.39	-3.16

glob - Global Energy, the binding energy of the solution.
aVdW, rVdW - Softened attractive and repulsive van der Waals energy.
ACE - Atomic contact energy (ACE).
HB - Hydrogen and disulfide bonds.
Transformation - Ligand transformation after refinement.

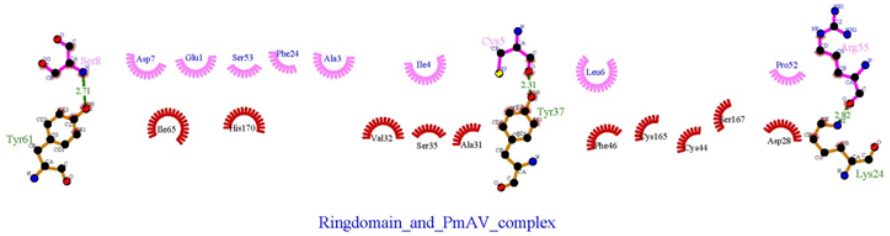

Figure 5: Interaction between shrimp antiviral protein PmAV with WSSV RING finger domain.

infection. This can further lead to reduced modification of host's ubiquitination pathway resulting in decreased diseased condition. Additional studies similar to molecular dynamics simulation [25,26] of the protein-protein complex may be useful for revealing new aspects for prevention of WSD. However, detailed *in vitro* and *in vivo* studies are needed to elucidate the specific anti-viral activity of *PmAV*.

Acknowledgement

Department of Science and Technology, India are highly appreciated for the funding through DST Ramanujan Fellowship award no. SR/S2/RJN-22/2011.

References

1. Lightner DV and Redman RM (1998) Shrimp diseases and current diagnostic methods. Aquaculture 164: 201-220.
2. Lo CF, Ho CH, Peng SE, Chen CH, Hsu HC, et al. (1996) White spot syndrome baculovirus (WSBV) detected in cultured and captured shrimp, crabs and other arthropods. Diseases of Aquatic Organism. 27: 215-225.
3. van Hulten MC, Witteveldt J, Snippe M, Vlak JM (2001) White spot syndrome virus envelope protein VP28 is involved in the systemic infection of shrimp. Virology 285: 228-233.
4. Yang F, He J, Lin X, Li Q, Pan D, et al. (2001) Complete genome sequence of the shrimp white spot bacilliform virus. J Virol 75: 11811-11820.
5. Wang Z, Chua HK, Gusti AA, He F, Fenner B, et al. (2005) RING-H2 protein WSSV249 from white spot syndrome virus sequesters a shrimp ubiquitin-conjugating enzyme, PvUbc, for viral pathogenesis. Journal of virology. 79: 8764-8772.
6. He F, Fenner BJ, Godwin AK, Kwang J (2006) White spot syndrome virus open reading frame 222 encodes a viral E3 ligase and mediates degradation of a host tumor suppressor via ubiquitination. J Virol 80: 3884-3892.
7. Luo T, Zhang X, Shao Z, Xu X (2003) *PmAV*, a novel gene involved in virus resistance of shrimp Penaeus monodon. FEBS Lett 551: 53-57.
8. Drickamer K (1993) Ca2+-dependent carbohydrate-recognition domains in animal proteins. Current Opinion in Structural Biology 3: 393-400.
9. Hoffmann JA, Kafatos FC, Janeway CA, Ezekowitz RA (1999) Phylogenetic perspectives in innate immunity. Science 284: 1313-1318.
10. Yu XQ, Kanost MR (2004) Immulectin-2, a pattern recognition receptor that stimulates hemocyte encapsulation and melanization in the tobacco hornworm, Manduca sexta. Developmental Dev Comp Immunol 28: 891-900.
11. Feizi T (2000) Carbohydrate-mediated recognition systems in innate immunity. Immunol Rev 173: 79-88.
12. Aiyar A (2000) The use of CLUSTAL W and CLUSTAL X for multiple sequence alignment. Methods Mol Biol 132: 221-241.
13. Eswar N, Eramian D, Webb B, Shen MY and Sali A (2008) Protein structure modeling with MODELLER. Methods in Molecular Biology 426: 145-159.
14. Zhang Y (2008) I-TASSER server for protein 3D structure prediction. BMC Bioinformatics 9: 40.
15. Guex N, Peitsch MC (1997) SWISS-MODEL and the Swiss-PdbViewer: an environment for comparative protein modeling. Electrophoresis 18: 2714-2723.
16. Laskowski RA, MacArthur MW, Moss DS, Thornton JM (1993) PROCHECK: a program to check the stereo chemical quality of protein structures. J Appl Cryst 26: 283-291.
17. Schneidman-Duhovny D, Inbar Y, Nussinov R, Wolfson HJ (2005) PROCHECK: a program to check the stereo chemical quality of protein structures. Nucleic Acids Research 33: W363-W367.
18. Andrusier N, Nussinov R, Wolfson HJ (2007) FireDock: fast interaction refinement in molecular docking. Proteins 69: 139-159.
19. Mashiach E, Schneidman-Duhovny D, Andrusier N, Nussinov R, Wolfson HJ (2008) FireDock: a web server for fast interaction refinement in molecular docking. Nucleic Acids Res 36: W229-W232.
20. Mashiach E, Nussinov R, Wolfson HJ (2010) FiberDock: Flexible induced-fit backbone refinement in molecular docking. Proteins 78: 1503-1519.
21. Mashiach E, Nussinov R, Wolfson HJ (2010) FiberDock: a web server for flexible induced-fit backbone refinement in molecular docking. Nucleic Acids Res 38: W457-W461.
22. Laskowski RA, Swindells MB (2011) LigPlot+: multiple ligand-protein interaction diagrams for drug discovery. J Chem Inf Model 51: 2778-2786.
23. Wallace AC, Laskowski RA, Thornton JM (1995) LIGPLOT: a program to generate schematic diagrams of protein-ligand interactions. Protein Eng 8: 127-134.
24. Cerenius L, Söderhäll K (2004) The prophenoloxidase-activating system in invertebrates. Immunological Immunol Rev 198: 116-126.
25. Prasad Gajula MN, Vogel KP, Rai A, Dietrich F, Steinhoff HJ (2013) How far in-silico computing meets real experiments. A study on the structure and dynamics of spin labeled vinculin tail protein by molecular dynamics simulations and EPR spectroscopy. BMC Genomics 14: S4.
26. Gajula P, Borovykh IV, Beier C, Shkuropatova T, Gast P, et al. (2007) Spin-labeled photosynthetic reaction centers from Rhodobactersphaeroides studied by electron paramagnetic resonance spectroscopy and molecular dynamics simulations. Applied Magnetic Resonance 31: 167-178.

Author Affiliation

Top

[1]*Indian Agricultural Statistics Research Institute, Pusa Road, New Delhi, India-110012*
[2]*Department of Biotechnology, Delhi Technological University, Delhi, India-110042*
[3]*Fish Genetics and Biotechnology, CIFE, ICAR, Mumbai, India-400061*

NFC Based Secure Mobile Healthcare System

Divyashikha Sethia[1], Daya Gupta[1],
Tanuj Mittal, Ujjwal Arora
Department of Computer Engineering
Delhi Technological University
New Delhi, India
[1] (divyashikha@dce.edu, dgupta@dce.ac.in)

Huzur Saran[2]
Department of Computer Engineering
Indian Institute of Technology
New Delhi, India
[2](saran@iitd.cse.ac.in)

***Abstract*— With the recent increase in usage of mobile devices especially in developing countries, they can be used for an efficient healthcare management. In this work, we have proposed a novel architecture for improving healthcare system with the help of Android based mobile devices with NFC [1] and Bluetooth interfaces, smartcard technology on tamper resistant secure element (SE) for storing credentials and secure data, and a HealthSecure service on a hybrid cloud for security and health record management. The main contribution of this paper is proposal of applications for i) Secure Medical Tags for reducing medical errors and ii) Secure Healthcard for storing Electronic Health Record (EHR) based on Secure NFC Tags, mobile device using NFC P2P Mode or Card Emulation Mode. We have also briefly mentioned a basic security framework requirement for the applications. Since NFC NDEF format is prone to security attacks [2], we have utilized low level APIs on Android based mobile devices, to securely access NFC tags such as MIFARE Classic tags with NFC-A (ISO 1443-3A) properties. Simple touch of NFC enabled mobile devices can benefit both the patient as well as the medical doctors by providing a robust and secure health flow. It can also provide portability of devices and usability for health management in emergency situation, overpopulated hospitals and remote locations.**

Keywords— mobile based secure healthcare; NFC in healthcare; e-Health card; medical object identifier; RFID; MIFARE Classic; java card; secure element; patient health record

I. INTRODUCTION

Robust healthcare is a requirement for both developed countries, where the cost of healthcare is high and security and privacy are critical issues and developing countries like India, where there is a mass population to handle in hospitals and robust healthcare procedures are required. An efficient, reliable, robust and secure health flow is important to manage patients, their health records smoothly and for the right care to reach to the patient at the right time.

Identification of objects for secure medical procedures is very essential for a secure workflow. For example, secure identifiers on the medicines can help healthcare professional to administer correct medication to a patient to reduce errors.

Along with this issue the Patient Health Record management is important both for patients as well as hospital management. In developing countries like India, there is no centralized management of health records and records are mostly retained by patients in a paper format OPD (Out Patient Department) card, which is both cumbersome to maintain along with the paper based reports and also unreliable. Work is still being done for a secure, electronic patient record management as a Healthcard on a Smartcard in developing countries like India [3] and other nations [4]. Most of the public healthcare services issue a Healthcard on a Smartcard, which retains just the primary information of the patient. All other records are stored on a centralized medical storage server. In developing countries like India, there are challenges like costly infrastructure, connectivity problem for accessing centralized medical records and acceptability of the Healthcard uniformly across different hospitals.

With the recent advancements in mobile devices involving secure credential storage, larger storage capability, wireless communication interfaces and computational power, they can be used in healthcare for not only gathering vital health parameters, as in the Body Area Networks, but also for healthcare management. Privacy and security is a very important aspect of healthcare [5].We propose that the patient should retain all or major patient's EHR electronically, on a Healthcard that is either on a external Smartcard accessible by a mobile device or on the mobile device retained by a patient. A Healthcard retained on a mobile device can retain the entire EHR including reports and tests. Permitted portion can be accessed securely by an authorized medical provider by a simple tap of mobile device. Due to the computational capabilities the records can be summarized and organized for a quicker action to be taken.

Healthcard on a mobile device can be helpful in developed countries also, where healthcare cost is high and privacy and security are critical. The patient can retain all records and can manage the privacy concerns of which portion of the records are to be accessible. The records can occasionally be synced to the central server for backup or storing past history. EHR on Healthcards retained by people can also help in providing the right care in an emergency situation when the patient is unconscious. It can also help determine location of the patient in case of emergency through location service on recent mobile devices. The business logic of using Healthcard on mobile devices can be beneficial to a medical professional since it can securely identify patients using simple portable mobile devices and also get a concise health report. A simple tap of NFC enabled mobile device, will not only improve the workflow of medical professionals but also prove to be beneficial in emergency and chaotic conditions like mass populated

978-1-4799-3635-9/14/$31.00 ©2014 IEEE

hospitals. Simplified workflows will result in faster and more efficient patient-doctor interaction.

The main contribution of this paper is proposal of a robust secure healthcare architecture using Android based mobile device with Near Field Communication (NFC) [1] and Bluetooth interfaces and smartcard technology on Secure Element (SE) for retaining security credentials and EHR. NFC is already being used for applications related to financial payments and ticketing. We propose a novel usage of NFC enabled mobile devices to access secure external medical tags for identifying medical objects like medicines and patient Healthcards. The Healthcard could be on an external tag or retained on the patient mobile device using NFC P2P or card emulation modes. This can provide greater control of sharing personal records with any authorized doctor by a simple tap of mobile devices. Bluetooth can be used along with NFC to provide faster access of bulky data from mobile device.

There is a strong cryptographic framework required for healthcare data. We have briefly mentioned the security requirement in section VII. However the detailed design, threat analysis, implementation and testing of the framework is still in progress and is beyond the scope of this paper.

The mobile devices and Healthcards can be authorized by a HealthSecure service on a hybrid cloud, to provide services for enhanced security and extended storage for health records. We plan to work on the architecture of the Healthsecure service in the future.

The paper is broadly divided into seven sections. Section II provides an overview of technologies for NFC, NFC tags, SE and Java Card. In section III we discuss about the proposed architecture. Section IV illustrates the implementation part followed by a brief overview of the security framework requirement in section V. In section VI we discuss briefly about some related work, followed by section VII which presents the conclusion and future work.

II. TECHNOLOGY

NFC [1] is an upcoming wireless technology which provides simple interfaces for device to device communication as well as access to NFC, RFID and smartcard tags [6]. NFC enabled mobile device can operate in three modes: i) Reader mode: in which device can read and write to NFC based passive tags. ii) Peer to Peer (P2P) mode in which NFC devices can interact and exchange information with each other iii) Card emulation mode: in which NFC device can operate as a contactless card.

NFC tags are of different types and use NDEF (NFC Data Exchange Format) [6] for storing and sending data. NFC tags must have a secure read and write access for critical applications such as those related to healthcare. NDEF provides no protection against data manipulation, overwrite protections and digital signature records cannot avoid malicious modification of tags [2]. Hence we utilize MIFARE Classic 1 K tags [7], which employ a proprietary protocol compliant to parts of ISO/IEC 14443-3 Type A, and write raw data using NFC-A (ISO 14443-3A) [8] properties for improved security. The MIFARE Classic 1K tag offers 1024 bytes of data storage, split into 16 sectors. Each sector is protected by two different keys, called key A and key B for secure access.

NFC enabled mobile devices have a secure element (SE) which is a secure microprocessor (a smart card chip) that includes a cryptographic processor to facilitate transaction with authentication and security, and provides secure memory for storing applications and credentials. It comes in different form factors such as embedded, microSD card or a UICC (SIM) card [9]. Due to simplicity of accessibility we have used SWP enabled microSD card (by GO-Trust [10]) as a SE to manage cryptographic keys as well as patient medical records. SWP is a contact based protocol between Contactless frontend (CLF) and UICC. It is Java Card 2.2.2 compliant.

Java Card [11] is a technology which enables Java based applets to run on smartcards with very limited memory and processing capabilities and provides data encapsulation, firewall and cryptography. The smart card specification standards [12], ISO/IEC 7816 for contact and ISO/IEC 14443 for contactless, specify that communication between a host application and a smart card is done through Application Protocol Data Units (APDUs).

III. PROPOSED APPLICATION MODELS

We have proposed an architecture for NFC based secure healthcare as illustrated in Fig. 1 for i) secure medical identifiers as in flow steps 1.1 to 1.5 and ii) Healthcard retaining EHR using Android mobile devices as in flow steps 2.1 to 2.5. We have proposed a secure healthcare service like HealthSecure on a hybrid cloud to which all hospitals can subscribe. The HealthSecure hybrid cloud provides service for maintaining Cryptographic servers for secure framework and Storage server to provide backup as well as space for extended EHR. $Mobile_{ADMIN}$ is a mobile device of an authorized medical admin. $Mobile_{PAT}$ is the patient's mobile device with the Healthcard and $Mobile_{DOC}$ is the doctor's mobile device. Since a larger screen would be better suited to view and update the health records, $Mobile_{DOC}$ could either be an NFC enabled tablet, for portability, or a laptop with external smartcard reader. K_A and K_B are the read and write access keys respectively for a secure tag based on MIFARE Classic. For NFC P2P based and card emulation based Healthcards, we use patient's and doctor's set of public and private keys, which are K_{PUBPAT}, K_{PRIPAT} and K_{PUBDOC},K_{PRIDOC} respectively. A symmetrical shared key K_{SH} is used for encrypting data.

Hospital administration has an application for securely reading/writing with a mobile device, $Mobile_{ADMIN}$, to manage smartcard based tags and patient Healthcards. $Mobile_{ADMIN}$ can register with the proposed HealthSecure cloud service on a hybrid cloud, which can issue security keys for our architecture. The mobiles use SE and simple interfaces of NFC and Bluetooth for credential storage and communication. We discuss the architecture of the applications briefly in the following subsections and give the details of the implementation in section IV and security framework requirement in section V.

A. Secure Medical Object Identification using NFC Tags

Reliable medical object identifiers are important for reducing errors in the hospital workflow, like giving correct

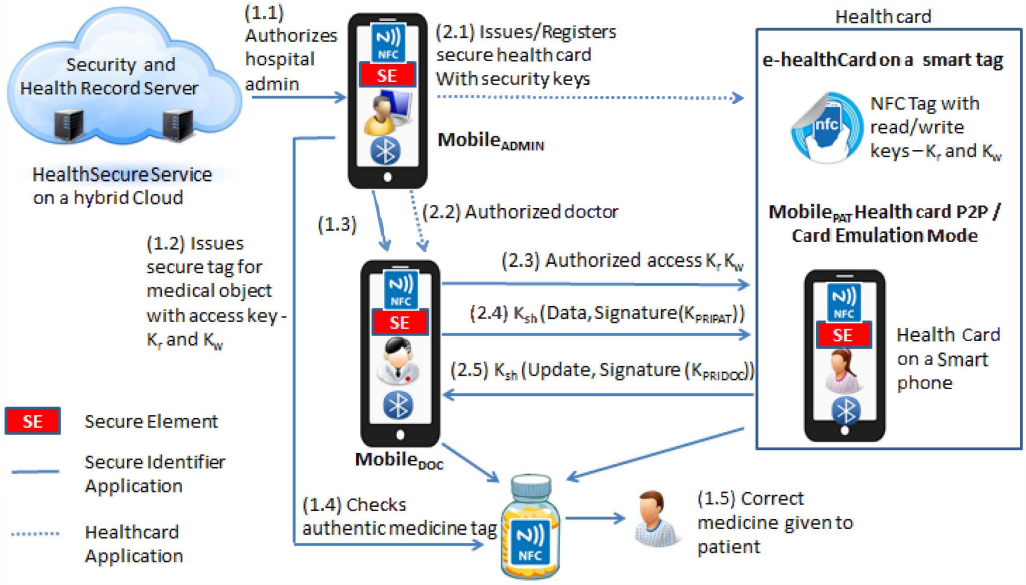

Fig. 1. NFC Based Secure Healthcare Architecture

medicine to a patient [13]. We propose architecture of an application for issuing secure identifiers to reduce the error and also to prevent security attacks like modification, repudiation and masquerading. The secure NFC passive tags have been used for identifiers, specifically MIFARE Classic. Bluetooth Low Energy (BTLE) stickers [14] have lately been used to identify objects. But since they require a dedicated battery to operate, NFC passive tags are cheaper for identifiers to be used in healthcare. As discussed in section II, NFC tags with NDEF format are prone to security flaws [2]. Hence basic NFC-A interface can be used to access smartcards from a mobile device. A valid mobile reader must have security key K_R for read access and a valid writer must have security key K_W for update access. The tag is issued by a healthcare admin mobile device, $Mobile_{ADMIN}$, which has registered to a HealthSecure service. It retains security keys in its SE for issuing tags. To enhance security, the access keys of the tag could be updated on a periodic basis for retaining secure IDs on the medical objects. Fig. 1, steps 1.1 to 1.5, shows the workflow of secure tag identifiers in bold. Along with medical identification records, information related to timestamp can also be updated.

B. e-Health Card using NFC Tags

The secure tags used for application in III-A, are used for a different application for storing EHR on Healthcard of a patient. This is similar to a smartcard based Healthcard. But here we suggest smartcards that can be securely and easily be accessed using mobile devices. The tag could retain patient identification information along with emergency information, insurance information and health records. The tag could be organized into different sections, each administered separately by different set of security access keys. Similar to the secure tag application, this card can be issued and updated by an authorized health admin mobile device $Mobile_{ADMIN}$. A patient can register at the $Mobile_{ADMIN}$ and then later show to an authorized doctor with $Mobile_{DOC}$ in an OPD which would have the required access keys K_R and K_W for reading and updating the health records respectively. All NFC information can be retained with a timestamp. Due to limitation of space on the card, it can only retain recent health records. Detailed health records can be retained on a storage server of the HealthSecure service on hybrid cloud. At the end of the visit the patient can present the tag back to the administrator to tap and store his visit detail on the hybrid cloud. At any point of time if patient's past records are required, they can be retrieved over secure wireless interface (like HTTPS) from the hybrid cloud, using the patient ID on the tag. This application will help the patient to retain the recent health records on a cheap yet secure tag equivalent to a smartcard.

C. e-Health Card based on P2P NFC mode

This application architecture is based on retaining a Healthcard on a mobile device using NFC P2P mode. The EHR is retained on the mobile device in a secure region instead of NFC tag as in III-B. The patient can tap his mobile device onto the doctor's mobile device to exchange his records using NFC NDEF format. The doctor can read and update the records and tap them back onto the patient's mobile device. Both patient and doctor register for the OPD session with the health admin, $Mobile_{ADMIN}$, to get secure keys. The patient's public and private keys K_{PUBPAT}, K_{PRIPAT} and doctor's public and private keys K_{PUBDOC}, K_{PRIDOC} get stored on the SE of their respective mobile devices for the OPD session.

This Healthcard offers more storage space as compared to what a smartcard based tag can provide as in application III-B. It also ensures that only the permitted records of the patient are accessed by an authorized doctor, thus retaining security and privacy of the patient. NFC P2P mode can be utilized for information exchange. But very large health records exchanged over NFC can be slow due to the low data rate of NFC. Bluetooth can be used along with NFC for exchange of larger

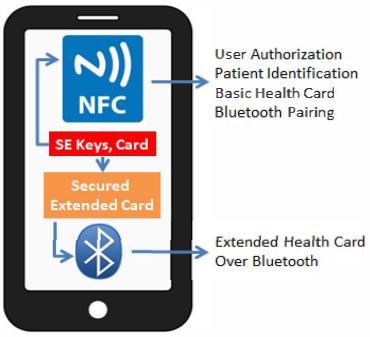

Fig. 2. Proposed Card emulation architecture

health record data. A basic security framework requirement is discussed in section V.

D. e-Health Card based on NFC card emulation

In this application architecture, Healthcard is retained on a mobile device using card emulation and Java card applets installed on the SE. We propose usage of a SE in the form of an SWP enabled microSD card as provided by GoTrust [10], which can be issued to the patient by HealthSecure service. Java Card applet can be used to authenticate and authorize the reader to access and update the health records using NFC SWP protocol. Since the SE has limited space, it can only retain part of the health records. The remaining health records can be retained outside the SE region on the SD card in a secure manner. The Card on the $Mobile_{PAT}$ can be accessed externally by a PC/SC reader that is attached to $Mobile_{DOC}$. Since the SE has limited space, an extended card consisting of past records and other health information, like images and reports, can be stored in encrypted format on an insecure region. Hence this Healthcard is different from a standard plastic smartcard used for Healthcard in the previous scenario. Since NFC has lower data rate, Bluetooth can be used to access the extended card. The Java card applet can be used to initiate Bluetooth pairing between mobile devices. This Healthcard is most secure and can also be used to retain larger information on the mobile device and is similar in idea to the Wireless Medical Card [17]. Fig. 2 shows the proposed card emulation architecture. A basic security framework requirement is discussed in section V.

IV. IMPLEMENTATION

We have developed applications for both Android devices, using Android APIs, and administrative server, using PHP and MySQL, for secure, reliable and robust healthcare system. Mobile applications have been tested on Google Nexus 7 and Samsung Galaxy S3 devices. We have used MIFARE Classic 1K tags for reading and writing data using APIs in Android framework (Android 2.3.3 and above). The Android framework provides android.nfc.tech package, which contains necessary classes and methods to enable interaction with tags. We have used a SWP Secure microSD card (by GO-Trust), which provides a microSD based Java Card 2.2.2 solution. The card supports running Java Card applets on a hardware-backed SE. It also provides a contactless interface (ISO 14443) via SWP which can be used to interact with compliant PC/SC readers. We have tested it using a Samsung Galaxy S3 (i9300, by Samsung) mobile device with Android 4.1.2. The card can be accessed from an authorized Android application developed using Go-Trust library. Since the card supports Global Platform 2.1.1 [15], the installation can be done using custom Global Platform APDUs. Java card applets have been developed to store credentials for security framework and for card emulation mode.

Implementation of Security framework and hybrid cloud service is in progress and will be tested and deployed in the field in our future work.

V. SECURITY FRAMEWORK REQUIREMENT

There is a strong security framework required for the healthcare management. It is different from the financial data security which is small in size and is handled by a set of trained professionals with standardized models [16]. The healthcare data can be large in size as in a Healthcard with entire HER in section III.D. Also the health card could be accessed by various persons: patient, medical professional, emergency person and insurance. The patient should be able to securely manage the access control of the EHR. We provide a brief overview of a basic security framework requirement for the application of Health card on a patient mobile device using NFC P2P or Card Emulation mode as in Figure 3. There is a requirement of confidentiality, integrity, mutual authentication, access control of EHR, privacy threats leading to identity thefts and insurance security breach [5].

The security framework involves various entities. A cryptographic server is used to generate, verify and store security keys. An administrator is present to issue Healthcards / tags and register patients/doctors. Mobile devices used by doctors are equipped with a Doctor App and a secure element (Doctor SE). Healthcard used by patients is called Patient card which in this case is using a NFC P2P or card emulation mode. The SEs involved, like Doctor SE, run a Java Card applet to manage cryptographic keys as well as patient medical records. Since the health card could be accessed by various persons: patient, medical professional and emergency person, they could use the concept of shared key based on Attribute Based Encryption [18]. The patient could access the card using combination of Patient key in the form of a PIN and Biometrics. There could be a separate Doctor PIN for doctor and a super key for emergency team when patient is unconscious. In case of loss of mobile devices the keys which are maintained by the HealthSecure service can be invalidated.

We have suggested usage of Public Key Infrastructure (PKI) for the security framework. The security flow consists of 1. Healthcard personalization 2. Mutual Authentication between the patient and the medical doctor to assure the correct patient is appearing before an authorized doctor and there is no relay attack 3. Access control for data viewable by the doctor 4. Secure healthcard retrieval and updation.

There is an initial phase of personalization in which the Patient Card and the Doctor SE get a unique identification ID (UID_{PAT} and UID_{DOC}) and a set of public and private keys (K_{PUBPAT}, K_{PRIPAT} and K_{PUBDOC}, K_{PRIDOC}) from the security server based on the respective card ID and/or secure element ID. This phase ensures that both the Patient Card and the

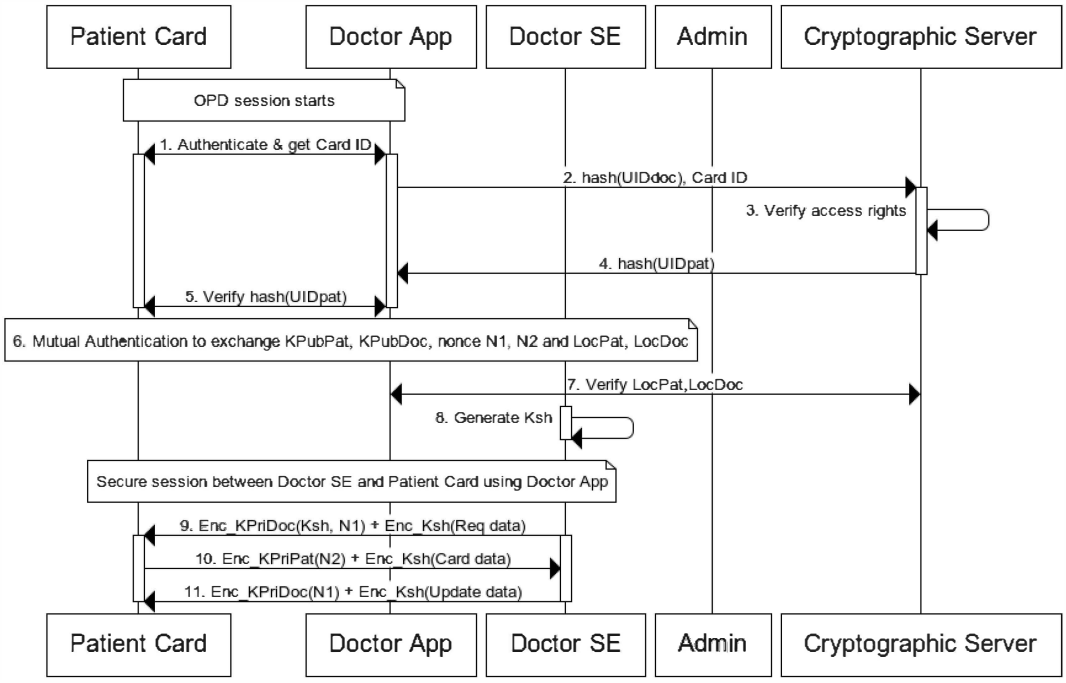

Fig. 3. Sequence diagram of basic security framework

Doctor SE have their respective UIDs and keys securely stored locally.

Now the OPD session can start between the patient and the doctor as detailed under Fig. 3. The Doctor App authenticates the Patient Card and retrieves the card ID. The card ID along with hash (UID_{DOC}) is sent to the server to verify access rights of doctor. Once verified, the server returns hash (UID_{PAT}), which is used to verify the authenticity of doctor by the patient. Now, as given in step 6, the patient and doctor mutually authenticate to exchange respective public keys, K_{PUBPAT}, K_{PUBDOC} and randomly generated nonce, N1 and N2 by patient and doctor SE respectively using algorithm suggested in [19], to prevent man in the middle attack. The location of patient is also shared with doctor, and with the help of server, validation is done to make sure both are same to avoid relay attacks. Loc_{PAT} and Loc_{DOC} could be GPS location or a related parameter in the ambience gathered from audio or light sensors on the mobile devices [20]. Now a symmetric key K_{SH} is generated by the Doctor SE for efficient encryption of health data and secure communication is held (steps 9 to 11). The doctor sends K_{SH} along with its request securely and receives the data. Similarly, an update, like a prescription, can be sent back securely to the Patient Card. A encrypted and signed data communications ensures confidentiality and integrity. This a basic framework requirement and we are working on designing a stronger framework as mentioned in section VII.

VI. Related Work

Emergency NFC tags [21] retain patient medical emergency information. But the work does not consider write protection and reusable NFC tags. NFC mobile devices have been used for storing credentials to be used for billing and identity [22]. We propose using it for healthcare applications with credentials and a much stronger security requirement since it is accessed by number of people and the quantity of data could be large. Smart poster [23] proposes using secure NFC tags since "NFC tags are vulnerable to spoofing as well as cloning", with a web server to securely retain the details of the poster. An application using NFC to track patients with pneumonia has been deployed in Karachi [24]. NFC based tags have also been used to tag medicines to reduce medical errors [13]. None of this work takes care of NFC tag security. We have suggested a novel manner of secure tags based on NFC-A protocol for our applications based on secure NFC tags. In our previous work [25] we have used NFC tags for reliable patient records and automating the health flow with Body Sensors. We have further expanded the work for new applications of NFC enabled devices for health flow data management with medical identifiers and Healthcards. The applications suggested in this paper for the improved workflow management with NFC enable mobile devices are unique to the best of our knowledge. Secure records can be stored on a mobile device for emergency purpose [18] using concept of shared keys. But they do not use any hardware tamper resistant device. Work has been done [17] for a wireless medical card with NFC and high speed interface with bulk memory card. Our work is different since we have proposed a similar larger card as in section III.D using a hardware tamper resistant SE based on a microSD card on a mobile device with NFC and Bluetooth interface.

VII. Conclusion and Future Work

In this work, we have proposed applications based on NFC enabled Android mobile devices for improving healthcare process for secure medical object identification and patient

Healthcard on an external tag or mobile device itself. The applications are simple to use with a simple touch of NFC for secure communication. This will improve the health flow in crowded hospitals of developing countries like India as well as of developed nations. The business model will benefit the patients as well as medical professional since they can use the commonly retained mobile devices conveniently. The cost of the architecture can be reduced by using microSD cards or UICC cards with inbuilt NFC antenna. These forms of SEs can be issued as Healthcards on mass scale to reduce the cost and to be operational on non NFC mobile devices. The proposed architecture can be used for applications other than healthcare with secure identifiers and secure transfer of large data between devices.

Although MIFARE Classic security algorithm Crypto1 has been broken [26], any other secure smartcard based tags like MIFARE DESIRE could be used in future based on the availability of the APIs. We have suggested a basic security framework requirement in this paper. A detailed design, implementation, testing and field deployment of the he security framework is in progress and will be addressed in our future work. We also plan to enhance the security framework using identity encryption using zero knowledge proofs and attribute based encryption for shared key management, access control of health data, and delegation of rights by patient to other trusted person for collection of health data. The current security framework is based on Public Key Infrastructure. Identity based Encryption and Attribute Based Encryption techniques can also be compared in future. We need to work on the security issues of NFC and Bluetooth for accessing secure Healthcard in future for security threats of theft, cloning, man in the middle and relay attacks and loss of a mobile device.

We plan to design architecture of the HealthSecure service on a hybrid cloud in the future with replicated Kerberos cryptographic servers and a Hospital Information System for backup of EHR. We also need to compare NFC and BTLE for card emulation. NFC has higher energy requirement, compared to BTLE, when it is in a reader mode to activate the passive tag. But NFC has an advantage of smoother interfaces and getting initiated by a simple tap, while BTLE requires pairing.

REFERENCES

[1] Vedat Coskun, Busra Ozdenizci and Kerem Ok, "A Survey on Near Field Communication (NFC) Technology", J. Wireless Personal Communications: An International Journal, vol. 71, pp. 2259-2294, 2013.

[2] M. Roland and J. Langer, "Digital Signature Records for the NFC Data Exchange Format", IEEE Proceedings of the Second International Workshop on Near Field Communication (NFC), pp, 71-76, 2010.

[3] Rashtriya Bima Yojana, http://en.wikipedia.org/wiki/Rashtriya_Swasthya_Bima_Yojan

[4] Smart Card Technology in U.S. Healthcare: Frequently Asked Questions, http://www.smartcardalliance.org/resources/pdf/Smart_Card_Technology_in_Healthcare_FAQ_FINAL_096012.pdf, 2012

[5] Sasikanth Avancha, Amit Baxi, and David Kotz, "Privacy in mobile technology for personal healthcare", ACM Computing Surveys (CSUR), vol. 45 Issue 1, article 3, 2012.

[6] NFC Forum Tedchnical Specifications, http://www.nfc-forum.org/specs/spec_list/ndefts

[7] MIFARE Classic 1K specification document, http://www.nxp.com/documents/data_sheet/MF1S50YYX.pdf

[8] NFCA on Android, http://developer.android.com/reference/android/nfc/tech/NfcA.html

[9] Mobile/NFC Security Fundamentals Secure Elements 101, http://www.smartcardalliance.org/resources/webinars/Secure_Elements_101_FINAL3_032813.pdf, 2013

[10] GO-Trust® Secure microSD Java, http://www.go-trust.com/products/microsd-java/

[11] Java Card™ Platform Security, http://www.oracle.com/technetwork/java/javacard/documentation/javacardsecuritywhitepaper-149957.pdf

[12] Smart Card Standards for contact and contactless interfaces, http://www.smartcardalliance.org/pages/smart-cards-intro-standards

[13] Lahtela, A., Hassinen, M.and Jylha, V., "RFID and NFC in healthcare: Safety of hospitals medication care", IEEE proceedings on Pervasive Computing Technologies for Healthcare, pp. 241—244, 2008.

[14] Saroj Kumar Panigrahy, Sanjay Kumar Jena, and Ashok Kumar Turuk, "Security in Bluetooth, RFID and wireless sensor networks", ACM Proceedings on 2011 International Conference on Communication, Computing & Security, pp. 628-633, 2011.

[15] Global Platform Specifications, http://www.globalplatform.org/specificationscard.asp

[16] Why healthcare IT security is harder than the rest, http://www.csoonline.com/article/print/693941

[17] Stefan Krone, Bjoern Almeroth, Falko Guderian and Gerhard Fettweis, "Towards A Wireless Medical Smart Card", IEEE Design, Automation & Test in Europe Conference & Exhibition,pp 1483 – 1488, 2012

[18] Ryan W. Gardner, Sujata Garera, Matthew W. Pagano, Matthew Green, and Aviel D. Rubin, "Securing medical records on smart phones", Proceedings of the first ACM workshop on Security and privacy in medical and home-care systems, pp. 31-40, 2009.

[19] Yun-Seok Lee, Eun Kim, and Min-Soo Jung, "A NFC based Authentication method for defense of the Man in the Middle Attack", 3 rd International Conference on Computer Science and Information Technology (ICCSIT'2013) January 4-5, 2013 Bali, Indonesia

[20] Tzipora Halevi, Di Ma, Nitesh Saxena, and Tuo Xiang, "Secure Proximity Detection for NFC Devices Based on Ambient Sensor Data", Computer Security – ESORICS 2012. Lecture Notes in Computer Science, vol 7459, pp 379-396, 2012.

[21] Sebastian Dunnebeil, Felix Kobler, Philip Koene, Jan Marco Leimeister, and Helmut Krcmar, "Encrypted NFC Emergency Tags Based on the German Telematics Infrastructure", IEEE proceedings on Near Field Communication (NFC), 2011 3rd International Workshop, pp. 50-55.IEEE Press, 2011.

[22] Gergely Alp´ar, Lejla Batina, and Roel Verdult, "Using NFC phones for proving credentials", 16th Measurement, Modelling, and Evaluation of Computing Systems and Dependability and Fault Tolerance. LNCS, vol. 7201, pp. 317-330. Springer Verlag, 2012.

[23] Jason Wu, Lin Qi, Ram Shankar Siva Kumar, Nishant Kumar, and Patrick Tague, "S-SPAN: Secure Smart Posters in Android using NFC", IEEE International Symposium on World of Wireless, Mobile and Multimedia Networks, pp. 1-3, IEEE Press, 2012

[24] Adam Marcus_, Guido Davidzony, Denise Law, Namrata Verma, Rich Fletcher, Aamir Khanz and Luis Sarnenta, "Using NFC-enabled Mobile Phones for Public Health in Developing Countries", IEEE Proceedings on First International Workshop on Near Field Communication, pp. 30-35. 2009.

[25] Divyashikha Sethia, Shantanu Jain and Himadri Kakkar, "Automated NFC enabled Rural Healthcare for reliable patient record maintenance", Proceedings of Global Telehealth Conference, vol. 182, pp. 104-113, 2012.

[26] Gerhard de Koning Gans, Jaap-Henk Hoepman, and Flavio D. Garcia, " A Practical Attack on the MIFARE Classic", Smart Card Research and Advanced Applications. LNCS, vol. 5189, pp. 267—282, 2008.

2012 Third International Conference on Computer and Communication Technology

Novel single input five output voltage mode universal filter based on DDCCTA

Neeta Pandey[1], Rajeshwari Pandey[2], Sajal K. Paul[3]
[1,2]Department of Electronics and Communication Engineeing,Delhi Technological University,Delhi
[3]Department of Electronics and Communication Engineeing, ISM Dhanbad

Abstract: A novel single input five output voltage mode universal filter based on differential difference current conveyor transconductance amplifier (DDCCTA) is presented. It employs grounded passive components namely two capacitors and a resistor. The proposed filter offers the following advantageous features: high input impedance—a desirable property of voltage mode filters; simultaneous availability of low pass, band pass, high pass, notch, and all pass; no matching constraint; low sensitivity performance and use of grounded capacitors suitable for integration. The effect of DDCCTA non-idealities on filter behaviour has also been addressed. The functionality of the design is verified through SPICE simulations using 0.25 μm TSMC CMOS technology.

I. INTRODUCTION

There is a growing interest in designing analog signal processing circuits and systems using current mode approach due to some potential performance features like wide bandwidth, less circuit complexity, wide dynamic range, low power consumption and high operating speed [1]. The current mode active elements can process signals in current or voltage or mixed mode so a wide variety of these elements are available in the literature [2-9]. Some recently proposed elements [10-15] employ current conveyor blocks and transconductance amplifier (TA) cascades in monolithic chip; and give compact implementation of signal processing circuits and systems. Current conveyor transconductance amplifier (CCTA) [10-11], current controlled current conveyor transconductance amplifier (CCCCTA) [12], differential voltage current conveyor transconductance amplifier (DVCCTA) [13], differential voltage current controlled conveyor transconductance amplifier DVCCCTA [14] and differential difference current conveyor transconductance amplifier (DDCCTA) [15] are example of such building blocks. The DVCCTA, DVCCCTA and DDCCTA are more flexible blocks as they inherit the advantageous characteristics of CCTA and CCCCTA along with one or two additional high input impedance terminals which may be used for applications demanding differential and floating inputs. Considering these features some applications of these elements have been reported in the literature [13-19].

The main intention of this paper is to present a single input five output voltage mode universal filter using DDCCTA. The literature survey of the available literature on such filters [20-29] shows that these structures

- use excessive number of resistors [20-28] ,
- employ floating resistors [20-23, 25-28],
- require component matching [20-22, 24-28],
- do not present high input impedance [20,21,23,25,27,28] which eases the cascading of voltage mode filter, and
- do not provide electronic tunability to the filter parameters [20-29].

It is clear form the above discussion that there is no structure available that simultaneously presents the features of minimum number of passive elements, all grounded passive elements, high input impedance and tunability of filter parameters. The proposed filter is derived from [15, 16] and employs two DDCCTAs, two grounded capacitor and a single grounded resistor. The proposed filter has high input impedance; requires no matching constraint; enjoys tunability of filter parameters and low sensitivity performance; and uses grounded passive components suitable from integration viewpoint. The effect of DDCCTA non-idealities on filter behaviour has also been discussed. The functionality of the proposed circuit has been verified through SPICE simulations using 0.25 μm TSMC CMOS technology.

II. CIRCUIT DESCRIPTION

The DDCCTA is based on DDCC [7] and consists of differential amplifier, current mirrors and TA. The port relationships of the DDCCTA as shown in Fig. 1 can be characterized by the following matrix:

$$\begin{bmatrix} I_{Y1} \\ I_{Y2} \\ I_{Y3} \\ V_X \\ I_Z \\ I_O \end{bmatrix} = \begin{bmatrix} 0 & 0 & 0 & 0 & 0 & 0 & 0 & 0 \\ 0 & 0 & 0 & 0 & 0 & 0 & 0 & 0 \\ 0 & 0 & 0 & 0 & 0 & 0 & 0 & 0 \\ 1 & -1 & 1 & 0 & 0 & 0 & 0 & 0 \\ 0 & 0 & 0 & 1 & 0 & 0 & 0 & 0 \\ 0 & 0 & 0 & 0 & -g_m & 0 & 0 & 0 \end{bmatrix} \begin{bmatrix} V_{Y1} \\ V_{Y2} \\ V_{Y3} \\ I_X \\ V_Z \\ V_O \end{bmatrix} \quad (1)$$

where g_m is transconductance of the DDCCTA.

978-0-7695-4872-2/12 $26.00 © 2012 IEEE
DOI 10.1109/ICCCT.2012.18

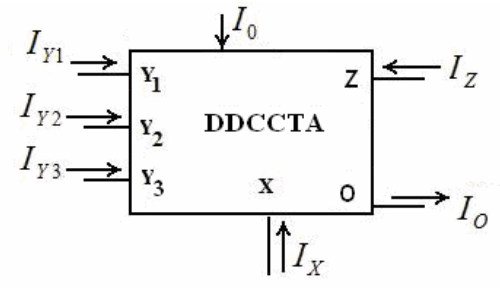

Fig. 1. Circuit symbol of DDCCTA

The CMOS based internal circuit of DDCCTA [15] in CMOS is depicted in Fig.2. It consists of the circuit of DDCC [7] followed by a transconductance amplifier. The value of g_m is obtained as $\sqrt{2\mu_n C_{ox}(W/L)I_0}$ which can be adjusted by bias current I_0.

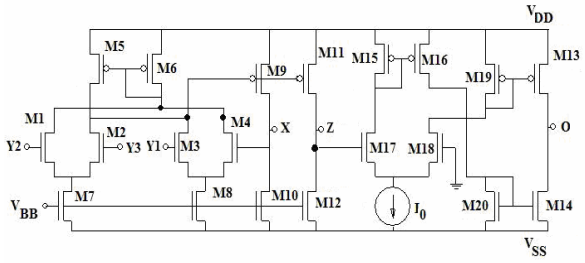

Fig. 2. DDCCTA internal circuit

The proposed voltage mode (VM) filter is shown in Fig. 3 which employs two DDCCTA, two grounded capacitors and a grounded resistor. The analysis of circuit yields the output voltages at various nodes as:

$$\frac{V_{out1}}{V_{in}} = \frac{s^2 C_1 C_2 R}{D(s)} \tag{2}$$

$$\frac{V_{out2}}{V_{in}} = \frac{sC_2}{D(s)} \tag{3}$$

$$\frac{V_{out3}}{V_{in}} = -\frac{g_m}{D(s)} \tag{4}$$

$$\frac{V_{out4}}{V_{in}} = \frac{s^2 C_1 C_2 R + g_m}{D(s)} \tag{5}$$

$$\frac{V_{out5}}{V_{in}} = \frac{s^2 C_1 C_2 R - sC_2 + g_m}{D(s)} \tag{6}$$

where

$$D(s) = s^2 C_1 C_2 R + sC_2 + g_m \tag{7}$$

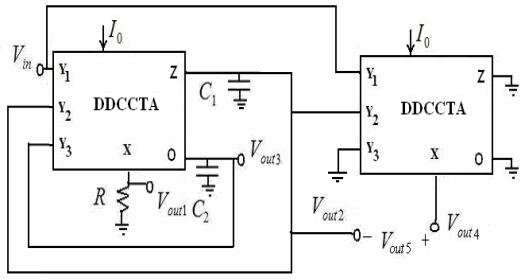

Fig. 3. Proposed voltage mode filter

It may be observed from (2) to (6) that high pass, band pass, low pass, notch and all pass responses are available at V_{out1}, V_{out2} V_{out3}, V_{out4} and V_{out5} simultaneously. Thus the proposed structure is a single input and five output voltage mode filter. It may further be noted that no component matching constraint is required. The responses are characterized by pole frequency (ω_0), bandwidth (ω_0/Q_0) and quality factor (Q_0) as

$$\omega_0 = \left(\frac{g_m}{RC_1C_2}\right)^{1/2}, \frac{\omega_0}{Q_0} = \frac{1}{RC_1}, Q_0 = \left(\frac{g_m RC_1}{C_2}\right)^{1/2} \tag{8}$$

It may be noted from (8) that the pole frequency (ω_0) and quality factor (Q_0) can be adjusted by g_m, i.e. by bias current of DDCCTA, without disturbing ω_0/Q_0. The ω_0 and Q_0 are orthogonally adjustable with simultaneous adjustment of g_m and R such that the product g_m R remains constant and the quotient g_m /R varies and vice versa**.** The resistance R being a grounded one may easily be implemented as a variable resistance using only two MOS [30]. Equation (8) also indicates that high values of Q-factor will be obtained from moderate values of ratios of passive components i.e. from low component spread [31]. These ratios can be chosen as $g_m R = (C_1/C_2) = Q_0$. Hence the spread of the component values becomes of the order of $\sqrt{Q_0}$. This feature of the filter related to the component spread allows the realization of high Q_0 values more accurately compares to the topologies where the spread of passive components becomes Q_0 or Q_0^2. It can also be easily evaluated to show that the sensitivities of pole ω_0 and pole Q_0 are within unity in magnitude. Thus the proposed structures can be classified as insensitive.

III. EFFECT OF NONIDEALITIES

In practice, the performance of the filter circuit may deviate from the ideal one due to non-idealities of DDCCTA. The non-idealities effects are categorized in two groups. The first comes from internal current and voltage transfers of DDCCTA and results in a modified port relationships as

$$\begin{bmatrix} I_{Y1} \\ I_{Y2} \\ I_{Y3} \\ V_X \\ I_Z \\ I_O \end{bmatrix} = \begin{bmatrix} 0 & 0 & 0 & 0 & 0 & 0 \\ 0 & 0 & 0 & 0 & 0 & 0 \\ 0 & 0 & 0 & 0 & 0 & 0 \\ \beta_1 & -\beta_2 & \beta_3 & 0 & 0 & 0 \\ 0 & 0 & \alpha & 0 & 0 & 0 \\ 0 & 0 & 0 & -\gamma g_m & 0 & 0 \end{bmatrix} \begin{bmatrix} V_{Y1} \\ V_{Y2} \\ V_{Y3} \\ I_X \\ V_Z \\ V_O \end{bmatrix} \tag{9}$$

where the coefficients $\beta_1 = 1 - \varepsilon_{v1}$, $\beta_2 = 1 - \varepsilon_{v2}$ and $\beta_3 = 1 - \varepsilon_{v3}$. The ε_{v1}, ε_{v2} and ε_{v3} denote voltage tracking errors from Y1, Y2 and Y3 terminals to X terminal respectively. The coefficient $\alpha = 1 - \varepsilon_i$ where ε_i denotes current tracking errors from X to Z terminal. The coefficient γ denotes current gain from Z terminal to O terminal. Taking these effects into account, (2) to (7) are changed to

$$\left.\frac{V_{out1}}{V_{in}}\right|_{NI} = \frac{\beta_1 s^2 C_1 C_2 R}{D_n(s)} \tag{10}$$

$$\left.\frac{V_{out2}}{V_{in}}\right|_{NI} = \frac{\alpha\beta_1 s C_2}{D_n(s)} \tag{11}$$

$$\left.\frac{V_{out3}}{V_{in}}\right|_{NI} = -\frac{\alpha\beta_1\gamma g_m}{D_n(s)} \tag{12}$$

$$\left.\frac{V_{out4}}{V_{in}}\right|_{NI} = \frac{\beta_1(s^2 C_1 C_2 R + \alpha\beta_3\gamma g_m)}{D_n(s)} \tag{13}$$

$$\left.\frac{V_{out5}}{V_{in}}\right|_{NI} = \frac{\beta_1(s^2 C_1 C_2 R + \alpha\beta_3\gamma g_m) - \alpha\beta_1 s C_2}{D_n(s)} \tag{14}$$

where

$$D(s)\big|_{NI} = s^2 C_1 C_2 R + \alpha\beta_2 s C_2 + \alpha\beta_3\gamma g_m \tag{15}$$

and NI stands for non-ideal.

It may be noted that the non-ideal current and voltage transfers do affect the filter parameter. The filter parameters expressed in (8) are modified to

$$\omega_0\big|_{NI} = \left(\frac{\alpha\beta_3\gamma g_m}{RC_1C_2}\right)^{1/2}, \qquad \left.\frac{\omega_0}{Q_0}\right|_{NI} = \frac{\alpha\beta_2}{RC_1} \quad \text{and}$$

$$Q_0\big|_{NI} = \left(\frac{\beta_3\gamma g_m RC_1}{\alpha\beta_2 C_2}\right)^{1/2} \tag{16}$$

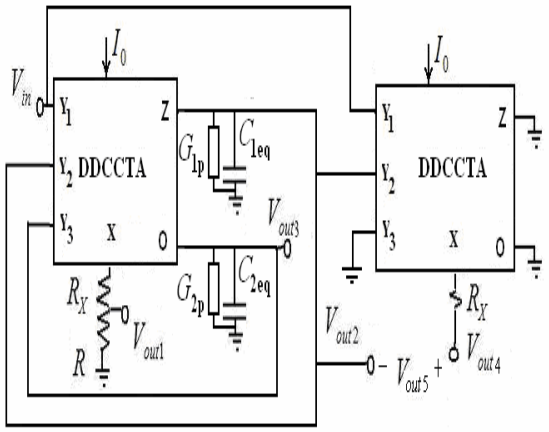

Fig. 4. Proposed voltage mode filter in presence of non-idealities

The current and voltage transfer functions apart from having non-unity values, also have poles at high frequencies. The maximum frequency of operation will be limited by poles of voltage (f_β) and current (f_α, f_γ) transfers which are simulated to be 236 MHz, 223MHz and 201MHz respectively for the implementation of DDCCTA depicted in Fig. 2. Their influence on filter performance can however be ignored if the operating frequencies are chosen sufficiently smaller than voltage and current transfer pole frequencies of the DDCCTA.

The second group of non-idealities comes from parasites of DDCCTA comprising of resistances and capacitances connected in parallel at terminals Y1, Y2, Y3, Z and O (i.e. $R_{Y1}, C_{Y1}, R_{Y2}, C_{Y2}, R_{Y3}, C_{Y3}, R_Z, C_Z, R_O, C_O$) and an intrinsic resistance R_X at terminal X. The effects of these parasites on filter response depend strongly on circuit topology. The proposed filter topology of Fig. 3, in the presence of these parasites, modifies to Fig. 4 where $C_{1eq} = C_1 // 2C_{Y2} // C_Z$, $C_{2eq} = C_2 // C_{Y3} // C_O$, $G_{1p} = 1/(R_Z // (R_{Y2}/2))$ and $G_{2p} = 1/(R_{Y3} // R_O)$. The intrinsic resistance (R_x) and parasitic capacitances can be accommodated respectively in external resistance R and capacitances C_1 and C_2. The effect of parasitic resistances can also be ignored if $sC_1 << G_{1p}$ and $sC_2 << G_{2p}$.

IV. SIMULATION RESULTS

To verify the theoretical propositions, the proposed filter is simulated with SPICE simulations using CMOS schematic of DDCCTA as given in Fig. 2. The TSMC 0.25μm CMOS process model parameters and supply voltages of $V_{DD} = -V_{SS} = 1.25V$ and $V_{BB} = -0.8V$ are used. The aspect ratio of various transistors is given in Table 1. The filter is designed for a pole frequency of $f_0 = 3.16$ MHz, $Q_0 = 1$, the component values are found to be $C_1 = C_2 = 50$ pF, R = 1 kΩ and bias current of DDCCTA equals to 100 μA. Figure 5(a) shows the simulation results for high pass (V_{out1}) and low pass (V_{out3}) filter responses. Figure 5(b) shows the simulation results for band pass (V_{out2}) and notch (V_{out4}) filter responses. The magnitude and phase responses for all pass filter are shown in Fig. 5(c).

To study the time domain behaviour of the proposed filter, an input sinusoidal signal of 3.16 MHz frequency and amplitude 100 mV is applied. The transient response for high pass output (V_{out1}) is shown in Fig. 6. Another simulation is performed by applying two sinusoidal signals of frequencies of 3.16 MHz and 30 MHz having an amplitude of 50mV each; and. The transient response at V_{out3} with its spectrum for input and output is shown in Fig. 7, which clearly shows that the 30 MHz signal is significantly attenuated. Large signal behavior of the proposed circuit is investigated by observing the dependence of the output total harmonic distortion (%THD) upon the level of input signal. The result as illustrated in Fig. 8.

Table 1. Aspect ratio of various transistors

Transistor	Aspect ratio (W(μm)/L(μm))
M1 – M4	10/0.5
M5 ,M6	5/0.5
M7,M8	27.25/0.5
M9,M11,M13	8.5/0.5
M10,M12,M14	44/0.5
M13,M14,M15,M16,M19-M20	5/0.5
M17,M18	27/0.5

V. CONCLUSION

A novel single input five output universal voltage mode filter has been presented that uses two DDCCTAs, two grounded capacitors and a grounded resistor. The proposed filter has high input impedance which is suitable from cascading viewpoint. It can simultaneously realize low pass, band pass, notch, high pass and all pass responses. The filter parameters can be adjusted electronically. All the passive elements are grounded which is preferred for IC implementation. The simulation results verify the theory.

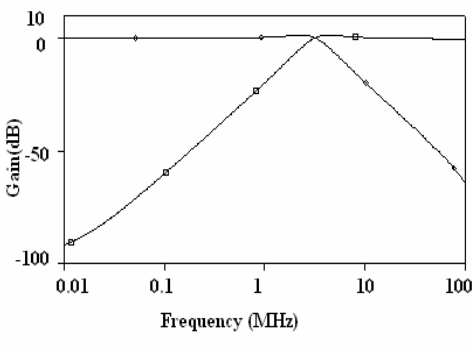

(a)

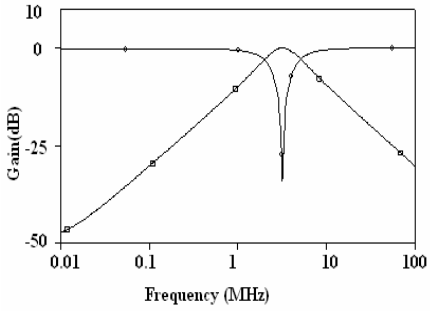

(b)

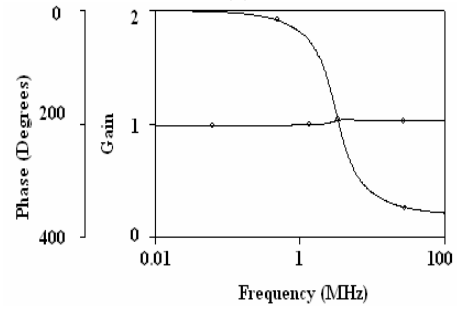

(c)

Fig. 5 Simulated responses of the proposed filter: (a) Low pass and High pass, (b) Band pass and Notch, (c) All pass

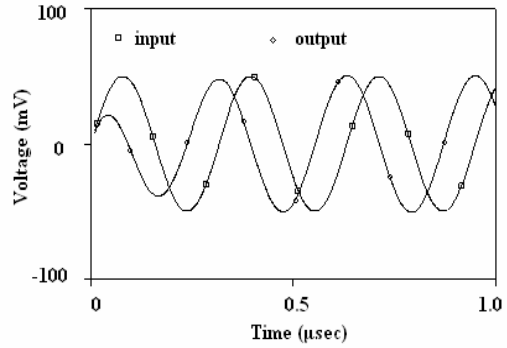

Fig. 6 Transient response for high pass output

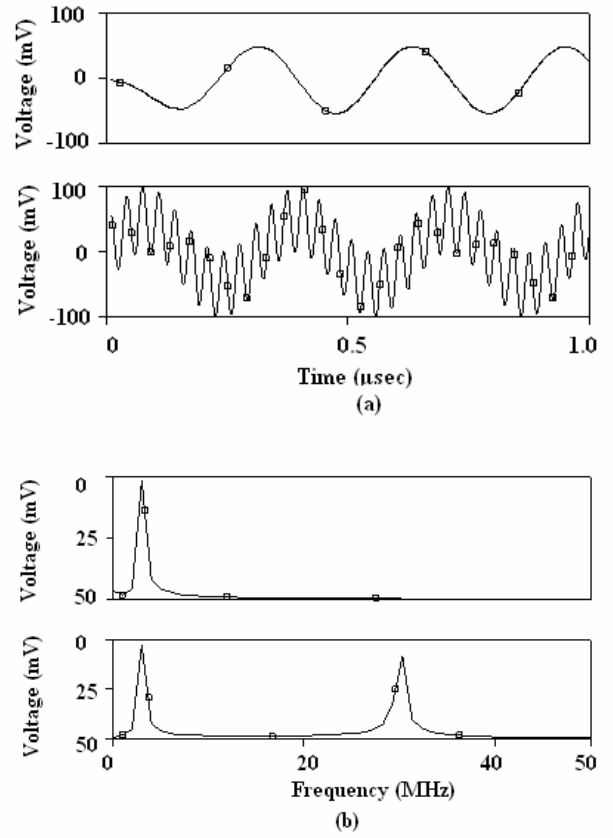

Fig. 7. Transient response (a) output and input signals (b) their spectrum

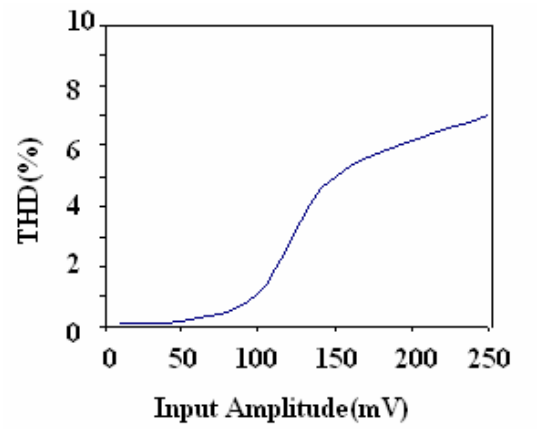

Fig. 8 Variation of % THD with input signal amplitude

REFERENCES

[1] Ferri G., & Guerrini N. C., Low-voltage low-power CMOS current conveyors. Kluwer Academic Publishers, 2000.

[2] R. L. Geiger, E. Sanchez-Sinencio, Active filter design using operational transconductance amplifiers: A tutorial, IEEE Circuits and Devices Magazine, 1, pp. 20 – 23, 1985.

[3] A. S. Sedra, K. C. Smith, A second generation current conveyor its application, IEEE Transactions on Circuit Theory, 17, pp. 132-134, 1970.

[4] A. Fabre, O. Saaid , F. Wiest, C. Boucheron, High frequency applications based on a new current controlled conveyor, IEEE Transactions on Circuit and Systems I, 43, pp. 82-91, 1996.

[5] I. A. Awad, A. M. Soliman, Inverting second generation current conveyors: the missing building blocks, CMOS realizations and applications, International Journal of Electronics, 86, pp. 413-432, 1999.

[6] H. O. Elwan, A. M. Soliman, Novel CMOS differential voltage current conveyor and its applications, IEE Proceedings - Circuits Devices Systems, 144, pp. 195-200, 1997.

[7] W. Chiu, S. I. Liu, H. W. Tsao, J. J. Chen, CMOS differential difference current conveyor and their applications, IEE Proceedings - Circuits Devices Systems, 143, pp. 91 – 96, 1996.

[8] D. Biolek, CDTA—building block for current-mode analog signal processing, Proceedings of the European conference on circuit theory and design (ECCTD 2003), pp. 397–400.

[9] J. W. Horng, W. Y. Chiu, H.Y. Wei, Voltage-mode highpass, bandpass and lowpass filters using two DDCCs, International Journal of Electronics, 91, pp. 461-464, 2004.

[10] R. Prokop, V. Musil, CCTA-a new modern circuit block and its internal realization, Proceedings of International Conference on Electronic devices and systems (IMAPSCZ 2005), pp. 89–93.

[11] W. Jaikla, P. Silapan, C. Chanapromma, M. Siripruchyanun, Practical Implementation of CCTA Based on Commercial CCII and OTA, Proceedings of International Symposium on Intelligent Signal Processing and Communication Systems (ISPACS2008).

[12] M. Siripruchyanun, W. Jaikla, Current controlled current conveyor transconductance amplifier (CCCCTA): a building block for analog signal processing, Electrical Engineering, 90, pp. 443–453, 2008.

[13] A. Jantakun, N. Pisutthipong, M. Siripruchyanun, A Synthesis of Temperature Insensitive/Electronically Controllable floating simulators based on DV-CCTAs, Proceedings of 6th International Conference on electrical engineering/ electronics, computer, telecommunications, and information technology (ECTI-CON 2009), pp. 560–563.

[14] W. Jaikla, M. Siripruchyanun, A. Lahiri, Resistorless dual-mode quadrature sinusoidal oscillator using a single

active building block, Microelectronics Journal, 42, pp. 135–140, 2011.
[15] N. Pandey, S. K. Paul, Differential Difference Current Conveyor Transconductance Amplifier: A New Analog Building Block for Signal Processing, Journal of Electrical and Computer Engineering, doi:10.1155/2011/361384, 2011.
[16] W. Tangsrirat, O. Channumsin, High-Input Impedance Voltage-Mode Multifunction Filter Using a Single DDCCTA and Grounded Passive Elements Radioengineeing vol. 20, pp. 905-910, 2011.
[17] N. Pandey, P. Kumar, Realization of Resistorless Wave Active Filter using Differential Voltage Current Controlled Conveyor Transconductance Amplifier Radioengineeing,20, pp. 911-916, 2011.
[18] N. Pandey, S. K. Paul, VM and CM Universal Filters Based on Single DVCCTA Active and Passive Electronic Components, doi:10.1155/2011/929507, 2011
[19] A. Lahiri , W. Jaikla, M. Siripruchyanun, Voltage-mode quadrature sinusoidal oscillator with current tunable properties (DVCCTA), Analog Integrated Circuit Signal Processing, 65, pp. 321–325, 2010.
[20] J. W. Horng, C. L. Hou, C. M. Chang, W. Y. Chung, H. Y. Wei, Voltage-mode universal biquadratic filters with one input and five outputs using MOCCIIs, Computers and Electrical Engineering, 31, pp. 190–202, 2005.
[21] J. W. Horng, C. L. Hou, C. M. Chang, W. Y. Chung, Voltage-Mode Universal Biquadratic Filters with One Input and Five Outputs, Analog Integrated Circuits and Signal Processing, 47, pp. 73—83, 2006.
[22] J. W.Horng, H. P. Chou, C. L. Hou, C. M. Chang, and C. T. Lin, High input impedance voltage-mode universal biquadratic filter with one input and five outputs using current conveyors, Circuits Systems Signal Processing, 25, pp. 767-777, 2006.
[23] H. P. Chen, S. S. Shen, A versatile universal capacitor-grounded voltage mode filter using DVCCs, ETRI Journal, 29, pp. 470 – 476, 2007.
[24] S. Minaei, E. Yuce, All-Grounded Passive Elements Voltage-Mode DVCC-Based Universal Filters Circuits Systems Signal Processing, 29, pp. 295-309, 2010.
[25] H. P. Chen, Universal voltage-mode filter using only plus-type DDCCs, Analog Integrated Circuits and Signal Processing. 50, pp. 137-139, 2007
[26] W. Y. Chiu, J. W. Horng, S. T. Cheng, Universal filter with one input and five outputs with DDCCs, Inernational Symposium On Intelligent signal processing and communication (ISPACS2008) Bankok Thailand 2008.
[27] H. P.Chen, Versatile universal voltage-mode filter employing DDCCs International Journal Electronics Communication (AEÜ), 63, pp. 78 – 82, 2009.
[28] J. W. Horng, Lossless inductance simulation and voltage-mode universal biquadratic filter with one input and five outputs using DVCCs, Analog Integrated Circuits and Signal Processing, 62, pp. 407–413, 2010.
[29] H. P. Chen, Voltage-mode FDCCII-based universal filters, International Journal Electronics Communication (AEÜ), 62, pp. 320 – 323 2008.
[30] H. P. Chen, High-Input Impedance Voltage-Mode Multifunction Filter with Four Grounded Components and Only Two Plus-Type DDCCs, Active and Passive Electronic Components, doi:10.1155/2010/362516, 2010.
[31] S. I. Liu, High input impedance filter with low component spread using current feedback amplifiers, Electronics Letters, 31, pp. 1042–1043, 1995.

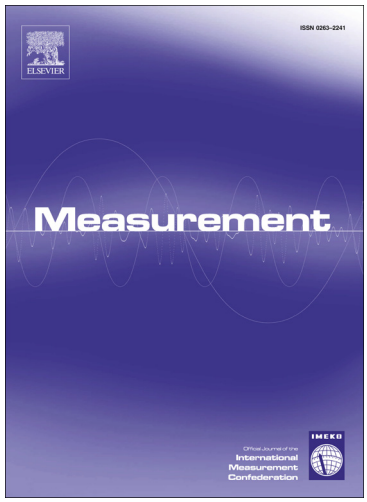

Reaffirmation of Measurement Uncertainty in Pressure Sensitivity Determination of Ls2p Microphones by Reciprocity Method

N. Garg, Anil Kumar, Arif Sanjid M, K.P. Chaudhary, S. Maji

PII: S0263-2241(14)00052-9
DOI: http://dx.doi.org/10.1016/j.measurement.2014.02.002
Reference: MEASUR 2728

To appear in: *Measurement*

Received Date: 26 March 2013
Revised Date: 25 December 2013
Accepted Date: 4 February 2014

Please cite this article as: N. Garg, A. Kumar, A. Sanjid M, K.P. Chaudhary, S. Maji, Reaffirmation of Measurement Uncertainty in Pressure Sensitivity Determination of Ls2p Microphones by Reciprocity Method, *Measurement* (2014), doi: http://dx.doi.org/10.1016/j.measurement.2014.02.002

REAFFIRMATION OF MEASUREMENT UNCERTAINTY IN PRESSURE SENSITIVITY DETERMINATION OF LS2P MICROPHONES BY RECIPROCITY METHOD

N Garg[1,2)], Anil Kumar[1)], Arif Sanjid M[1)], K P Chaudhary[1)] & S. Maji[2)]

1) Apex Level Standards and Industrial Metrology Division, CSIR-National Physical Laboratory, New Delhi-110 012, India
(E-mail: ngarg@mail.nplindia.ernet.in)
2) Deptt of Mechanical, Production & Industrial Engg., Delhi Technological University, Delhi- 110 042,India.

Abstract

The paper presents the accuracy and precision associated with realization of primary standard of sound using the reciprocity method. An experimental determination of the front cavity volume on Universal Measuring Machine has lead to reaffirmation of measurement uncertainty in pressure sensitivity determination to 0.04 to 0.15 dB in frequency range 31.5 Hz to 25 kHz. The reduced measurement uncertainty has also been validated from the results of the recent APMP Key comparison and also by comparison to the manufacturer's value for LS2P microphones. The use of optical method for measuring the front cavity volume has refined the measurement methodology followed with adaptation of a self reliant, traceable and systematic measurement procedure in comparison to the earlier use of nominal values for sensitivity fitting exercise conducted on *MP.EXE* program. Consequently, the measurement uncertainty associated with the calibration of working standard microphones, multifunction acoustic calibrator and A-weighted sound pressure level measurements is also reduced.

Keywords: Reciprocity method, Front cavity depth, Front cavity volume, LS2P microphones, *MP.EXE* program, sensitivity fitting exercise.

1. Introduction

The primary standard of sound pressure is the utmost and precise standard with highest levels of stability, accuracy and precision and is maintained through primary calibration of laboratory standard microphones (LS1P and LS2P) in a closed coupler cavity by reciprocity technique in the frequency range of 31.5 Hz to 25 kHz with an expanded uncertainty of 0.05 dB to 0.17 dB (k=2 and 95 % confidence level) [1,2]. The designation LS2P refers to a laboratory standard microphone of mechanical configuration 2 having nearly constant presssure sensitivity as a function of frequency [3]. The reference standard LS2P microphones used at NPL, India is Brüel & Kjær (B&K) type 4180. The Reciprocity calibration apparatus of NPLI is Brüel & Kjær (B&K) type 9699 system. During reciprocity calibration, the microphones are acoustically coupled in pairs by the air enclosed in the cavity of precisely determined mechanical dimensions. For each pair, one microphone is used as sound source (transmitter) and other as receiver. The electrical transfer impedance i.e the ratio of open circuit voltage of receiver microphone to the input current of transmitter microphone for each of three different microphone pairs is thus measured. The system determines the transmitter current by measuring the voltage across a calibrated capacitance, which is connected in series with the transmitter microphone. After determining the acoustic coupling conditions and measurement of three voltage ratios, the sensitivity of each microphone can be calculated as per IEC 61094-2 [4] solving three equations with three sensitivities as unknown parameters. The methodology of realizing sound pressure by primary standard is almost the same by all National Metrology Institutes (NMIs) whereby the difference lies in the signal processing part and in the sensitivity fitting exercise performed in primary microphone calibrations [5].

The pressure sensitivity measurement of microphones is influenced by various factors affecting the electrical and acoustic transfer impedance contributing to the expanded measurement uncertainty. The major components of uncertainty comprises of the electrical transfer impedance which depends on the uncertainty in measurement of voltage and capacitance; acoustic transfer impedance that depends on the uncertainty of dimensions, measurement of voltage ratio, environmental conditions, polarization voltage, heat conduction and wave motion corrections. Precise measurement of the equivalent volume of the cavity including the equivalent volume of the microphone is pivotal factor in reciprocity method. NPLI had been using the nominal values specified by B&K since last few years for the sensitivity fitting exercise for two standard plane wave couplers in *MP.EXE* software untill the sensitivity deviations i.e difference in the sensitivity of microphone under test calculated for two couplers in range 200 Hz to 2 kHz is less than 0.01 dB.

Fig. 1. Deviation in Sensitivity (in dB) from mean value of all participants in APMP.AUV.A-K3 comparison with the expanded uncertainty (dark lines) as the limits in sensitivity deviation.

The experience gained in the recent key comparsion exercises viz., Bilateral comparison of NPLI with Danish Primary Laboratory in Acoustics (DPLA), APMP.AUV.A-K1 and APMP.AUV.A-K3 comparison (fig 1) have not only inculcated a confidence in the system procedure and methodology realized, but also provided a scope for further improvement for achieving the highest levels of accuracy and precision at par with other NMIs [6-8]. The Key comparison results of sensitivity deviation (in dB re 1 V/Pa) are within ± 0.03 dB in range 200 Hz to 20 kHz in comparison to the pilot laboratory, while the highest deviation of 0.11 dB is observed at 25 kHz [8]. NPLI Calibration and Measurement Capabilities (CMCs) for sound have already been appended in Key comparison data base (KCDB) since year 2009 and the recent Key comparison APMP.AUV.A-S1 [9] for multifunction acoustic calibrator (B&K 4226) initiated in 2009 with NIMT, Thailand as pilot laboratory and 13 participating laboratories has validated NPLI CMCs for sound pressure level determination of multi-frequency acoustic calibrators. Thus, it is imperative to continuously upgrade the primary standard for achieving highest levels of accuracy and precision and establish a strong traceability chain through out the country. The paper demonstrates the use of optical method for determination of front cavity depth of microphone and focuses on reaffirmation of measurement uncertainty associated with LS2P microphone calibrations by reciprocity method.

2. Experimental analysis

The open circuit sensitivity is determined by means of reciprocity method. The microphone under test is subsequently acoustically coupled in pairs with two microphones in a closed coupler. The sensitivity of the microphone is obtained from measurements of the electrical transfer impedance between the pair of microphones and acoustical transfer impedance between the microphones in compliance with IEC 61094-2. The electrical transfer impedance is measured using the main unit of B&K reciprocity set up 5998, sine generator type, B&K 1051, a band pass filter, type B&K 1617 and a digital voltmeter, Datron 1281 [10]. The polarising voltage applied to the microphones is (200 ± 0.01) V. All measurements are conducted in a temperature controlled laboratory at (23 ± 2)º C and relative humidity within the range (50 ± 10) %. While conducting the reciprocity measurements, for the standard deviation of measurements at a particular frequency, it is ensured that standard

deviation of measurements *STDEV* < 400 ppm and *S/N* ratio is greater than 46 dB [10]. Each single calibration run comprehended three cycles of measurements for three microphones pairs for a single coupler. A total of five calibration runs are conducted wherein each single run comprehended three cycles of measurements for three microphone pairs. Two plane wave couplers are used in each measurement for LS2P microphones. The long coupler and short coupler used in case of LS2P microphones have nominal length 4.7 mm and 9.4 mm and each has diameter of 9.3 mm. It may be noted that short coupler measurements cater to frequency range 31.5 Hz to 2 kHz, while that in case of long coupler, the measurement range extends from 31.5 Hz to 25 kHz. The measurement data is analysed using computer software *MP.EXE* developed by Brüel & Kjær (B&K), Denmark.

3. Dimensional Measurements

The front cavity volume (V_f) is equal to $\pi/4\ d^2 L_f$; where d and L_f are microphone diameter and front cavity depth respectively. The front cavity volume is also measured as the product of cross sectional area of coupler and cavity depth, wherein the nominal diameter of coupler is 9.3 mm for 4.7 mm (B&K Model UA1430) and 9.4 mm (B&K Model UA1414) long couplers. The diameter and front cavity depth are measured on Universal Measuring Machine (Model: UMM-219, Make: SIP, Switzerland). UMM is a fundamental displacement measuring machine equipped with reference standard scale attached to its movable bed. It is fitted with an optical depth focusing microscope and displacement measuring laser interferometer (Model: HP 5529, Make: Agilent, USA). Optical microscope is mounted on a vertical translation stage of UMM. The resolution of the optical microscope is 0.5 µm. The heterodyne laser interferometer is also fixed on the same vertical translation stage of UMM to measure the cavity depth. The microscope locates the graduation marks of the reference scale and matches with vernier scale. The displacement of the movable bed of UMM can be read in unison by reading microscope of UMM and in computer screen of Laser interferometer. Fig 2 shows the experimental setup for dimensional measurements of microphone. The uncertainty of measurement of laser interferometer is ± 0.1 µm (k=2). The expanded uncertainty (k=2) in length (L in metres) measurement using laser interferometer and UMM has been calculated as $\sqrt{\left(144.34^2 + 2031.38^2 L^2\right)} \times 10^{-9}$ m [11] and corresponding Calibration and Measurement Capability (*CMC*) has been enlisted in KCDB website.

3.1 Cavity depth measurement

The reference standard microphone cavity is fixed under the optical depth focusing microscope. The measurement of cavity depth is as follows:

- The microscope is focussed on to the surface of annulus of reference standard microphone by observing its image in the eyepiece. Then the laser interferometer reading is preset to zero.
- The reference standard microphone is transversely moved to locate the diaphragm surface of reference standard microphone cavity under the optical depth focusing microscope.
- The vertical stage of UMM is moved downwards till a best focussed image of diaphragm surface in the eyepiece is sought.
- The vertical displacement (Z-axis) will be measured by the laser interferometer. This reading gives the cavity depth of reference standard microphone.

Fig. 2. Pictorial view of Universal Measuring Machine for measuring diameter of coupler (LHS) and the front cavity depth (RHS).

3.2 Diameter measurement

The laser interferometer is realigned in X-Axis for inner diameter measurement. The reference standard microphone cavity is fixed under the optical depth focusing microscope. The inner diameter of the microphone is measured as follows:

- The microscope is focussed on to the edge of annulus of reference standard microphone by observing its image in the eyepiece. Then the laser interferometer reading is preset to zero.
- The reference standard microphone is transversely moved to locate the other edge of annulus of reference standard microphone under the optical depth focusing microscope.
- The X translation stage displacement will be measured by the laser interferometer. This reading gives the diameter of the cavity reference standard microphone.

These measurements are repeated several times to ensure their precision and also to determine the random uncertainty. The microphone is rotated by 90° about the optical axis of depth focusing microscope to acquire diametric measurements in orthogonal direction of microphone. The front cavity depth of the one such test microphone (B&K 4180, S. No. 2702577) is measured as 0.5039 mm and diameter as 9.3070 mm and thus the front cavity volume is calculated as 34.26 mm^3. The expanded measurement uncertainty of cavity depth is calculated as shown in table 1.

Table 1. Expanded uncertainty in microphone cavity depth measurements

The expanded uncertainty in diameter measurement is calculated as 1.8 µm by taking into account all the sources of uncertainty discussed in table 1 and additional uncertainty of 1 µm normally distributed attributed to taper, roughness and sealing ring. The measurement uncertainty of front cavity volume is calculated to be 0.103 mm^3 (k=2) by substituting the values of measurement uncertainty of cavity depth and measurement uncertainty of diameter in equation $u_v^2 = \left(\frac{\pi}{2} d L_f\right)^2 u_d^2 + \left(\frac{\pi}{4} d^2\right)^2 u_{Lf}^2$ wherein u_d is uncertainty in diametric measurements, u_{Lf} is uncertainty in cavity depth measurements and u_v is uncertainty is front cavity volume measurements.

4. Sensitivity fitting exercise

The nominal values of parameters such as equivalent volume, loss factor, resonance frequency, static pressure and temperature coefficient are used. The measured front cavity volume is taken as the starting value, which is then iteratively fitted in fine increment of 0.05 mm^3 for achieving the sensitivity deviations of an order of 0.005 dB for the long and short couplers. The other microphone parameters viz., equivalent volume, resonance frequency, loss factor values in conjunction with front cavity volume are also iteratively adjusted starting from their nominal values and calculation of its sensitivity level is repeated for both long and short couplers until agreement in these calculated levels over the frequency range 200 Hz to 2

kHz in the two couplers is acceptably close (typically about 0.005 dB or better). The fine adjustment fitting in front cavity volume in this exercise is done to account for the excess volume of cavity which is difference between actual volume and volume calculated from cross sectional area of coupler and cavity depth. The sensitivity fitting exercise is varied in various National Metrology Institutes [5]. NPLI participation in International Key comparison APMP.AUV.A-K3 with use of nominal values of microphone parameters has revealed a maximum difference of 1 mm^3 in front cavity volume, 0.042 mm in cavity depth, 0.86 mm^3 in equivalent volume, 0.4 kHz in resonance frequency measurements for LS2P microphones [8]. However, with the dimensional characterization of front cavity depth, it is envisaged that measurement uncertainty in reporting the microphone parameters shall be reduced that will in-turn reduce the uncertainty in sensitivity determination especially at high frequencies [12]. The absolute difference in sensitivity determined by two couplers is much smaller than expanded uncertainty in frequency range 31.5 Hz to 2 kHz and as such the values of microphone front cavity are adequately determined by iterative fitting procedure [13].

5. Reaffirmed Measurement Uncertainty

The greatest contribution to the standard uncertainty at low frequency is uncertainty in equivalent diaphragm volume, which reduces as frequency increases [14]. As frequency approaches the resonance frequency of the diaphragm, the greatest contribution arises from unpredictability of radial wave motion and of viscous losses in the coupler. The wave motion correction significant at higher frequency and heat conduction correction pronounced at low frequencies are incorporated as parameter $Cor_{HW,xy}$ which is dependent upon the length of cavity and speed of sound in cavity [10,13]. The heat conduction corrections is dependent on the length to diameter ratio of coupler, volume to surface ratio of coupler, thermal diffusivity of enclosed air and ratio of specific heat of air. The expanded uncertainty for heat conduction correction is taken as 0.011 dB, while that for radial wave motion is 0.023 dB at 25 kHz. Variation of environmental conditions from reference value (23ºC, 101.325 kPa, 50 % R.H) also influences the sensitivity determination. The maximal deviation between calculated sensitivity level and corresponding sensitivity level measured in environmental chamber is 0.0144 dB over the pressure range 94 kPa to 106 kPa from B&K 4180 microphones [15]. The uncertainty in temperature and pressure coefficient is caused by uncertainty due to resonance frequency and uncertainty of temperature or pressure coefficient at 250 Hz. The uncertainty of temperature coefficient at 250 Hz is reported to be 0.0015 dB/K and uncertainty of pressure coefficient at 250 Hz was 0.0002 dB/kPa for B&K 4180 microphones [16,17]. The expanded uncertainty of 0.2ºC in temperature measurement, 0.4 % RH in relative humidity measurement and 0.06 kPa in pressure measurement in conjunction with uncertainty in sensitivity coefficients (dB/K; dB/10%RH; dB/kPa) measured at different frequencies induces the maximum uncertainty in sensitivity determination by 0.008 dB for temperature, 0.005 dB for humidity and 0.008 dB for pressure at 25 kHz. The contribution of relative humidity has not much effect as a variation of 20 % RH affects the sensitivity maximum by 0.02 dB at 25 kHz [10]. The digital multimeter used is traceable to the national voltage standards and an uncertainty of 0.0055 mV has been stated at 250 Hz for range 10 to 100 mV. Systematic error of voltage ratio measurements using an electrical reference standard have been measured to be less than 0.005 dB upto 12.5 kHz, after which it increases to a maximum value of 0.015 dB [18]. The voltage ratio is dependent on output and reference voltage of receiver and transmitter channel and has been accounted to be 0.025 dB at 25 kHz in table 2. The capacitor is a part of ZE0796 transmitter unit (S. No. 2209196) having nominal value of 4.737 pF at 1 kHz with an associated uncertainty of 0.0001 nF. For a signal to noise ratio > 46 dB, the effect on sensitivity is reckoned to be < 0.0001 dB [5].

The relative uncertainty [4] on non-zero frequency speed of sound is 3×10^{-4}, density of humid air as 22×10^{-6}, ratio of specific heats as 3.2×10^{-4}.

Table 2. Uncertainty calculation (All values in dB) for determination of sensitivity (dB re 1V/Pa) of LS2P microphones

The type-A uncertainty associated with five measurements runs is less than 0.05 dB in measurement frequency range of 31.5 Hz to 25 kHz. The effect of viscous losses arising from inner thread in front cavity, surface roughness, excess volume of front cavity and deviations from theoretical calculation of acoustic transfer impedance especially at high frequencies have been substituted in uncertainty contribution due to equivalent and front cavity volume in table 2. The accuracy and precision in determination of microphone parameters is crucial for the determination of the microphone sensitivity (dB re 1V/Pa). The uncertainty associated with the determination of microphone parameters viz., equivalent diaphragm volume, resonance frequency, loss factor etc have been taken slightly on higher side as the exact sensitivity coefficient is very difficult to analyze. The maximum influence of 0.1 mm difference from nominal value in cavity depth is at high frequency starting from 0.02 dB at 16 kHz, 0.03 dB at 20 kHz and 0.07 dB at 25 kHz [10]. With the dimensional characterization of cavity depth, a conservative estimate of uncertainty of 0.02 dB is taken at 25 kHz. The equivalent diaphragm volume is difficult to be determined by any means other than iterative process followed in sensitivity fitting exercise. The nominal value of 9.2 mm^3 is used as starting value and uncertainty of 1 mm^3 is stated to account for the variations due to various dimensional and type specific features of B&K 4180 microphones and adjustment followed in sensitivity fitting exercise. The uncertainty in measurement of front cavity depth is shown in section 3 to be 1.5 µm for a nominal value of 0.5 mm for LS2P microphones. It may be note here that the excess volume of the cavity, which is difference between the actual front volume and volume calculated from cross sectional area of coupler and front cavity depth is also an additional terminating impedance when calculating the acoustic impedance as referred in IEC 61094-2. Fig 3 shows the expanded uncertainty (k=2) in sensitivity determination (in dB re 1V/Pa) for B&K 4180 reference standard microphones measured by reciprocity set up.

Fig. 3. Expanded uncertainty (k=2) in sensitivity determination (in dB re 1V/Pa) for B&K 4180 reference standard microphones measured by reciprocity set up.

Thus, an uncertainty of 0.5 mm^3 is stated for the front cavity volume to account for the excess volume and fine adjustments pursued in sensitivity fitting exercise for matching the sensitivities in both couplers. The heat conduction in cavity behind the diaphragm at very low frequencies results in increase in equivalent volume and errors in calculation of acoustic impedance of microphone influence the accuracy particularly at high frequencies [4], which have been incorporated in table 2. The nominal value of damping factor is 1.05 and it is possible to determine within 0.02 or 2 % consistent with the key comparison results. Loss factor can be determined as ratio of sensitivities at resonance and asymptotic value at low frequencies. For a nominal frequency of 22 kHz, the uncertainty specified is 1.5 kHz [19]. The nominal values and expanded uncertainties for various microphone parameters are shown in table 3. The nominal effective diaphragm diameter of diaphragm is taken as 8.95 mm for calculation of radial modes, while nominal height is taken as 11.9 mm as specified by manufacturer. Fig. 4 shows the sensitivity of B&K 4180 microphone calculated using the sensitivity fitting exercise discussed in section 4. The validation of the stated uncertainties was done in two ways, wherein one of the way followed was the periodic calibration of the

reference standard LS2P microphones for establishment of traceability chain and the deviations in observed sensitivities from the previous values have been observed to be less than 0.1 dB, as shown in fig. 5, which lies within the domains of uncertainties stated for both the microphones. Another validation was done for the recently procured LS2P microphones calibrated by Danish Primary Laboratory in Acoustics (DPLA) and E_n value less than 0.3 was observed for microphone sensitivity at five discrete frequencies (125 Hz to 2 kHz) as the DPLA values were available only for these frequencies.

Table 3. Nominal Values and Expanded Uncertainties (*k*=2) of microphone parameters

The difference in front cavity depth as compared to the manufacturer's value was observed to be 0.4 µm. The front cavity volume was measured to be 34.3 mm^3 in each case with a deviation of 0.1 mm^3 to that value reported by manufacturer for one microphone. All the microphone parameters measured were within the domains of uncertainty stated in table 3, which has validated this methodology and reaffirmed the uncertainties calculated.

Fig. 4. Sensitivity (dB re 1V/Pa) for B&K 4180 (S. No. 1863694) microphone

It may be noted here that recent key comparisons results as shown in fig. 1 also validates these uncertainties as the result are well within the domains of the reaffirmed measurement uncertainties stated for calibration of LS2P microphones. The stability of the condenser microphones is very essential for measurement accuracy of secondary standard. Periodic calibrations of LS2P microphones have revealed the change in sensitivity within ± 0.1 dB in span of past three years. Wong [20] investigations on measurement of microphones open circuit sensitivity levels of three LS1P standard microphones over a period of 31 months reveal the stability of microphone to be approx 0.01 dB for measurements from 125 Hz to 8 kHz. B&K analysis [18] also shows the deviation from a linear regression line is < 0.01 dB (2σ) over a period of 14 years at 250 Hz**.** Reciprocity calibration results (125 Hz and 2 kHz) obtained with a type 4180 microphones reveal the deviations (2σ) from the linear regression lines are < 0.012 dB over a period of 6 years. Changes in the sensitivity of microphone may occur due to change in tension of the diaphragm or due to change is distance between diaphragm and back plate. Artificial ageing at high temperatures after the final tensioning of diaphragm causes the microphone to settle into a state of very high operating stability. Fig. 5 shows the deviation in sensitivity with past three years for B&K 4180/1863694 microphone. The deviation in sensitivity from mean value of sensitivity measured from reciprocity method in three years has been observed to be within ± 0.10 dB, which confirms the stability of these microphones. It can be observed that at 250 Hz, the deviations are less than 0.03 dB. In case of negative deviations from the mean value of sensitivity over the years, the maximum deviation observed is less than 0.08 dB.

Fig. 5. Stability of LS2P microphone (B&K 4180, S. No. 1863694) with the expanded uncertainty as the limits in sensitivity deviation.

6. Implications of reaffirmed measurement uncertainty

The reduced expanded uncertainty calculated for reciprocity calibrations thus affect the measurement uncertainty associated with secondary calibrations also. The expanded uncertainty (k=2) in secondary microphone calibration is reaffirmed to be 0.08 dB to 0.34 dB in frequency range 31.5 Hz to 20 kHz for working standard (WS2P) B&K microphones 4133-34-49.

Fig. 6. Expanded Uncertainty in calibration of reference standard microphones, working standard microphones and multifunction acoustic calibrator.

The expanded uncertainty (k=2) calculated for calibration of WS1P working standard microphones is 0.08 dB to 0.23 dB in frequency range 31.5 Hz to 10 kHz whereby it differs due to uncertainty contribution of reference standard microphones. The detailed uncertainty budget has been discussed in reference [21]. However the static pressure and temperature coefficients, preamplifier characteristics etc. further vary for different working standard microphones influencing the calibration uncertainty, the details of which can be referred from [22,23]. The expanded uncertainty (k=2) in calibration of sound calibrators and multi-frequency acoustic calibrator is reaffirmed to be 0.12 dB to 0.22 dB in frequency range 31.5 Hz to 16 kHz. Fig 6 shows the expanded uncertainty in calibration of reference standard microphones, working standard microphones and multifunction acoustic calibrator. It may be noted here that as the uncertainty contribution due to microphone calibration and calibration of sound calibrators are contributing factors in determination of expanded uncertainty in A-weighted sound pressure level measurements using Sound level Meter as discussed in reference [21], the reaffirmed measurement uncertainty (k=2) is calculated to be 0.40 dB to 0.90 dB in range 31.5 Hz to 10 kHz. Thus, it is envisaged that with the reduction of measurement uncertainty in primary standards, the entire measurement traceability chain from reference standards to field measurements is strengthened [21,24].

7. Conclusions

The paper presents an indigenous approach of dimensional characterization of the reference standard microphones by Universal Measuring Machine at NPL India, due to which the measurement uncertainty attributed to the microphone parameters in closed coupler reciprocity measurements is reduced. The type-A uncertainty has been measured to be less than 0.05 dB in the measurement frequency range 31.5 Hz to 25 kHz for both the microphones. The reaffirmed expanded uncertainty (k=2) is calculated to be 0.04 dB to 0.15 dB. The validation of the reaffirmed uncertainties and microphone parameters was done in comparison to the manufacturer's value for newly procured LS2P microphones that has inculcated a confidence on the measurement approach and methodology followed. The present investigations not only enhance the measurement accuracy and precision associated with reciprocity calibrations at NPLI, but also refine the measurement methodology followed with adaptation of a self reliant, traceable and automated measurement procedure in compliance with the ISO & IEC 17025 standards for realizing the primary standard of sound with measurement uncertainties at par with other NMIs. Consequently, the methodology followed for realizing the primary standard with reduced uncertainties in turn also reduces the measurement uncertainty associated with calibration of working standard microphones, sound calibrators, field sound pressure level measurements. However, efforts are still in progress to

reduce the measurement uncertainties further by better control of the ambient environmental conditions; replacement of the voltmeter, band pass filter and sine generator with a Lab View controlled hardware to achieve higher dynamic range and less distortion and also to realize the low frequency range beyond 31.5 Hz with a definite uncertainty. It is envisaged that these investigations shall further reduce the claimed uncertainties in microphone reciprocity calibrations to a range of 0.03 dB - 0.10 dB at par with other NMIs and also strengthen the entire measurement traceability chain associated with sound parameter throughout the country.

Acknowledgments

Authors are thankful to the Director, National Physical Laboratory, New Delhi and Dr. A. K. Bandyopadhyay, Head, ALSIM for their constant encouragements and for the permission to publish this work. Authors thank retired colleagues Mr. Omkar Sharma and Dr. Ashok Kumar and Head, AUV& EIC, Dr. T. K. Saxena for their valuable guidance and Mr B. K. Sharma and Mr Vijay Kumar of NPLI for their significant help in dimensional measurements. The work was supported by the Networking Project, *NWP-45* for enhancement of Acoustics and Vibration metrology at CSIR-NPL, India.

References

[1] Garg N., Singh M., Sharma O., Mohanan V. Current status of Acoustic measurement standards at National Physical Laboratory of India (NPLI). New Delhi, Part 1: Sound Pressure, J Metrology Soc India, 22 (2007) 77-90.

[2] Garg N. Accuracy and precision realized in microphone reciprocity calibrations at NPL, India, Proceedings 8th International Conference on Advances in Metrology, *Admet* 2013, 21st to 23rd February, PP-37, (2013) 177-178.

[3] IEC 61094-1, IEC standard: Measurement microphones-Part 1- specifications for laboratory standard microphones, International Electrotechnical Commission, Switzerland, 2000.

[4] IEC 61094-2, Measurement microphones-Part 2- Primary method for pressure calibration of laboratory standard microphones by reciprocity technique, International Electrotechnical Commission, Switzerland, 1992.

[5] Rasmussen K, Final report on the key comparison CCAUV.A-K3, May 2006.

[6] Figueroa S. B., Nielsen L., Rasmussen K. Report on the Bilateral comparison between DPLA-DFM and NPLI.

[7] Horiuchi R., Takahashi H., T. Fujimori T., Sato S. Final report on key comparison APMP.AUV.A-K1, Metrologia 44 09001, 2007.

[8] Kwon H. S., Narang P. Report on key comparison APMP.AUV.A-K3, Metrologia 46 09001, 2009.

[9] Plangsangmas V. and Leeudomwong S., Report on regional supplementary comparison, APMP.AUV.A-S1. Draft B, November, 2011

[10] B&K User Manual for Reciprocity Calibration Apparatus Type 9699, 1997.

[11] Sanjid M. A., Nasrin M., Chaudhary K. P., Singhal R. P., Ramification of uncertainty due to limited resolution of universal measuring machine, Indian Journal of Pure and Applied Physics, 43 (2005) 319-328.

[12] Nedzelnitsky V., Wagner R. P., Non-Contact Methods for Measuring Front Cavity Depths of Laboratory Standard Microphones Using a Depth-Measuring Microscope, J. Res. Natl. Inst. Stand. Technol. 113 (2008) 97-119.

[13] Wagner R. P., Nedzelnitsky V., Fick S. E., New Measurement Service for Determining Pressure Sensitivity of Type LS2aP Microphones by the Reciprocity Method, J. Res. Natl. Inst. Stand. Technol. 116 (2011) 761-769.

[14] Hanes P. Monte Carlo simulation for calculation of uncertainty in reciprocity calibration of microphones, Canadian Acoustics, 35 (2007) 154-155.

[15] Li Wu, Wong G. S. K., Hanes P., Ohm W. S., Measurement of sensitivity level pressure correction for LS2P laboratory standard microphones, Metrologia 42 (2005) 45-48.

[16] Horiuchi R., T. Fujimori T., Sato S., Uncertainty analysis for pressure sensitivities of laboratory standard microphones, Acoustical Science & Technology 25 (2004) 354-363.

[17] Rasmussen K. The static pressure and temperature coefficients of laboratory standard microphones, *Metrologia* 36 (1999) 265-273.

[18] Microphone Reciprocity calibration calculation program for Reciprocity Calibration, 1998, http:// *http://www.bksv.com/doc/bv0051.pdf*.

[19] Frederiksen E. DPLA determination of microphone parameters in connection with accreditated client calibrations, WW-6081-11 Type 9699.

[20] Wong G. S. K. and Wu L., Primary microphone calibration system stability (L). J Acoustical Society of America 114 (2003) 577-579.

[21] Garg N., Sharma O., Measurement accuracy of secondary standards of sound pressure in comparison to primary standards, J. Metrology Society of India, 27(2012) 219-229.

[22] B&K. User Manual for Microphone calibration system, Type 9721, 2011.

[23] Properties and Calibration of laboratory Standard microphones, Uncertainty in microphone frequency responses, B&K report, *2001*. *http://bruel.ru/UserFiles/File/Review1_01.pdf*

[24] Garg N., Sharma O., Kumar A. & Schiefer M. I., A novel approach for realization of Primary Vibration Calibration Standard by homodyne laser interferometer in frequency range of 0.1 Hz to 20 kHz, *Measurement* 45 (2012) 1941-1950.

Figures in Paper

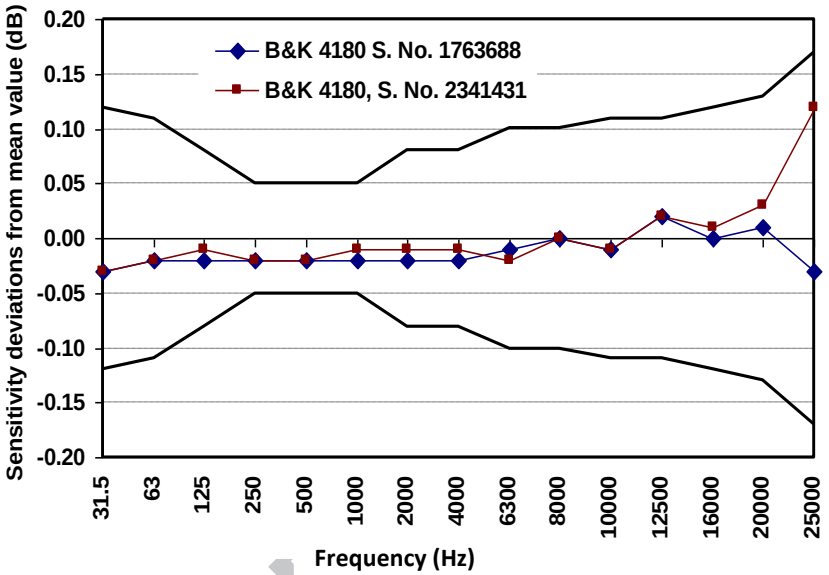

Fig. 1. Deviation in Sensitivity (in dB) from mean value of all participants in APMP.AUV.A-K3 comparison with the expanded uncertainty (dark lines) as the limits in sensitivity deviation.

Fig. 2. Pictorial view of Universal Measuring Machine for measuring diameter of coupler (LHS) and the front cavity depth (RHS).

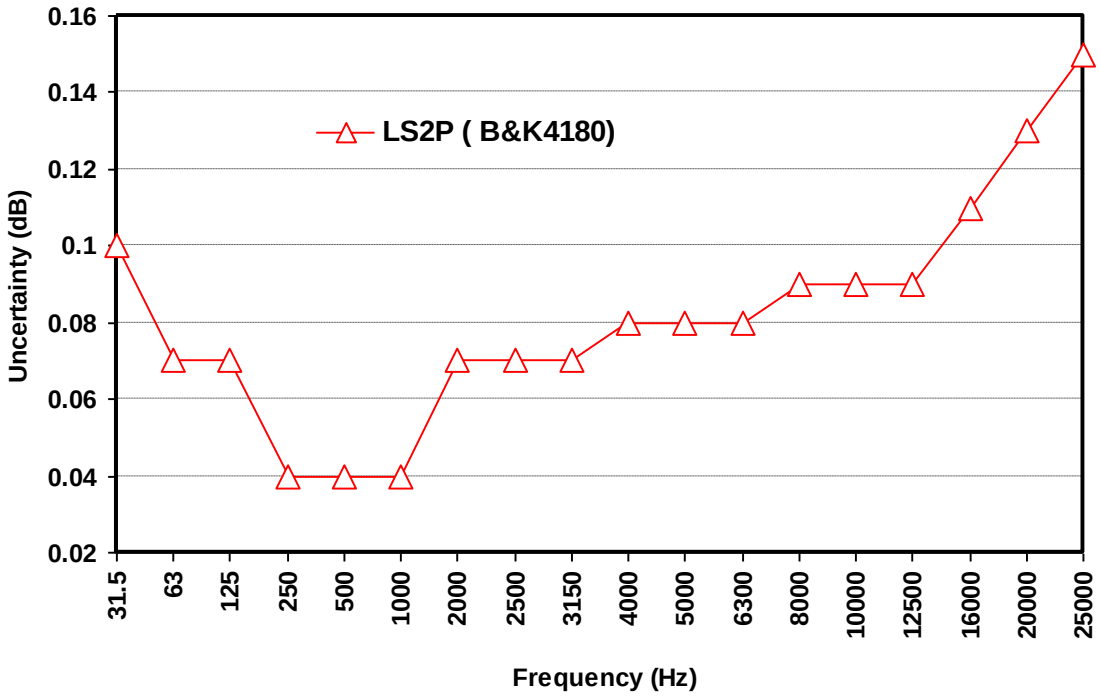

Fig. 3. Expanded uncertainty (*k*=2) in sensitivity determination (in dB re 1V/Pa) for B&K 4180 reference standard microphones measured by reciprocity set up.

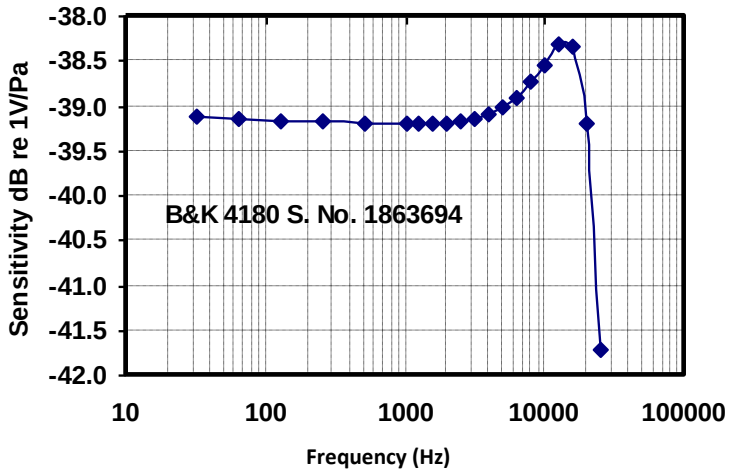

Fig. 4. Sensitivity (dB re 1V/Pa) for B&K 4180 (S. No. 1863694) microphone

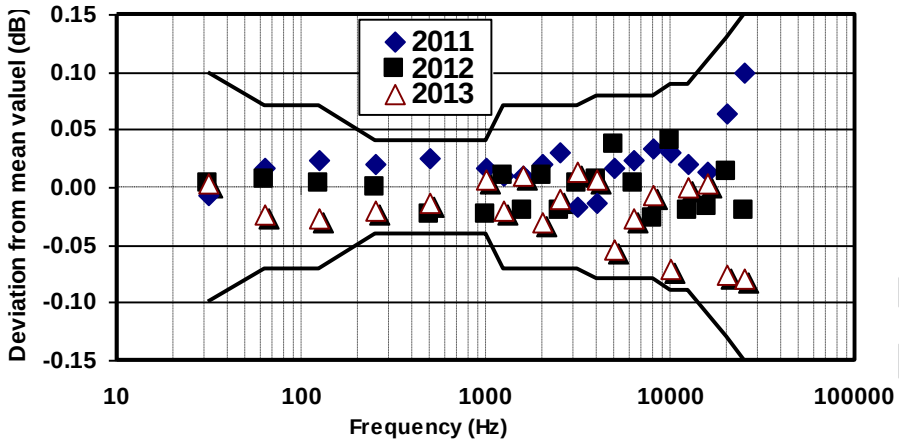

Fig. 5. Stability of LS2P microphone (B&K 4180, S. No. 1863694) with the expanded uncertainty as the limits in sensitivity deviation.

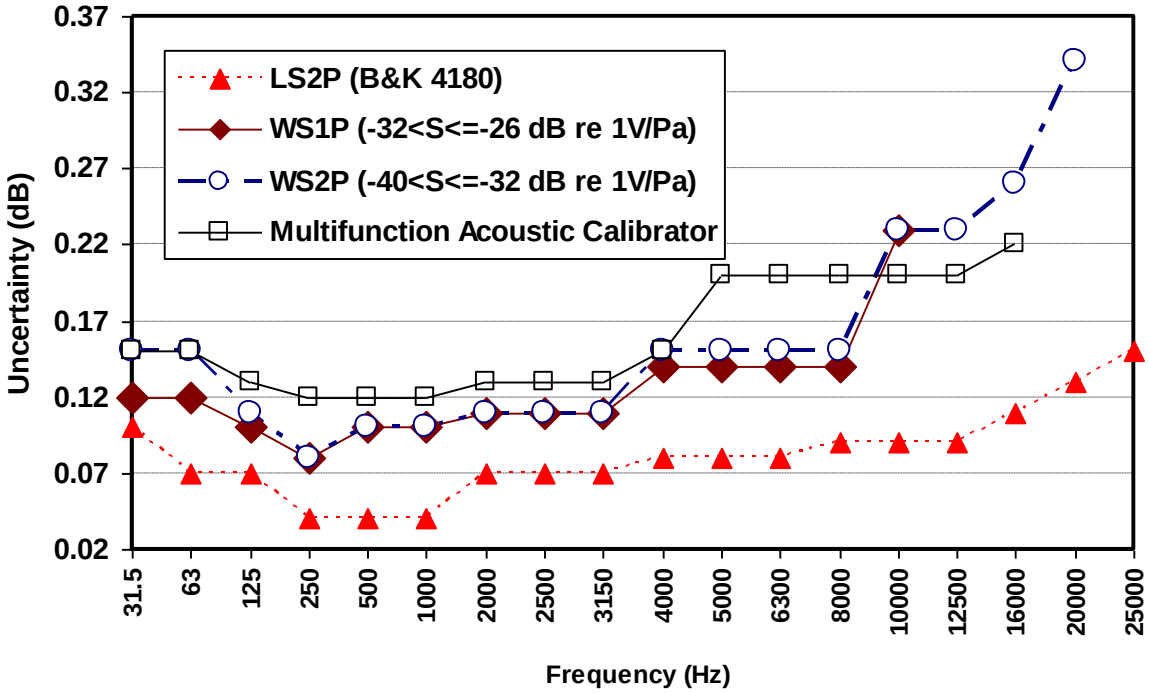

Fig. 6. Expanded Uncertainty in calibration of reference standard microphones, working standard microphones and multifunction acoustic calibrator.

Tables in paper

Table 1. Expanded uncertainty in microphone cavity depth measurements

Source of uncertainty	**Uncertainty contribution (in µm)**
Depth focusing Microscope	0.29
Laser Interferometer	0.05
Alignment Error	0.40
Repeatability	0.54
Combined Uncertainty (k =1)	0.73
Expanded Uncertainty (k=2)	**1.46**

Table 2. Uncertainty calculation (All values in dB) for determination of sensitivity (dB re 1V/Pa) of LS2P microphones.

Uncertainty Component	**Probability Distribution**	**31.5 Hz**	**≥ 250 Hz to < 2 kHz**	**≥2 kHz to <4 kHz & ≥ 63 Hz to <250 Hz**	**≥ 4 kHz to <8 kHz**	**≥ 8 kHz to 12.5 kHz**	**16 kHz**	**20 kHz**	**25 kHz**
Electrical Transfer impedance									
Series impedance	Rectangular	0.015	0.010	0.011	0.011	0.011	0.011	0.011	0.015
Voltage ratio	Normal	0.020	0.011	0.015	0.015	0.015	0.020	0.021	0.025
Cross-talk	Rectangular	0.0035	0.0035	0.0035	0.0035	0.0035	0.0035	0.0035	0.0035
Distortion	Rectangular	0.0011	0.0005	0.0005	0.0005	0.0005	0.0005	0.0005	0.0011
Receiver & transmitter ground shield	Rectangular	0.0005	0.0005	0.0005	0.0005	0.0005	0.0005	0.0005	0.0005
Coupler Properties									
Coupler Volume	Rectangular	0.011	0.008	0.011	0.011	0.011	0.011	0.014	0.017
Leakage	Rectangular	0.0017	0.0011	0.0017	0.0017	0.0017	0.0017	0.0017	0.002
Microphone Parameters									
Equivalent & Front cavity volume	Normal	0.01	0.005	0.01	0.01	0.01	0.02	0.03	0.035
Cavity depth	Rectangular	0.0004	0.0004	0.0004	0.0004	0.0004	0.0007	0.010	0.020
Resonance frequency	Rectangular	0.0003	0.0001	0.0001	0.0001	0.0002	0.0002	0.0003	0.0003
Loss factor	Rectangular	0.0008	0.0002	0.0008	0.0008	0.0008	0.011	0.011	0.011
General Factors									
Heat conduction	Normal	0.011	0.006	0.006	0.002	0.002	0.001	0.001	0.001
Radial wave motion	Normal	0.0000	0.0000	0.0000	0.0020	0.011	0.020	0.020	0.023
Static Pressure	Normal	0.0002	0.0002	0.0002	0.002	0.0002	0.0006	0.001	0.008
Temperature	Normal	0.0015	0.0015	0.0015	0.0015	0.0015	0.002	0.008	0.008
Relative Humidity	Normal	0.0002	0.0002	0.0002	0.002	0.0002	0.0006	0.001	0.008
Rounding error	Rectangular	0.0029	0.0029	0.0029	0.0029	0.0029	0.0029	0.0029	0.0029
Air properties	Rectangular	0.0001	0.0001	0.0002	0.0002	0.0002	0.0003	0.0003	0.0006
Repeatability	Normal	0.031	0.01	0.023	0.034	0.036	0.036	0.041	0.044
Expanded Uncertainty (*k*=2) (dB)		**0.10**	**0.04**	**0.07**	**0.08**	**0.09**	**0.11**	**0.13**	**0.15**

Table 3. Nominal Values and Expanded Uncertainties (*k*=2) of microphone parameters

Microphone Type	**B&K 4180**
Front Cavity Volume (mm^3)	34.0 ± 0.5
Equivalent Volume (mm^3)	9.2 ± 1.0
Diameter of cavity (mm)	9.3000 ± 0.0018
Resonance Frequency (kHz)	22.0 ± 1.5
Front Cavity depth (mm)	0.5030 ± 0.0015
Damping factor	1.05 ± 0.02

Research Highlights:

- National Primary Sound standard is discussed
- Measurement uncertainty in frequency range 31.5 Hz to 25 kHz is reaffirmed.
- Use of optical method for measuring front cavity depth is described

International Journal of Soft Computing and Engineering (IJSCE)
ISSN: 2231-2307, Volume-3, Issue-3, July 2013

Real Time Object Tracking Using Different Mean Shift Techniques–a Review

Snekha, Chetna Sachdeva, Rajesh Birok

Abstract*— The many different mean shift techniques for object tracking in real time are discussed in this paper. The mean shift is a non-parametric feature space analysis technique. It is a method for finding local maxima of a density function from given discrete data samples.There are several approaches that use the mean shift techniques for locating target objects. These techniques are taken from the literature dating back to the earliest methods. It is shown that at least 07 distinct methods have been introduced in the literature, with many variations on implementation. This paper should serve as a convenient reference for future work in real time object tracking.

***Index Terms*— Mean shift, CAMshift, ABCshift, Path assigned mean shift , SOAMST and Fuzzy clustering mean shift**

I. INTRODUCTION

Object tracking refers to method to track an object (or multiple objects) over a sequence of images. Tracking of visual objects can be done either by forward-tracking or by back-tracking. Mean shift analysis is a possible forward-tracking technique because it estimates the positions of the regions in the current frame from the previous frame. Mean-shift tracking is a technique for following an object of interest as it moves through a video sequence. It is a gradient ascent approach that models the image region to be tracked by its color histogram. The mean shift is a non-parametric feature space analysis technique. The mean shift is a method for finding local maxima of a density function from given discrete data samples.It works with a search window that is positioned over a section of the distribution. The mean shift technique is an application independent tool .It is suitable for real data analysis because it does not assume any prior shape (e.g. elliptical) on data clusters. Therefore, there are numerous approaches employing the mean shift algorithm in object tracking. A large number of papers exist on mean shift tracking techniques. This paper provides a single reference of the great majority of papers and techniques presented on mean shift technique. We compiled over 10 years' papers pertaining to different Mean shift methods published up to the date of submission of this manuscript. Papers referencing mean shift methods from previous papers without any modification or improvement have been omitted. It is possible that one or more papers were unintentionally omitted. We apologize if an important method or improvement was left out. This manuscript steps through a wide variety of methods with a brief discussion and categorization of each. We have avoided discussing slight modifications of existing methods as distinct methods.

Manuscript received on July 2013

Snekha, Electronics and Communication Department, Delhi Technological University, New Delhi, India.

Chetna Sachdeva ,Electronics and Communication Department ,Delhi Technological University, New Delhi, India.

Rajesh Birok , Associate professor ,Electronics and Communication Department ,Delhi Technological University, New Delhi, India.

1.1 Related Work

There are numerous methods employing the mean shift algorithm on object tracking. Cominiciu et al [1] proposed tracking of non-rigid objects from a moving camera using Mean Shift method. Further, a general nonparametric technique was proposed for the analysis of a complex multimodal feature space and to delineate arbitrarily shaped clusters in it. The basic computational module of the technique is the mean shift [2]. Histogram-based target representation was improved by spatially masking the object to be tracked (spatially smoothness achieved in similarity function) with an isotropic kernel [3]. Bradski [4] proposed an improved version of Mean Shift, CAMShift (Continously Adaptive Mean Shift) Method. In this method the mean shift algorithm is modified to deal with dynamically changing color probability distributions derived from video frame sequences. Allan et al [5] extended the method of Bradski [4] by a default implementation to allow tracking in an arbitrary number and type of feature spaces. Stolkin et al [6] described a new color based tracking algorithm, ABCshift (the Adaptive Background CAMSHIFT) tracker. Pooransingh et al [7] proposed a new method for color image segmentation derived from the mean shift theorem. When applied to color image segmentation tasks, the path assigned mean shift algorithm performed faster than existing fast mean shift methods. Ming-Yi Ju [8] proposed a fuzzy color histogram generated by a self-constructing fuzzy cluster to reduce the interference from lighting changes for the mean shift tracking algorithm. The number of color bins generated by the
proposed fuzzy cluster varies according to the target image. J. Ning [9] proposed scale and orientation adaptive mean shift tracking (SOAMST) algorithm to enable estimation of the scale and orientation changes of the target under the mean shift tracking framework.

Previous surveys and the number of conferences, and research papers on object tracking show that it is a highly researched area. Fig. 1 shows the frequency of publications in the area of object tracking published between 2002 and 2011.

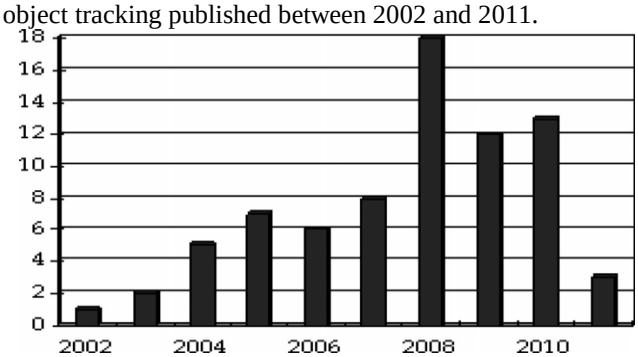

Figure 1: Frequency of publications in the area of object tracking between 2002 and 2011 as reviewed in this review. Note the rising trend in research interest in the area

The rest of the paper is organized as follows: Section 2 describes various approaches of mean shift for object tracking. In Section 3 the results and discussion finally, conclusions are summarized.

II. VARIOUS MEAN SHIFT TECHNIQUES

2.1 CAMshift [4-5]

It is Continuously Adaptive Mean Shift Tracking. It is based on an adaptation of Mean Shift that, given a probability density image, finds the mean (mode) of the distribution by iterating in the direction of maximum increase in probability density.Unlike Mean Shift that uses Static Distributions, it uses continuously adaptive probability distributions (that is, distributions that may be recomputed for each frame). It is one of the simplest methods and supplies reliable and robust results, if the colors in the background differ significantly from those in the target object.

1. Set the region of interest (ROI) of the probability distribution image to the entire image.
2. Select an initial location of the Mean Shift search window. The selected location is the target distribution to be tracked.
3. Calculate a color probability distribution of the region centered at the Mean Shift search window.
4. Iterate Mean Shift algorithm to find the centroid of the probability image. Store the zeroth moment (distribution area) and centroid location.
5. For the following frame, center the search window at the mean location found in Step 4 and set the window size to a function of the zeroth moment. Go to Step 3.

2.2 ABCshift [6]

It is acronym for Adaptive Background CAMshift Tracking. CAMSHIFT was designed for close range tracking from a stationary camera and failed when color of tracked object resembled its background. ABCshift achieves robustness against camera motion and other scene changes by continuously relearning its background model at every frame. It tracks efficiently even when the object shares common color with the background. Therefore, it enables robustness in difficult scenes where the tracked object moves past backgrounds with which it shares significant colors.

1. Identify an object region in the first image and train the object model, P(C|O).
2. Center the search window on the estimated object centroid and resize it to have an area r times greater than the estimated object size.
3. Learn the color distribution, P(C), by building a histogram of the colors of all pixels within the search window.
4. Use Bayes' law, equation (1), to assign object probabilities, P(O|C), to every pixel in the search window, creating a 2D distribution of object location.
5. Estimate the new object position as the centroid of this distribution and estimate the new object size (in pixels) as the sum of all pixel probabilities within the search window.
6. Repeat steps 2-6 until the object position estimate converges.
7. Return to step 2 for the next image frame .

2.3 PAMshift [7]

It is short for Path Assigned Mean shift tracking. It is a fast tracking method. In PAMS assignment, all points along the path towards the mode point are assigned to that final mode value. Points already assigned modes are eliminated from the mean shift process and are not traversed in the future. Since large swathes of feature space vectors are now assigned in one iteration step, the complete mean shift process converges much faster.

1. Select a point site (p, q) at random in the image.
2. Extract the colour values vector of the pixel at that point $I_{U,V}(p,q)$.
3. Find the j neighbourhood vector, $I_{(U,V)j}(t)$, within the colour bandwidth, hc.
4. Compute the Center of Mass, CoM_c in the colour domain.
5. Translate by the mean shift vector, $m_c(U, V)$.
6. Repeat 3 and 5 till convergence to stationary mode vector,$I_{(Um,Vm)}$. Assign the final mode vector,$I_{(Um,Vm)}$, to the entire mean shift path, $U^{t=i}_{t=0} I_{(U,V)j}(t)$, where i is the number of iterations to convergence.

2.4 Fuzzy Clustering Mean Shift [8]

Color information has been extensively used for characterizing an object in the application of computer vision. However the conventional approaches use fixed number of color bins to quantize the RGB color space for generating the color histogram as the tracked features. Such approaches may result in unfeasible classification and are sensitive to noisy interference such as lighting changes and quantization errors. In order to properly classify the color information, a sequential version of self-constructing fuzzy cluster is generated from the training data set, i.e. the target image, based on similarity tests. During the training phase, one data pattern is considered in each time. The similarity between the input pattern and the existing fuzzy clusters is calculated to decide whether to combine the considered pattern into the most similar existing cluster or to create a new cluster for the pattern. Once a new cluster is created, the corresponding membership function should be initialized. On the contrary, when the considered pattern is combined into the most similar existing cluster, the corresponding membership function of that cluster should be updated according to the statistical mean and deviation of the data points included in the cluster. After all the training patters are considered as above, we finally obtain a set of fuzzy clusters and corresponding membership functions.

2.5 SOAMST [9]

It is a scale and orientation adaptive mean shift tracking. SOAMST algorithm employs the weight image derived from the target model and the target candidate model in the target candidate region to estimate the target scale and orientation. Such a weight image can be regarded as the density distribution function of the object in the target candidate region, and the weight value of each pixel represents the possibility that it belongs to the target. Using this density distribution function, we can compute the moment features and then estimate effectively the width, height and orientation of the object based on the zeroth-order moment, the second-order center moment and the Bhattacharyya coefficient between target model and target candidate model.

1. Initialisation: Calculate the target model $\hat{q}$ and initialise the position y_0 of the target candidate model in the previous frame.
2. Initialise the iteration number k $\leftarrow$0.
3. Calculate the target candidate model $p(y_0)$ in the current frame.
4. Calculate the weight vector $\{w\}_{i=1\ldots n}$.

5. Calculate the new position y_1 of the candidate target model.
6. Let d $\leftarrow \| y_1 - y_0 \|$, $y_0 \leftarrow y_1$. Set the error threshold ε (default 0.1) and the maximum iteration number N (default 15)

a. If (d< ε or k≥ N) Stop and go to step 7
b. Otherwise k$\leftarrow$k+1 and go to step 3

7. Estimate the width, height and orientation of the candidate target model using covariance matrix.
8. Estimate the initial target model for the next frame.

III. RESULT AND DISCUSSION

In this section, the results of applying the mean shift methods on various test sequences are shown.

Figure 2 shows the result of CAMShift method on a test sequence of an orange ball. In this example, the color of the object being tracked, that is orange ball, has similarity with its background. In such case, the CAMShift algorithm fails to track the object, rather it keeps on adapting its window to include the background. It works well only when the object significantly differs from its background in color. Similar situation is shown in Figure 3, where the tracking window saturates itself to background and tracking fails. Figure 4 shows the result of applying ABCShift method where the object color is similar to its background. As shown this method tracks the object well. Thus, the shortcoming of CAMShift is overcome by ABCShift method.

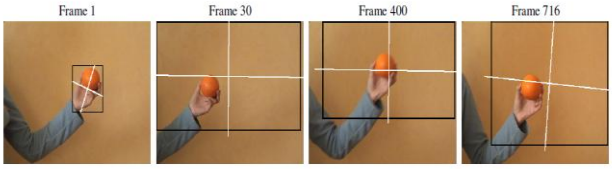

Figure 2. CAMshift at frame1,frame 30,frame 400,frame 716 [10]

Figure 3. Person tracking with CAMshift from a moving camera in outdoors environment [6]

Figure 4.ABCshift successfully tracks throughout the sequence and is not disturbed by red regions of background [6]

The result of fast mean shift method PAMS is shown in Figure 5. It improves the complexity inherent in traditional mean shift method. It is efficiently applied to color segmentation problems as shown. It performs 1.5 to 5 times faster than other existing fast methods when applied to segmentation tasks.

Figure 6 shows the result of Fuzzy Mean Shift method. As mean shift method suffers from quantization error, it is unable to efficiently track the object. This shortcoming is overcome by Fuzzy Mean shift Method as clear from the example shown. In addition to this, this also reduces the complexity associated with the mean shift method.

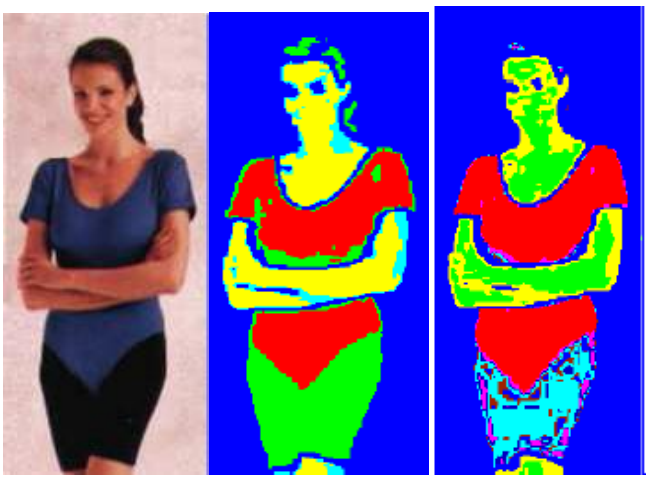

Figure5(a) Original (b) PAMS (c)Mean shift Image [7]

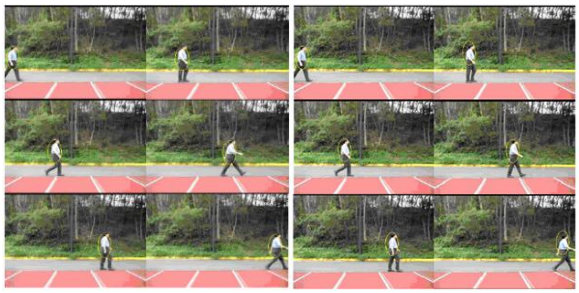

Figure 6 [8](a) Mean shift (b)Fuzzy clustering mean shift

a

b

Figure 7: (a) Traditional Mean Shift Method; (b) SOAMS Method [9]

Figure 7 shows the result of Scale and Orientation adaptive mean shift method for tracking hand of a person, which undergoes changes in orientation and scale both. As clear from Figure 7(a) traditional mean shift method is unable to adapt to changes in orientation and scale and thus fails to track the object efficiently. This has been improved by SOAMS technique that tracks scale and orientation changes of the object, as is clear from Figure 7(b).

IV. RESEARCH PAPERS' REVIEW

Table 1 summarises the works of mean shift object tracking techniques. It identifies the advantages and shortcomings of a particular method, along with the improvements proposed for each of those methods. Any improvements, if possible in future, are also summarised in the table.

Paper	Pros and Cons	Improvements Proposed/ Possible
1.Real-time Tracking of Non-rigid Objects using Mean Shift *By: Dorin Comaniciu, Peter Meer*[1]	1.Superior Tracking Performance with low computational Complexity 2.Direct projection into new frame produces large bias in estimated location, i.e., target scale variant	Further improvement proposed in [2] and [3]
2.Mean Shift: A Robust Approach towards Feature Space Analysis *By: Dorin Comaniciu, Peter Meer*[2]	1. The presence of a significant feature when pooled together provides an excellent tolerance to noise levels. 2. Features with lesser support in the feature space may not be detected in spite of being salient for the task to be executed.	The disadvantage of missing a salient feature can be largely avoided by either augmenting the feature space with additional (spatial) parameters from the input domain, or by robust post/pre processing of the input domain guided by the results of the feature space analysis. These improvements have been proposed by Comaniciu in [3] and by many other authors.
3.Kernel Based Object Tracking *By: Dorin Comaniciu, Peter Meer*[3]	1. Coped well with camera motion, partial occlusions, clutter and target scale variations 2. Sophisticated motion filter required , if occlusions present	The traditional mean shift process is limited by the fixed kernel bandwidth. It was overcome by CAMshift [4]
4.Computer Vision Face Tracking For Use in a Perceptual User Interface *By: Bradski*[4]	1. CAMSHIFT handles noise well without the need for extra filtering or adaptive smoothing. 2. Since CAMSHIFT relies on color distributions alone, errors in color (colored lighting, dim illumination, too much illumination) will cause errors in tracking	This work was extended for multiple quantized feature spaces in [5].
5.Object Tracking Using Camshift Algorithm And Multiple Quantized Feature Spaces *By:John G. Allen, Richard Y. D. Xu, Jesse S. Jin*[5]	1. CAMSHIFT fails with camera motion, since it relies on a static background model which is unable to adequately represent changing scenery. 2. CAMSHIFT tracker also fails to detect target when target shares color pixels with its background.	These problems were addressed by ABCshift algorithm proposed by [6]. Scale and orientation adaptive tracking has been further improved by Ning et al [9].
6.Efficient Visual Servoing With The ABCshift Tracking Algorithm *By: Rustam Stolkin, Ionut Florescu, Morgan Baron, Colin Harrier and Boris Kocherov*[6]	Robustness against camera motion and similar color pixels of object and background	Future work concentrates in both developing further the algorithm as well as modifying the platform and the mechanical issues involved.
7.The Path Assigned Mean Shift Algorithm: A New Fast Mean Shift Implementation For Color Image Segmentation [7]	1. Fast mean-shift method 2. Improper selection of bandwidth and kernel	Future work will focus on the proper selection of bandwidth and kernel to minimize the mislabeling rate.
8. Shift Tracking Using Fuzzy Color Histogram *By: Ming-Yi Ju, Chen-Sen Ouyang, Hao-Shiu Chang* [8]	1. Robust and reliable 2. Less mean shift iterations required than the conventional algorithm for tracking a moving object.	This paper proposed the method only for RGB model. It can be further extended to other color models and texture as well.
9.Scale And Orientation Adaptive Mean Shift Tracking *By: J. Ning, L. Zhang, D. Zhang, C. Wu*[9]	1. Adaptive to object's scale and orientation changes 2. Restricted to only ellipse and rectangular model	Future work will focus on how to detect and use the true shape of the target, instead of an ellipse or a rectangle model, for a more robust tracking.

Table 1:Pros, Cons and Improvements

V.CONCLUSION AND COMMENTS FOR FURTHER RESEARCH

Several Mean shift techniques taken from the literature are discussed and analyzed herein, with their pros and cons. The traditional mean shift process limited by the fixed kernel bandwidth has been improved by the CAMshift algorithm. Camshift algorithm for object tracking does reasonably well when the object significantly differs in color from its background. ABCshift tracking overcomes the shortcomings of CAMshift tracking. It tracks an object efficiently despite the camera motion and resemblance of object color with the background.

To improve computational complexity of standard mean shift algorithm, fast mean shift methods have been proposed. These include PAMS and Parallel Mean Shift Method. Recent work on object tracking has included texture in the feature space, instead of only color. Fuzzy color clustering for tracking has also been proposed to overcome the effects of quantization inherent in fixed bin histogram. The concluding discussion and table should serve as a useful guide in choosing the right Mean shift method for object tracking.

REFERENCES

[1] Dorin Coamaniciu, Peter Meer ,"Real-time Tracking using Non-rigid Objects using Mean Shift", Proc. IEEE Conf.Computer Vision and Pattern Recognition, vol. II, pp. 142-149, June 2000.

[2] Dorin Coamaniciu, Peter Meer," Mean Shift: A Robust Approach towards Feature Space Analysis",IEEE Trans. Pattern Analysis and Machine Intelligence,vol. 24, no. 5, pp. 603-619, May 2002.

[3] Dorin Coamaniciu, Peter Meer," Kernel Based Object Tracking", IEEE Transactions on Pattern Analysis and Machine Intelligence, Vol. 25, No. 5, pp. 564-577, May 2003.

[4] Gary R Bradski, "Computer Vision Face Tracking For Use in a Perceptual User Interface", Proc. IEEE Workshop Applications of Computer Vision, pp. 214-219, Oct. 1998.

[5] John G. Allen, Richard Y. D. Xu, Jesse S. Jin, "Object Tracking Using Camshift Algorithm And Multiple Quantized Feature Spaces", Proceedings of the Pan-Sydney area workshop on Visual information processing, ser. ACM International Conference Proceeding Series, vol. 100. Darlinghurst, Australia: Australian Computer Society, Inc., 2004, pp. 3–7.

[6] Rustam Stolkin, Ionut Florescu, Morgan Baron, Colin Harrier and Boris Kocherov, "Efficient Visual Servoing With The ABCshift Tracking Algorithm", 2008 IEEE International Conference on Robotics and Automation Pasadena, CA, USA, May 19-23, 2008.

[7] Akash Pooransingh, Cathy-Ann Radix, Anil Kokaram, "The Path Assigned Mean Shift Algorithm: A New Fast Mean Shift Implementation For Colour Image Segmentation", 2008. ICIP 2008. 15th IEEE International Conference on Image Processing.

[8] Ming-Yi Ju, Chen-Sen Ouyang, Hao-Shiu Chang," Mean Shift Tracking Using Fuzzy Color Histogram", Proceedings of the Ninth International Conference on Machine Learning and Cybernetics, Qingdao, 11-14 July 2010, IEEE.

[9] J. Ning, L. Zhang, D. Zhang, C. Wu, "Scale And Orientation Adaptive Mean Shift Tracking", IET Computer. Vision, 2012, Vol. 6, Iss. 1, pp. 52–61

[10] Nicole M. Artner, "A Comparison Of Mean Shift Tracking Methods", in 12th Central European Seminar on Computer Graphics, 2008, pp. 197-204.

[11] Sang Gu Lee, "Image Object Tracking System Using Parallel Mean Shift Algorithm", The 2012 International Conference on Image Processing, Computer Vision, and Pattern Recognition (IPCV'12), 2012.

International Journal of Environmental Science: Development and Monitoring (IJESDM)
ISSN No. 2231-1289, Volume 4 No. 3 (2013)

Role of technological advancements in enhancing sustainable development.

Ujjwal Raheja* and Abhinav Malik^
*Bachelor of Technology, Delhi Technological University Shahbad Daulatpur Delhi
^ Bachelor of Technology, Bhagwan Parshuram Institute of Technology, Rohini Delhi

Abstract:

Sustainable development today has crossed national boundaries. Today every nation raises the importance of developing technologies for sustaining our comforting lifestyles at minimal costs and load on our planet's resources. It has become a priority to develop such technology that enhances our ability to consume efficiently, reduce wastage and which can be adopted easily. Every nation is eager to share what they have developed because sustainability cannot exist at one point or nation on earth, it has to be globally adopted for better living and existence. Globally geologists are concerned about the depleting levels of liquid fuels and the increase in our dependency on them. Some also fear that is this our descend back into the Stone Age era. This makes sustainable development of utmost importance for all the world. The load on this planet can exist in many forms from a delayed existence of a disease to wrong driving habits leading to over consumption of fuels. The technology we developed for comforting our lives today puts a lot of pressure on our planet's resources and to sustain our comfortable lives with minimal changes we again look back to technology that may help us do so. It may be technologies for eradication of diseases to technologies for harnessing renewable sources of energy.

Introduction

The world has seen many conventions, commissions, reforms and guidelines on sustainable development. Developed nations like United States of America have spent more than 100 billion USD on cancer research. Many nations have invested great amounts in biotechnology and renewable energy forms. The US Energy Information Administration in its STEO report clearly points to the increasing consumption of liquid fuels from 0.8 million bbl/d in 2012 to 0.9 million bbl/d in 2013 and is forecasted to reach up to 1.2 million bbl/d in 2014. This increase in consumption not only fastens the pace towards the end of non-renewable resources but also indicates increase in global pollution levels by greenhouse gases.

Ahmed and Stein in 2004 suggested that for sustainable development one needs to bring uniformity in technological progress, reduce poverty to new levels that all parts of the society can co-exist while following the sustainable paths and reforms laid out.

This paper covers various arenas in which vast research has yielded positive results or which are being constantly explored in order to find suitable technologies. The ongoing research in the field of biotechnology and it's ever increasing importance today has been also discussed. World communication technologies and the renewable energy sources, their advancements and extents to which they can be incorporated in our lives have been discussed.

Biotechnology

Recent times have seen an upsurge in the investments nations are putting in the field of biotechnological research. Not only this upcoming and vast field offers problems to serious world problems but also gives an extra edge to human race in the field of medicine.

Biotechnology solved a great problem of food security. Earlier the food sources were totally dependent on natural conditions from rainfall to soil content. But today biotechnology has helped us ensure that we are able to meet our food demands even when adverse natural conditions are met. Transgenic crops are developed for imparting desirable traits to a plant and for obtaining the required useful product from it in minimal favorable conditions. Traits like pesticide tolerance and insect resistance are majorly worked upon in plants (Rastogi and Pathak, 2009).

The first transgenic crop Flavr Savr Tomato was introduced in 1994, which had an increased shelf life due to slow ripening.

In 1990s there was an increase in global crop yield due to development of Bt crops which were generated by insertion of cryAc gene obtained from B.thuringiensis. These crops were resistant to a wide range of insects as they produced toxin substances which were harmless when consumed by humans, Bt cotton being one of them (Carriere et al. 2003). Over the years Bt brinjal, Bt maize and many more crops resistant to insects were developed through this technique. Furthermore crops resistant to water scarcity were also developed to minimize the effects of famine (Thomson 2002, Zhang et al. 2004, Vinocur et al. 2005).

Another aspect of biotechnology is medicine and research. Biotechnology has provided man with tools that can be used to manipulate an organism or a disease at DNA level and provide ways to eradicate it from the root level. Yet Cancer remains undefeated. Every year the world spends billions of dollars on cancer research, some fields have shown positive results in preventing cancer to a great extent. Biotechnology has been used to explore genetic disorders and cure them thereby increasing the expected life of a human on this planet. Genetic disorder occurred because of changes in the DNA due to inheritance, lifestyle problems and environmental factors have been observed at molecular level and these interpretations have been used to cure various illness which were not pathogen associated (Bell and Beck, 2010).

Nanotechnology

Nanotechnology has been majorly explored in the field of disease detection and in the field of electronics. Gold nanoparticles have been proposed to be used for early and accurate detection of Cancer. Oral cancer was successfully detected using gold nanoparticles by Ivan et al. 2005 due to difference in the amount of absorption of these nanoparticles by cancerous and non-cancerous cells. Bajaj et al 2009 also proposed a similar test for early detection of cancer using gold nanoparticles and fluorophores. It could differentiate between various stages of cancer. Nanoparticles are also preferred as a suitable drug delivery system for cancer drugs as they are very specific to delivery site and do no release toxic drugs at other than the affected sites. These nanoparticles are also known to cross blood brain barrier hence are able to deliver drugs to cure anomalies of central nervous system (Muldoon et al. 2006).

Nanoparticles have been used in food packaging industry for their anti-microbial properties and their thermal resistance (Holly et al. 2005, Brody et al. 2006). Nanoparticles have also found use in development of biosensors for detection of blood sugar levels using minimal amount of blood sample (Rivas et al. 2006).

Information and communication technologies; and Artificial Intelligence

The term information and communication technology in a broader sense refers to the use of information and communication techniques in the fields of social and economic development along with fields involving human rights. It is meant to deal with resource deficit population anywhere around the world.

Kurzweil Ray suggests that the emergence of information society and new economic models along with the development of affordable and efficient information and communication techniques has given way to the contribution towards sustainable development (Kurzweil Ray, 2005).

It is believed that the people with economically privileged background would for long tend to stay in constant interaction and communication with people around the world through the means of internet, telephones, audio and video conferencing. Ray Kurzweil, adumbrates a significant increase in technologies like genetics, nanotechnology, robotics and many more. According to him ,this would leads to a technological singularity in the year 2045 and at this point the machine intelligence would be more powerful than human intelligence combined together.

The issue of realizing long term environmental and societal sustainability is a challenge for individual and collective decision making. However, certain findings in behavioral economics suggest that human decision making is biased and short sighted when it comes to sustaining healthy planet and there lies the utility of artificial intelligence for sustainability (McElroy, Mark W. 2006) , (Fisher, D. H. 2011).

Norio Shiratori and Mohammed Atiquzzaman (2004) have collectively proposed a routing schedule, named as Shaped Deficit Round Robin (SDRR). The scheme proposed by them offers better weighted throughput and improvements in packet suspension per flow. Their prime concern is to bring out the capabilities of a Label Switched Router in the presence of non real-time and real time applications wherein the non-real time applications dealt with packet loss and the real time applications dealt with packet loss.

Today information and communication technology is used across the world among people of varying ages to have access to information on various subjects and assistance in areas of their interest ranging from psychological issues , to sports , music or any sort of medical assistance. Amongst the young generation the social media and online gaming are gaining importance.

Renewable energy for sustainable development and environment

It is believed and estimated that around the world that buildings contribute towards a large percentage of the total world's annual energy consumption. This energy is consumed for a large number of purposes. Exploiting renewable energy in buildings and agricultural greenhouse can significantly contribute towards a much lesser dependence on fossil fuels.

Renewable energy resources seem to be an alternative and a solution to preserve the natural resources and bridge an intimate relationship between the renewable energy and sustainable development. It is also essential to use energy more rationally in order to bridge a transition from fossil fuels to non -polluting fuels, and technologies such as photovoltaic (PV) cells and fuel cells (WEO, 1995).

It is estimated that worlds energy consumption is estimated to be 22billion kwh per year and about 66 billion metric ton of carbon emission are released in atmosphere to meet the energy demands (Bos et al , 1994). This demands for an approach which is essential to integrate renewable energies. However, renewable energy resources are geographically diffused and demand for one of the following two approaches (EUO, 2000):

1. The effective utilization of capture area, greater than that by community which is to be supplied.

2. Significant reduction of community's energy demands with locally available resources to a level commensurate.

Recently with new technological innovations being brought up, the advent of fuel cells is being considered as an alternative for power generation for mobile and stationary uses (Jacobson MZ, Colella WG, Golden DM (2005); Steele BCH, Heinzel A (2001)). Fuel cells of different types have been developed, some of them include: polymer electrolyte fuel cell (PEFC), molten carbonate fuel cell (MCFC) , alkaline fuel cell (AFC), phosphoric acid fuel cell (PAFC). Amongst these fuel cells PEFC is the one which has been most developed in the past 20 years and is suitable for vehicle applications which require high power density and rapid start up (Jacobson MZ, Colella WG, Golden DM (2005) ; Steele BCH, Heinzel A (2001) Borup R, et al (2007)). In comparison to the electrolytic cells that were used earlier the polymer electrolytes separate the fuels and the oxidants used effectively using a thin film of microns and thus can eliminate the problem of electrolytic leakage completely.

Thus it can be said that renewable resources if harvested sustainably can reduce the threats of air pollution, water pollution, destruction of natural habitat and problems of land degradation (Benefits of Renewable Energy Use, 1999). The reinforcement of renewable energy market and the promotion of innovative renewable applications will lead to preservation of environment by reducing emission at all levels.

Discussion

The world today is at a stage where looking back at past we see many follies committed in haste and due to lack of knowledge. Today the requirement is to survive and preserve life as it is. When we talk about biotechnological developments and future perspectives in terms of sustainable development we mean to focus on the need of such developments that decrease the ever-increasing load on our health systems, our agricultural lands and in turn our planet. A simple example is early detection of cancer, for a patient this may lead to longer life, for the planet it

would mean a person who didn't undergo radiation therapy hence saved a lot of energy. Such small contributions mass up and contribute towards significant sustainable development.

When we discuss better communication systems we focus upon our ability to spread the knowledge to farthest of arenas so that exploitation of resources does not take place. Renewable energy perhaps is the most discussed field when it comes to sustainable development. With increasing oil prices and decreasing availability one would have to look upon the non-conventional ways of energy. Harnessing solar energy has been a project since many decades now and with each passing year we strive to develop systems which are more efficient than their predecessors to harness solar energy.

There are a number of obstacles which a new technology faces, people may not accept to incorporate it as a part of their lives for example solar heaters are being used by a fraction of population in regions where sunlight is ample. GM crops though have helped us fill the food banks are many times protested against by some organizations and members of the society (Greenpeace 1999, King and Gordon. 2001). Some oil companies claim we have enough oil for next 40 to 60 years but in the end the after all these technological developments and future prospects, we will only survive if we are prepared for the future and have gained a mass acceptance for technology that will aid us in survival.

References

Ahmed, A. and Stein, J.A. (2004) 'Science, technology and sustainable development: a world review', World Review of Science, Technology and Sustainable Development, Vol. 1, No. 1, pp.5–24. brain barrier disruption consortium meeting. Am J Neuroradiol 27:715–721

Avinash Bajaj, Oscar R. Miranda, Ik-Bum Kim, Ronnie L. Phillips, D. Joseph Jerry, Uwe H. F. Bunz, and Vincent M. Rotelloa Detection and differentiation of normal, cancerous, and metastatic cells using nanoparticle-polymer sensor arrays Proc Natl Acad Sci U S A. 2009 July 7; 106(27): 10912–10916. Chemistry, Applied Biological Sciences

Bell, C. G. and Beck, S. (2010) The epigenomic interface between genome and environment in common complex diseases. Brief Funct Genomics 9: 477-485

Benefits of Renewable Energy Use. Union of Concerned Scientists. 1999. Retrieved 2013-01-04.

Borup R, et al (2007) Scientific aspects of polymer electrolyte fuel cell durability and degradation. Chem Rev 107:3904 –3951.

Bos, E., My, T., Vu, E. and Bulatao R. 1994. World population projection: 1994-95. Edition, published for the World Bank by the John Hopkins University Press. Baltimore and London.

Brody AL. 2006. Nano and food packaging technologies converge. Food Technol 60:92–94

Carriere, Y., C. Ellers-Kirk, M. Sisterson, L. Antilla, M. Whit-low, T. J. Dennehy, and B. E. Tabashnik. 2003.Long-term regional suppression of pink bollworm by Bacillus thuringiensis cotton. Proc. Natl. Acad. Sci. USA 100: 1519-1523

D. King and A. Gordon, "Contaminant found in taco bell taco shells," Friends of the Earth, 2001, http://www.foe.org/.

Energy use in offices (EUO). 2000. Energy Consumption Guide 19 (ECG019). Energy efficiency best practice programme. UK Government. London.

Fisher, D. H. 2011. Sustainability, Chapter 23 from Leadership in Science and Technology: A Reference Handbook, William Sims Bainbridge, ed., Sage Publications. Retrieved. From http://www.vuse.vanderbilt.edu/~dfisher/SustainLeader.final.htm

Greenpeace, "Genetically engineered food,," Greenpeace, 1999, http://www.greenpeace.org/.

Holley C. 2005. Nanotechnology and packaging. Secure protection for the future. Verpackungs-

Rundschau 56:53–56.

Ivan H. El-Sayed,Xiaohua Huang,and Mostafa A. El-Sayed Surface Plasmon Resonance Scattering and Absorption of anti-EGFR Antibody Conjugated Gold Nanoparticles in Cancer Diagnostics: Applications inOral Cancer 2005

Jacobson MZ, Colella WG, Golden DM (2005) Cleaning the air and improving health with hydrogen fuel-cell vehicles. Science 308:1901–1905.

Kurzweil, Ray (2005), The Singularity is Near, New York: Viking Books, ISBN 978-0-670-03384-3.

McElroy, Mark W. 2006. The Sustainability Code -- A Policy Model for Achieving Sustainability in Human Social Systems. Center for Sustainable Organizations, University of Groningen. Retrieved from http://www.sustainableorganizations.org/The-Sustainability-Code.pdf.

Muldoon LL, Tratnyek PG, Jacobs PM, Doolittle ND, Christoforidis GA, Frank JA, Lindau M, Lockman PR, Manninger SP, Qiang Y, Spence AM, Stupp SI, Zhang M, and Neuwelt EA. 2006. Imaging and nanomedicine for diagnosis and therapy in the central nervous system: Report of the eleventh annual blood.

Norio Shiratori (Tohoku University, Japan) and Mohammed Atiquzzaman (University of Oklahoma, USA), Telecommunication Systems 25:3,4, 169–172, 2004

Rivas GA, Miscoria SA, Desbrieres J, and Barrera GD. 2006. New biosensing platforms based on the layer-by-layer self-assembling polyelectrolytes on Nafion/carbon nanotubes-coated glassy carbon electrodes. Talanta (in press, 2006).

S. Rastogi and N. Pathak, Genetic Engineering, Oxford University Press, New Delhi, India, 2009.

Steele BCH, Heinzel A (2001) Materials for fuel-cell technologies. Nature 414:345–352.

Thomson, J. A. (2002) J. Nutr. 132, 3441S–3442S.

US Energy Information Administration Short Term Energy Outlook (STEO) July 2013

Vinocur, B. & Altman, A. (2005) Curr. Opin. Biotechnol. 16, 123–132.

World Energy Outlook (WEO). 1995. International Energy Agency. OECD Publications. 2 rue Andre Pascal. Paris. France.

Zhang, J. Z., Creelman, R. A. & Zhu, J.-K. (2004) Plant Physiol. 135, 615–621.

International Journal of Advanced Science and Technology
Vol.62, (2014), pp.19-30
http://dx.doi.org/10.14257/ijast.2014.62.02

Sensing Performance Evaluation over Multihop System with Composite Fading Channel

Deepti Kakkar[1], Arun Khosla[1] and Moin Uddin[2]

[1]*Department of ECE, National Institute of Technology, Jalandhar, India*
[2]*Delhi Technological University*

Kakkard@nitj.ac.in, khoslaak@nitj.ac.in, prof_moin@yahoo.com

Abstract

Cognitive radio has been demonstrated for improved spectrum utilization by secondary users in the presence of spectrum holes. In this paper, a Cognitive Radio (CR) network is implemented over the cooperative multihop wireless link. A multihop network is a collection of relay nodes within transmitter and receiver. A fixed infrastructure based multihop architecture is assumed for the performance analysis of energy detection algorithm for spectrum sensing in CR. System performance estimation against channel impairments dominated by fading and shadowing effects is one of the prerequisite for performance analysis of such networks. An effort has been made for exact performance analysis of multihop wireless network over composite fading channels. The investigation lead to the findings i.e., *for a given value of fading or shadowing parameter, the preferable detection probability is always dependent upon the optimum number of hops. Depending upon SNR a three- or five- hop link may perform better. For severe fading conditions,* the *one-hop link performs best.*

Keywords: *Energy Detection, Spectrum sensing, Multi-hop System, Performance Evaluation, Composite Fading channel*

1. Introduction

Radio frequency is a natural resource but unlike other resources it will not deplete when used. Most of its usable or beneficial part has been allocated to different services or has already been licensed by the government agencies in respective countries. Therefore there exists an apparent spectrum scarcity for new wireless services. It has also been noticed that licensed users rarely utilize all the allocated frequency bands at all the time and at different geographical locations. The underutilization of allotted frequency bands occurs and spectrum usage becomes inefficient. Such spectrum underutilization has motivated cognitive radio (CR) technology. Spectrum detection and spectrum traffic allocation are the main two challenges to enhance the spectrum utilization. The unlicensed users first sense the primary user's activities, *i.e.*, detecting the presence of signals in the frequency spectrum is spectrum sensing. The motto behind the development of CR technology is primary user detection with better transmission opportunity exploration [1, 2]. Spectrum holes are the unused frequency bands allocated to primary user at any point of time [3]. The performance of energy detection based spectrum sensing has been principally discussed for two hop relay networks [4, 5]. The recent studies illustrated that the cooperative relaying protocols can be used to fulfill all the basic requirements of CR networks [6, 7]. Many authors have been proposed that the cooperative spectrum sensing with accurately chosen fusion method will significantly improve the probability of detection [8]. CR has not been implemented on cascaded multihop

ISSN: 2005-4238 IJAST

relay networks over wireless link with composite fading characteristics. The potential of broader coverage in low transmitting power makes cooperative multihop scenarios more powerful communication technology [9]. In the last few years, numerous contributions addressed the performance of multihop relayed transmission, Hasna and Alouini [10-12] and Karagiannidis *et al.*, [13] studied average bit error rates and outage probability for different types of relays over Rayleigh, Nakagami-m fading channels. A relay network is thus expected to provide an improved return on assets, which means higher average revenue per user with superior grade of service at low incremental cost. The idea behind this approach is to split up the wireless link into multiple shorter hops, so that the source communicates with the destination only indirectly via a set of intermediate relay stations. Since the individual hops are generally much shorter than the distance between source and destination, the detrimental effects of path loss can be mitigated and therefore the total transmit power might be reduced compared to systems without relays [14]. If less transmit power is used, this also leads to a reduction of both the inter- and intra-cell interference level and might facilitate a cell capacity gain since multiple nodes within one cell might transmit data at the same time if they are far enough apart. Further, multihop relaying gives better trunking efficiency at aggregation points. Such networks are well suited for deployments in emergency and disaster scenarios. Also in rural areas, where traffic density is low and population is sparsely distributed, it may not be economically viable to build traditional cellular access networks with full fledged base stations (BS), rather a network architecture with a BS flanked by relay nodes to improve capacity and range extension may be a more flexible approach. The channel condition within all the hops of a cascaded multihop network does not remain same. In a wireless link, the data to be transferred from the sender to receiver has to propagate through air. During this propagation, the signal (data) gets distorted due to several phenomenon's that occur within the wireless link. Issues like hidden terminal problem, multipath fading, shadowing and noise all makes it difficult to detect and extract the exact transmitted signal at the receiver. Also, the spectrum bands that lie above the 2GHz frequency are affected severely by these environmental conditions.

The remainder of paper is organized as follows: Section 2 describes multihop systems and spectrum sensing in cognitive radios. Section 3 briefly describes the composite fading channel chacteristics over multihop network. In Section 4 provides performance analysis and simulation results. Finally, in Section 5, we summarize the conclusions of our studies.

2. Multihop Systems and Spectrum Sensing

To meet the objective of low cost radio network deployment, for wide-area coverage, multihop transmission is likely to play important role in future wireless communication systems. Wireless relays help overcome current dependencies on wired backbones and enable cost-effective enhancement of coverage, throughput and system capacity of cellular networks as well as a fundamental enabling-technology for wireless ad-hoc and sensor networks.

Motivating by the practical deployment, an infrastructure based multihop wireless network with the relays is considered for the performance analysis. The simple multihop technology is synonymous with packet radio networking, MANET and mesh networking. The *L*-hop system model with *(N-1)* intermediate relays between source *S* and destination *D*, R_1, R_2,...,R_{N-1} respectively is considered, as shown in Figure 1. Relays are equipped with wireless communication devices to exchange the information between source to destination. In fact relay nodes do offer high flexibility in placing base stations, allowing fast network roll-out and adaptive traffic capacity engineering. The system is such that source *S* and destination *D* are away from each other and does not follow line of sight mechanism. All the nodes are placed equidistant to each other for the ease of analysis. The corresponding SNR at each hop

are $\gamma_1, \gamma_2, ..., \gamma_{L-1}$. The relay is capable to receive radio signal from its predecessor and retransmit to its successor in a multihop network. The relays may operate in different possible schemes, depending upon how the received signal is processed: Amplify and Forward (AF) and Decode and Forward (DF). In the Amplify and Forward (AF) scheme (Analogue Repeaters), the relay node just amplifies and re-transmits the input symbols. The received signal is deteriorated by link fading and additive receiver noise. The degraded signal and noise are amplified and forwarded, thereby raising the noise level of the system. Serial relay transmission is used for long distance communication and range-extension in shadowing. It also provides power gain. In this topology signals propagate from one relay to another relay and the channels of neighboring hop are orthogonal to avoid any interference. In Decode and Forward (DF) Relay Protocols (Digital Repeaters), the relay demodulates and decodes the received signal before the retransmission. In this case, the forwarded signal does not contain supplementary filth, but degrade the system performance by symbol errors. Following the model, the exact performance investigation of (DF) and (AF) relay links having random number of hops has been accomplished. The wireless channels between successive relay nodes are slow varying and frequency non-selective composite fading channels in our investigations.

Figure 1. Schematic of a multihop network with source *S* is transmitting towards destination *D* via *N-1* intermediate relays

This paper perform the spectrum sensing in such a infrastructure based networks and shows that the probability of detection will also varies w.r.t the number of relays between source to destination. Spectrum sensing identifies unused spectrum and provides awareness regarding to the radio environment. The performance of spectrum sensing is investigated by means of energy detection technique and using their comparison property. Energy detector acts as a non-coherent detection because it is having a very low implementation complexity as it does not need any prior information about the primary user's signal. Such features make the energy detector the most commonly used detector in spectrum sensing. In spectrum sensing the accuracy is very much desirable. We consider detection probability (DP) and false-alarm probability (FP) for the analysis. The DP is defined as the probability of correctly detecting the Primary user (PU) when it is actually present and the FP is probability of incorrect detection of PU when it is not present. The vacant spectrum detection mainly depends upon the SNR condition of the wireless link and the sensing time. CR user need to sense the presence of PU, and transmit their data within same time duration, if the channel found to be free. In a infrastructure based multihop network such as shown in Figure 1, where the defined number of nodes are in between the transmitter and receiver, the repetitive sensing will lead to maximizing the sensing time. Which further results in lesser data transmission time with more power consumption. In this paper, the cooperative spectrum sensing is not incorporated, but single time sensing within the last hop and destination is accomplished, by keeping the view in mind that the signal to noise ratio at the last hop is dependent upon the probability of outage of first *(L-1)* relays within a wireless link . To simplify the analysis, cascaded multihop transmission link can be reduced to an equivalent point-to-point link and the PDF of the end-to-end SNR is given as [15].

$$p(\gamma) = N\delta(\gamma) + (1-N)\, p_{\gamma_L}(\gamma) \quad \textbf{(1)}$$

Where, N represents probability that outage occur with first (L-1) link, $p_{\gamma_L}(\gamma)$ is the SNR of last hop. Assuming channels of L hops independent and relays in Fig.1 are separated by sufficient distance, the SNRs γ_l, l=1, 2…, L are mutually independent. The probability N can be expressed as

$$\begin{aligned} N &= 1 - \Pr\{\gamma_1 > \gamma_{th}, \gamma_2 > \gamma_{th}, ..., \gamma_{L-1} > \gamma_{th}\} \\ &= 1 - \prod_{l=1}^{L-1} \Pr\{\gamma_l > \gamma_{th}\} \\ &= 1 - \prod_{l=1}^{L-1} \left[1 - P_{\gamma_l}(\gamma_{th})\right] \end{aligned} \quad \textbf{(2)}$$

Where, $P_{\gamma_l}(\gamma_{th})$ is the cumulative distribution function (CDF) of γ_l.

The longer sensing time reduces the data transmission time that degraded the channel efficiency. The energy detector is used to test the two different conditions of received signals (hypotheses H_0 and H_1) at time t and can be described as:

$$\begin{aligned} y(t) &= n(t)\ ; && H_0 \\ y(t) &= n(t) + x(t); && H_1 \end{aligned}$$

The PDF of the received signal for hypothesis H_0 and H_1 is given by [16]

$$\begin{aligned} Y &= \chi^2_{2u}, H_0 \\ Y &= \chi^2_{2u}(2\gamma), H_1 \end{aligned} \quad \textbf{(3)}$$

Where $\Gamma(.)$ is the gamma function , $I_v(.)$ is the vth order modified Bessel function of the first kind, and $u = TW$ is the time bandwidth product. γ is the signal to noise ratio at the cognitive coordinator. The detection probability (P_d) and false alarm probability (P_f) can be generally evaluated by $Pr(Y > \lambda | H1)$ and $Pr(Y > \lambda | H0)$. Spectrum sensing performance mainly degraded when, channels within hops experiences deep fading and shadowing.

3. Composite Fading Channel Model

The wireless channels with slow varying and frequency non-selective characteristics are considered. For a composite fading channel, the received signal envelops of the N-hops X_1, X2,…, X_N are random variable with composite Nakagami-lognormal PDF given by [17]. By change of variable $t = \dfrac{\ln y_l - \mu_l}{\sqrt{2}\sigma_l}$, the PDF in can be expressed as

$$p_{X_N}(x_N) = \frac{2 m_N^{\,m_N} x_N^{\,2m_N - 1}}{\sqrt{\pi}\Gamma(m_N)} \int_{-\infty}^{\infty} e^{-t^2} h(t) dt \quad \textbf{(4)}$$

Where, $x_l \geq 0$, m_l is the Nakagami fading parameter, μ_l and σ_l represent mean and

standard deviation of lognormal shadowing respectively. $\Gamma(.)$ is the standard gamma function. The m_l parameter is inversely related to the severity of the fading, m_l=1 for Rayleigh case and m_l=∞ for no fading case. σ_l is associated with the shadowing, σ_l=0 for no shadowing. $h(t) = e^{-m_l(\sqrt{2}\sigma_l t+\mu_l+x_l^2 e^{-(\sqrt{2}\sigma_l t+\mu_l)})}$, The integral form in Eq. (4), $\int_{-\infty}^{\infty} e^{-t^2} h(t)dt$ is a Gauss-Hermite integration, approximated as:

$$\int_{-\infty}^{\infty} e^{-t^2} h(t)dt \approx \sum_{i=1}^{N} w_i h(t_i) \quad \textbf{(5)}$$

Where t_i and w_i are the roots of Hermite polynomial of degree N and the weight factors of Gauss-Hermite Integration for the lth hop, t_i and w_i for different values of n are available in [18]. Therefore, Eq. (4) can be re-written as:

$$p_{X_l}(x_l) = \frac{2{m_l}^{m_l} {x_l}^{2m_l-1}}{\sqrt{\pi}\Gamma(m_l)} \sum_{i=1}^{N} w_i h(t_i) \quad \textbf{(6)}$$

An equivalent approximation for Eq. (6) is given by [14]

$$p_{X_l}(x_l) = K\sum_{i=1}^{N} a_i {x_l}^{2m_l-1} e^{-b_i {x_l}^2} \quad \textbf{(7)}$$

Where $x_l \geq 0$, $a_i = \frac{2{m_l}^{m_l} w_i e^{-m_l(\sqrt{2}\sigma_l t_i+\mu_l)}}{\sqrt{\pi}\Gamma(m_l)}$, $b_i = me^{-(\sqrt{2}\sigma t_i+\mu)}$,

$K = \frac{\sqrt{\pi}}{\sum_{i=1}^{N} w_i}$, K is the normalization factor. Based on the amplitude distribution in Eq. (7) PDF

for the random variable γ_l can be evaluated as

$$p_{\gamma_l}(\gamma_l) = \frac{K}{2\rho^{m_l}} \sum_{i=1}^{N} a_i {\gamma_l}^{m_l-1} e^{-b_i \frac{\gamma_l}{\rho}} \quad \textbf{(8)}$$

$p_{\gamma_l}(\gamma_l)$ in Eq. (8) is a Mixture of Gamma Distributions [19]. For the PDF in Eq. (8), CDF of the SNR per hop $P_\gamma(\gamma)$ can be evaluated as

$$P_{\gamma_l}(\gamma_l) = \frac{K}{2\rho^{m_l}} \sum_{i=1}^{N} a_i \int_0^{\gamma_l} t^{m_l-1} e^{-\frac{b_i}{\rho}t} dt$$

The CDF of received SNR is rewritten by using [20]

$$P_{\gamma_l}(\gamma_l) = \frac{K}{2}\sum_{i=1}^{N}\frac{a_i}{b_i^{m_l}}\gamma\left(m_l, \frac{b_i\gamma_l}{\rho}\right) \quad \textbf{(9)}$$

Where, $\gamma(.,.)$ is the incomplete gamma function.

4. Performance Analysis and Simulation Results for Multihop System

The simulations are done for Nakagami-lognormal fading within the hops of wireless link. For simulations, MATLAB software is adopted. In simulations, it is assumed that wireless channels for each hop are independent and not identically distributed (i.n.i.d.). The signal to noise ratio (SNR) at the receiver is dependent upon the distance between source to destination and number of hops in a wireless link. Figure 2 clearly represents the receiver operating characteristic curve (ROC) analysis with various number of hops in case of cascaded multi-hopped network over composite fading channel. The direct link with average SNR of 8 dB is also included in performance analysis. Figure clearly reveals that the detection probability is dependent upon the number of relays/hops in a cascaded wireless link. As the number of hops starts increasing the detection probability gets decreased.

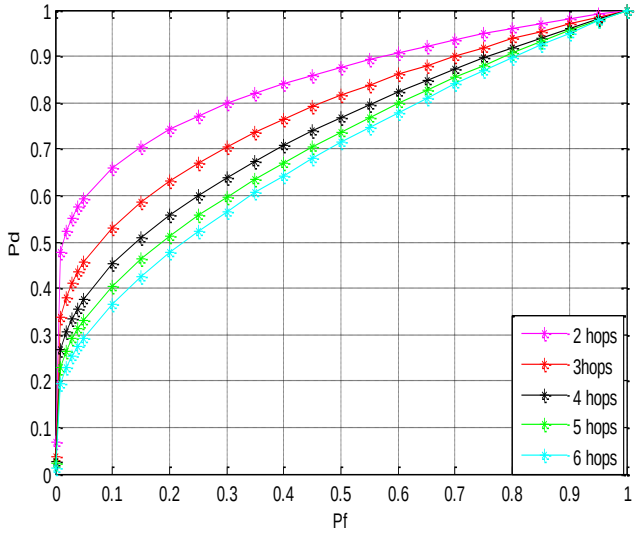

Figure 2. ROC for six-hop link for different number of hops at *m=1* and *σ = 8.* With Avg.SNR=8dB.

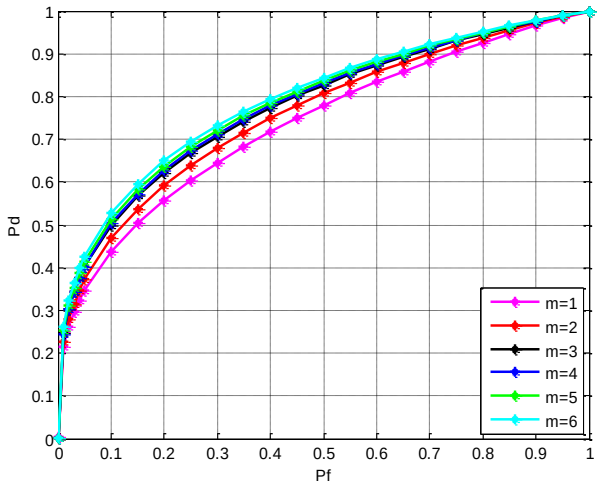

Figure 3. ROC analysis in Nakagami-lognormal faded (i.i.d) channel with different values of fading parameter (m) in a three hop network

In Figure 3 the simulations are carried out for 3 hop scenarios with the average SNR between each link is assumed to be 8 dB and the value of *u* is set to be 2. For the simulation the Receiver operating characteristic curves (ROC) has been drawn for the variable value of nakagami-m parameter having fixed value of standard deviation σ=8. From the figure it is revealed that as the channel conditions improve, the detection probability also improves significantly. Further, there is not significant improvement in detection probability for the values of *m* greater than 5

Figure 4 also represents the equivalent results, but the simulations are carried out for 5 hop network, assuming the average SNR within between each link is not identical. For the simulations, it is assumed that the average SNR goes on increasing as with the number of hops. The simulations are carried out for 5 hop scenarios with the average SNR between each hop are assumed to be (5dB, 8dB, 12dB, 15dB and 18dB).

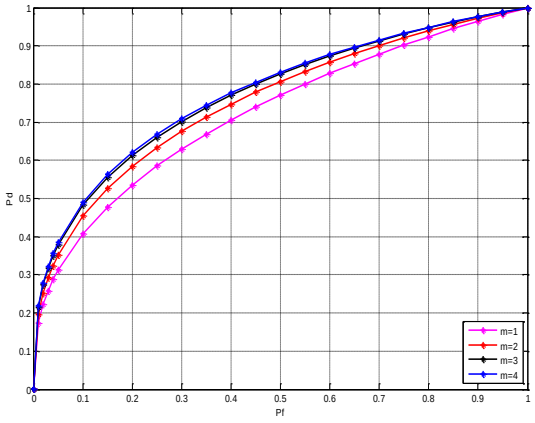

Figure 4. ROC analysis in Nakagami-lognormal fading (i.n.i.d) channel with different values of fading parameter (m) in five hop network

In depth analysis of graph shown in Figure 5 represents that the variation in P_d with standard deviation (σ) in (i.i.d) wireless links. Figure clearly describes that the as shadowing severity increases, the detection probability decreases for composite fading channel with m=2. Both the parameters follow the inverse relation property. The simulations are carried out for 3 hops network with each hop carries wireless links with an average SNR of 8dB. Similar analysis can be performed for 4 and 5 hopped networks with different average SNR within channel.

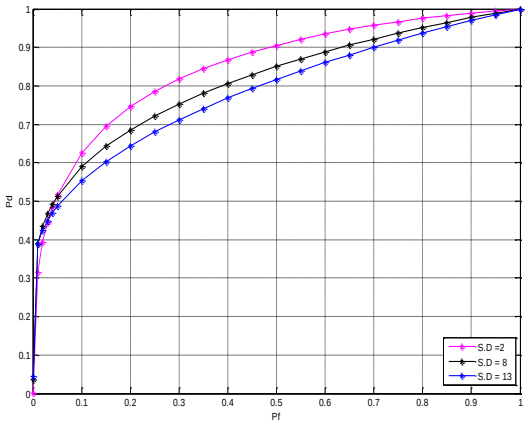

Figure 5. ROC analyses in Nakagami-lognormal faded (i.i.d) channel with different values of shadowing parameter (σ) in a three hop network

Similar analysis has been also been performed in Figure 6 by considering (i.n.i.d) wireless channels within hops of 4 hop network. The SNR within hops are the variable parameter with the assumption that it goes on increasing as the number of hops. For the simulations the direct channel with SNR 5dB is also associated with multihop network. The SNR within hops are assumed as (8dB, 12dB, 15dB and 18dB) respectively. It is clearly revealed from the both the Figures 4 and 5 that the shadowing severity affects the detection probability irrespective of the type of channel and number of hops.

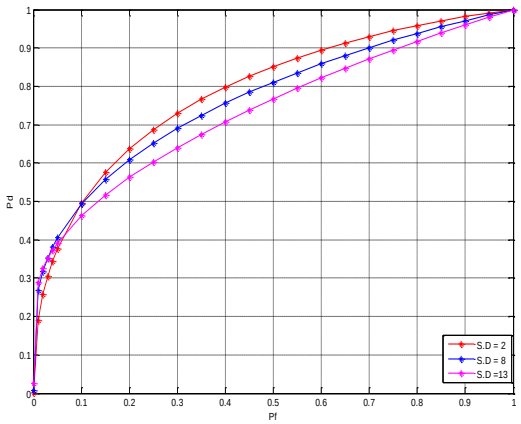

Figure 6. ROC analysis in Nakagami-lognormal faded (i.n.i.d) channel with different values of shadowing parameter (σ) in a four hop network.

Figures 7 and 8 represents an interesting fact that the type of relay within a multihop network also affects the sensing performance. The value of *Pd* is greater for the fixed value of *Pf*, in case we take up DF relays rather than the AF relays within a multihop wireless link. In Figure 6 we have analyzed the spectrum sensing with different types of relays by considering Nakagami-lognormal faded (i.i.d) channel with 8dB average SNR and having fixed value of standard deviation σ=8 within hops of the three hop network. Similar analysis has been also performed in Figure 7 by considering (i.n.i.d) wireless channels within hops of 3 hop network. The direct channel with average SNR 8dB is also associated with multihop branch. The SNR within hops are assumed as (8dB, 12dB and 15dB) respectively.

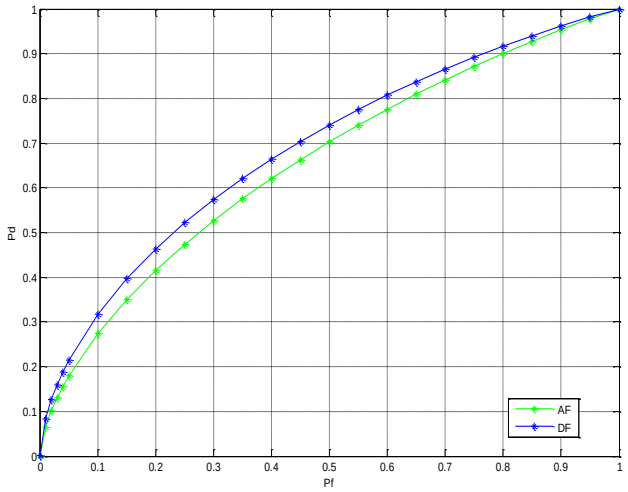

Figure 7. ROC analysis for Nakagami-lognormal faded (i.i.d) channels within 3 hop network

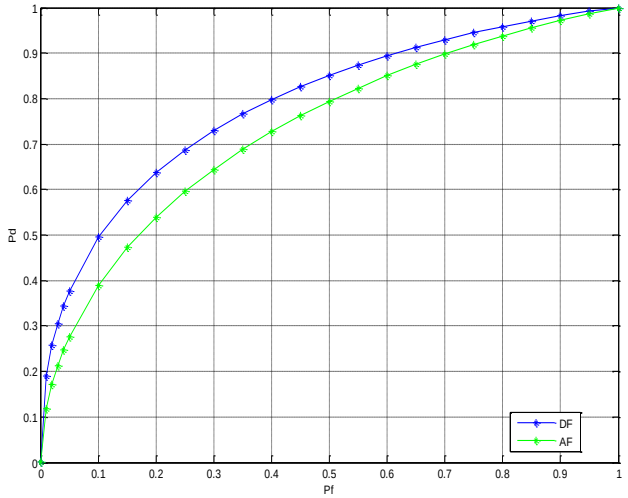

Figure 8. ROC analysis for Nakagami-lognormal faded (i.n.i.d) channels within 3 hop network

5. Conclusion

We have deliberated to do the spectrum sensing with an energy detector for a cognitive radio network with composite fading channels. All the wireless transmission systems are characterized by inefficient static spectrum allocations, imperfect channel distributions, fixed radio frequency bands, random distance between source to destination and imperfect network coordination. In wireless networks, as the distance between sources to destination keeps on increasing, for better reception it is necessary to incorporate relays within a link. The lesser power is need for transmission in multihop networks, but smaller number of hops reduces path loss. The analysis covers the receiver operating curves (ROC) representing detection probability for cascaded multihop link. It is also shown that the spectrum sensing employed in the cognitive radio network depends upon channel conditions. For good channel conditions higher number of hops can be used to achieve desired detection probability. Further for future work, the single branch multihop network can be augmented to multi-branch multihop network for the performance analysis with different diversity combining techniques at the receiver.

References

[1] J. Mitola, III and G. Q. Maguire Jr., "Cognitive radio: Making software radios more personal", IEEE Pers. Commun., vol. 6, no. 4, **(1999)**, pp. 13–18.
[2] S. Haykin, "Cognitive radio: Brain-empowered wireless communications", IEEE Journal on Selected Areas in Communications, vol. 23, no. 2, **(2005)**, pp. 201–220,.
[3] FCC, "Spectrum Policy Task Force", ET Docket 02-135, **(2002)**.
[4] F. F. Digham, M. -S. Alouini and M. K. Simon, "On the Energy Detection of Unknown Signals Over Fading Channels", IEEE International Conference on Commun., ICC, vol. 5, **(2003)**, pp. 3575–3579.
[5] S. Atapattu, C. Tellambura and H. Jiang, "Relay based cooperative spectrum sensing in cognitive radio networks", in Proc. IEEE Global Telecommun. Conf., (**2009)**.
[6] G. Ganesan and Y. Li, "Cooperative spectrum sensing in cognitive radio, part I: Two user networks", IEEE Transactions on Wireless Communications, vol. 6, no. 6, **(2007)**, pp. 2204–2213.
[7] I. F. Akyildiz, W. Y. Lee, M. C. Vuran and S. Mohanty, "Next generation/dynamic spectrum access/cognitive radio wireless networks: A Survey", Elsevier Computer Networks Journal, vol. 50, **(2006)**, pp. 2127-2159.
[8] S. Attapattu, C. Tellembura and H. jiang, "Energy Detection Based Cooperative Spectrum Sensing in Cognitive Radio Network", IEEE Transaction on Wireless Communication, vol. 10 no. 4, **(2011)**, pp. 1223-1241
[9] V. Ashgari, D. B. da-Costa and S. Aissa, "Performance Analysis of Multihop Relaying Channels with Nakagami-m Fading: Ergodic Capacity Upper-Bounds and Outage Probability", IEEE Transactions on Communications, vol. 60, no. 10, **(2012)**.
[10] M. O. Hasna and M. S. Alouini, "End-to-End Performance of Transmission Systems with Relays over Rayleigh Fading Channels", in IEEE Transactions on Wireless Communications, vol. 2, no. 6, **(2003)**, pp. 1126 -1131.
[11] M. O. Hasna and M. S. Alouini, "Outage Probability of Multihop Transmission over Nakagami Fading Channels", IEEE Communication Letters, vol. 7, no. 5, **(2003)**, pp. 216-218.
[12] M. O. Hasna and M. S. Alouini, "Harmonic Mean and End-to-end Performance of Transmission Systems with Relays", IEEE Transactionson on Communication, vol. 52, no. 1, **(2004)**, pp. 130– 135.
[13] G. K. Karagiannidis, T. A. Tsiftsis and R. A. Mallik, "Bounds for Multihop Relayed Communications in Nakagami-m Fading", IEEE Transactions on Communications, vol. 54, no. 1, **(2006)**, pp. 18 – 22.
[14] M. O. Hasna and M. S. Alouini, "A Performance Study of Dual-Hop Transmissions with Fixed Gain Relays", IEEE Transactions on Wireless Communications, vol. 3, no. 6, **(2004)**.
[15] N. C. Beaulieu and J. Hu, "A Closed-form Expression for the Outage Probability of decode-and-forward Relaying in dissimilar Rayleigh Fading Channels", IEEE Communication Letters, vol. 10, no. 12, **(2006)**, pp. 813-815.
[16] I. S. Gradshteyn and I. M. Ryzhik, "Table of Integrals, Series, and Products", San-Diego, CA: Academic Press, sixth edition, **(2000).**
[17] G. L. Stüber, "Principles of Mobile Communication", 3rd ed. Norwell, MA, USA: Kluwer Academic Publishers; **(2001)**.

[18] M. Abramowitz and I. A. Stegun, (Eds.), "Handbook of Mathematical Functions: with Formulas, Graphs and Mathematical Tables", New York: Dover Publications; **(1965)**.
[19] M. Wiper, D. R. Insua and F. Ruggeri, "Mixtures of Gamma Distributions with Applications", Journal of Computational and Graphical Statistics, vol. 10, no. 3, **(2001)**, pp. 440-454.
[20] I. S. Gradshteyn and I. M. Rhyzik, "Table of Integrals, Series and Products", 7th ed. New York: Academic press; **(2007)**.

Authors

Deepti Kakkar

Deepti Kakkar was born in 1982, in Jalandhar, Punjab, India. She did her Bachelor of Technology in Electronics and Communication Engineering from Himachal Pradesh University, India in 2003 and Masters of Engineering in electronics product design and technology from Punjab University, Chandigarh. Deepti is currently pursuing her research in Cognitive Radios towards completion of her PhD from Dr. B.R. Ambedkar National Institute of Technology, Jalandhar, India. She has a total academic experience of 7 years and at present she is ASSISTANT PROFESSOR in Electronics and Communication department with Dr. B. R. Ambedkar National Institute of Technology, Jalandhar, India. Earlier, she had worked as lecturer in Electronics and Communication department with DAV Institute of Engineering and Technology, Jalandhar, Punjab. She has guided 9 post graduate engineering dissertations and several projects. She has ten papers in the proceedings of various International Journals and Conferences. Her recent research interests include dynamic spectrum allocation, spectrum sensing, software defined radios and Cognitive Radios.

Arun Khosla

Arun Khosla received his Ph.D degree from Indraprastha University, Delhi in the field of Information Technology. He is presently working as ASSOCIATE PROFESSOR and HEAD of Department of Electronics and Communication Engineering, National Institute of Technology, Jalandhar. India. **Dr. Khosla** has been reviewer for various IEEE and other National and International conferences and also serves on the editorial board of International Journal of Swarm Intelligence Research. He is a life member of Indian Society of Technical Education. He has a total academic experience of 24 years and at present he is ASSOCIATE PROFESSOR and HEAD in Electronics and Communication Department with Dr. B. R. Ambedkar National Institute of Technology, Jalandhar, India. Four research scholars have completed their Ph.D under his guidance and three more are pursuing the same. He has guided more than 10 post graduate engineering dissertations and several projects.

Moin Uddin

Moin Uddin is a senior member, IEEE. Moin Uddin did his B.Sc Engineering in 1972 and M.Sc. Engineering in 1978 from Aligarh Muslim University, Uttar Pradesh, India. He completed his Ph.D in 1993 from Roorkee University, India. He has more than 35 years of total experience in academics and research and was former PRO-VICE CHANCELLOR of Delhi Technical University, Delhi, India. Prior to that he was Director of Dr. B. R. Ambedkar National Institute of Technology, Jalandhar, India, since 2005. Prior to this, he was PROFESSOR and HEAD, Electrical Department at Jamia Millia Islamia University, New Delhi. Twenty five research scholars have completed their Ph.D under his guidance and seven more are pursuing the same. He has designed the computer engineering curriculum of many international and national universities and institutions and is among the expert panel of these universities. Prof. Moin Uddin is a life member ISTE national society and member, board of studies of many institutions. He has successfully completed several projects under Ministry of Human Resource Development and All India Council for Technical education, Govt. of India.

International Journal of ChemTech Research
CODEN(USA): IJCRGG ISSN : 0974-4290
Vol.6, No.1, pp 236-247, Jan-March 2014

Spectrophotometric Determination of Complexation of Ruthenium (IV) with 2-[(5-Bromo-2-Pyridylazo)]-5-Diethylaminophenol and N-Hydroxy-N, N′-Diphenylbenzamidine

Pushpa Ratre[1]* and Devendra Kumar[2]

[1, 2]Department of Applied Chemistry and Polymer Technology
Delhi Technological University (Formerly Delhi College of Engineering)
Shahbad Daulatpur, Bawana Road, Delhi-110042, India

*Corres. Author: pushpa.ratre.delhi@gmail.com

Abstract: A new, simple and selective spectrophotometric method has been developed for the determination of trace amount of Ru(IV) which is based on the formation of orange colored mixed complex of ruthenate ion (RuO_4^{2-}) with 2-[(5-bromo-2-pyridylazo)]-5-diethylamino-phenol (5-Br-PADAP). The orange color complex was extractable with seven derivative of N-hydroxy-N,N'-diphenylbenzamidine (HDPBA) in dichloromethane in the ratio of tri-sodium citrate dehydrate to sodium acetate at 1:3. The molar absorptivity of Ru(IV)-(5-Br-PADAP)-HDPBA complex in dichloromethane at absorption maxima of 560 nm was calculated to be 3.0×10^4 Lit mol^{-1} cm^{-1} with the mole ratio of metal to ligand in the complex being at 1:1:1. The stability constant of the complex was calculated to be 4.73 dm^3mol^{-1} at 28°C. The system obeyed Beer's law up to 1.0 to 14.0 µg Ru(IV) per 5 mL in organic phase with the detection limit of the method at 2σ being 12.0 ng mL^{-1}. Most of the foreign ions do not interfere with the proposed method except palladium. The method has been successfully applied for the determination of trace analysis of Ru(IV) in real sample, synthetic mixture and different sources of water with the RSD value ranging between ±0.71% and ±4.75%. The proposed method caused the recovery of metal ions to be in the range of 86.0% to 101.5%.

Keywords: Ru(IV), 5-Br-PADAP, HDPBA, Spectrophotometric, Orange color complex.

1. Introduction

Ruthenium, which is associated with platinum ores, is a rare transition element found in about 10^{-8} % of the earth's crust. It is a hard, white metal discovered by Karl Klaus in 1844. The larger amount of ruthenium is found in chondrite and iron meteorites (10^{-6}–10^{-4})%[1]. All ruthenium compounds are highly toxic and carcinogenic. Compounds of ruthenium stain the skin very strongly and the ingested ruthenium is seen to be retained strongly in bones[2]. Nowadays, compounds and complexes of ruthenium have come to be used as drugs for treatment of cancer and tumor[3]. Some other applications include a ruthenium NO donors,

cis-[Ru(NO)(bpy)$_2$L]X*n* being used for Chagas's disease[4], ruthenium octahedral metal complexes being used as inducer for structural analysis of DNA[5], a ruthenium based catalysts being used for synthesis of ammonia, pharmaceutical industry[6] and fabrication of dye-sensitized solar cells (DSSCs)[7], etc.

In the proposed method, the hydroxyamidine is used as extracting analytical reagent. These reagent forms orange colored complexes with ruthenium (IV)-2-[(5-bromo-2-pyridylazo)]-5-diethylaminophenol (5-Br-PADAP) in the presence of the halo-group attached to the carbon atom and carbon-nitrogen double bond [8-10]. These hydroxyamidine is widely used in quantitative determination of metal ions in environment, organic, inorganic and pharmaceutical analysis. Recently, it has found a way in biotechnology as prodrugs of amidines (amidoximes) to study the reduction and hydrolytical metabolism of ximelagatran via two mono-prodrugs (*N*-hydroxy-melagatran and ethyl-melagatran)[11, 12].

Nowadays, new analytical techniques have been developed for the determination of ruthenium in trace quantities in various complex matrices, e.g., ores, alloys, seawater, biological samples, etc and in synthetic samples, e.g., electrothermal atomic absorption spectrometry[13], atomic absorption spectrometry (AAS)[14], flow injection analysis (FIA)[15], x-ray photoelectron spectroscopy[16], high-performance liquid chromatography [17], voltametric method[18], flow injection chemiluminescent[19], etc. Although all these techniques are highly sensitive but required costly maintenance and skilled hands for operation and are quite expensive. Instead, the spectrophotometric method is more popular and cheaper technique.

A survey of literature reveals that a lot of reagents, compound and surfactant have been employed for the determination of ruthenium. Kuchekar et al.[20] used a reagent *o*-methylphenyl thiourea for the extraction of ruthenium but the method was less sensitive. Gopala Krishna et al.[21] developed a 4-Hydroxy 3,5-dimethoxy Benzaldehyde-4-hydroxy Benzoylhydrazone [HDBHB] for the extraction of ruthenium but the method suffered from interference of Cu^{+2} and Fe^{+3}. Mathew et al.[22] developed a method which suffered from interferences of foreign ions using schiff's base derived from a triazine. Lokhande et al.[23] developed a less sensitive method for the analysis of ruthenium using Pyrimidine-2-thiol as reagent along with *N*-octylaniline as an extractant. El-Shahawi et al.[24] developed a less sensitive method using benzyltributylammonium chloride for the determination of ruthenium. Alaa et al.[25] described the solid phase extraction method using quinoxaline dyes into microcrystalline *p*-dichlorobenzene for trace analysis of ruthenium but it is a tedious job to filter the derivative of reagent mixed with ruthenium. El-Shahawi et al.[26] used a sodium periodate as a reagent for developing a iodometry titration and spectrophotometric method for the determination of ruthenium but the drawback of these method is precipitation of iodine which decreases the molar absorptivity. Islam et al.[27] used a reagent 3-(2-Pyridyl)-5,6-diphenyl-*as*-triazine (PDT) and ferrozine together to reduce the extraction time of ruthenium but was not able to increase its molar absorptivity. Keyvanfard et al.[28] studied the kinetic reaction and oxidation of metaperiodate in micellar medium for the determination of ruthenium but the method had low sensitivity. Solovey-Vandersteen et al.[29] used a reagent "xylenol orange" for the determination of ruthenium but the method had low molar absorptivity. Balcerzak et al.[30] used a high molecular weight amines for analysis of ruthenium but method was based on tedious job of preparation of compound. Druskovic et al.[31] used a reagent 4-pyridone derivatives for determination of ruthenium but the method had low molar absorptivity. Rezaei et al.[32] developed a less sensitive method for estimation of ruthenium which was based on oxidation of safranin O by metaperiodate. Hong-fu et al.[33] using a reagent malachite green, Praveen Kumar et al.[34] using a reagent 1,10-phenanthroline and Zhi-rong et.al[35] using a reagent chrome blue K contributed to a less sensitive method for ruthenium.

The chief goal of the present work is to achieve a new, simple, more sensitive and reproducible method for the determination of Ru(IV) in the environmental samples. The trace amount of Ru(IV) has spectrophotometrically determined with 5-Br-PADAP in the presence of appropriate ratio of tri-sodium citrate and sodium acetate and its subsequent extraction with hydroxyamidines (HOA) in dichloromethane. By using the extraction method of Ru(IV) with HOA, most of the common ions do not interfere with the proposed method.

2. Experimental

2.1 Instrumentation

For characterization of ruthenium (IV) complex, double beam UV-Visible spectrophotometer 54440SS model equipped with 1cm quartz cell was used. A digital pH meter (DB-1011) was calibrated regularly with a standard buffer solution before use.

2.2 Reagents

All chemicals used were procured from Sigma Aldrich and E. Merck. Millipore double distilled water was used for the preparation of all solutions. The standard solution of ruthenium ($RuO_2.XH_2O$) was prepared by fusion of 75.0 mg of pure ruthenium powder in a 15 mL silver crucible with 1.0 g of sodium hydroxide and 0.20 g of sodium peroxide at dull-red heat for 10 min. The residue was dissolved with 2.0 mol L^{-1} sodium hydroxide in a 500 ml standard flask and made up to the mark[36]. The stock solution of 9.92×10^{-3}mol L^{-1} was standardized by thiourea method[37]. The lower concentration of solutions was prepared by diluting the stock solution.

A 3.47×10^{-3} mol L^{-1} (0.1%, w/v) solution of N-Hydroxy-N, N'-diphenylbenzamidine (HDPBA) (98.0% pure) was prepared in dichloromethane. A 2.89×10^{-4} mol L^{-1} (0.01%, w/v) 2-[2-(5-bromopyridyl) azo]-5-dimethylaminophenol **(**5-Br-PADAP) (97.0% pure) solution in methanol (95.0% pure) was employed for color development. A 3.40×10^{-2} mol L^{-1} (1.0%, w/v) of tri-sodium citrate dihydrate (TSC) and 2.0 mol L^{-1} (16.4%, w/v) solution of sodium acetate (SC) were prepared in distilled water. The above solutions were mixed in a volume ratio of 1:3, 1:2, 1:1, 2:3 (TSC: SC) in a final 12.0 mL volume is equivalent to pH 11.0±02. The solutions of diverse ions were prepared in mg/mL solutions of the ions as given in the literature[38].

2.3 General Procedure

Take an aliquot of the standard solution containing up to (1.0 to 14) µg/mL or (6.62×10^{-6} to 9.26×10^{-5}) mol L^{-1}Ru (IV) in a 125mL separatory funnel. To the above solution, add 0.6 mL of 5-Br-PADAP and then buffering the complex with mixture of (1:3) TSC-SC solutions up to total volume of 10.0 mL. The orange colored complex formed immediately within 2 min which was extracted with 3.0 mL of HDPBA solution prepared in dichloromethane. Wash the aqueous phase with 2x1 ml fresh dichloromethane. Then separate the orange colored dichloromethane extracts and dry over anhydrous sodium sulfate (≈2 gm) in a 10.0 mL beaker. Transfer the combined extract into a 5.0 mL volumetric flask. Measure the absorbance of the complex against the solvent at λ_{max} 600 nm and 560 nm.

2.4 Sampling and Sample Preparation

2.4.1 Platinum Crucible

A different known amount of platinum crucible were weighed and dissolved in hot aquaregia to remove Osmium, if present in the solution. The resultant solution was evaporated three times with small amount of hydrochloric acid in order to remove nitric acid. The residues were diluted with 2 mol L^{-1} sulphuric acid and RuO_4 was separated by distillation after the oxidation of ruthenium by 0.02 mol L^{-1} $KMnO_4$. The volatile RuO_4 was absorbed in 2.0 mL of hydrochloric acid and the solutions were diluted to 10 mL in a volumetric flask with distilled water. The amount of ruthenium present in different sample solutions prepared as above was determined by the proposed method with the help of the pre-determined calibration plot.

2.4.2 Synthetic Mixtures and Water Samples

The synthetic mixtures were prepared according to the composition of ruthenium alloys which contain ruthenium and other platinum group metals and some transition series elements. Take a portion of synthetic mixture and follow the above procedure. The concentration of Ru (IV) present in mixture was determined with help of standard addition method.

The sample bottles were soaked in 10 percent HNO_3 for 24 h and rinsed several times with double distilled water prior to use. The water samples were filtered through 0.45 µm membranes filter and preserved with concentrated nitric acid to bring down the pH to < 2.0. The samples thus preserved were stored at 4ºC in

sampling kits and brought to the laboratory for metal analysis. The concentrations of Ru (IV) present in water samples were determined with the help of standard addition method.

3. Results and Discussion

The development of new analytical method for determination of Ru (IV) has been done by extracting Ru (IV)-(5-Br-PADAP)-HDPBA complex from dichloromethane in the presence of TSC-SC mixture. The optimum experimental conditions and some important spectral and statistical data obtained for the determination of Ru (IV) in the proposed method have been summarized in Table 1.

3.1 Spectral Studies

The complex Ru (IV)-(5-Br-PADAP) in aqueous and organic (HDPBA-dichloromethane), exhibits maximum absorbance at around 600 nm and 560 nm against the solvent (Figure 1). The reagent blank in both phase shows some absorbance (A=0.04) at this region and hence it was used in all experimental work.

3.2 Effect of Extraction Solvent

Ruthenium(IV) complex is extractable into many polar and non-polar solvents, such as ethyl acetate ($\varepsilon = 1.10\times10^4$ L mol^{-1} cm^{-1}), isobutyl methyl ketone ($\varepsilon = 0.62\times10^4$ L mol^{-1} cm^{-1}), toluene ($\varepsilon = 2.81\times10^4$ L mol^{-1} cm^{-1}), benzene($\varepsilon = 1.73\times10^4$ L mol^{-1} cm^{-1}), chloroform ($\varepsilon = 2.99\times10^4$ L mol^{-1} cm^{-1}), dichloromethane ($\varepsilon = 2.99\times10^4$ L mol^{-1} cm^{-1}), *etc.* with value of $\lambda_{max,}$ 560 nm in all cases as shown in Table 2. The sensitivity of complex in terms of molar absorptivity in both dichloromethane and chloroform is maximum and similar. However, dichloromethane is preferred because of its less toxic nature than chloroform. Thus, due to its superiority, dichloromethane was therefore chosen as solvent for the extraction of Ru(IV)-(5-Br-PADAP)-HDPBA complex.

Figure 1 Absorption spectra of Ru(IV)-(5-Br-PADAP) complex in aqueous and organic phase against solvent. Ru(IV)[1.97×10^{-5} mol L^{-1}], aqueous phase; 5-Br-PADAP [5.72×10^{-5} mol L^{-1}]; TSC-SA[1:3] ; HDPBA[2.08×10^{-3} mol L^{-1}]

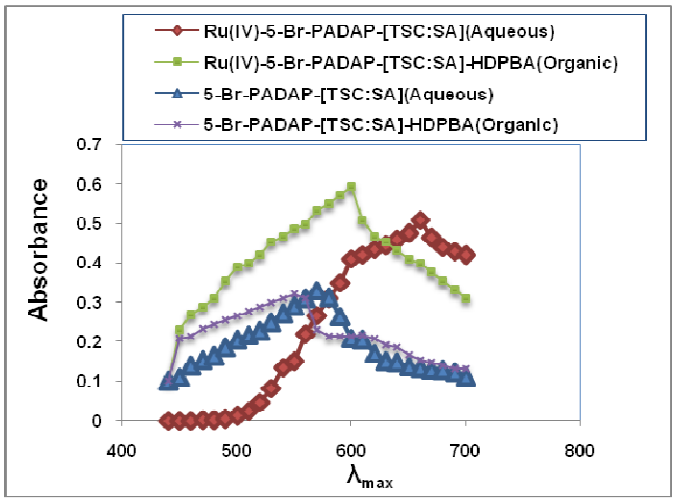

Table 1. Analytical Parameters of Ru(IV)-5-Br-PADAP-HDPBA in dichloromethane.

Colour of the complex	Orange
λ_{max}	600 nm[aqueous], 560 nm [organic phase]
TSC: Sodium Acetate	[1:3]
Concentration of 5-Br-PADAP	5.72×10^{-5} mol L^{-1}
Concentration of HDPBA	2.08×10^{-3} mol L^{-1}
Composition of complex (M: L:L)	1:1:1
Stability constant of the complex	4.731 dm^3mol^{-1} at 28°C
Beer's law	1.0 to 14 μg/5 mL
Molar absorptivity	3.0×10^4 L mol^{-1} cm^{-1}
Standard deviation (SD) N=10, Relative standard deviation(RSD) N=10	±0.0031, 0.52%
Stability of complex	24h
Sendell's Sensitivity, Detection limit (2σ) N=10	0.0033 μg cm^{-2}, 12 ng mL^{-1}
Intercept, slope, correlation coefficient	-0.00070, 0.060, 1.0

Table 2 Effect of solvent on the extraction of Ru(IV)-(5-Br-PADAP)-HDPBA complex

Solvent	**Ru(IV), $\lambda_{max,}$ nm**	**Molar absorptivity(ε) L mol^{-1} cm^{-1} $\times10^4$**	**% Extraction**
Ethyl acetate	500	1.113	53.5
Isobutyl methyl ketone	505	0.620	85.5
Xylene	560	0.235	75.0
Benzene	410	1.732	50.5
Toluene	400	2.810	50.0
Carbon tetrachloride	500	0.121	70.5
Chloroform	560	3.070	99.5
Dichloromethane	560	3.270	99.5

3.3 Effect of Derivatives of N-Hydroxy-N,N'-Diphenylbenzamidine (HDPBA)

The spectral characteristics of Ru(IV)-5-Br-PADAP complexes were examined using seven different derivatives of hydroxyamidines (HOAs) in dichloromethane. Compounds with chloro(Ph)- and methyl(Ph')-substitution in two phenyl rings of N'-atom in HOA were used. The complexes with various HOAs show different values of molar absorptivity, at their respective λ_{max}. Introduction of methyl (+I) or chloro (-I) group at *N'*-phenyl ring of HOAs slightly reduces the sensitivity in the following order C_6H_5 >4-CH_3-C_6H_4 (Ph'-) > 3-CH_3-C_6H_4 (Ph'-) > 2-CH_3-C_6H_4 (Ph'-) > 4-Cl-C_6H_4(Ph-) > 3-Cl-C_6H_4(Ph-) > 2-Cl-C_6H_4(Ph-) as shown in Figure 2. The parent compound, HDPBA was chosen due to reasons, namely relatively easier synthesis, large yield of the compound and high reproducibility of the result.

3.4 Effect of Reagents

The result obtained indicated that at least $(4.00\text{-}6.29)\times10^{-5}$ mol L^{-1} of the reagent in ethanol is required for maximum complexation. In subsequent studies, 5.72×10^{-5} mol L^{-1} of 5-Br-PADAP was used. The concentration of HDPBA in dichloromethane in the range of $(1.73\text{-}3.12)\times10^{-3}$ mol L^{-1} was adequate for the complete extraction of the complex. Therefore, a 2.08×10^{-3} mol L^{-1} HDPBA was employed throughout the experiment. The concentration ranges of both the reagent were shown in the Figure 3.

3.4.1 Effect of Mixed Ratio of Tri-sodium Citrate (TSC)-Sodium Acetate (SC)

Tri-sodium citrate dihydrate and sodium acetate are widely used in foods, beverages and various technical applications in industry, mainly as buffering, sequestering or emulsifying agent and stabilization of reactions. The TSC-SC mixture is used as stabilizer in our experiment.

The effect of concentration and volume ratio of TSC and SC on the absorbance and percentage of extraction of the complex were studied. The concentration range of $(2.72\text{-}4.76)\times10^{-3}$ mol L^{-1} TSC and 0.4-1.2

mol L^{-1} SC was sufficient for maximum color development and stabilization of complex. Hence the author has chosen the mixture ratio of 3.40×10^{-3} mol L^{-1} TSC and 0.60 mol L^{-1} sodium acetate solution for further studies.

The effect of volume ratio of TSC: SC on the percentage of extraction of Ru (IV)-complex is as shown in Figure 4. The volume ratio of 1:2, 2:3, 1:1 and 1:3 were sufficient for the stability of the complex and show a maximum percentage of extraction of (89.4 to 89.8) of the complex at wavelength of 560 nm. There were no change in the *p*H of the complex up to (~ 11.0 ± 0.2), since RuO_4 was prepared in strong alkaline medium using NaOH fusion process.

3.5 Effect of Temperature, Electrolyte and Dilution

The variation in temperature of the aqueous phase from 10 to 50°C has no adverse effect on the extraction of the metal ions. Beyond this temperature range, the absorbance of the complex starts decreasing. Hence, all extraction work was carried out at room temperature.

Addition of 1 molL^{-1} $KCl/NH_4Cl/K_2SO_4$ solutions does not change the absorption characteristics and neither the shift in λ_{max} nor any change in absorbance of the complex was observed.

The effect of variation in the volume of the aqueous phase, keeping the other variables constant, on the extraction of the metal with HDPBA was studied. No change in the absorbance of the metal complex was observed on varying the volume ratio of the organic to aqueous phase from 1:4 to 1:1. For the sake of uniformity, all extraction was performed at a 1:1 volume ratio for both phases.

3.6 Stability Constant, Ionic Strength and Composition of the Ru(IV)-Complex

The stability constant(K') of the complex formed were calculated through Job's method[40] at the ratio of TSC: SC[1:3] and ionic strength (mμ) of 7.94×10^{-4} mol L^{-1} was calculated to be 4.731 dm^3mol^{-1} at 28°C for the complex Ru(IV)-(5-Br-PADAP)-HDPBA.

Figure 2 Absorption spectra of Ru(IV)- (HOA'S) Deivatives Complexes. Ru(IV)[1.97×10^{-5} mol L^{-1}]; 5-Br-PADAP[5.72×10^{-5} mol L^{-1}]; TSC-SA(1:3) ; HOA'S[2.08×10^{-3} mol L^{-1}]; [a] C_6H_5 ; [b] 4-CH_3-C_6H_4 (Ph'-); [c] 2-CH_3-C_6H_4 (Ph'-) ; [d] 4-Cl-C_6H_4(Ph-); [e] 3-Cl-C_6H_4(Ph-) [f] 2-Cl-C_6H_4(Ph-)

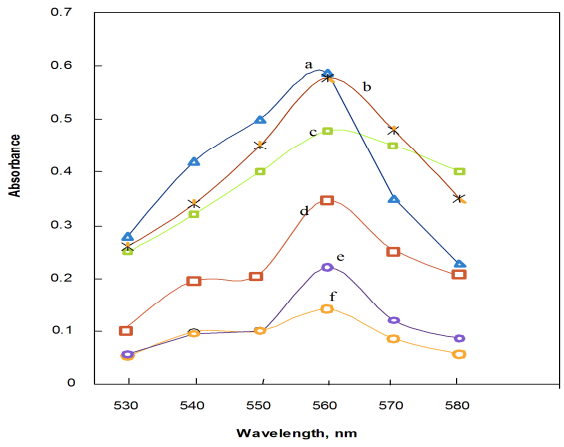

Figure 3 Effect of Reagent concentrations on Ru(IV)- complex in dichloromethane. Ru(IV)[1.97×10^{-5} mol L^{-1}]; TSC-SA(1:3)

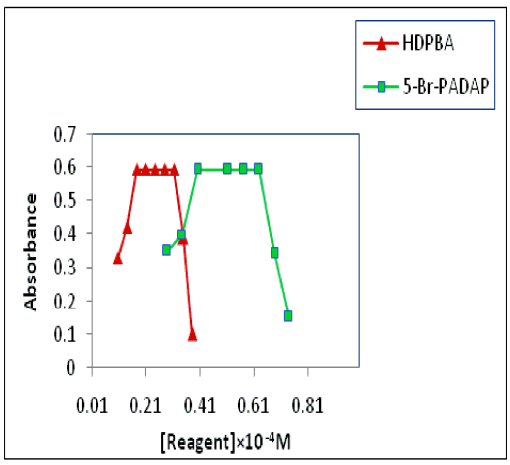

The composition of the ruthenium (IV) complex was determined by the curve fitting method[39] and Job's continuous variation method[40]. The molar ratio of metal to 5-Br-PADAP and HDPBA was determined by plotting logarithmic value of distribution ratio of metal versus logarithmic values of varied known concentrations of 5-Br-PADAP/ HDPBA in dichloromethane. The inclination of the curves for 5-Br-PADAP and HDPBA were found to be very close to integer 1 in all cases. Thus Figure 5 shows a 1:1:1 molar ratio complex of Ru(IV): 5-Br-PADAP: HDPBA in dichloromethane. The ruthanate ion, RuO_4^{2-}, forms a stable 1:1 mixed ligand complex by replacing H^+ available essentially in alkaline medium (pH > 9.0) from both OH-groups present in 5-Br-PADAP as well as in HOA. The probable reaction mechanism is as shown below.

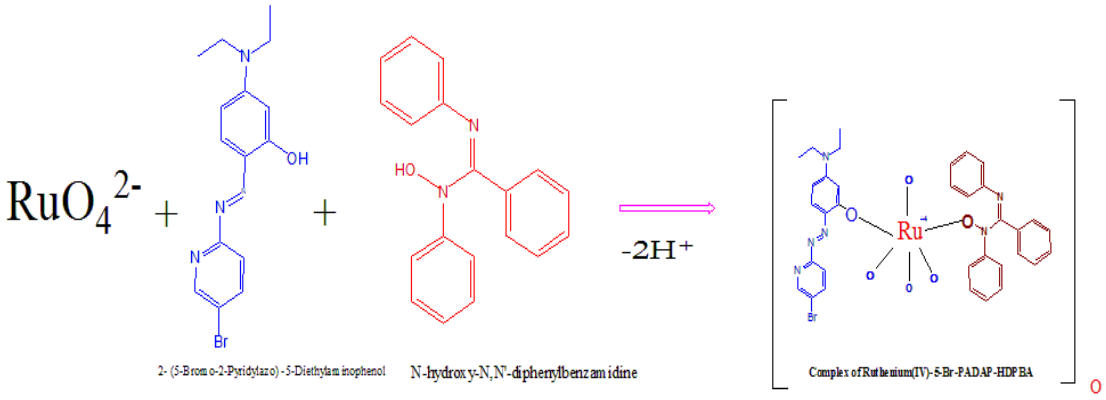

Subscript "$_o$" here indicates organic phase *i.e.* dichloromethane and abbreviations HL and HOA have been used for representing 5-Br-PADAP and N-hydroxy-N,N'-diphenylbenzamidine, respectively.

Figure 4 Effect of volume ratio of TSC and SA on extraction of Ru(IV)-(5-Br-PADAP)-HDPBA complex. Ru(IV)[1.97×10^{-5} mol L^{-1}] ; 5-Br-PADAP[5.72×10^{-5} mol L^{-1}]; HDPBA[2.08×10^{-3} mol L^{-1}].

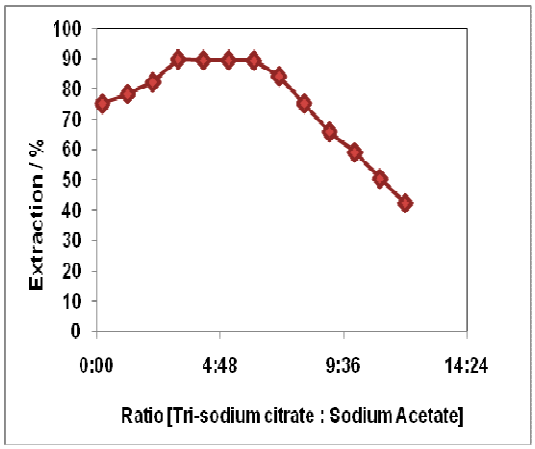

Figure 5. Plot of curve-fitting method for determination of molar ratio of Ru(IV) to 5-Br-PADAP and HDPBA in Ru(IV)- complex.

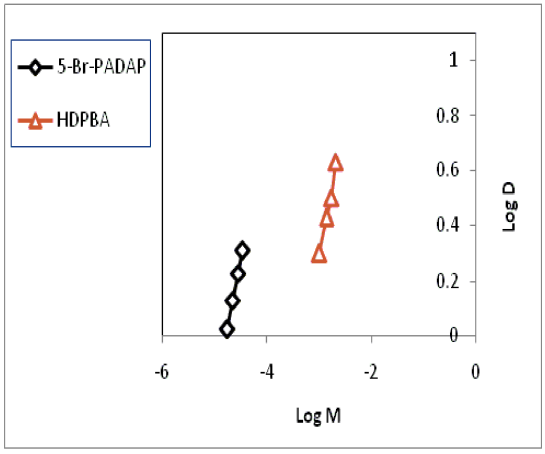

3.7 Beer's law, correlation Coefficient, Molar Absorptivity, Sensitivity, Detection Limit and Precision

The orange coloured Ru(IV)-5-Br-PADAP-HDPBA complex obeyed Beer's law up to 1.0-14.0µg Ru(IV)/5mL in both aqueous and organic phase at λ_{max} 600 nm and 560 nm respectively, as shown in Figure 6. Intercept, slope, correlation coefficient, (2σ) detection limit, Sandell's sensitivity [41] are as given in Table 1. The molar absorptivity value of the complex with various hydroxyamidines (HOA) tested to lie in the range is (2.8-3.0)×10^4 L mol^{-1} cm^{-1}. The molar absorptivity value of orange colored Ru(IV)- 5-Br-PADAP complex in aqueous and organic phase were 2.57×10^4 L mol^{-1}cm^{-1} at 600 nm and 3.0×10^4 L mol^{-1}cm^{-1} at 560 nm respectively. The precision of the method was checked by taking 10 replicate measurements each containing 6.62×10^{-5} mol L^{-1} Ru(IV) per 5 mL organic phase. The mean absorbance value and the standard deviation value

were calculated to be 0.593 and ±0.003, respectively which gave a relative standard deviation of 0.52%. The range within which the value of molar absorptivity of the system may fall with the measured precision at 95% confidence level was calculated and the value of confidence limit [41] in terms of molar absorptivity was found to be $(3.0\pm0.03)\times10^4$ L $mol^{-1}cm^{-1}$.

3.8 Effect of Diverse Ions

To study the effect of diverse ions [42], variable amounts of foreign ions were introduced to a fixed amount of ruthenium (IV). PGEs, namely Pd (II) interferes at concentrations > 2-fold excess. However, interference due to Pd (II) may be minimized by masking it with 3 ml of 4% sodium thiosulphate. Mn(II) and Pb(II) are tolerated not more than 10-fold excess concentration. The tolerance limit of various diverse ions, in mg, in the determination of 1.0 µg Ru(IV)/mL is summarized in Table 4.

3.9 Applications

The proposed method was successfully applied for the determination of Ruthenium (IV) in real samples (Platinum crucible), synthetic mixture and different sources of water samples. The trace amount of Ruthenium (IV) present was determined by standard addition method and actual concentration is calculated from a pre-determined calibration plot. The result presented in Table 5 shows a concentration of Ru(IV) present in real samples was found to lie between 2.87-3.0 µg / mL with RSD value ranging from ±1.50 % to ± 2.85 % and percentage recovery of metal ions was determined between 96.0 % and 98.50 %. The RSD value obtained for Ru(IV) content in the synthetic mixture and in different sources of water samples ranged between ±1.0 % and ±4.75% . The result obtained from the proposed method was highly satisfactory and it was also verified from the reported method [29] as shown in Table 5,6 and 7.

Table 4 Tolerance limit (TL) of diverse ions in the determination of 10 µg Ru(IV) / 5 mL aqueous phase.

Foreign Ions Added	TL*mg/mL	Foreign Ions Added	TL*mg/mL
Rh(III), Pd(II), Pt(IV),Os(VIII)	2.0, 0. 014[a], 1.0	Bi(III), Mo(VI)	2000, 1000
V(V)	0.9	Co(II), Mg(II), Fe(III)	15, 18, 25
Cu(II),Mn(II),Sb(III),Se(IV),	1.0	Ca(II), Ni(II), Cr(III), Ti(IV), Zr(IV), W(VI)	50
Pb(II), La(III)	2.0, 3.0	Zn(II)	40
Nb(V), U(VI)	4.0, 3.5	Fluoride, Phosphate, Nitrate, Citrate	2.0, 4.0, 10.0, 100
Th(IV), Sr(II)	5.0, 6.0	EDTA, Tartrate, Bromide	140, 300, 200
Hg(II), Be(II)	1.0	Thiosulphate, Oxalate	500, 1000

***Ions were considered to be interfere when they caused a change in the absorbance of the Ru(IV)-(5-Br-PADAP)-HDPBA complex (A=0.593) by ≥ ±≤ 2%. a- Masked by 3 ml of 4% sodium thiosulphate.**

Figure 6 Applicability of Beer's law on Ru(IV)-complex in dichloromethane.

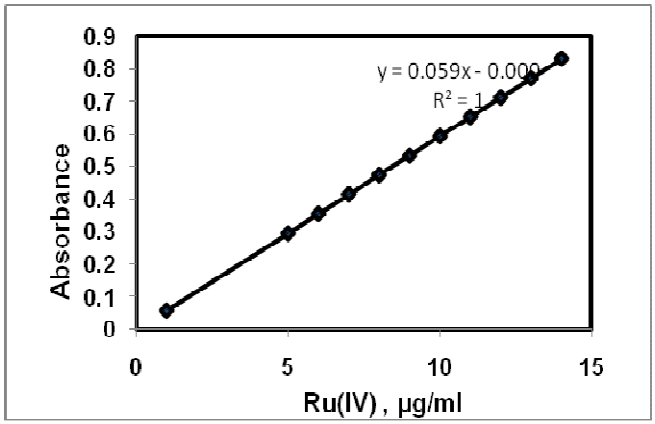

Table 5 Determination of Ru(IV) in Platinum crucible

Weight of the sample (g)	Ru(IV) added, (µg)/mL	Ru(IV) found, (µg) / mL	RSD* ±, %, N=4	(Recovery ± RSD) %, N=4
1.0	----------	2.87	2.00	----
2.0	----------	3.75	2.50	----
2.5	----------	4.00	2.85	------
2.0	5.0	8.25	1.50	96.02 ± 1.7
2.5	5.0	9.50	2.45	97.06 ± 1.5
3.0	5.0	10.55	1.50	98.50 1.7

LEGENDS- N: Number of analysis, RSD: Relative Standard Deviation

Table 6 Determination of Ru (IV) in the Synthetic Mixture.

Sample No.	Synthetic Mixture	Ru found in µg/ 5 mL			
		Proposed method*		Reported method[29]	
		Concentration of Ru(IV), µg/mL	RSD*±, %, N=4	Concentration of Ru(IV), µg/mL	RSD*±, %, N=4
[S-1]	Ru^{IV}(10); Pd^{II}(5);Os^{VIII}(30); Fe^{III}(30); Pt^{IV}(20); Mn^{II}(10).	9.96	1.17	9.90	1.01
[S-2]	Ru^{IV}(20); Co^{II}(10); Ni^{II}(20); Mo^{VI}(10); Fe^{III}(30); Rh^{III}(10).	19.96	1.19	20.1	1.31
[S-3]	Ru^{IV}(10); Rh^{III}(10);Os^{VIII}(15); Pd^{II}(5); Co^{II}(10); Pt^{IV}(20).	10.10	1.58	9.90	1.01

LEGENDS-S-1, S-2, S-3 are the synthetic mixture, N: Number of analysis, RSD: Relative Standard Deviation

Table 7 Determination of ruthenium in different sources of water samples by standard addition method.

Water Samples	Ru(IV) Added, µg / mL	Proposed method, Ru(IV) found, µg/ mL	RSD ±, %, N=4	(Recovery±RSD)%, N=4	Reported method[29] Ru(IV) found, µg/ mL	RSD ±, %, N=4	(Recovery ± RSD)%, N=4
River water	10.0	9.5, 10.0, 10.0, 9.9	2.50	98.5 ± 0.1	9.9, 10.1, 10.0, 9.9	0.71	99.75 ± 0.2
Bore well	10.0	8.5, 9.0, 9.2, 8.7	3.50	88.5 ± 0.1	8.2, 9.0, 9.1, 8.7	4.75	87.5 ± 0.50
Sea water	10.0	10.1, 10.2, 10.0, 10.2	1.70	101.0 ± 0.1	10.1, 10.1, 10.0,10.2	1.80	101.5 ± 0.2
Dam	10.0	8.5, 8.5, 8.9, 8.7	2.20	86.5 ± 0.2	8.5, 8.5, 8.7, 8.7	1.34	86.0 ± 0.30

LEGENDS- N: Number of analysis, RSD: Relative Standard Deviation

4. Conclusion

The spectrophotometric method are more selective, sensitive and rapid for the determination of trace amount of Ru(IV) using reagent 2-[(5-bromo-2-pyridylazo)]-5-diethylaminophenol (5-Br-PADAP) along with *N*-hydroxy-*N,N'*-diphenylbenzamidine. The selected reagent advantageously increases the sensitivity and selectivity of the method. The accuracy of the method is comparable with other reported methods in the literature. Most of the foreign ions, even at high concentration, do not interfere with determination of Ru(IV). Only palladium interferes in this method which could effectively be masked by the addition of sodium thiosulfate. The proposed method has been successfully applied for the determination of Ru(IV) in real samples, synthetic mixture and different sources of water samples. The proposed method overcomes with many drawbacks of classical photometric methods.

5. Acknowledgment

Authors are thankful to Delhi Technological University for providing financial assistance and laboratory facilities.

References

1. R. Hamond, The elements, in Lide, D. R., ed., CRC Handbook of Chemistry and Physics, 86th ed., CRC Press: Boca Raton (FL), 2005.
2. W. P. Griffith, "Ruthenium Oxidation Complexes: Their Uses as Homogenous Organic Catalysts," *Platinum Metals Rev.*, vol. 55 (3), July 2011, pp.193-195.
3. S. Atak and M. S. Celik, Innovations in Mineral and Coal Processing, 1st ed., Taylor and Francis, 1998.
4. L. Staurengo-Ferrari, S.S. Mizokami, J. J. Silva, F.O. da Silva, E. H. Sousa, L. G. da Franca, M.L. Matuoka, S.R. Georgetti, M.M. Baracat, R. Casagrande, W. R. Pavanelli and Jr. W. A. Verri, "The ruthenium NO donor, [Ru(bpy)2(NO)SO3](PF6), inhibits inflammatory pain: involvement of TRPV1 and cGMP/PKG/ATP-sensitive potassium channel signaling pathway," *Pharmacol Biochem Behav*., vol.105, Apr 2013, pp.157-165.
5. A. D. Richards and A. Rodger, "Synthetic Metallomolecules as Agents for the control of DNA structure," *Chem. Soc. Rev.*, vol. 36, 2007, pp. 471-475.
6. D. Kuang, S. Ito, B. Wenger, K. Cedric, J-E. Moser, B. Humphry, Z. Robin, M. Shaik and M. Gratzel, "High Molar Extinction Coefficient Heteroleptic Ruthenium Complexes for Thin Film Dye-Sensitized Solar Cells," *J. American Chem. Soc*., vol. 128, 2006, pp. 4146-4154.
7. C-L Lee, W-H Lee and C-H Yang, "The effects of co-sensitization in dye-sensitized solar cells," *J. Mat. Sci.*, vol. 48 (9), May 2013, pp. 3448-3453.
8. P. Ratre and D. Kumar, "Spectrophotometric Determination of Trace Amounts of Samarium in Environmental Samples," *American Inter. J. Res. Formal, Appl. Nat. Sci.* vol. 3 (1), June-Aug 2013, pp. 110-118.
9. P. Ratre and D. Kumar, "Spectrophotometric Determination of Pt (II) and Pd (II) in Environmental Samples Collected from Highly Polluted Areas of Delhi Region of India," *Inter. J. Emerging Techno. Computational. Appl. Sci.*, vol. 5 (4), June-Aug 2013, pp. 421- 429.
10. S. Biswas, P. N. Pathak and S. B. Roy, "Development of an extractive spectrophotometric method for estimation of uranium in ore leach solutions using 2-ethylhexyl phosphonic acid-mono-2-ethylhexyl ester (PC88A) and tri-n-octyl phosphine oxide (TOPO) mixture as extractant and 2-(5-bromo-2-pyridylozo)-5-diethyl aminophenol (Br-PADAP) as chromophore," *Spectrochim Acta A Mol Biomol Spectrosc.* vol. 91, Jun 2012, pp. 222-227.
11. M. P. Gulseth, , "Ximelagatran: an orally active direct thrombin inhibitor," *American Journal of Health System Pharmacy*, vol. 62 (14), Jul 2005, pp.1451-1467.
12. C. Colwell and P. Mouret, "Ximelagatran for the prevention of venous thromboembolism following elective hip or knee replacement surgery," *Semin Vasc Med.*, vol. 5 (3), Aug 2005, pp. 266-275.
13. M. Taddia, C. Lucano and A. Juris, "Analytical characterization of supramolecular species determination of ruthenium and osmium in dendrimers by electrothermal atomic absorption spectrometry," *Analytica Chimica Acta*, vol. 375 (3), Nov. 1998, pp. 285–292.
14. W. Heinig and K. Mauersberger, "Ruthenium determination in synthetic purex waste solutions by AAS," *Talanta*, vol. 32(2), Feb. 1985, pp. 145-147.
15. A. A. Ensafi, M. Arab Chamjangali and H. R. Mansour, "Catalytic spectrophotometric determination of ruthenium by flow injection method," *Talanta*, vol. 55 (4), 2001, pp. 715-720.
16. E. Giuseppe De Benedetto, R. Maria Guascito, R. Ciriello and R. I. Tommaso Cataldi, "Analysis by X-ray photoelectron spectroscopy of ruthenium stabilised polynuclear hexacyanometallate film electrodes," *Analytica Chimica Acta*, vol. 410 (1-2), Apr. 2000, pp. 143-152.
17. H. Yoshida, K. Hidaka, J. Ishida, K. Yoshikuni, H. Nohta and M. Yamaguchi, "Highly selective and sensitive determination of tricyclic antidepressants in human plasma using high-performance liquid

chromatography with post-column tris(2,2′-bipyridyl) ruthenium(III) chemiluminescence detection, " *Analytica Chimica Acta*, vol. 413 (1-2), May 2000, pp. 137-145.

18. B. Nalini and S. Sriman Narayanan, "Amperometric determination of ascorbic acid based on electrocatalytic oxidation using a ruthenium(III) diphenyldithiocarbamate-modified carbon paste electrode," *Anal. Chim. Acta*, vol. 405 (1-2), Jan 2000, pp. 93-97.
19. P-R. Tomas, M-L. Carmen, T. Virginia and M. Jesus, "Flow injection chemiluminescent determination of N-nitrosodimethylamine using photogenerated tris(2,2′-bipyridyl) ruthenium (III), *Analytica Chimica Acta*, vol. 541 (1-2), June 2005, pp. 67-72.
20. R. S. Kuchekar, S. Y. Shelar, R. H. Aher, H. S. Han, "Development of a reliable analytical method for extraction spectrophotometric determination of ruthenium(III) from catalyst and fissium alloy using o-methylphenyl thiourea as a chromogenic chelating ligand," *Spectrochimica Acta Part A: Molecular and Biomolecular Spectroscopy*, vol. 106, 2013, pp. 1-11.
21. D. Gopala Krishna, N. Devanna, K. B. Chandrasekhar, "Direct And Derivative Spectrophotometric Determination Of Ruthenium (III) In Presence Of Micellar Medium In Water And In Alloy Samples Using 4-Hydroxy 3,5dimethoxy Benzaldehyde-4-hydroxy Benzoylhydra-zone (Hdmbhbh)," *International Journal of Inorganic and Bioinorganic Chemistry*, vol.1(1), 2011, pp. 8-12.
22. B. Mathew,V. Mini, A.Vinnifred, "Microquantitative determination of ruthenium(III) spectrophoto metrically using a schiff's base derived from a triazine," *Der Chemica Sinica*, vol. 1(3), 2010, pp. 7-14.
23. N. Lokhande, G. B. Kolekar, M. A. Anuse and M. B. Chavan, "Extraction of Ruthenium(IV) from Hydrochloric Acid Medium with N-Octylaniline and Its Determination Spectrophotometrically with Pyrimidine-2-thiol," *Separation Science and Technology*, vol. 35 (1), 2000, pp. 153-157.
24. M. S. El-Shahawi, A. Z. Abu Zuhri, and S.M. Al-Daheri, "Spectrophotometric determination of ruthenium after extraction of perruth-enate with benzyltributylammonium chloride," *Fresenius' J. Anal. Chem.*, vol. 350 (12), 1994, pp. 674-677.
25. S. A. Alaa, "Simple and Selective Spectrophotometric Determination of ruthenium after Solid Phase Extraction with some Quinoxaline Dyes into Microcrystalline P-Dichlorobenzene," *Spectrochim. Acta Part A: Molecular and Biomolecular Spectroscopy*, vol. 58 (9), July 2002, pp. 1831-1837.
26. B. Rezaei and N. Majidi, "A Simple and High Sensitive Spectrophotometric Method for Ultra Trace Determination of Ruthenium With Its Catalytic Effect On The Oxidation Of Pyronin B By Periodate," *Spectrochim. Acta Part A: Molecular and Biomolecular Spectroscopy*, vol. 66 (4-5), April 2007, pp. 869–873.
27. M. A. Islam and W. I. Stephen, "Evaluation of some as-triazines and re-evaluation of PDT and ferrozine as reagents for spectrophotometric determination of ruthenium," *Talanta* , vol. 39 (11), Nov. 1992, pp. 1429–1435.
28. M. Keyvanfard and M. Karamian, "Spectrophotometric Reaction Rate Method for the Determination of Trace Amounts of Ruthenium(III) by Its Catalytic Effect on the Oxidation of Spadns by Metaperiodate in Micellar Medium," *Asian Journal of Chemistry*, vol. 21 (2), 2009, pp. 942-948.
29. A. Solovey-Vandersteen, "T. Vrublevska and H. Lang, UV-Visible and IR Spectroscopic Studies of Ruthenium(II)-Xylenol Orange Complex," *Acta Chimica Slovnica.*, vol. 51, 2004, pp. 95-106.
30. M. Balcerzak and E. Wyrzykowska, "Extraction Preconcentration of Platinum and Ruthenium using High Molecular Weight Amines Prior to Simultaneous Determination by Derivative Spectrophotometry," *Analusis*, vol. 27(10), 1999, pp. 829-834.
31. V. Druskovic, V.Vojkovic and T. Antonic, "Extraction of Ruthenium and Its Separation from Rhodium and Palladium with 4-Pyridone Derivatives," *Croatica Chemica Acta*, vol. 78, 2005, pp. 617-626.
32. B. Rezaei and M. Keyvanfard, "Spectrophotometric Reaction Rate Method for the Determinationof Ultra Trace Amounts of Ruthenium(III) by its Catalytic Effect on the Oxidation of Safranin O by Metaperiodate," *Canadian Journal of analytical sciences and spectroscopy*, vol. 50 (6), 2005, pp. 311-316.
33. W. Hong-fu, Z. Su-lan, SU Zhi-xian, HE Li-ming and Y. Qin, "Determination of trace Ruthenium(III) by Catalytic Kinetic spectrophotometry with malachite green, *Chinese Journal of Analysis Laboratory*, vol. 8, 2009, pp. 90-93.

34. A. Praveen Kumar, P. Raveendra Reddy, and V. Krishna Reddy, "Direct and Derivative Spectrophoto metric Determination of Ruthenium(III)," *International Journal of ChemTech Research CODEN(USA)*, vol. 5 (4), April-June 2013, pp 1442-1447.
35. Z. Zhi-rong, W. Qun and Z. Shu-yuan, "Kinetic spectrophotometric determination of trace ruthenium(III) based on catalytic effect of ruthenium(III) on oxidation of acid chrome blue K by potassium bromate," M*etallurgical Analysis*, vol. 7, 2007, pp. 13-19.
36. M. Balcerzak, "Sample Digestion Methods for the Determination of Traces of Precious Metals by Spectrometric Techniques," *Analytical sciences*, vol.18, 2002, pp. 737-750.
37. G. H. Ayres and Y. Frederick, "Spectrophotometric Study of Ruthenium-Thiourea Complex,". *Analytical Chemistry*, vol. *22* (10), October 1950, pp. 1277-1280.
38. E. B. Sandell and O. Hiroshi, Photometric determination of traces of metals, John Wiley & Sons: New York, 1978.
39. L.G. Sillen, "Some graphical methods for determing equilibrium constant II on Curve-fitting method for two-variables data", *Acta Chemica Scandinavica*, vol. 10, 1956, pp.186-202.
40. P. Job, "Job plot", *Annali di Chimica Applicata*, vol. 9, 1928, pp. 113-203.
41. B. S. Furniss, A. J. Hannaford, P. W. G. Smith and A. Tatchell, Vogel's textbook of Practical organic chemistry, Pearson Education: London, 2005.
42. D.D. Perin, Chemical Analysis-Masking and Demasking, vol. 33, 4th. ed. John Wiley & Sons: New York, 1999.

*****

UNFAIR ADVERTISING AND SALES PROMOTION: CONSUMERS' PERCEPTION

Dr. P.V. Khatri and Ms. Rashmi***

ABSTRACT

Advertising and sales promotion tools play an important role in boosting sales of a business firm. It constitutes the most sensitive area of marketing. Businessmen make use of advertising which often extols the merits of their product or service. Advertising is a potent tool in the hands of the business man to influence consumer behaviour. When used indiscriminately and unscrupulously, this tool harms the consumer interest. It is here that advertising policy and practices become a matter of public concern. A seller is often tempted to magnify and exaggerate the qualities and beneficial characteristics of his product or service. This exaggeration, which is often deliberate, misleads the buyers. However, there has been a great deal of controversy over the role of advertising and sales promotion in the national economy. Advertising has a great potential of increasing the sale and profits of an organization. It can be effective, used for creating awareness about a product or service, increasing knowledge, building brand preference, developing conviction, inducing trial, and triggering off the sales. In a competitive situation, advertising is a major tool of product differentiation and competition. By increasing the sales volume, advertising helps reduce average production and distribution costs per unit and thus contributes to the national economic development. Unscrupulous and excessive advertising not only leads to the increased distribution costs, thereby resulting in excessive costs to the consumers but tends to persuade the buyer to buy products not only what he does not need but also what he actually does not want. Economists traditionally either ignored advertising or viewed it with skepticism. Many criticism against marketing communication (advertising, sales promotion, public relations, personal selling) have been voiced by legislators, professional consumer advocates, and public at large. The present paper investigates and analyses the

* is a Senior Faculty in the Department of Commerce, Swami Shraddhanand College, University of Delhi. Email id drpvkhatri@gmail.com

** BE from Delhi College of Engineering, University of Delhi and PGDM from Indian Institute of Management, Kozhikode (IIMK) has worked in Deloitte Consulting, Hindustan Unilever Ltd. and HCL Technologies as a business executive, is presently a Faculty in the Department of Management Studies, College of Vocational Studies, University of Delhi. Email id rashmikhatri2009@gmail.com

extent of prevalence of unfair and deceptive advertising practices from the consumers' perception.

Keywords: Unfair trade practices, Unfair, Misleading, Deceptive, Alluring, False, Disparaging, Exaggerated, Discount schemes, Warranty, Guarantee and Performance.

INTRODUCTION

Advertising and sales promotion constitute the most sensitive area of marketing. Businessmen make use of advertising which often extols the merits of their product or service. However, there has been a great deal of controversy over the role of advertising and sales promotion in the national economy. Advertising has a great potential of increasing the sale and profits of an organization. It can be effective, used for creating awareness about a product or service, increasing knowledge, building brand preference, developing conviction, inducing trial, and triggering off the sales. In a competitive situation, advertising is a major tool of product differentiation and competition. By increasing the sales volume, advertising helps reduce average production and distribution costs per unit and thus contributes to the national economic development.

LITERATURE REVIEW

Unscrupulous and excessive advertising not only leads to the increased distribution costs, thereby resulting in excessive costs to the consumers but tends to persuade the buyer to buy products not only what he does not need but also what he actually does not want. (Ref. Verma, DPS., "Advertising: Need for Effective Regulatory Measures", paper presented at the Faculty Development Seminar on "Marketing Strategies for the Third World Countries", held under the auspicious of the Department of Commerce, Delhi School of Economics, University of Delhi, India. Dec. 14-15, 1989.) Heavy advertising also acts as a barrier to the entry of new entrepreneurs to a particular industry.

According to Adlai Sterenson, the American standard of living is due in no small measure to the imaginative genius of advertising which not only create and sharpen demand but also, by its impact upon the competitive process, stimulates the never ceasing quest of improvement in quality of the product.

Sir William Churchill spoke very high of advertising when he said, "Advertising nourishes the consuming power of human beings". It creates better standard of living. It set up before a man the goal of a better home, better clothing, and better food for himself and family. It spurs individual exertion and greater production. It brings together in fertile union those things which otherwise would never have met.

Economists traditionally either ignored advertising or viewed it with skepticism. For example, Alfred Marshall, father of the neo-classical school of economics, divided advertising into two categories: (i) informative, and (ii) persuasive. He admitted that benefits of providing information

about new products, but disapproved of the persuasive advertising on the ground that it merely shifted demand from one brand to another without serving any socially useful purpose. Advertising has not been favourably viewed by modern economists also. Many of them believe that persuasion is opposed to the concept of an 'economic man' who should make his decision rationally rather than emotionally. (Marshal, 1980.) Samuelson emphasizes that disadvantages of promotion but admits certain economic advantage. (Samuelson, 1985: 500.)

The economic effects of advertising, which could be harmful to consumer interests, can be classified under two categories:

1. Preventing, distorting, or restricting competition in the relevant market; and
2. Misleading the consumers to buy products which may not be in their best interest.
   a) While advertising falling under the first category is referred to as anti-competitive advertising, the second category is called *unfair advertising*.
   b) The extent, impact, and persuasiveness of advertising and other forms of marketing communication about goods and services in an industrializing society can scarcely be exaggerated. Every level of trade, from manufacturer to retailer, uses advertising, whether through radio, television, magazines, newspapers, billboards, lables, in-store signs or direct mail. Many firms advertise a multitude of products and make a variety of claims in its advertising copy frequently. (Stone, 1980: 167-68.)
   c) A purchaser will choose among the products based on their advertised claims, even when those claims are false. (Kintner, 1971: 348) Large scale efforts are being made, often with an impressive success, to channel the buyer's thought processes and purchasing decisions by the use of insights, gleaned from psychometric and social sciences, with the result that many of us are being influenced and manipulated far more than we realize, in the patterns of our every day lives. (Packard, 1957: 1). Deceptive pictures, as well statements, can be used to lure potential customers into their first purchase. Such deceptive inducements may come in a variety of forms.
   d) The positive contribution of advertising cannot be denied. However, advertising has great manipulative power and capacity to harm the consumer and the public interest. The problem lies not in the extent of advertising but in the judgement that a significant, but undetermined portion of it, is either false or deceptive. Estimates of the proportion that is false or deceptive vary widely, but if it is only a small percentage of the total, the problem for the customer is, in absolute terms, substantial. (Sutherland, 1949 and Raymond 1968).
3. Many criticism against marketing communication (advertising, sales promotion, public relations, personal selling) have been voiced by legislators, professional consumer advocates, and public at large. (Webster, 1974: 29-30). These includes:
4. Marketing communication makes people buy things they do not need.
5. Marketing communication has created materialistic values in the society that are not sufficient as goals for national policy and personal life style.

6. Marketing communication is at times annoying and in poor taste.
7. Marketing communication is often deceptive and misleading, especially for disadvantaged consumers.
8. Marketing communication often provides inadequate information to the consumer making it difficult for him in making buying decisions about complex products.
9. Marketing Communication power leads to reduced competition which, in turn, creates higher prices and reduced consumer welfare.

Borden (Borden, 1944: 10) in his classic study, has concluded that consumers are confused by the large number of meaningless product differentiation, caused by advertising, and consequently they cannot make wise choice.

Besides being harmful to the consumer, misleading or false advertising also adversely affect the operation of the macro-marketing system. In a consumer oriented marketing system, the customer is considered sovereign and his wise choice rewards those who supply superior products and services and penalizes those who ignore product quality and fail to render efficient service. Misleading the buyer through untrue advertising would cause the entire marketing system to work imperfectly.

Advertising is a potent tool in the hands of the business man to influence consumer behaviour. When used indiscriminately and unscrupulously, this tool harms the consumer interest. It is here that advertising policy and practices become a matter of public concern. A seller is often tempted to magnify and exaggerate the qualities and beneficial characteristics of his product or service. This exaggeration, which is often deliberate, misleads the buyers. Often it is difficult to distinguish between an exaggerated claim about the product and a deliberate misrepresentation of fact. This distinction between the two is a matter of degree and intent. Businessmen spend huge amounts of money on advertising.

In India, a number of legislations have been enacted to protect the consumers from various unfair trade practices such as unfair, deceptive or misleading advertising. These legislations deals with specific aspects of consumer protection such as standardization of products; grading, packaging and branding; prevention of adulteration short weights and measures; advertising of specific products; hoarding; profiteering; black marketing, etc. These legislations are:

1. The Indian Contract Act, 1872.
2. The Sale of Goods Act, 1930.
3. The Agricultural Produce (Grading and Marking) Act, 1937.
4. The Drugs and Cosmetics Act, 1940.
5. The Drugs (Control) Act, 1950.
6. The Industries (Development and Regulation) Act, 1951
7. The Prevention of Food Adulteration Act, 1954.
8. The Drugs and Magic Remedies (Objectionable Advertisements) Act, 1954.

9. The Essential Commodities Act, 1955.
10. The Trade and Merchandise Marks Act, 1958.
11. The Monopolies and Restrictive Trade Practices Act, 1969.
12. The Essential Services Maintenance Act, 1981.
13. The Standards of Weights and Measures Act, 1976.
14. The Prevention of Black Marketing and Maintenance of Supplies of Essential Commodities Act, 1980.
15. The Bureau of Indian Standards Act, 1986.
16. The Consumer Protection Act, 1986.

Advertising is sought to be regulated through various laws passed by the central legislature or state legislatures, Guidelines issued by various departments or agencies of government of India, code of conduct for advertising framed by the advertising standards framed by the Advertising Standard Council of India (ASCI), Code for Commercial Advertising on Doordarshan, Code of Standard in Relation to the Advertising of Medicines and Treatments, Standard of Practice for Advertising Agencies as approved by the Advertising Agencies Association of India, Bombay.

The Consumer Protection Act, 1986 is a land mark legislation which sought to regulate unfair advertising under the category of unfair trade practices, which is defined under Sec (r) which reads:

Section 2 (r) "unfair trade practice" means a trade practice which, for the purpose of promoting the sale, use or supply of any goods or for the provision of any service, adopts any unfair method or unfair or deceptive practice including any of the following practices, namely:

1. The practice of making any statement, whether orally or in writing or by visible representation which,
   (i) falsely represents that the goods are of a particular standard, quality, quantity, grade, composition, style or model;
   (ii) falsely represents that the services are of a particular standard, quality or grade;
   (iii) falsely represents any re-built, second-hand, renovated, reconditioned or old goods as new goods;
   (iv) represents that the goods or services have sponsorship, approval, performance, characteristics, accesso-ries, uses or benefits which such goods or services do not have;
   (v) represents that the seller or the supplier has a sponsorship or approval or affiliation which such seller or supplier does not have;
   (vi) makes a false or misleading representation concerning the need for, or the usefulness of, any goods or services;

(vii) gives to the public any warranty or guarantee of the performance, efficacy or length of life of a product or of any goods that is not based on an adequate or proper test thereof

1. Provided that where a defence is raised to the effect that such warranty or guarantee is based on adequate or proper test, the burden of proof of such defence shall lie on the person raising such defence;

(viii) makes to the public a representation in a form that purports to be

(a) a warranty or guarantee of a product or of any goods or services; or

(b) a promise to replace, maintain or repair an article or any part thereof or to repeat or continue a service until it has achieved a specified result, if such purported warranty or guarantee or promise is materially misleading or if there is no reasonable prospect that such warranty, guarantee or promise will be carried out;

(ix) materially misleads the public concerning the price at which a product or like products or goods or services, have been or are, ordinarily sold or provided, and, for this purpose, a representation as to price shall be deemed to refer to the price at which the product or goods or services has or have been sold by sellers or provided by suppliers generally in the relevant market unless it is clearly specified to be the price at which the product has been sold or services have been provided by the person by whom or on whose behalf the representation is made;

(x) gives false or misleading facts disparaging the goods, services or trade of another person.

Explanation - For the purposes of clause (1), a statement that is

(a) expressed on an article offered or displayed for sale, or on its wrapper or container; or

(b) expressed on anything attached to, inserted in, or accompanying, an article offered or displayed for sale, or on anything on which the article is mounted for display or sale; or

(c) contained in or on anything that is sold, sent, delivered, transmitted or in any other manner whatsoever made available to a member of the public, shall be deemed to be a statement made to the public by, and only by, the person who had caused the statement to be so expressed, made or contained.

2. Permits the publication of any advertisement whether in any newspaper or otherwise, for the sale or supply at a bargain price, of goods or services that are not intended to be offered for sale or supply at the bargain price, or for a period that is, and in quantities that are, reasonable, having regard to the nature of the market in which the business is carried on, the nature and size of business, and the nature of the advertisement.

Explanation —For the purpose of clause (2), "bargaining price" means—

(a) a price that is stated in any advertisement to be a bargain price, by reference to an ordinary price or otherwise, or

(b) a price that a person who reads, hears or sees the advertisement, would reasonably understand to be a bargain price having regard to the prices at which the product advertised or like products are ordinarily sold;

3. permits

(a) the offering of gifts, prizes or other items with the intention of not providing them as offered or creating impression that something is being given or offered free of charge when it is fully or partly covered by the amount charged in the transaction as a whole;

(b) the conduct of any contest, lottery, game of chance or skill, for the purpose of promoting, directly or indirectly, the sale, use or supply of any product or any business interest;

(3A) withholding from the participants of any scheme offering gifts, prizes or other items free of charge, on its closure the information about final results of the scheme.

Explanation — For the purposes of this sub-clause, the participants of a scheme shall be deemed to have been informed of the final results of the scheme where such results are within a reasonable time, published, prominently in the same newspapers in which the scheme was originally advertised;

4. permits the sale or supply of goods intended to be used, or are of a kind likely to be used, by consumers, knowing or having reason to believe that the goods do not comply with the standards prescribed by competent authority relating to performance, composition, contents, design, constructions, finishing or packaging as are necessary to prevent or reduce the risk of injury to the person using the goods;

5. permits the hoarding or destruction of goods, or refuses to sell the goods or to make them available for sale or to provide any service, if such hoarding or destruction or refusal raises or tends to raise or is intended to raise, the cost of those or other similar goods or services:

6. manufacture of spurious goods or offering such goods for sale or adopts deceptive practices in the provision of services.

Briefly stated, an unfair trade practice is a trade practice which involves an unfair method or unfair or deceptive practice adopted for promoting the sale, use or supply of any goods or for the provision of services. Deceptive, misleading or untrue advertising is also a unfair trade practice. The following advertising practices, in particular, amount to unfair trade practice:

1. Making false claim and misleading advertisements about any goods or services;
2. Advertising of bargain price for any goods or services;

Whether a particular advertising method or practice used in a business or trade is unfair or not can be seen in the light of the facts and circumstances of the particular case. In the same manner, what advertising practice is 'deceptive' also depends on the facts and circumstances of the case. The term 'unfair' is used in a variety of ways. According to the Collins Paperback

Thesaurus, the word 'unfair' means arbitrary, biased, discriminatory, inequitable, one sided, partial, partisan, prejudiced, unjust, crooked, dishonest, dishonorable, and uncalled for, unsupporting, unwarranted or wrongful.

Similarly, the term 'deception' is used in a variety of ways as craftiness, cunning, deceitfulness, deceptiveness, dissimulation, duplicity, fraud, fraudulence, guile, hypocrisy, imposition, insincerity, treachery, trickery, artifice, bluff, cheat, decoy, feint, fraud, hoax, illusion, imposture, leg-pull lie, ruse, sham, snare, stratagem, subterfuge or tricky.

The term 'deceptive' is used in many senses such as ambiguous, deceitful, delusive, and dishonest, fake, fallacious, false, fraudulent, illusory, misleading, mock, specious, spurious and unreliable.

The concept of 'unfair' and 'deceptive' advertising practice is based upon developments in the Anglo-American law of torts. The law of torts is designed to provide for social stability by declaring conduct that may lead to breach of peace to be an actionable wrong. Included in such conduct are assault, deceit, negligence, and delicious prosecution, and these acts constitute torts whether or not they take place in a commercial context. Independent legal considerations began to develop concerning some of these practices, however, when they occurred in a commercial context. (Ref. American Jurisprudence, vol. 55, 739, p.50)

In United States, most of the Federal Trade Commission (FTC) actions against deceptive advertising acts, or practices are based on section 5 of the FTC Act, 1914, which, after revision, were incorporated in the Wheeler–Lea Act in 1938. The amended FTC Act states that "……unfair or deceptive acts or practices in commerce are hereby declared illegal". The statute does not define the 'unfair' and 'deceptive', and the FTC has often been criticized for not doing so itself, especially after assuming in the 1970s a more aggressive posture in dealing with consumer protection matters. (Ford, and Calfee, 1986: 82-100; Posner, 1973: 47-89). The United States' Supreme Court in 1972 laid down criteria to determine whether an advertising trade practice was unfair or not. They are:

(i) Whether practice offends the public policy;

(ii) Whether it is against the law of the land or accepted customs or practices;

(iii) Whether the practice is immoral, unethical, oppressive or unscrupulous;

(iv) Whether it affects the customer monetarily or physically. (Garden, 1982: 6-15).

On a complaint filed by any consumer/consumer association/governmentabout any unfair trade practice involving advertising, the consumer redressal agencies can pass a suitable order against such advertising under the Consumer Protection Act.

Objective of the Study

The objective of the present study is to find out the extent of prevalence of unfair trade practices relating to advertising and sales promotion in the market.

METHODOLOGY

A detailed survey of selected consumers has been conducted with a structured questionnaire.

Hypotheses

H1: The trade practices relating to unfair, deceptive, false and misleading advertising are prevailing to a large extent in the market.

H2: There is no significant difference in the consumers' perception about the prevalence of such unfair practices on the basis of various demographic variables across a large section of customers or consumers.

Analysis

Prevalence of Unfair Advertising and Sales Promotion Practices: The Consumers' Perception towards the prevalence of unfair trade practices relating to advertising and sales promotion is measured on a five point scale across different statements. The percentage score of consumers' opinion about the extent of prevalence of these practices in the market is shown in Table 1.

Table 1: Prevalence of UTPs Relating to Advertising and Sales Promotion: Consumers' Perception

Statement	*Per cent Score (N=100)*					*Descriptive Statistics*		
	5	*4*	*3*	*2*	*1*	*Mean*	*S.D.*	*C.V.*
1. In many advertisements, the manufacturer or dealer makes exaggerated claims regarding the various features of the product or service	-	88.9	11.1	-	-	3.89	.320	8.22
2. The product is often not available at the advertiseddiscounted price	-	22.2	27.8	50.0	-	2.72	.83	30.51
3. Manufacturers/dealers often use product warranty and guarantee to allure the buyer	-	11.1	33.3	55.6	-	2.56	.70	27.34
4. The manufacturers or dealers often increase the selling price before announcing any discount scheme, sales contests, games, gifts or prizes	-	72.2	22.2	5.6	-	3.67	.59	16.07
5. In most of the advertisements, the manufacturer or dealer use the word 'free' with a view to deceive the customers	-	72.2	27.8	-	-	3.72	.57	15.32

Contd. table 1...

Contd. table 1...

6. TV advertisements are generally more deceptive as compared to other advertisements	-	5.6	16.7	61.1	16.7	2.11	.76	36.01
7. Generally, the advertisers resort to unethical and obscene advertising practices to promote their products or services	-	61.1	38.9	-	-	3.61	.50	13.85
8. TV is as more potent weapon as compared to other media of advertisements of advertising exaggerated claims about the quality/ usefulness/benefits/performance of the product or service	-	72.2	27.8	-	-	3.72	.46	12.36
9. The celebrities, like film starts and sportspersons, are generally used by the manufacturers or dealers in their advertisements to mislead the customer	-	88.9	11.1	-	-	3.89	.32	8.22
10. Most of the advertisements falsely represent the standard or grade of their products or service	5.6	77.8	16.7	-	-	3.89	.47	12.08
11. Most of the manufacturers or dealers make deceptive use of the term 'new' in their advertisements	5.6	72.2	22.2	-	-	3.83	.51	13.31
12. In most of the cases, the advertiser falsely represents that his goods or services have sponsorship or approval of well-known persons or organizations	5.6	72.2	22.2	-	-	3.83	.51	13.31
13. The advertisers often make misleading representation concerning the need for or the usefulness of any goods or services	5.6	66.7	27.8	-	-	3.78	.55	14.55
14. The advertisers generally give to the public warranty or guarantee of the performance or life of the product that is not based on an adequate test	-	55.6	38.9	5.6	-	3.5	.62	17.71
15. Advertisements generally give information disparaging the goods, services or trade of another persons(s)	-	11.1	50.0	38.9	-	2.72	.67	24.63

Source: Key: 5=Strongly 4=Agree 3=Uncertain 2=Disagree 1=Strongly Disagree

EXAGGERATED CLAIMS ABOUT PRODUCT FEATURES

In order to increase their sales and profit, manufacturers and dealers often make exaggerated claims in their advertisements about the product or service. The survey has revealed that a very large majority (73.8 percent) of consumers perceived manufacturers and dealers making exaggerated claims regarding the features of the product or service. For instance, advertisements for lotion that would make hair "healthier", cosmetics that would make "wrinkles fade away in just 10 minutes", devices that would remove "ugly" hairs forever, creams and devices for bust development, and diet plans, and hundreds of such other advertisements kin the magazines and newspapers make questionable claims of this sort. (Stone, 1980:70). Many such examples of exaggerated claims in advertisements about the goods or services can be added, *i.e.*, advertisements relating to reducing weights and size of body in just one hour. (In re Body Wrap Company, Bombay (MRTP Commission UTP Inquiry No. 83 of 1985, order dated 27.10.1986.)

FALSE CLAIMS ABOUT PRODUCT STANDARDS

False representation that the product is of a particular standard, quality, quantity, grade composition, style or model, is often made in the advertisement. More than half (58.8 per cent) of the consumers were of the view that most of the advertisements falsely represent the standard or grade of the product or service. Very few (7.3 per cent) of the consumers expressed a different viewpoint. Not many (30.3 per cent) of the consumers were uncertain on the issue. The mean score (3.6) of the consumers signify that on an average the consumers feel that the practice of making false claims about the quality etc. of the products is widely prevailing in the market.

MEDIA AND DECEPTION

Manufacturers and dealers use various modes of advertisements for advertising their goods and services. In utter violation of the Code of Commercial Advertising on Doordarshan, a large number of advertisements on TV were perceived to be misleading, deceptive and unfair. A very large majority (78 per cent) of consumers felt that TV, which is a more potent advertising medium compared to others, was used to make exaggerated claims about the quality, usefulness, benefits, and performance of the product or the service concerned. A good number (40.6 per cent) of consumers consider TV advertisements more deceptive than advertisement in other media. Somewhat similar observations were made in a leading case on misleading advertising in the United States of America (Kinter, 1971: 354).

Deception through T.V. advertising has its peculiar nature. Everyone knows that on television all that glitters is not gold. On black and white screen white looks grey and blue looks white; the lily must be painted. Coffee looks like mud. Real ice cream melts much more quickly than the firm but false sundae. The plain fact is, except by props and mockups, some objects cannot be shown on television as the viewer, in his mind's eye, knows the essence of the object. A mock up is an object to aid in the creation of a desired effect. Specifically, its use in a television commercial is to stimulate a real object which, because of technical requirements of the medium,

is impractical and impossible to use in the commercial. The advertising agency has been most ingenious in its solution to television's inherent weakness. By key lighting on one of two shirts, sheets or towels, it can make one appear lighter than the other. Glycerin is used to give a frosty appearance to soft drinks. Tea is made triple strength, so that it appears normal rather than as water. Grenadine is added to orange juice to keep it from looking like milk. Colour corrections are made— blue appear white and white appears gray. Shampoo and other foamy substances are used to give a lasting head to beer, and ice cream is often whipped potatoes, which of course will not melt.

Thus, the most potent media of advertising is most susceptible to manipulation and used as a carrier of misleading advertisements.

Use of Gifts as Sale Gimmicks

As a device to attract customers, offering and giving free goods is a commonly accepted sales promotion method. Any consumer can be easily lured by an offer of getting something for nothing. An offer that is truly free in fact as well as description will be rare. The word 'free' refers to an offer involving something other than an unconditional gift for which the customer pays nothing and/or does something. The usual 'free deal' will be an offer to give something for nothing, contingent upon the purchase of goods or hiring of services. The consumers suffer no harm if he gets free gift but it is not the case always.

The manufacturers and dealers already include the cost of so called free gifts and prizes in the price of product or service. Most of the gift or prize schemes are conditional and full of deception. The survey has revealed that large majority of the consumers (61.3 %) feels that in most of the advertisements, the manufacturers and dealers use the word 'free' with a view to deceiving the consumers. Moreover, 73% of consumers feel that manufacturers and dealers often increase the selling price before announcing any discount schemes, sales contests, games, gifts, or prizes. Despite their awareness, about these gifts and sales gimmicks, the consumers fall in to their trap.

Use of Celebrities

Manufactures and dealers often use celebrities like film stars and sportsperson for the promotion of their goods and services. There is no harm in doing so but when these celebrities are used to mislead customers, the practice becomes unquestionable. It has been revealed by the study that a large majority of consumers (79%) feel that celebrities are used by businessman in their advertisements to mislead the customers.

False Sponsorship or Approval

Many a seller or supplier represent in their advertisements that the goods or services has sponsorship or approval, performance, characteristics, accessories, uses, benefits, etc. which such goods and services do not have. Where a seller or supplier of shock-absorbers that they

have been certified by the Bureau of Indian Standards, when in fact the certification was under consideration, it is false representation as to approval and characteristics which such certification normally carries. False representations as to durability of goods or the efficacy of services would be covered by the expression 'performance/characteristics'. The advertisement falsely representing that 'a particular management course' is approved by a foreign university or a particular school is recognized by CBSE.

The study has revealed more than half of the consumers (57.3%) were of the opinion that in most of the cases advertisers falsely represent that their goods or services has sponsorship or approval of well-known persons or organizations.

Obscenity in Advertisements

As to the practice of resorting to unethical and obscene advertising for the promotion of goods or services, a little over half of the consumers (51.3%) expressed the opinion that the advertisers often resorted to unethical and obscene advertising practices to promote their goods or services.

Disparaging of Competitor's Product

The tort of commercial disparagement, often referred to as trade libel, is just another deceptive practice for the diversion of customers. Disparagement consists of a false assertion of fact about the quality of competitors' product or services by someone intending to harm his competitor's business which directly results in financial loss. Closely associated with, but distinguishable from disparagement, is the tort of defamation. Defamation includes, but is not limited to situations where false statements are made to injure one in his business by impeaching his integrity, skill, diligence or credit. Simply stated, it impugns the integrity or credit of a person in connection with his business as opposed to the quality of product.

In competitive advertising, product comparisons are among the most effecting means of influencing the consuming public. As a result, comparative misrepresentation is a route frequently observed by business rivals. Yet of all the forms of disparagement, this one is often the most difficult to circumscribe in terms of what is and what is not actionable. As to the prevalence of the practice of disparaging advertising a good number of consumers (39.3 %) were uncertain whereas not many of the consumers (28.8%) agree that the advertisements generally give information disparaging the goods, service or trade of another person(s). Thus, the unfair trade practice of disparaging advertisements is not found to be prevailing to any significant extent.

Misleading Product Warranty

Manufacturers and dealers generally convey to the consuming public a representation in the form that purports to be —a warranty or guarantee of a product or any goods or services *e.g.* the advertisements 'satisfaction of your money back; one week free trial or lifelong guarantee or guaranteed treatment of——'. It is often felt by the consumers that such purported guarantee or

warranty was either false or misleading or the same was just to allure the buyers. A majority of the consumers (67%) felt that manufacturers and dealers often used product guarantee or warranty to allure the buyers. This view was not shared by most of the voluntary consumer's organizations. Thus, the prevalence of unfair trade practice of giving advertisements containing misleading warranty was felt to be prevailing in the market to a significant extent by the individual consumers.

The extent of prevalence of unfair trade practice relating to advertising and sales promotion is considered to be on higher side. Taking a composite view of the practices concerning advertising and sales promotion, the study has revealed that an overwhelming majority of consumers (87.5%) agreed about the prevalence of unfair trade practice concerned.

A comparative view of the consumers' opinion as to the extent of the prevalence of unfair advertising and sales promotion practices in the market are shown in Figure 1 which indicates that the practices were prevailing to an alarming extent.

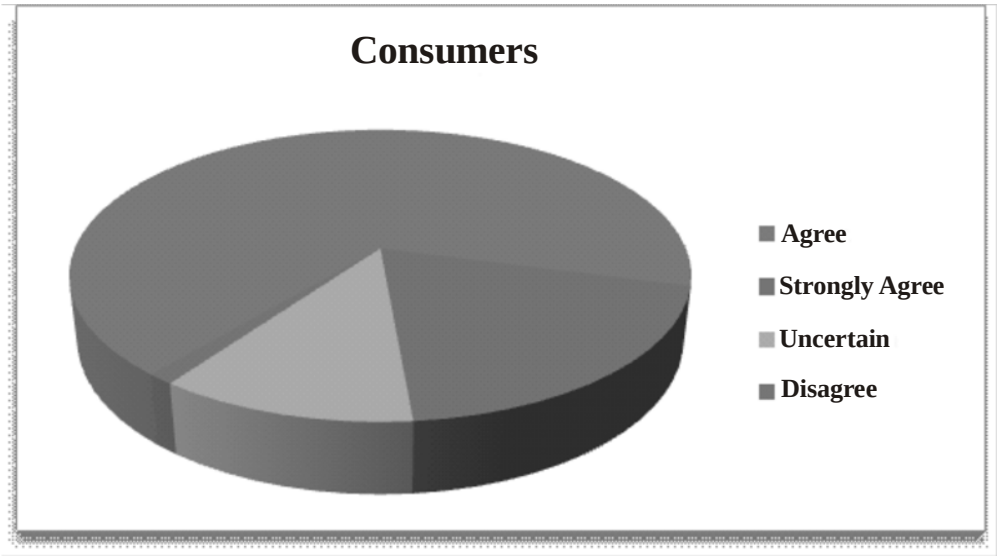

Figure 1: Prevalence of UTPs of Advertising and Sales Promotions: Consumers' Perception

CONCLUSION

The survey of consumers' opinion about the extent of prevalence of certain unfair trade practices pertaining to advertising and sales promotion has revealed that the practices are prevailing in the market to a significant extent. Consumers have felt that manufacturers and dealers resort to the practice of making exaggerated claims about various features of the product or services. The manufacturers and dealers often increase the selling price before announcing any discount scheme, sales contest, games, gifts and prizes. Moreover, the advertisers use the word 'free' in their advertisements with a view to allure the buyers. The celebrities, like film stars and sports

persons, were often used in advertisements. The false claims about approval and sponsorship were also made for promoting sale. The vehicle of advertising and other sales promotion techniques used by the dealers for promoting the sale of their goods and services were found to be unfair and deceptive in a big way by the consumers.

REFERENCES

Borden, Neil H. (1944). *The Economic Effects of Advertising*, Homewood, Ill., Richard D. Irwin, Inc.

Ford, Gary T., and Calfee, John E. (1986). Recent Developments in FTC Policy on Deception. *Journal of Marketing*, vol. 50, 82-100.

Kintner, Earl W. (1971). *A Primer on the Law of Deceptive Practices: A Guide for the Businessmen*, New York: Macmillan Publishing Co., 348.

Marshal, Alfred (1980). *Principles of Economics*, London: Macmillan & Co. Ltd..

Packard, Vance (1957). *The Hidden Persuaders*, New York: Pocket Books, Inc.

Posner, R. (1973). The Federal Trade Commission, University of Chicago *Law Review*, 37, No.10, 47-89. Regulation of Advertising by the FTC, Washington D.C. American Enterprise Institute.

Raymond Baumhart, S.J. (1968). *Ethics in Business*, New York: Holt, Rincechart and Winston.

Samuelson, Paul A. (1985). *Economics: An Introductory Analysis*, New York: McGraw Hill, Inc.

Stone, Alan (1980). *Economic Regulation and the Public Interest: Federal Trade Commission in Theory and Practice*, London: Cornell University Press.

Stone, Allan (1980). *Economic Regulation and the Public Interest*, London: Cornell University Press. 167-68.

Sutherland, Edwin H. (1949). *White Collar Crime*, New York: Holt, Rinehart and Winston.

Verma, DPS. (1989). *Advertising: Need for Effective Regulatory Measures*, paper presented at the Faculty Development Seminar on "Marketing Strategies for the Third World Countries", held under the auspicious of the Department of Commerce, Delhi School of Economics, University of Delhi, India. Dec. 14-15.

Webster, Frederick E. (1974). *Social Aspects of Marketing*, New Jersey, Englewood Cliffs: Prentice Hall, Inc.

Transportation Research Part C 40 (2014) 111–122

Contents lists available at ScienceDirect

Transportation Research Part C

journal homepage: www.elsevier.com/locate/trc

Vehicular traffic noise modeling using artificial neural network approach

Paras Kumar [a,*], S.P. Nigam [b], Narotam Kumar [b]

[a] Mechanical Engineering Department, Delhi Technological University, Delhi 110042, India
[b] Mechanical Engineering Department, Thapar University, Patiala 147004, India

ARTICLE INFO

Article history:
Received 27 August 2012
Received in revised form 10 January 2014
Accepted 10 January 2014

Keywords:
Artificial Neural Network (ANN)
Modeling
Vehicular traffic noise
Back propagation (BP)
Prediction capability

ABSTRACT

In India, the transportation sector is growing rapidly and the number of vehicles on Indian roads is increasing at a very fast rate leading to overcrowded roads and noise pollution. The traffic scenario is typically different from other countries due to predominance of a variety of two-wheelers which has doubled in the last decade and forms a major chunk of heterogeneous volume of vehicles. Also tendency of not following the traffic norms and poor maintenance adds to the noise generation.

In the present study, Multilayer feed forward back propagation (BP) neural network has been trained by Levenberg–Marquardt (L–M) algorithm to develop an Artificial Neural Network (ANN) model for predicting highway traffic noise. The developed ANN model is used to predict 10 Percentile exceeded sound level (L_{10}) and Equivalent continuous sound level (L_{eq}) in dB (A). The model input parameters are total vehicle volume/hour, percentage of heavy vehicles and average vehicle speed. The predicted highway noise descriptors, L_{eq} and L_{10} from ANN approach and regression analysis have also been compared with the field measurement. The results show that the percentage difference is much less using ANN approach as compared to regression analysis. Further goodness-of-fit of the models against field data has been checked by statistical *t*-test at 5% significance level and proved the Artificial Neural Network (ANN) approach as a powerful technique for traffic noise modeling.

1. Introduction

Traffic noise is a major contributor to overall noise pollution. Traffic noise from highways creates problems for surrounding areas, especially when there are high traffic volumes and high speeds. Vehicular traffic noise problem is contributed by various kinds of vehicles like heavy and medium trucks/buses, automobiles and two wheelers.

Different traffic noise prediction models have been developed by many researchers in different countries based on the field measurement of different highway noise descriptors and traffic noise parameters.

Steele (2001) has critically reviewed the most commonly used traffic noise prediction models like CORTN, FHWA and ASJ. Johnson and Saunders (1968) predicted the noise level from freely flowing road traffic on sites ranging from motorway to urban roads and showed how basic variables such as traffic density, speed and distance from road side have an effect on the observed pattern of noise. A prediction models was developed which incorporate the effects of flow rate, speed of the vehicle, composition of the traffic and adjustment for gradient and road surface for predicting L_{10} (1 h) and L_{10} (18 h) (Delany et al., 1976). This model was used by Hammad and Abdelazeez (1987) in Amman (Jordan) and found a 4 dB difference in L_{10}

* Corresponding author. Address: Mechanical Engineering Department, Delhi Technological University, Bawana Road, Delhi 110042, India. Tel.: +91 9560063121; fax: +91 11 27871023.
E-mail address: paraskum007@rediffmail.com (P. Kumar).

0968-090X/$ - see front matter © 2014 Elsevier Ltd. All rights reserved.
http://dx.doi.org/10.1016/j.trc.2014.01.006

(1 h) and a correlation coefficient of 0.91 in L_{10} (18 h) between experimental and predicted values. Pamanikabud and Vivitjinda (2002) formulated a model of highway traffic noise based on vehicles types in Thailand under free flow traffic conditions and estimated reference mean energy emission level for each type of vehicle based on direct measurement of L_{eq} (10 s). Gorai et al. (2007) have developed six different statistical relationships (models) to predict L_{eq} based on the total traffic volume per hour (Q) and percentage of heavy vehicles over total number of vehicles (P) as input parameters. The deviation between observed value and predicted value from each model at different locations was within the order of ±1.5 dB (A) except at one location. Cho and Mun (2008) considered several types of road surface and developed a highway traffic noise prediction model for environmental assessment in South Korea.

The linear regression analysis for traffic noise modeling, used in early models, was replaced by advanced modeling techniques (Cammarata et al., 1995; Givargis and Karimi, 2009; Rahmani et al., 2011). Cammarata et al. (1995) proposed the ANN model to predict the equivalent sound pressure level caused by urban traffic where the data was collected with typical features of commercial, residential and industrial area. Initially the ANN model proposed has three input parameters i.e. equivalent number of vehicles, average height of the buildings and width of the street and later on, to achieve the better prediction capability, the number of vehicles has been decomposed into the numbers of cars, motor cycles and trucks. Now the new ANN model has five inputs and one output parameter with 20 numbers of neurons in hidden layer. The result obtained using BPN based approach has been compared with classical models proposed by Burgess (1977), Josse (1972), CSTB (Bertoni et al., 1987) and a favorable agreement was observed between the predicted and measured result using ANN. Givargis and Karimi (2009) have presented the mathematical logarithmic, statistical linear regression and neural models to predict maximum A – weighted noise level ($L_{A,max}$) for Teran-karaj express train. The models have been developed on the basis of data recorded at a distance of 25 m, 45 m, and 65 m from the centerline of the track and at a height of 1.5 m while the prediction capabilities have been tested on the data associated with 35 m and 55 m. Different non-parametric tests have showed satisfactory result for all the models and none of the models outweighs the others. As far as the neural network is concern, the authors have built and tested a neural network via statistical neural networks (SNN) module of STATISTICA software (version 7.0). This network was a two layered network with no hidden layer i.e. a perceptron with two input neurons and one output neuron. The neural network input parameters were train speed and distance while output was maximum A – weighted noise level ($L_{A,max}$). The training algorithm adapted was pseudo-inverse, linear least squares optimization. The mean training and testing error were observed as 0.5 dB (A) and 0.3 dB (A) respectively, indicate a sign of good fitness between the predicted and measured values.

Even many western countries have also developed different prediction models based on L_{10}, L_{eq} and other descriptors. But the highway noise descriptors, L_{eq} (in North America, Continental Europe) and L_{10} (in United Kingdom), are increasingly being used for quantitative assessment of nuisance associated with traffic noise.

Further, these models are unreliable for predicting highway noise in India because of different traffic conditions and traffic characteristics. The traffic load on Indian road is also increasing day by day, with the introduction of varieties of new vehicle models. This paper is thus aimed to develop a more relevant and accurate free-flow traffic noise prediction model for highways in India i.e. a model which predict the output accurately by accounting the input traffic parameters, more relevant to Indian traffic conditions and characteristics. It is realized that the vehicle volume/hr, percentage of heavy vehicles and average vehicle speed are the three more relevant traffic parameters in India which affect the noise level to a large extent. Artificial Neural Network (ANN) approach has been used in the present study to develop a precise traffic noise prediction model.

2. Highway noise descriptors and traffic parameters

The different highway noise descriptors are Percentile Exceeded Sound Level (L_x), Equivalent Continuous (A-weighted) Sound Level (L_{eq}), Day Night Average Sound level (L_{dn}), Traffic Noise Index (TNI) and Noise Pollution Level (NPL). Out of the above, the two noise descriptors which have been mostly used in many countries to describe highway traffic noise are L_{10} and L_{eq} levels. The different traffic parameters normally considered are vehicle volume, vehicle mix and the average speed.

2.1. Percentile exceeded sound level, L_{10}

L_{10} is defined as the level which is exceeded for 10% of time and provides a good measure of intermittent or intrusive noise, i.e. traffic noise, aircraft flyovers, etc.

2.2. Equivalent continuous (A-weighted) sound level, L_{eq}

Equivalent continuous (A-weighted) sound level is defined as the steady sound level that transmits to the receiver the same amount of acoustic energy as the actual time varying sound over the prescribed time period. The Equivalent sound level in the time period from t_1 to t_2 is given by

$$L_{eq} = 10\,\mathrm{Log}\left[\frac{1}{(t_2 - t_1)}\int_{t_1}^{t_2}\frac{p^2(t)}{p_{ref}^2}\mathrm{dt}\right] \tag{1}$$

Table 1
Vehicle classification.

S. no.	Type of vehicle	Description
1	Heavy truck	Single-unit truck with 10 wheels
2	Medium truck	Single-unit truck with 6 wheels
3	Bus	Normal buses
4	Tractors	All tractors
5	Cars	All four wheelers
6	Tempos	All three wheelers
7	Scooter/mopeds/motorcycles	All two wheelers

where $p(t)$ is the A-weighted instantaneous acoustic pressure and p_{ref} is the reference acoustic pressure (20×10^{-5} N/m^2).

2.3. Traffic volume, Q

Traffic volume is defined as the total number of vehicles flowing per hour. The noise level increases with an increase in traffic volume. The vehicles are divided into seven categories according to Indian conditions as shown in Table 1. The number of each type of vehicle passing through a fixed point on the road is to be counted and recorded for 1 h duration. Several such samples are to be taken in different time slots ranging between 8.00 A.M. and 7.00 P.M. It is generally accepted that over a wide range of traffic flow, the variation of L_{10} with flow rate can be represented by a logarithmic relation (Delany et al., 1976). So the traffic volume has been considered in logarithmic form in the present paper.

2.4. Truck-traffic mix ratio, P

Trucks and buses are contributing more noise to the environment as compared to other category of vehicles. The ratio of heavy trucks and buses to total traffic is called truck traffic mix ratio. An increase in this ratio will increase the noise level. From the hourly recorded data for traffic volume (Q), the truck-traffic mix ratio was computed and incorporated in the model in terms of percentage of heavy vehicles.

2.5. Speed of vehicle, V

Vehicle speed is taken as an average speed of all vehicle categories. If the vehicle is traveling within the limited range of road speeds, the noise produced is related to the engine, which would vary with each vehicle type. The speed for each category of vehicle has been measured and then the vehicle average speed is computed. Delany et al. (1976) has discussed that the noise output of a composite vehicle stream can be approximated as a logarithmic function of speed. Therefore, the speed of the vehicle is introduced in the form of Log V in the model.

3. Vehicle classification and noise standard in India

Vehicles are divided into seven categories according to Indian conditions as shown in Table 1.

One of the earliest noise standards available is due to the Occupational Safety and Health Act (OSHA) enacted in USA in 1971 which happens to be a landmark step in the direction of environmental noise control.

In India, noise figured only incidentally in general legislation of the Govt. of India as a component in Indian Penal Code, Motor Vehicles Act (1939), and Industries Act (1951). Some of the states also had noise limits incorporated in certain manner in their legislation. In 1986, the Environment (Protection) Act was legislated.

A review of the status report indicates that noise surveys were made in India in the sixties by the National Physical Laboratory, New Delhi. The findings of this survey clearly established the existence of high noise levels in Delhi, Bombay and Calcutta.

An expert committee on noise Pollution was set up by the Ministry of Environment, Govt. of India, in early 1986 to look into the present status of noise pollution in India. Expert Committee submitted its report in June 1987.

The permissible sound pressure level for automotive vehicles in India as per Central Pollution Control Board (Noise limits for vehicles, 2005) is given in Table 2.

4. Site Selection, Instrument and Method of Measurement

Patiala (Punjab) city is considered as a representative candidate to develop a highway noise prediction model in India. After a survey of different areas and location where continuous flow of vehicles occurs without any obstructions like traffic signal lights, a two lane straight patch was selected at a distance of 4.0 km from Patiala (India) towards Sirhind road as shown in Fig. 1. Systematic noise monitoring was done during day-time at 8.00 A.M to 7.00 P.M from April 2009 to May 2009 using Sound Level Meter (Cesva SC-310).

Table 2
Noise limits for vehicles at manufacturing stage applicable from 1st April, 2005.

S. no.	Type of vehicle	Noise limits in dB (A)
1	Two wheeler	
	• Displacement up to 80 cc	75
	• Displacement more than 80 cc but up to 175 cc	77
	• Displacement more than 175 cc	80
2	Three wheeler	
	• Displacement up to 175 cc	77
	• Displacement more than 175 cc	80
3	Vehicles used for carriage of passengers and capable of having not more than nine seats, including the driver's seat	74
4	Vehicles used for carriage of passengers having more than nine seats, including the driver's seat, and a maximum gross vehicle weight (GVW) of more than 3.5 tonnes	
	• With an engine power less than150 kW	78
	• With an engine power of 150 kW or above	80
5	Vehicles used for carriage of passengers having more than nine seats, including the driver's seat: vehicles used for carriage goods	
	• With maximum GVW not exceeding 2 tonnes	76
	• With maximum GVW greater than 3 tonnes but not exceeding 3.5 tonnes	77
6	Vehicles used for transport of goods with a maximum GVW exceeding 3.5 tonnes	
	• With an engine power less than 75 kW	77
	• With an engine power of 75 kW or above but less than 150 kW	78
	• With an engine power of 150 kW or above	80

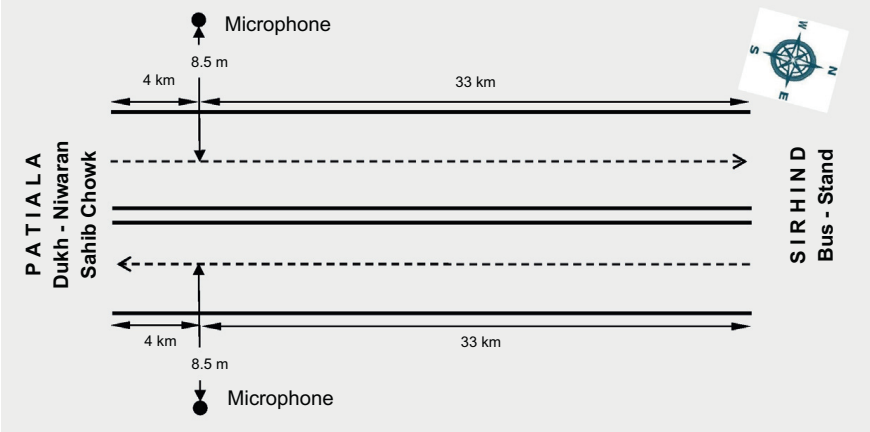

Fig. 1. Location of noise measurement on highway section.

The SLM was mounted at a height of 1.2 m above the ground level and was located at the side of the road as per ISO R-362 (Rao and Rao, 1991). The noise descriptors, L_{eq} and L_{10} were measured for 1 h duration in dB (A) weighting with slow response. Besides noise monitoring, vehicle number and vehicle speed, temperature, humidity and wind conditions were also measured continuously.

A large number of sets of data were recorded for 1 h duration on different dates and timings in a random or staggered manner in order to account for statistical temporal variations in traffic flow characteristics. The measured parameters have been divided into two classes i.e. output parameters (L_{10}, L_{eq}) and input parameters (vehicle volume/hour, percentage of heavy vehicles and average vehicle speed). The complete recorded data, as shown in Tables 3 and 4, is further used for training and testing the ANN model.

5. Artificial Neural Network (ANN)

An Artificial Neural Network (ANN) is a computational model that is inspired by the structure and functional aspect of biological neural network. The feature that makes the neural network more flexible and powerful is its ability to learn by example. The neural network has multi-disciplinary applications which include neurobiology, philosophy, economics, finances, engineering, mathematics and computer science, etc.

There exists the different types of neural network architecture but the multilayer feed forward network (MFFN) (Fausett, 1994) is more popular. The architecture of multilayer feed forward network consist of interconnection of several layers i.e.

Table 3
Experimental training data sets.

Sample number	Input parameters[a]			Output parameters[b]	
	Log Q	P (%)	Log V	L_{10}	L_{eq}
1	3.14	10.2	1.62	77.4	75.3
2	3.06	9.4	1.71	76.0	74.1
3	3.03	7.4	1.74	76.4	73.7
4	3.06	13.3	1.73	75.4	73.2
5	3.01	12.9	1.73	75.8	74.5
6	3.09	10.7	1.71	76.4	74.4
7	3.2	9.1	1.74	77.8	75.9
8	3.24	7.1	1.75	77.1	75.0
9	3.23	8.1	1.76	77.3	75.0
10	3.11	10.3	1.74	75.8	72.9
11	3.14	7.3	1.72	76.2	74.2
12	3.16	7.2	1.74	75.8	73.2
13	3.23	10.4	1.73	78.2	76.1
14	3.2	7.8	1.75	76.2	73.2
15	3.19	10.7	1.74	77.8	75.9
16	3.12	12.4	1.75	76.1	73.8
17	3.14	9.3	1.76	76.4	74.2
18	3.17	11.3	1.75	76.2	74.0
19	3.18	9.2	1.70	78.3	75.7
20	3.17	9.4	1.68	78.2	75.4
21	3.16	8.1	1.73	77.7	75.5
22	3.1	9.9	1.70	77.6	74.5
23	3.14	9.6	1.75	77.8	75.4
24	3.21	8.9	1.71	79.9	77.4
25	3.11	11.0	1.68	78.8	76.1
26	3.14	11.0	1.73	77.7	75.4
27	3.11	9.3	1.72	77.3	75.0
28	3.07	12.4	1.73	75.7	73.6
29	3.07	12.1	1.74	76.5	74.2
30	3.19	10.2	1.71	78.6	76.8
31	3.20	8.8	1.74	77.1	75.8
32	3.24	6.3	1.73	76.6	75.2
33	3.22	7.2	1.75	77.2	75.9
34	3.08	9.7	1.74	75.8	74.4
35	3.09	7.8	1.75	76.4	74.9
36	3.23	6.1	1.75	75.3	74.1

[a] Q – traffic volume (vehicle/hour), P – heavy vehicles (%), V – average vehicle speed (km/h).
[b] All levels are in dB (A) referred to 20 micro-Pascal.

Table 4
Experimental testing data sets.

Sample number	Input parameters			Output parameters	
	Log Q	P (%)	Log V	L_{10}	L_{eq}
1	3.14	10.2	1.70	77.8	75.0
2	3.09	10.7	1.69	77.9	76.4
3	3.07	12.2	1.73	76.7	74.2
4	3.13	10.8	1.74	77.3	74.6
5	3.14	6.9	1.68	75.6	72.9
6	3.07	9.2	1.72	76.0	74.1
7	3.12	9.4	1.70	77.0	75.2
8	3.09	10.1	1.75	77.1	75.8
9	3.03	12.8	1.73	76.4	74.8
10	3.08	8.5	1.72	76.2	74.5

input layer, hidden layer and output layer and have at least one intermediate hidden layer between input and output layer. The basic processing elements of neural networks are the artificial neurons (nodes). All these neurons are connected to each other to transmit the information or signal from input layer to output layer through hidden layer. A network is said feed forward if no neurons in the output layer take part as a feedback element to any of the neuron. Each neuron produces the output signal as it receives the input signal according to the chosen activation function. In a simplified mathematical model of the neuron, the effects of the synapses are represented by connection weights that modulate the effect of the associated input signals, and the nonlinear characteristic exhibited by neurons is represented by a transfer function. The neuron impulse is

then computed as the weighted sum of the input signals, transformed by the transfer function. The learning capability of an artificial neuron is achieved by adjusting the weights in accordance to the chosen learning algorithm. Various methods are existing to set the strengths of the connections. One way is to set the weights explicitly using a priori knowledge and the other way is to change the weights automatically by feeding the teaching patterns to the neural network. Thus the neural network is an adaptive system that can learn relationship through repeated presentation of data and is capable of generalizing to new previously unseen data.

In the present study, the multilayer feed forwarded neural network has been trained by the back-propagation learning algorithm which provides a procedure to update weights to correctly classify the training pair. The Levenberg–Marquardt optimization technique has been used to update weights in back-propagation algorithm. The training of a network by back-propagation involves the feed forward of the input training pattern, calculation of back propagation of the associated error and adjustment of weights to minimize the error. A multilayer feed forward network, as shown in Fig. 2, has i number of input neurons, j number of hidden neurons and k number of output neurons. To train the neural network, training data set is required which consists of input vector (x_i) and corresponding target output vector (t_k) while the network simulated output is (y_k). The weights between input-hidden layer neurons and hidden-output layer neurons are represented as w_{ij}, v_{jk} respectively. The training data set is given by vector (x_i, t_k).

To compute the network error, first the input and output vector for each neuron in the hidden and output layer is to be compute. Figs. 3 and 4 show the input and output vector computation process at hidden and output layer respectively. The input to any neuron is the weighted sum of the outputs of the previous layer neurons while its output is dependent on the activation function. The Hyperbolic tangent sigmoid transfer function is chosen for hidden layer, Eq. (2), and linear transfer

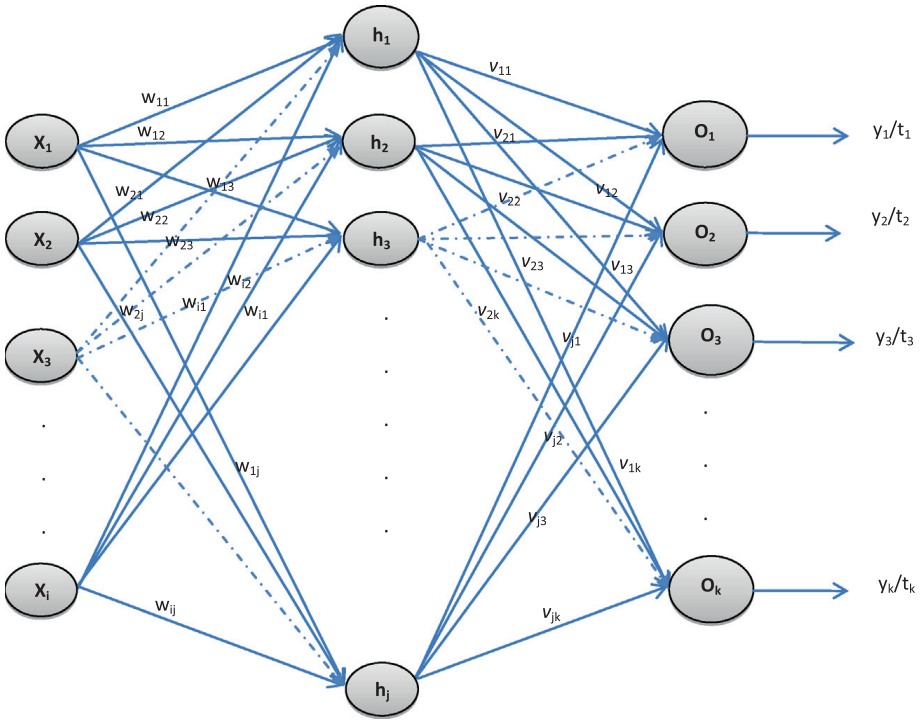

Fig. 2. Multilayer feed forward network.

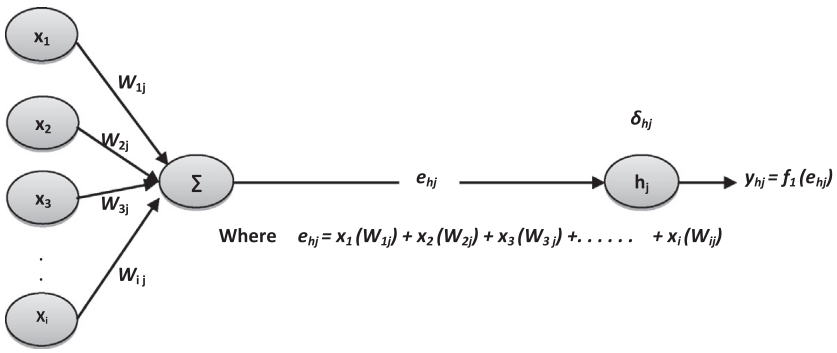

Fig. 3. Computation process of jth neuron at hidden layer.

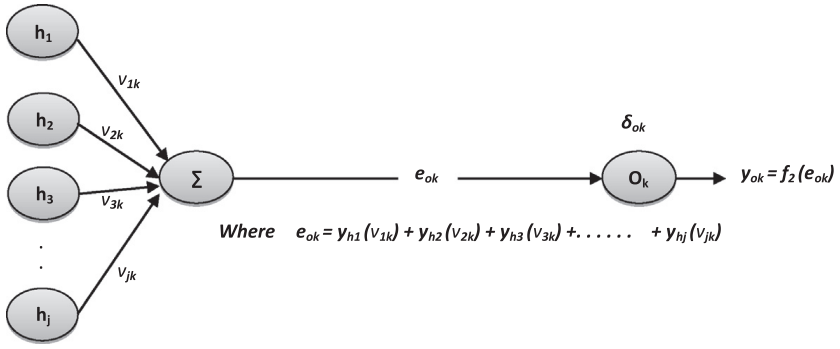

Fig. 4. Computation process of kth neuron at output layer.

function, Eq. (3), in output layer because a multilayer perception may learn faster in terms of number of epochs when the sigmoid function is symmetric rather than

$$f_1(x) = \frac{(e^x - e^{-x})}{(e^x + e^{-x})} \tag{2}$$

$$f_2(x) = x \tag{3}$$

when it is asymmetric (Haykin, 1999). The performance of the neural network has been evaluated in terms of mean square error (MSE) between the targeted output and predicted output for a given samples size.

The output and error vector of lth neuron for the hidden layer is expressed by the following equations:

$$output(y_{hl}) = f_1\left(\sum_{m=1}^{i} x_m w_{ml}\right) \tag{4}$$

$$Error(\delta_{hl}) = \sum_{p=1}^{k} v_{lp}\delta_{op} \tag{5}$$

While the output and error vector for the pth neuron of output layer is given by the following equations:

$$Output(y_p) = f_2\left(\sum_{l=1}^{j} y_{hl} v_{lp}\right) \tag{6}$$

$$Error(\delta_{op}) = t_p - y_p \tag{7}$$

where $m \to 1, 2, 3, \ldots, i$; $l \to 1, 2, 3, \ldots, j$ and $p \to 1, 2, 3, \ldots, k$.

The targeted output vector is compared with neural network simulated vector and the error vector is calculated for output layer neurons. The next step is to compute the mean square error (MSE) for the neural network, expressed by the following equation:

$$E = \frac{1}{k}\sum_{p=1}^{k} \delta_{op}^2 \tag{8}$$

If the MSE is less than the desired error (goal) i.e. the Neural Network training is complete and the network is ready for prediction. Otherwise the weights are updated until the desired error goal is achieved. The main purpose of neural network training is to obtain better memorization and generalization capability which is mainly dependent on the learning algorithm. The Levenberg–Marquardt (L–M) algorithm is used to update weights in the proposed ANN model. Once the training is completed, the prediction capability of the network is checked for unknown input data to verify whether it is correctly predicting or not.

The MATLAB neural network tool box is used for ANN analysis which includes neural network training, testing, performance evaluation and comparison.

5.1. Levenberg–Marquardt (L–M) algorithm

The gradient based search methods are the fast optimization techniques to update weights in Artificial Neural Network (ANN). The most commonly used optimization methods for ANN learning are gradient descent method (GDM), Gauss–Newton's method (GNM), Conjugate gradient method, variable-metric method and Levenberg–Marquardt method.

In gradient descent method (GDM) the error function decreases steeply in the direction of the negative of gradient. The better and efficient convergence in BPN depends upon the choice of learning rate coefficient and momentum factor. A large learning rate leads to slow convergence because of oscillation of weights while lower rate increases the time of convergence because of small steps. A proper choice of this coefficient is needed to avoid failure in convergence. The other way to improve the convergence with large learning rate is to add momentum factor to the previously changed weights. The addition of this term smoothens the oscillatory behavior of weights and leads to efficient rapid learning. After adding the momentum term, the weights at each connection are adjusted as per Eq. (9)

$$w^{\gamma+1} = w^{\gamma} - \rho\nabla E + \vartheta\delta w^{\gamma} \tag{9}$$

where $w^{\gamma+1}$ is the current weight, w^{γ} the previous weight, δw^{γ} the previous weight change, ∇E the gradient of error, ρ the learning rate and ϑ is the momentum coefficient.

The Newton's method (NM) uses second order derivative to converge faster as compared to gradient descent method. The weights are updated according to the following equation:

$$w^{\gamma+1} = w^{\gamma} - H^{-1}\nabla E \tag{10}$$

where H is Hessian matrix.

The gradient descent method functioning well when the initial weight guess are far away from the optimal weights while the Newton's method performs well when the initial weight guess are near to the optimal one. The Levenberg method (Levenberg, 1944) has taken the advantage of both the methods by combining them. Initially the GDM is used and later on switched over to the Newton's Method (NM) when the solution is near to optimal. The weights are updated as Eq. (11)

$$w^{\gamma+1} = w^{\gamma} - (H + \tau I)^{-1}\nabla E \tag{11}$$

where I is the Identity matrix and τ is a blending factor.

The blending factor determines the level of mixing between GDM and NM. Initially a large value of blending factor is used and the weights are updated as per GDM because there is little effect of Hessian matrix on weight update. The value of blending factor is adjusted depending upon whether the error (E) is increasing or decreasing. When the initial weights converge to optimal side, the value of blending factor becomes small and the weights are updated according to NM. If the error is increasing i.e. the NM is not converging to optimal weights, and then increases the blending factor (τ) and shift more towards GDM. On the contrary, if the error is decreasing i.e. the GDM is not converging then decrease blending factor and shift more towards NM, to obtain optimal weights.

Later on, Marquardt (1963) incorporated the local curvature information in the Levenberg method resulting into the Levenberg–Marquardt (L–M) method. The GDM is used when blending factor is high but still to move further in the directions of smaller gradient to achieve faster convergence, the advantage of Hessian matrix should be incorporated. So the identity matrix in Levenberg's equations is replaced with the diagonal of the Hessian and the weights are adjusted according to the following equation:

$$w^{\gamma+1} = w^{\gamma} - (H + \tau\ diag[H])^{-1}\nabla E \tag{12}$$

where $dig[H]$ is diagonal of Hessian matrix.

The Levenberg–Marquardt (L–M) algorithm interpolates between the Gauss–Newton's method (GNM) and gradient descent method (GDM). The L–M algorithm is more robust than the GNM which means that in many cases it finds solutions even if it starts far off from the final minimum.

6. Proposed ANN architecture for traffic noise modeling

The proposed ANN architecture for highway traffic noise modeling is shown in Fig. 5. The input parameters to the neural network model are vehicle volume/hour (Log Q), percentage of heavy vehicles (P) and average vehicle speed (Log V) and the output parameters are 10 Percentile Exceeded Sound Level (L_{10}), Equivalent Continuous Sound Level (L_{eq}) in dB (A).

Once the input and output parameters have been decided, the next step is to decide the number of neurons in the hidden layer. The prediction accuracy of any neural network is dependent on the number of hidden layers and the numbers of neurons in each layer. To find out the optimal neural network architecture, a number of neural networks architecture have been trained and tested by varying the number of hidden layers and number of neurons in each layer.

Total 46 field data sets (samples), including vehicle volume/hour (Log Q), percentage of heavy vehicles (P), average vehicle speed (Log V), L_{10}, L_{eq}, are randomly distributed for training and testing the ANN model. These randomly distributed 36-training and 10-testing samples are presented in Tables 3 and 4, respectively. The neural network is trained through a number of epochs and during each epoch a new set of data is fed to the network. The network program automatically generates the initial weights which are automatically updated depending upon the error between predicted and targeted output. The program was automatically terminates the training process if any one of the conditions is achieved:

- Maximum number of epochs.
- Error goal achieved.
- Minimum gradient reached.

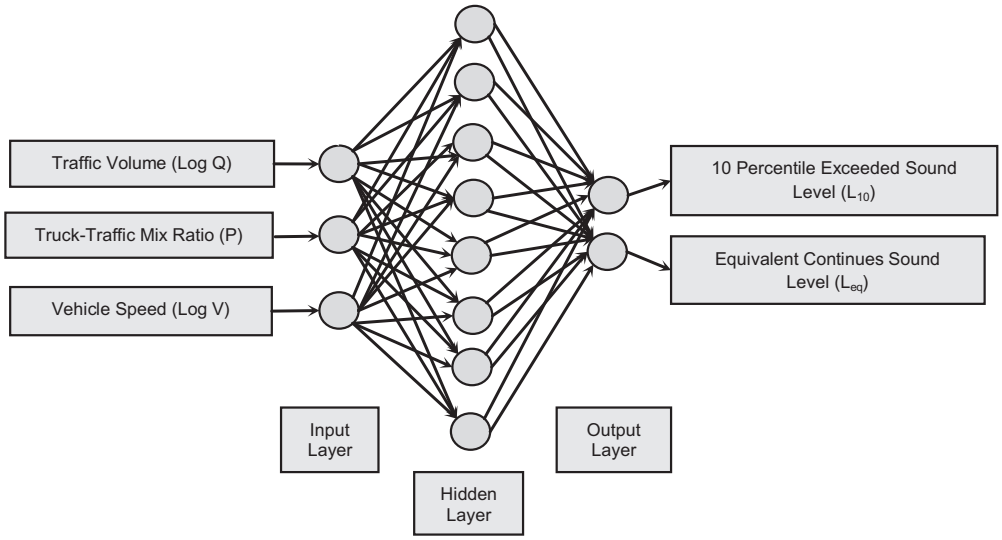

Fig. 5. Proposed ANN architecture for traffic noise modeling (3-8-2).

Table 5
Comparison of training and testing data for ANN architecture (3-*N*-2).

Hidden nodes (*N*)	Training				Testing			
	Correlation coefficient (*R*)		Mean square error		Correlation coefficient (*R*)		Mean square error	
	L_{10}	L_{eq}	L_{10}	L_{eq}	L_{10}	L_{eq}	L_{10}	L_{eq}
4	0.8878	0.8694	0.24047	0.26981	0.4958	0.3179	0.72389	1.19720
8	**0.9769**	**0.9453**	**0.05188**	**0.11772**	**0.8160**	**0.8524**	**0.50631**	**0.40434**
11	0.9688	0.9549	0.06966	0.09742	0.7254	0.6938	2.98290	5.74790
14	0.9188	0.8818	0.17687	0.24587	0.4660	0.1378	174388	6761.76
17	0.9943	0.9968	0.01293	0.00703	0.3079	0.1344	4.70330	7.57420
20	0.9958	0.9954	0.00956	0.01037	0.3502	−0.1623	2.17330	4.43940
25	0.9944	0.9968	0.01261	0.00710	0.8268	−0.4849	0.50894	38.8470
30	0.9965	0.9945	0.00782	0.01206	0.1147	0.1927	21.5323	16.6834

The comparative data between training and testing samples, for single hidden layer by varying the number of neurons from 4 to 30, is presented in Table 5. It has been observed that among the entire neural network tested, the single hidden layer neural network structure with eight numbers of neurons gave minimum mean square error and good correlation coefficient between the targeted and predicted output for training and testing data sets.

Therefore the optimal neural network structure is 3-8-2, as shown in Fig. 5, which connected 3-input parameters and 2-output parameters through 8-number of neurons in the hidden layer.

Once the number of neurons has been decided, the next step is to check the prediction capability of ANN using unseen samples. The testing samples are not used for training purpose, but are only used to check the predictive capability of trained ANN model.

7. Results and discussion

7.1. Regression result

After computing the relevant parameters, multiple regression analysis is carried out to predict the 10 Percentile Exceeded Sound Level (L_{10}) and Equivalent Continuous (A-weighted) Sound Level (L_{eq}) as a function of traffic volume ($\log Q$), heavy vehicle percentage (P %) and average vehicle speed ($\log V$). The following relations are found from regression analysis.

$$L_{10}[\mathrm{dB(A)}] = 75.87 + 6.53\ \log Q + 0.09P - 11.84\ \log V \tag{13}$$

$$L_{eq}[\mathrm{dB(A)}] = 67.6 + 5.8\ \log Q + 0.27P - 6.58\ \log V \tag{14}$$

The comparison of experimental and regression outputs for training and testing samples is summarized in Tables 6 and 7, respectively. The percentage difference (%) between experimental and regression output results for training samples are in the range of (−4.2) to (+2.7) for L_{10} and (−5.1) to (+2.6) for L_{eq}, while for testing samples it is in the range of (−4.1) to (−0.1) for L_{10} and (−4.8) to (+0.5) for L_{eq}.

7.2. Artificial Neural Network (ANN) result

Tables 6 and 7 show the comparison of experimental and ANN results for L_{10} and L_{eq} for training and testing samples respectively. These comparative results are also plotted in Figs. 6 and 7 for ANN architecture 3-8-2.

It is clear that the percentage difference (%) between experimental and ANN results during training are in the range of (−0.8) to (+1.0) for L_{10} and (−1.5) to (+0.9) for L_{eq}, while for testing it is in the range of (−1.7) to (+1.8) for L_{10} and (−0.6) to (+1.5) for L_{eq}. It can also be concluded that the ANN model predicts the output parameters close to the actual field results for both training and testing.

7.3. Goodness of fit

The model's goodness of fit against experimental data has been tested using *t*-test (Pamanikabud and Vivitjinda, 2002; Montgomery and Runger, 2004). *t*-Test is based on *t*-distribution i.e. an appropriate test for judging the significance difference between the means of two samples when the sample size is small. In this test, *t*-start (test statistic – calculated from the sample data) is compared with *t*-critical (probable value based on *t*-distribution read from table). If the *t*-start value is within the ±*t*-critical value for two-tailed test i.e. there is no significance difference between the two samples (accept null hypothesis or rejecting alternative hypothesis) otherwise there is a significance difference exist (rejecting null hypothesis or accept alternative hypothesis).

The predicted output parameter from regression and ANN models have been tested against field data for testing data samples at 5% significance level. The results are summarized in Table 8. The *t*-start values are −2.73 for L_{10} and −2.02 for L_{eq} against the *t*-critical value of ±2.10 using regression model. These values of *t*-start are greater than and near to the critical

Table 6
Comparison between experimental, regression and ANN result-training.

Sample number	Result						Percentage error (%)			
	Experimental		Regression		ANN		Regression[a]		ANN[b]	
	L_{10}	L_{eq}	L_{10}	L_{eq}	L_{10}	L_{eq}	L_{10}	L_{eq}	L_{10}	L_{eq}
1	77.4	75.3	78.5	76.0	77.5	75.2	−1.4	−0.9	−0.1	0.1
2	76.0	74.1	78.2	75.8	76.1	73.7	−2.9	−2.3	−0.1	0.5
3	76.4	73.7	78.2	75.7	76.2	74.0	−2.3	−2.7	0.2	−0.4
4	75.4	73.2	78.2	75.6	75.3	73.3	−3.7	−3.3	0.1	−0.1
5	75.8	74.5	77.8	75.3	75.8	74.5	−2.6	−1.1	0.0	0.0
6	76.4	74.4	78.4	75.9	76.7	74.3	−2.6	−2.0	−0.4	0.1
7	77.8	75.9	79.2	76.8	77.8	75.7	−1.8	−1.2	0.0	0.3
8	77.1	75.0	79.6	77.2	76.9	75.2	−3.2	−2.9	0.2	−0.3
9	77.3	75.0	79.5	77.1	76.9	74.7	−2.8	−2.8	0.5	0.4
10	75.8	72.9	78.6	76.1	75.7	73.5	−3.7	−4.4	0.1	−0.8
11	76.2	74.2	78.8	76.4	76.4	74.2	−3.4	−2.9	−0.3	0.1
12	75.8	73.2	79.0	76.6	75.8	73.6	−4.2	−4.6	0.0	−0.5
13	78.2	76.1	79.1	76.9	78.4	76.3	−1.1	−1.0	−0.3	−0.3
14	76.2	73.2	79.3	76.9	76.5	74.3	−4.0	−5.1	−0.4	−1.5
15	77.8	75.9	79.1	76.6	77.8	75.7	−1.7	−0.9	−0.1	0.3
16	76.1	73.8	78.6	76.1	76.0	73.8	−3.3	−3.1	0.1	0.0
17	76.4	74.2	78.9	76.4	76.2	74.2	−3.3	−2.9	0.2	−0.1
18	76.2	74.0	79.0	76.5	76.1	73.9	−3.7	−3.4	0.2	0.1
19	78.3	75.7	77.8	75.5	78.3	75.9	0.6	0.3	0.0	−0.2
20	78.2	75.4	78.2	75.8	78.0	75.4	0.0	−0.5	0.3	0.0
21	77.7	75.5	76.7	74.8	76.9	74.8	1.3	0.9	1.0	0.9
22	77.6	74.5	77.4	75.1	77.6	75.0	0.2	−0.8	0.1	−0.7
23	77.8	75.4	76.3	74.4	77.7	75.7	1.9	1.3	0.1	−0.4
24	79.9	77.4	77.7	75.4	79.7	77.7	2.7	2.6	0.3	−0.4
25	78.8	76.1	78.1	75.6	78.6	76.3	0.9	0.6	0.3	−0.2
26	77.7	75.4	77.0	74.9	77.7	75.4	0.9	0.7	−0.1	0.1
27	77.3	75.0	76.8	74.8	77.3	74.7	0.6	0.3	0.0	0.3
28	75.7	73.6	76.7	74.6	75.7	73.5	−1.3	−1.3	0.0	0.1
29	76.5	74.2	76.5	74.4	76.6	74.4	0.0	−0.3	−0.1	−0.2
30	78.6	76.8	77.7	75.4	78.8	76.5	1.1	1.8	−0.3	0.4
31	77.1	75.8	76.8	74.9	77.7	75.6	0.4	1.2	−0.8	0.3
32	76.6	75.2	77.0	75.1	76.6	75.2	−0.5	0.1	0.0	−0.1
33	77.2	75.9	76.5	74.7	77.4	75.3	0.9	1.6	−0.3	0.8
34	75.8	74.4	76.2	74.3	76.0	73.7	−0.5	0.1	−0.2	0.9
35	76.4	74.9	75.8	74.1	76.7	74.7	0.8	1.1	−0.4	0.2
36	75.3	74.1	76.4	74.7	75.4	73.9	−1.5	−0.8	−0.1	0.2

[a] % Error (Regression) = (1 − Regression result/Experimental Result) * 100.
[b] % Error (ANN) = (1 − ANN result/Experimental Result) * 100.

Table 7
Comparison of experimental, regression and ANN result – testing.

Sample number	Result						Percentage error (%)			
	Experimental		Regression		ANN		Regression		ANN	
	L_{10}	L_{eq}	L_{10}	L_{eq}	L_{10}	L_{eq}	L_{10}	L_{eq}	L_{10}	L_{eq}
1	77.8	75.0	78.7	76.2	77.5	74.9	−1.1	−1.6	0.4	0.2
2	77.9	76.4	78.3	75.8	78.4	76.1	−0.5	0.8	−0.7	0.3
3	76.7	74.2	78.3	75.7	76.0	73.8	−2.1	−2.0	0.9	0.5
4	77.3	74.6	78.7	76.2	75.9	73.8	−1.8	−2.1	1.8	1.1
5	75.6	72.9	78.7	76.4	75.6	73.3	−4.1	−4.8	0.0	−0.5
6	76.0	74.1	78.3	75.9	75.5	73.1	−3.0	−2.4	0.6	1.4
7	77.0	75.2	77.4	75.2	76.7	74.1	−0.5	0.0	0.4	1.5
8	77.1	75.8	76.9	74.8	77.4	75.4	−0.6	0.1	−0.4	0.5
9	76.4	74.8	76.5	74.4	75.9	74.3	−0.1	0.5	0.6	0.7
10	76.2	74.5	76.5	74.6	77.5	74.9	−0.4	−0.1	−1.7	−0.6

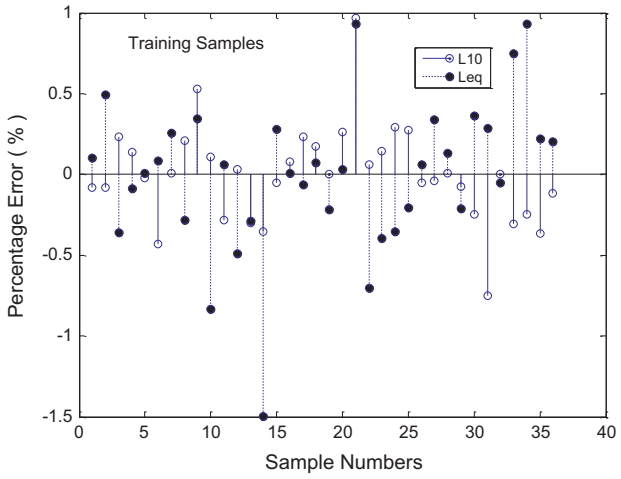

Fig. 6. Percentage error between experimental and ANN predicted output (training) for Neural Network Architecture 3-8-2.

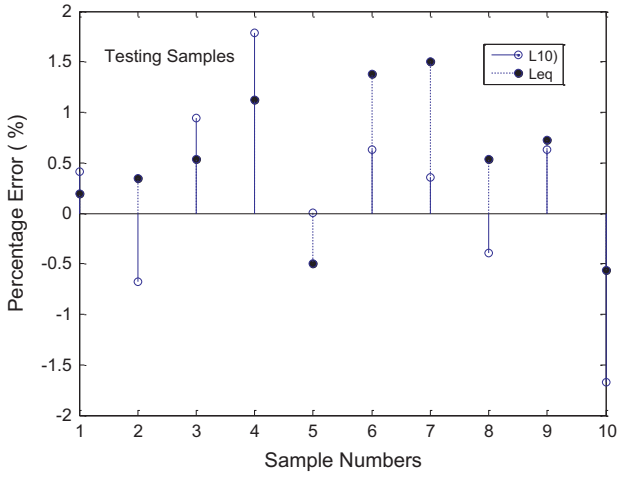

Fig. 7. Percentage error between experimental and ANN predicted output (testing) for Neural Network Architecture 3-8-2.

value respectively. This indicates that the predicted traffic noise level does not fit well with the field data using regression model. Using the ANN model the values of t-start are 0.40 for L_{10} and 0.89 for L_{eq} against the t-critical value of ±2.10. These two values are less than and far away from the critical value and are within the non-rejection region. This implies that predicted traffic noise level using ANN model fits well with the field data as compared to regression model at 5% significance level.

Table 8
Results of *t*-test at significance level (α) of 0.05 for testing data samples.

Output parameter in dB (A)	Regression model		ANN model	
	t-Start	*t*-Critical	*t*-Start	*t*-Critical
L_{10}	−2.73	±2.10	0.40	±2.10
L_{eq}	−2.02	±2.10	0.89	±2.10

t-Start: test statistic – calculated from the sample data.
t-Critical: probable value based on *t*-distribution read from table.

8. Conclusions

Many multilayer feed forward back propagation (BP) neural networks were trained and tested by Levenberg–Marquardt (L–M) optimization algorithm to predict L_{10} and L_{eq}, highway noise descriptors. Among all the neural network tested, one layered neural network architecture 3-8-2 (3-input neurons, 8-neurons in hidden layer and 2-output neurons) is found to be optimum because of better performance in terms of MSE during training and testing in both highway noise descriptors. The correlation coefficients are 0.9769, 0.9453 during training and 0.8160, 0.8524 during testing for L_{10} and L_{eq} respectively. A high correlation coefficient and less percentage error difference between experimental and predicted output is an indication of better prediction capability of neural network as compared to regression analysis. Further, better prediction capability of ANN model has also been verified by statistical *t*-test at 5% significance level.

References

Bertoni, D., Franchini, A., Magnoni, M., 1987. Il Rumore Urbano e l'Organizzazione de Territorio. Pitagora Editrice, Bologna, Italy, pp. 45–69.
Burgess, M.A., 1977. Noise prediction for urban traffic conditions-related to measurements in the Sydney metropolitan area. Appl. Acoust. 10, 1–7.
Cammarata, G., Cavalieri, S., Fichera, A., 1995. A neural network architecture for noise prediction. Neural Networks 8 (6), 963–973.
Central Pollution Control Board, 2005. Noise Limits for Vehicles Applicable at Manufacturing Stage, April. <http://cpcb.nic.in/divisionsofheadoffice/pci2/Noise-vehicle.pdf>.
Cho, D.S., Mun, S., 2008. Development of a highway traffic noise prediction model that considers various road surface types. Appl. Acoust. 69, 1120–1128.
Delany, M.E., Harland, D.G., Hood, R.A., Scholes, W.E., 1976. The prediction of noise levels L_{10} due to road traffic. J. Sound Vib. 48 (3), 305–325.
Fausett, L., 1994. Fundamentals of Neural Networks: Architectures, Algorithms and Applications. Prentice-Hall, NJ.
Givargis, S., Karimi, H., 2009. Mathematical, statistical and neural models capable of predicting $L_{A,\,max}$ for the Tehran-Karaj express train. Appl. Acoust. 70, 1015–1020.
Gorai, A.K., Maity, S., Pal, A.K., 2007. Development of the traffic noise prediction model. Asian J. Water Environ. Pollut. 4 (2), 65–74.
Hammad, R.N.S., Abdelazeez, M.K., 1987. Measurements and analysis of the traffic noise in Amman, Jordan and its effects. Appl. Acoust. 21 (4), 309–320.
Haykin, S., 1999. Neural Networks: A Comprehensive Foundation. Prentice-Hall, NJ.
Johnson, D.R., Saunders, E., 1968. The evaluation of noise from freely flowing road traffic. J. Sound Vib. 7 (2), 287–309.
Josse, R., 1972. Notions d'aeoustique Paris. Eyrolles, France.
Levenberg, K., 1944. A method for the solution of certain non-linear problems in least squares. J. Appl. Math. 2, 164–168.
Marquardt, D.W., 1963. An algorithm for least-squares estimation of nonlinear parameters. J. Soc. Ind. Appl. Math. 11 (2), 431–441.
Montgomery, D.C., Runger, G.C., 2004. Applied Statistics and Probability for Engineers. John Wiley & Sons, Inc., Singapore.
Pamanikabud, P., Vivitjinda, P., 2002. Noise prediction for highways in Thailand. Transport. Res. Part D 7, 441–449.
Rahmani, S., Mousavi, S.M., Kamali, M.J., 2011. Modeling of road-traffic noise with the use of genetic algorithm. Appl. Soft Comput. 11, 1008–1013.
Rao, P.R., Rao, M.G.S., 1991. Prediction of $LA_{10}T$ traffic noise levels in the city of Visakhapatnam, India. Appl. Acoust. 34 (2), 101–110.
Steele, C., 2001. A critical review of some traffic noise prediction models. Appl. Acoust. 62, 271–287.